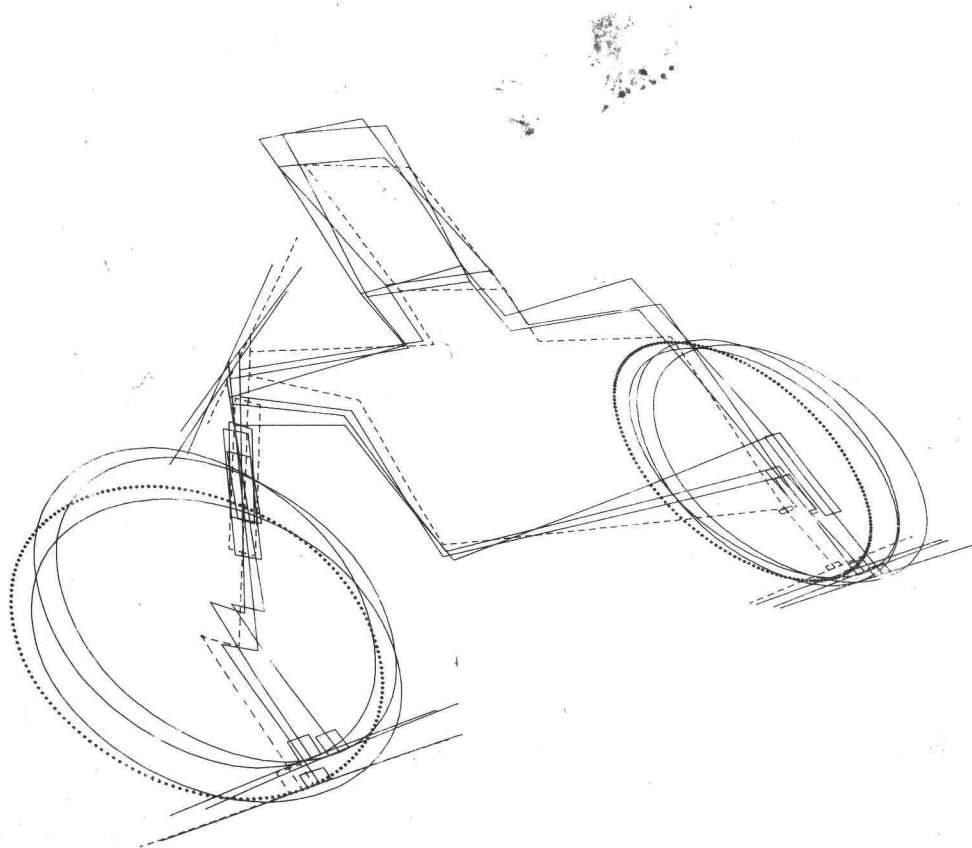


The Dynamic Behaviour of a Motorcycle when running straight ahead and when cornering



C. Koenen



The Dynamic Behaviour of a Motorcycle
when running straight ahead and when cornering



VERVALLEN

P1759
4244

C10084
51500

BIBLIOTHEEK TU Delft
P 1759 4244



C

845150

© 1983 by C. Koenen, Ureterp, The Netherlands

The Dynamic Behaviour of a Motorcycle when running straight ahead and when cornering

PROEFSCHRIFT ter verkrijging van
de graad van doctor in de
technische wetenschappen
aan de Technische Hogeschool Delft,
op gezag van de Rector Magnificus,
prof.ir. B.P.Th. Veltman,
in het openbaar te verdedigen
ten overstaan van het College van Dekanen
op donderdag 8 december 1983
te 14.00 uur door
Cornelis Koenen,
geboren te Den Haag,
werkтуigkundig ingenieur



Dit proefschrift is goedgekeurd door de promotor
Prof. dr. ir. H.B. Pacejka

*Voor mijn ouders
Voor Joppie*



page	contents
IX	SUMMARY
X	SAMENVATTING
XI	LIST OF SYMBOLS
	INTRODUCTION
1	1.1 previous work on motorcycle dynamics
2	1.2 delimitation of the problem area
3	1.3 objectives and approach
	THE MATHEMATICAL MODEL
4	2.1 introduction
5	2.2 aspects and consequences of cornering
9	2.3 co-ordinates / physical structure of the vehicle model
13	2.4 anti-symmetrical tyre behaviour
15	.1 general
19	.2 stationary behaviour
	.3 non-stationary behaviour
25	2.5 rider behaviour
26	.1 general
	.2 passive rider behaviour
27	2.6 environment
30	2.7 derivation of the equations of motion (principles)
32	.1 general
35	.2 kinematics of the vehicle
38	.3 kinematics of the wheel
38	.4 derivation of the constraint equations
38	.5 kinetic energy due to the speed of the mass centres
41	.6 kinetic energy due to the rotational speed of the bodies
43	.7 kinetic energy due to the speed of revolution of the wheels
44	.8 potential energy
45	.9 dissipation function
47	.10 right-hand members
47	.11 post-processing the equations of motion
48	.12 equations concerning the stationary situation
49	.13 equations concerning the non-stationary situation
	CALCULATIONS
51	3.1 procedure
53	3.2 solution of the steady state equations
54	3.3 calculation of the eigen-solutions
57	3.4 application of computer graphics

page	contents
	4.1 stationary behaviour
63	.1 steady state results
65	.2 front contact geometry
	4.2 non-stationary behaviour
67	.1 general
68	.2 presentation of the root-loci; baseline results
80	.3 presentation of the mode shapes; baseline results
	4.3 influence of model structure
96	.1 general
96	.2 simplified model
98	.3 frame elasticity
102	.4 tyre behaviour
107	.5 rider passive behaviour
107	.6 aerodynamic effects
110	.7 miscellaneous
	4.4 influence of some parameters
110	.1 suspension
113	.2 geometrical parameters
113	.3 inertia properties
	DISCUSSION AND CONCLUSION
119	5.1 validity of the model
120	5.2 discussion of the results concerning the running-straight-ahead situation
120	5.3 discussion of the results concerning the cornering situation
121	5.4 conclusion
	APPENDICES
123	A frame elasticity
127	B definition of the full model
130	C elaborated quantities
133	D definition of auxiliary quantities
136	E equations of the stationary motion
141	F equations of the non-stationary motion
162	G parameter values
164	REFERENCES

SUMMARY

The stationary and non-stationary behaviour of a running motorcycle provided with a passive rider has been modelled. The non-linear model, which is fit to describe situations with large values of the mean banking angle (roll angle), features eleven degrees of freedom (one of which being the forward speed u_s which has been kept stationary throughout this study). The behaviour of the system has been described relative to a moving-along system of axes. Regarding the permitted translatory and rotatory motion of this system of axes position and attitude in space are not relevant; thus the order of the system reduces by two.

Stationary aerodynamic forces have been included.

The tyre behaviour has been described by non-linear algebraic equations and first-order differential equations. The presence of these differential equations increases the order of the system by 10, the order of the full system now becoming 28.

The description of the non-stationary behaviour of the system has been linearized about a trim condition, which represents the stationary situation either when running-straight-ahead or when cornering. This trim condition is determined by the value of the chosen input parameters (stationary roll angle and forward speed) together with the non-linear model describing the stationary situation.

The stationary behaviour of the baseline model has been calculated, presented and interpreted. This has also been done extensively for the non-stationary behaviour. The eigenmotions have been calculated for a range of trim conditions and presented in the form of root-loci, supplemented by the mode shape information implied in the eigenvectors. A graphical presentation technique has been developed and employed to visualize the latter: with the aid of computer graphics at small intervals, sequential in time, images are being generated of a structure, representing a single-track-vehicle with a rider. The position and the attitude in space of each of the parts of this structure is being determined as a function of time in accordance with a specific eigen-mode of motion of the motorcycle model. The motion picture "Vibrational Modes of Single-Track-Vehicle" shows various vibrational modes of motion in this way.

At running-straight-ahead we distinguish between symmetrical and anti-symmetrical eigen-modes of motion, the symmetrical being: *pitch* and *bounce* (concerning the motion of the "sprung" mass), and *front hop* and *rear hop* (concerning the motion of the "unsprung" masses); the most relevant anti-symmetrical being: *weave* (eventually unstable at high speed), *wobble* (a steering oscillation, mostly lightly damped or unstable at moderate speed), *shake* (in which the rider upper body motion plays a major role), *twist* (frame torsion) and *rear wobble* (the wobble counterpart concerning the main frame motion). The most important monotonous mode of motion of the uncontrolled system is the so-called *capsize* mode which can be lightly unstable.

When cornering symmetrical motions get mixed up with anti-symmetrical motions and vice versa. The most important cornering modes of motion (at a stationary roll angle of .8 rad) are the "*cornering weave*" (unstable) and the "*wheel patter*" (combined wobble and front hop; unstable in some cases).

The effects of various model features on the dynamic behaviour have been traced. The sensitiveness of the model to variations of various model parameters has been determined.

SAMENVATTING

Van een motorfiets met een niet-regelende berijder is een fysisch model gemaakt. Het gedrag van dit model is wiskundig beschreven.

De wiskundige beschrijving staat toe het gedrag van het fysische model bij grote waarden van de gemiddelde rolhoek te berekenen. De gemiddelde rolhoek van een motorfiets heeft een grote waarde in scherpe en/of snel bereden bochten.

Het model kent 11 graden van vrijheid van beweging; de wiskundige beschrijving is niet-lineair. Eén van de vrijheidsgraden wordt beschreven door de voorwaartse snelheid; deze snelheid is echter verder steeds als konstant beschouwd. Het gedrag van het systeem wordt beschreven ten opzichte van een meebewegend assenstelsel. De plaats en stand met betrekking tot aan dit assenstelsel toegepaste verplaatsingen en verdraaiingen zijn niet relevant. Hierdoor vermindert de orde van het systeem met twee.

De invloed van stationaire aerodynamische krachten is in het model opgenomen.

Het gedrag van de banden wordt beschreven door niet-lineaire algebraïsche vergelijkingen en eerste-orde differentiaalvergelijkingen. De aanwezigheid van deze differentiaalvergelijkingen doet de orde van het systeem met tien toenemen. De orde van het totale systeem is 28.

De beschrijving van het niet-stationaire gedrag van het systeem is gelineariseerd rond een werkpunt, dat de stationaire toestand bij rechtruitrijden of in een bocht voorstelt. Dit werkpunt wordt bepaald door de waarde van de gekozen ingangsparameters (stationaire rolhoek en voorwaartse snelheid) en het niet-lineaire model dat de stationaire toestand beschrijft.

Het stationaire gedrag van het model is berekend, gepresenteerd en besproken. Hetzelfde is op een meer intensieve wijze gedaan voor het niet-stationaire gedrag. Dit niet-stationaire gedrag bij rechtruitrijden en in de bocht is voor een reeks van werkpunten beschouwd met behulp van een eigenwaarden/eigenvektoren-analyse. Om de eigenvektor-informatie toegankelijk te maken is een geschikte grafische presentatiemethode ontwikkeld en toegepast. Deze methode bestaat hierin, dat met behulp van computer graphics snel opeenvolgend in de tijd beelden worden gegenereerd van een draadfiguur, voorstellende een tweewieler met berijder, waarbij de stand en de plaats in de ruimte van elk van de delen van deze draadfiguur als functie van de tijd bepaald worden door een specifieke eigentrillingsvorm van het fysische model van de motorfiets. In de film "Vibrational Modes of Single-Track Vehicles" worden diverse eigentrillingsvormen op deze manier getoond.

Bij rechtruitrijden worden symmetrische en anti-symmetrische eigentrillingsvormen onderscheiden. De symmetrische zijn: *pitch* (dompen), *bounce* (stampen), *front hop* (stuiteren van het voorwiel) en *rear hop* (stuiteren van het achterwiel). De belangrijkste anti-symmetrische zijn: *weave* (slingerteren van de hele motorfiets, mogelijk instabiel bij hoge snelheid), *wobble* (stuurtrilling, vaak licht gedempt of instabiel bij matige snelheid), *shake* (slingerteren van voornamelijk het bovenlichaam van de berijder), *twist* (torderen van het frame) en *rear wobble* (wobble-achtig verschijnsel bij het hoofdframe). Van de monotone bewegingsvormen van het ongeregelde systeem is de -veelal instabiele- *capsize* (uit de koers raken en omvallen) de belangrijkste.

In de bocht treedt vermenging van symmetrische met anti-symmetrische bewegingen op v.v. De belangrijkste trillingsvormen in de bocht (bij een stationaire rolhoek van .8 rad) zijn "*cornering weave*" (instabiel) en "*wheel patter*" (stuurtrilling gekombineerd met stuiteren van het voorwiel; mogelijk instabiel bij bepaalde snelheden).

Er is nagegaan wat de invloed van diverse aspekten van de modellering op de resultaten is. Daarnaast is de gevoeligheid van de resultaten voor een aantal modelparameters bepaald.

LIST OF SYMBOLS

a (without indices)	: half contact length, cf. Fig. 21
\bar{a}	: position vector, cf. Figs. 29 and B3
\bar{b}	: id.
\bar{d}	: id.
\bar{e}	: unit vector
f	: function
\bar{F}	: position vector, cf. Figs. 29 and B3
g	: gravitational acceleration
\bar{g}	: position vector concerning point masses, cf. Figs. 29 and B3
h	: height / increment
\bar{h}	: position vector
\bar{j}	: normal to the wheel centre plane
k [-]	: dimensionless damping coefficient / integer value
\bar{k}	: position vector
l	: length in short notation, cf. Appendix D
m	: mass / number of dynamic equations
n	: stepnumber in iteration process / order of the set of dynamic equations
p	: number of stationary equations
p (indices α, γ) [rad $^{-1}$]	: coefficient in the tyre model, e.g. cf. Eq. (7)
p (indices D,L) [m]	: co-ordinate specifying the points of application of the aerodynamic forces
\bar{p}	: vector indicating the position of the specified point in (C_2, x_2, y_2, z_2)
q	: generalized co-ordinate (general)
q (indices α, γ) [rad $^{-1}$]	: coefficient in the tyre model, e.g. cf. Eq. (14)
r	: radius / yaw rate ($=\dot{\psi}$)
\bar{r}	: radius vector
\dot{s}	: slip speed vector
t (without indices)	: mechanical trail / time
t_p	: pneumatical trail
u	: longitudinal velocity* { with respect to
v	: lateral velocity } (C_2, x_2, y_2, z_2)
x	: variable quantity / x-axis*
\bar{x}	: vector of state variables in the set of 2 nd -order differential equations / with subscript s id. of stationary equations
y	: y-axis*

* all systems of axes are right-handed and orthogonal

z	: z-axis*
\bar{z}	: vector of state variables in the set of 1 st -order differential equations
A (without index)	: frontal area
A (with indices 1,2)	: wheel centre
\bar{A}^ζ	: transformation matrix rotating over ζ
\bar{A}	: matrix of coefficients in the set of 1 st -order differential equations
B	: point of the main frame, in the nominal situation coinciding with A_2
\bar{B}	: matrix of coefficients in the set of 1 st -order differential equations
C	: constant
C (with indices xz, zx)	: product of inertia (with minus sign in definition)
C (with indices D, L)	: aerodynamic coefficient
C (with indices M, F)	: coefficient in the tyre model
C (with indices 1,2)	: contact centre (defined in Fig. 10)
\bar{C}	: compliance matrix
D	: point defining the position of the reversed pendulum representing the upper part of the rider body / point at which the steer axis and the ground plane intersect / dissipation function
\bar{E}	: system matrix
F	: force
G	: mass centre
\bar{I}	: unity matrix
J	: moment of inertia
\bar{J}	: inertia matrix
K	: point / damping coefficient [Nsm^{-1}] or [$Nmsrad^{-1}$]
\bar{K}	: damping matrix
M	: mass matrix
P	: point at which the stiff wheel-torus touches the ground
Q	: generalized forces and moments
R	: radius of path
S	: point denoting the eye position of the spectator
T	: target point of view / kinetic energy
U	: potential energy
V	: running speed, cf. Fig. 13
\bar{V}	: absolute velocity vector
W	: work

\dot{x}	: X-component in (O,X,Y,Z) of the absolute velocity of C_2
\dot{y}	: Y-component in (O,X,Y,Z) of the absolute velocity of C_2
\bar{z}	: eigenvector
α	: tyre side slip angle
β	: angle describing the torsion due to frame compliance, cf. Appendix A
γ	: camber angle
δ	: steer angle
ε	: steering axis inclination or rake angle, cf. Fig. 12
ζ	: angle
η	: load dependency coefficient in the tyre model
θ	: pitch angle
λ	: spring compression / eigenvalue
ρ	: turn slip ($= \dot{\psi} / v$)
σ	: tyre relaxation length
ϕ	: roll angle
\dot{x}	: variable part of Ω
ψ	: yaw angle
$\bar{\omega}$: angular velocity vector
Ω	: angular velocity of the wheel about the wheel spindle (relative to the $(A_1, x_{A_1}, y_{A_1}, z_{A_1})$ -system of axes)
\circ	: nominal situation
1	: front sprung part; part 1s excluded / front assembly
1a	: front axle assembly
1s	: front sprung twisting part
1u	: front unsprung part
1w	: front wheel
2	: main frame assembly
2a	: rear axle assembly
2u	: rear unsprung part
2w	: rear wheel
3	: upper part of the rider body

subscripts

e	: effective
---	-------------

g	: due to gravity
i	: integer value
p	: pneumatic (-trail: t_p)
r	: radial (F) / relative to (c_2, x_2, y_2, z_2) ($\bar{\omega}$) / concerning the rider (C, ϕ)
s	: concerning the stationary situation / concerning a suspension spring (λ)
spect	: concerning the spectator
t	: concerning the tyre
tc	: concerning the tyre crown
u	: unsprung
w	: concerning the wheel
x	: component in x-direction / concerning the x-equation
y	: component in y-direction / concerning the y-equation
z	: component in z-direction
D	: drag
DUM	: dummy quantity (with no relevant influence on the results)
F	: concerning a force
GYR	: contribution due to gyroscopic effects arising from the compliance of the wheel
L	: lift
M	: concerning a moment
RE	: real part of the complex quantity
IM	: imaginary part of the complex quantity
α	: due to side slip (F,M) / 1 st index: concerning a contribution due to side slip / 2 nd index: coefficient describing the influence of side slip
β	: concerning the frame torsion motion
γ	: due to camber (F,M) / 1 st index: concerning a contribution due to camber / 2 nd index: coefficient describing the influence of camber
δ	: concerning the steer motion
ρ	: due to turn slip
ψ	: concerning the ψ -equation

o	: concerning the nominal situation
1	: concerning the front sprung part; part 1s excluded / concerning the front assembly / front / in x-direction (\bar{e}_1)
1a	: concerning the front axle assembly
1s	: concerning the front sprung twisting part
1u	: concerning the front unsprung part
1w	: concerning the front wheel
2	: concerning the main frame assembly / rear / in y-direction (\bar{e}_2)
2a	: concerning the rear axle assembly
2u	: concerning the rear unsprung part
2w	: concerning the rear wheel
3	: concerning the upper part of the rider body / in z-direction (\bar{e}_3)

superscripts

C2,G1u, etc.	: denoting the system of axes (C_2, x_2, y_2, z_2), resp. ($G_{1u}, x_{G1u}, y_{G1u}, z_{G1u}$)
L	: lagging component
NL	: non-lagging component
T	: transposed
.	: time derivative
'	: in the ground plane
-	: vector / matrix / linepiece
~	: variable part (concerning the non-stationary behaviour)
*	: material point

prescripts

d	: differential
δ	: virtual increment
∂	: partial differential
Δ	: finite variation

postscripts

| : under the condition

notations (examples)

\underline{p}_{G1a}^{C2}

: the vector \underline{p} denotes a position relative to (C_2, x_2, y_2, z_2) ; the subscript $G1a$ defines the point of which the position is being specified, in this case G_{1a} ; the superscript $C2$ specifies the system of axes, relative to which the components have been taken. If no superscript is explicitly provided, $C2$ is default.

Σ_δ

: summation over all parts rotating about the steering axis relative to the main frame assembly

Σ_5

: summation over 5 masses, specified in Appendix D

miscellaneous

c.g.

: centre of gravity

1.1 Previous work on motorcycle dynamics

Two aspects qualifying the behaviour of a motorcycle are handling and dynamic stability. This study focuses on the latter.

It is not known when the first serious problems concerning the dynamic stability of motorcycles occurred. In the early stages of motorcycle development (at the end of the 19th century) design in this respect was poor but at the same time speeds were relatively low. At present, however, dynamic instability is likely to be the cause of some severe accidents [9].

The first applications of mathematics to the behaviour of single track vehicles date back to about 1900 and were done by McGaw [7] (1898), Whipple [48] (1899) and several others (see [11] for a more complete bibliography). However, these studies all lacked several fundamental aspects of the dynamic system at hand. The mathematical approach of motorcycle free-control* dynamics that is generally recognized to be the archetype of the more elaborate models of recent time is that of Sharp [31] (1971)**. This model has since been used in several studies: e.g. to investigate the influence of accessories [18] and as a vehicle basis to investigate rider control [5], [46]; Schwarz even had the Sharp model running backwards [29].

However, the Sharp model still lacked one crucial aspect, resulting in a poor prediction of the properties of one specific oscillatory mode of motion, the so-called 'wobble mode'. The discrepancy between reality and model results being obvious, several attempts were made to get the model behaviour to be more realistic. A large effort was put into detailing the description of the tyre behaviour [5], [30], [36]. Unfortunately, the main model deficiency remained. In practice, obviously also frame compliance was important with respect to dynamic stability. Sharp [32] first investigated a lumped elasticity near the rear wheel which appeared to be not significant with respect to the theoretically obtained results. Koch [10] extended his model to include parameter excitation by wheel/tyre non-uniformities and attempted to explain the wobble properties in this way. An extension of the original

* free-control: without controlling actions of the rider involved.

** at the time this detailed mathematical approach was already common in the fields of aircraft, railway and automobile dynamics.

theory, however, appeared to be sufficient to cure the discrepancy. The detail required to be included turned out to be the frame torsional compliance between the front wheel and the engine block, as was found by Sharp and Alstead [38] and Spierings [39] at about the same time.*

Motorcycles in general are more prone to exhibit dynamic instability when cornering [9]. Sharp suggested research in this field [34]. Taylor and Adiele [40] calculated the root-loci of a cornering motorcycle, omitting suspension dynamics. Pacejka and Koenen did include full in-plane dynamics and presented the root-loci in [13] and [20]. Following Sharp and Alstead [38] and Spierings [39] they also added frame torsional compliance; furthermore simple lateral rider dynamics and elaborate tyre moment descriptions have been included in their extended model [14].

In-plane rider dynamics have been regarded by Taylor and Black [41] in a vehicle model describing in-plane dynamics only. The active behaviour of the rider has been the subject of various studies (e.g. [46], [5]).

The development of the theory describing the behaviour of single track vehicles has been stimulated by experimental research, reported on by many investigators. Experiments concerned e.g. the transient motion when entering a curve [6], the steady cornering situation [2], [50] and oscillations both when running straight ahead [26] and when cornering [47].

1.2 Delimitation of the problem area

Motorcycles in general are prone to exhibit various distinct oscillatory modes of motion. In the practice of motorcycling one may encounter terms as "wobble" (or "flutter" or "shimmy") and "weave" (or "speed wobble") denoting periodic motions when running straight ahead, and "wheel patter" and "cornering weave" denoting comparable phenomena occurring when cornering. The nature of these oscillatory motions varies from harmless to extremely dangerous.

The research at hand is aimed at studying the oscillatory behaviour of a motorcycle/rider system both when running straight ahead and when cornering. The model comprises a simplified version of the real system, as has been indicated by Fig. 1: the environment has been idealized, non-stationary aerodynamics has been omitted, and of the rider behaviour the passive part only has been included, cf. Fig. 2.

* structurally, Koch did include this necessary feature in his model. However, the parameter values employed by Koch did not provide realistic results.

1.3 Objectives and approach

The objective of this work is to achieve more theoretical knowledge on motorcycle dynamics especially regarding cornering situations. This knowledge comprises a detailed description of typical oscillatory modes of motion and the influence of some parameters and model features on the dynamic behaviour of the chosen physical model.

This objective has been approached by developing and employing a mathematical representation of the physical model. The dynamic behaviour has been described in terms of eigenvalues and eigenvectors. The mode shapes have been studied with the aid of computer graphics, employing a visual vehicle structure.

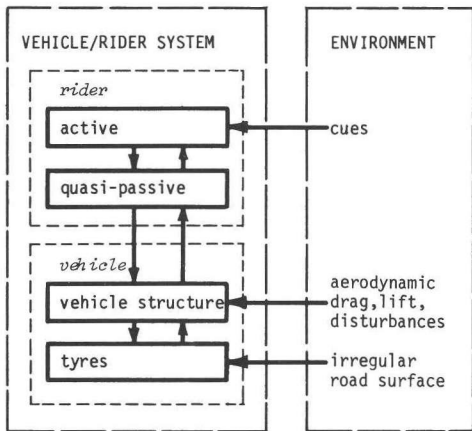


Fig. 1 full vehicle/rider/
environment system

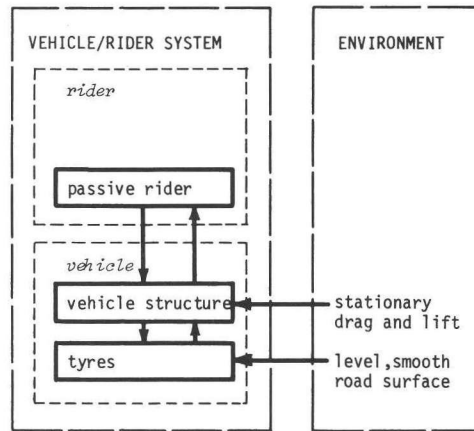


Fig. 2 vehicle/rider/environment
system, as modelled

2.1 Introduction

The mathematical model to be discussed describes the behaviour of a physical structure representing a motorcycle with a passive rider. The full non-linear equations of motion have been linearized about a state of equilibrium which is generally in a curve.

As a basis for the discussion of the mathematical model three main situations of the vehicle have been introduced:

- I the nominal situation;
- II the stationary situation;
- III the non-stationary situation.

The nominal situation has been defined as the situation of the vehicle loaded with a 50-percentile male rider in touring position (cf. [15]) at zero forward speed and zero roll angle. At this situation the vehicle geometry has been defined and all motion and geometrical variables have been set equal to zero. The nominal situation has been indicated by the subscript o.

The stationary situation or steady state has been defined as the equilibrium condition at a constant, non-zero forward speed. In this situation the vehicle may be cornering. The variables provided with subscript s describe the stationary situation. Some of these variables have been assumed to be very small, the remaining to be not necessarily small.

The non-stationary situation has been defined as the situation comprising infinitesimal perturbations from the stationary situation. Therefore all non-stationary variables have been assumed to be small. The non-stationary situation has been referred to by superscript ~.

Thus, in principle, the full value of a variable quantity x_i is composed as follows:

$$x_i = x_{is} + \tilde{x}_i \quad (1)$$

The nominal values x_{io} have been included in the stationary value x_{is} . For all motion variables the nominal contribution (vehicle at rest) equals to zero. The nominal situation has been accounted for in the description of the vehicle structure which serves as a starting-point for the calculations. The stationary situation has been described by a set of non-linear algebraic equations. Linear differential equations determine the non-stationary situation.

2.2 Aspects and consequences of cornering

When regarding the dynamic behaviour of a vehicle it is convenient to differentiate between two categories of interest (cf. Fig. 3):

- I symmetrical dynamics, or the sum total of longitudinal dynamics and suspension dynamics;
- II anti-symmetrical dynamics, or lateral dynamics.

The first category concerns motions of the vehicle or parts of it due to which the non-material plane of symmetry in question does not move (as is the case with spring deflections and bounce and pitch motions); the second category concerns motions due to which the plane of symmetry in question changes position and/or orientation (such as lateral translation, yaw, roll and steer motions).

In many cases symmetrical and anti-symmetrical dynamics can be regarded isolated from each other and still give an acceptable approximation of the phenomena in question. This holds for instance for motorcycle dynamics when small deviations from the running straight ahead condition are regarded, cf. Fig. 4 (examples from literature are [35] and [41] in which the symmetrical dynamics only, and [34] in which the anti-symmetrical dynamics only has been dealt with). In this case symmetrical and anti-symmetrical dynamics can be considered as orthogonal.

In curves, however, this orthogonality no longer holds true due to the fact that, when cornering, the plane of symmetry of the vehicle is not perpendicular to the road plane, cf. Fig. 5. As a result symmetrical and anti-symmetrical dynamics get mixed up.

Thus when investigating the dynamic behaviour of a cornering motorcycle symmetrical and anti-symmetrical dynamics may not be regarded isolated from each other. A number of the effects, causing cornering dynamics to differ from running straight ahead dynamics will be discussed in the sequel.

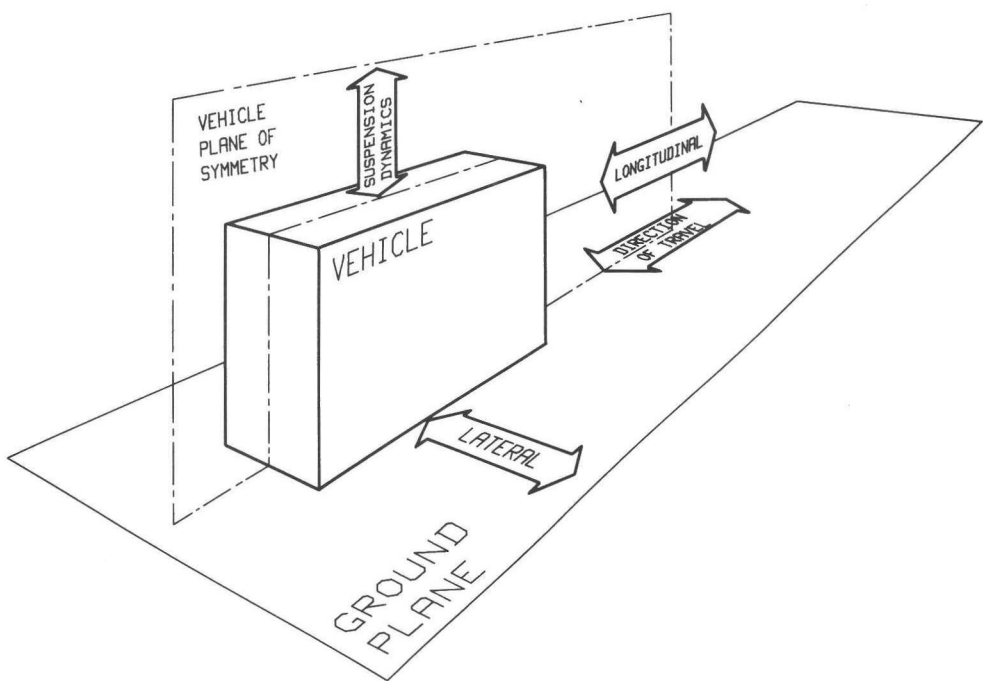


Fig. 3 symmetrical dynamics (longitudinal dynamics plus suspension dynamics) and anti-symmetrical dynamics (lateral dynamics). Note that longitudinal and suspension dynamics per definition denote motions in the vehicle plane of symmetry.

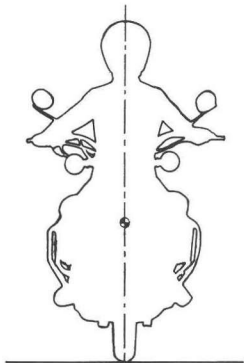


Fig. 4 running straight ahead

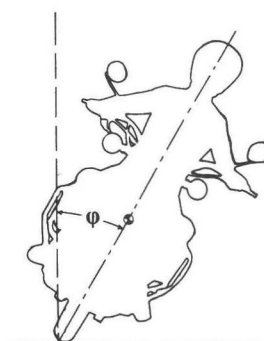


Fig. 5 cornering

geometrical coupling

If the vehicle plane of symmetry is not perpendicular to the ground plane, interaction between the symmetrical and the anti-symmetrical motion occurs due to geometrical properties of the system in question. For instance, at a non-zero roll angle the steer angle cannot be varied without affecting the symmetrical situation, due to the mechanical trail, cf. Fig. 6 and Fig. 7.

tyre coupling effects

Fluctuations of the values of symmetrical variables cause changes of the normal wheel loads. This causes the tyre side forces, which are present in the cornering situation, to vary, since the tyre side forces depend on the normal load (cf. Fig. 8).

tyre behaviour parameters

The dynamic behaviour of a cambered wheel differs from that of a wheel at zero inclination. At increasing camber angle both the camber and the side slip stiffness decrease.

geometrical parameters

In the event of cornering, extra spring compressions arise due to the in-plane component of the centripetal acceleration. In consequence the geometrical situation of the vehicle resulting from steady cornering conditions differs from the geometry when running straight ahead. In the case of non-linear suspension stiffness characteristics the extra stationary compressions in addition cause suspension parameters to change*.

The actual mechanical trail of the front wheel (cf. Fig. 6), the nominal value of which being an important design parameter, is subjected to significant changes if both the roll and the steer angle differ from zero. This matter will be dealt with in more detail in the discussion of the steady state behaviour.

inertia parameters

Lateral velocity and yaw rate, determining the path of the vehicle, have been defined in the road plane and about an axis perpendicular to the road plane respectively, cf. Fig. 9. Relative to this orientation the inertia properties of the vehicle vary with the roll angle.

other effects

Besides the effects mentioned above many more cornering effects occur. As far

* note that, when running straight ahead, at high speed also significant changes in the compression of the suspension springs occur due to aerodynamic forces.

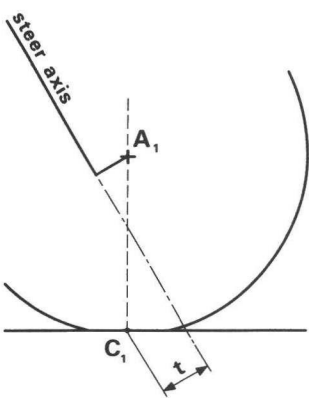


Fig. 6 mechanical trail t

rear view

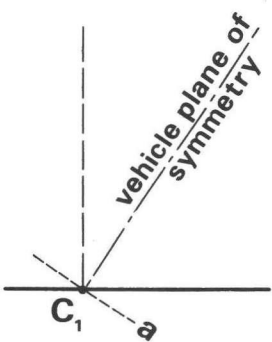


Fig. 7 geometrical coupling due to the mechanical trail: a is the tangent to the course of C_1 if the road level were adjusted to suit the new situation (main frame kept still)

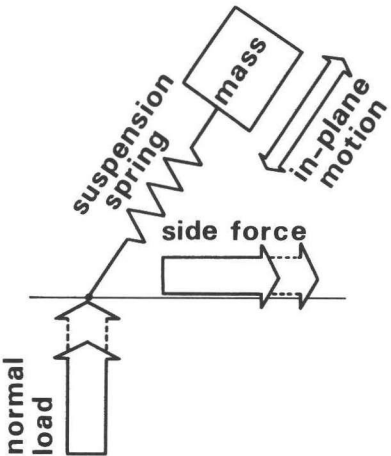


Fig. 8 a tyre coupling effect: an in-plane acceleration of the sprung mass causes the tyre normal load to vary, which in turn causes a variation of the tyre side force.

as these have been taken into account in the modelling, they can be traced from the terms of the full equations, as they have been presented in the Appendices E and F.

2.3 Co-ordinates / physical structure of the vehicle model

An earth-fixed system of axes (O, X, Y, Z) and a vehicle-based moving along system of axes (o, x, y, z) have been assumed as shown in Fig. 9. Both systems are right-handed orthogonal frames of reference. The origin of the moving along system of axes at any time coincides with the rear wheel contact centre C_2 ; furthermore the orientation is such that $(o, x, y, z) = (C_2, x_2, y_2, z_2)$. The contact centre of a wheel has been defined as the point of intersection of the wheel centre plane, the ground plane and a plane containing the wheel spin axis and the normal to the ground plane. The wheel centre plane has been defined as the plane perpendicular to the wheel axle centre line at the wheel centre, cf. Fig. 10. In the unloaded situation, the wheel centre plane coincides with the equatorial plane of symmetry of the wheel. The orientation of the moving along system of axes (C_2, x_2, y_2, z_2) is such that the x - and y -axes lie in the ground plane, the x -axis coinciding with the line of intersection of the rear wheel centre plane and the ground plane, the positive part pointing forward (relative to the direction of travel); the z -axis being directed perpendicular to the ground plane, pointing downwards in positive direction.

The rear wheel contact centre C_2 has been allowed to move in the ground plane. The component u of the velocity of C_2 along the x -axis will be assumed to be constant. The moving along system of axes has been allowed to rotate about the z -axis (yaw motion). The rear wheel centre plane has been allowed to rotate about the x -axis relative to the moving along system of axes (camber motion of the wheel or roll motion of the vehicle).

Concerning the vehicle plus rider itself, in this section a slightly simplified version of the full system will be regarded.* This reduced version is composed of seven rigid parts, interconnected by kinematic restraints (cf. Fig. 11):

- | | | | | |
|------|--------------------------------------|---|----------------------|------|
| (2w) | the rear wheel; | } | together forming the | (2u) |
| (2a) | the rear axle assembly;** | | rear unsprung part | |
| (2) | the main frame assembly;*** *** | } | together forming the | |
| (3) | the upper part of the rider body;*** | | rear sprung part | |
| (1) | the front sprung part; | } | together forming the | (1u) |
| (1a) | the front axle assembly; | | | |
| (1w) | the front wheel. | | | |

* the full system has been described in appendix B.

** the pivoting rear fork mass has been split up into a front and a rear part, assigned to and incorporated in the parts (2a) and (2) respectively.

*** the main frame assembly includes the lower part of the rider body.

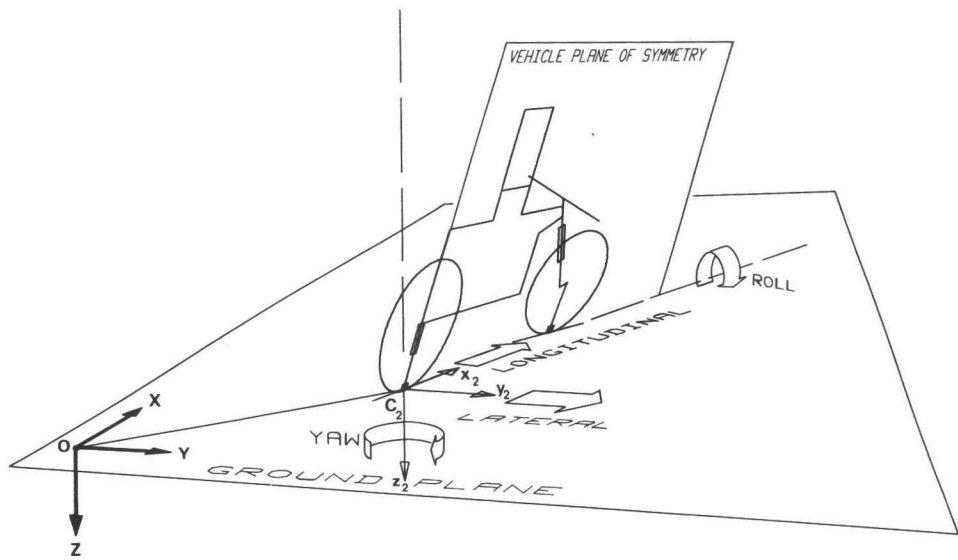


Fig. 9 earth-fixed and vehicle-fixed systems of axes; main vehicle motions: roll, yaw, longitudinal and lateral translation.

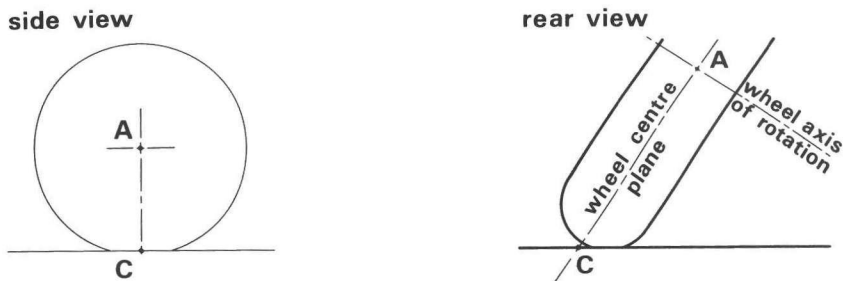


Fig. 10 definition of the contact centre C as the point of intersection of
 ● the ground plane;
 ● the wheel centre plane (defined in Sec. 2.3);
 ● a plane through the wheel axis of rotation and perpendicular to the ground plane.

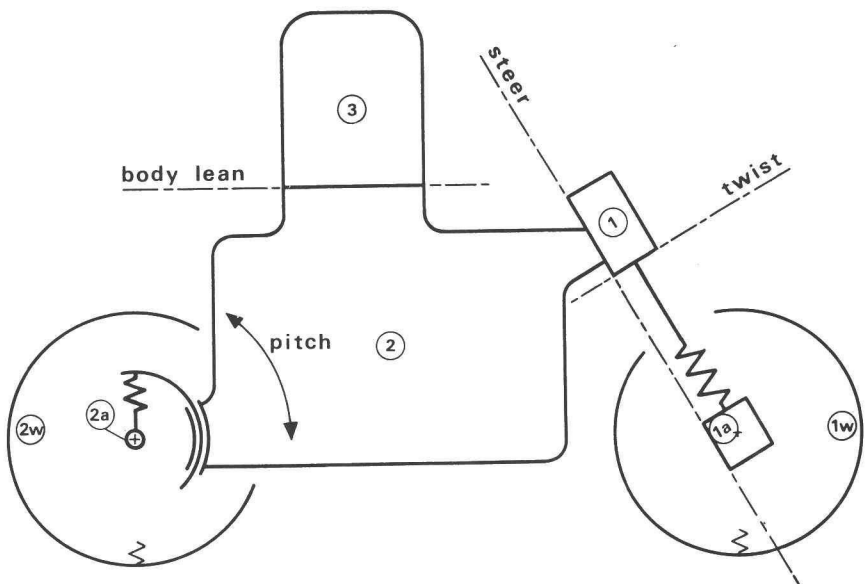


Fig. 11 the various parts composing the vehicle*

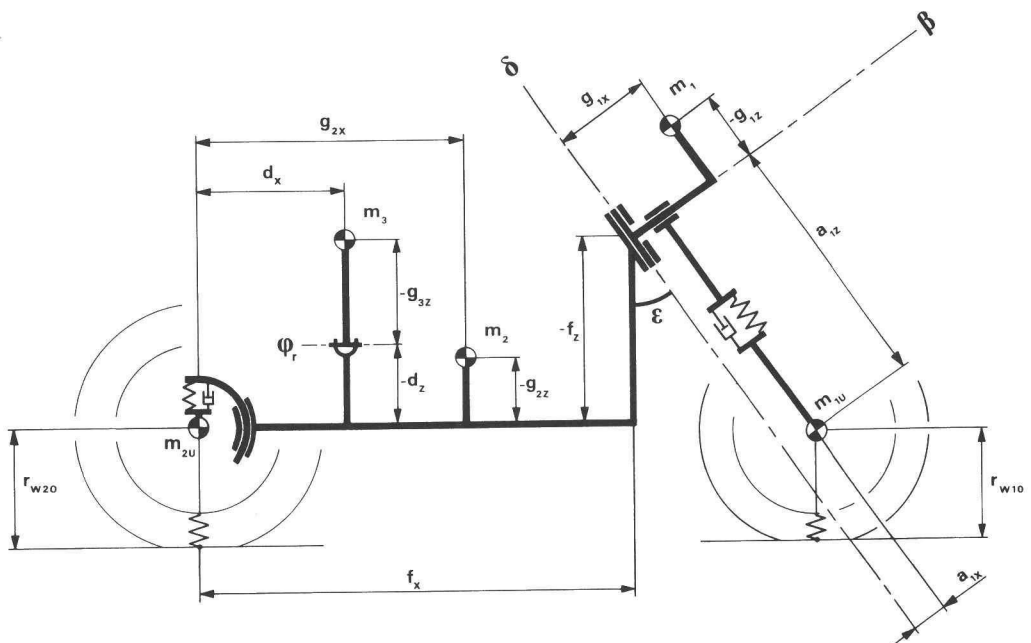


Fig. 12 geometry of the model*, cf. the vector structure, presented in Fig. 29

* slightly simplified version; the geometry of the full model has been described in appendix B.

The qualification 'sprung' indicates that the parts in question are directly or indirectly suspended by the suspension springs; the qualification 'unsprung' indicates that the parts in question are functionally between the suspension system and the ground plane.

All parts mentioned above have been assumed to be infinitely stiff. The most important elastic property of the real frame structure has been accounted for by the 'twist' degree of freedom, in which the distributed compliance of the structure has been lumped, as has been described in Appendix A. The lateral and torsional elasticity of wheels plus tyres has been accounted for in the tyre model; as far as the vehicle structure is concerned of the wheels only the wheel centre planes are relevant.

With respect to the moving along system of axes the rear unsprung mass ②u has been allowed to camber and to translate due to the radial tyre spring compression. Furthermore, the rear wheel has been allowed to rotate about its axle. The point of the main frame assembly ② which in the nominal condition coincides with the rear wheel centre A_2 , has been allowed to translate along a line coinciding with the line through A_2 and C_2 , thus compressing or expanding the rear suspension spring/damper system; the main frame assembly ② has been allowed to rotate about an axis through this point and perpendicular to the vehicle plane of symmetry (pitch motion). The upper part of the rider body ③ has been allowed to rotate relative to ② about an axis fixed to body ② parallel to the x-axis in the nominal condition.

At the front end of the rear sprung mass the steer pivot has been located. The parts ①, ①a and ①w together rotate as a whole relative to the whole of the parts ②w, ②a, ② and ③ about the inclined steering axis. The lumped frame compliance allows the whole of the parts ①a and ①w to rotate about the twist axis relative to the remainder of the vehicle. This front unsprung part has also been allowed to perform a translatory motion which is parallel to the steering axis in the nominal situation and relative to the remainder of the vehicle, thus compressing or expanding the front suspension spring/damper system. Finally the front wheel ①w has been allowed to rotate about its spindle.

The angular momentum due to rotation of the crankshaft, flywheel etc. has not been taken into account if the crankshaft rotates about a longitudinal axis, which is the case with the specific motorcycle considered in this study.

The geometry of the vehicle, expressed in the quantities to be used in the mathematical model, has been depicted in Fig. 12.

2.4 Anti-symmetrical tyre behaviour

2.4.1 general

Depending on its position, orientation and motion relative to its supporting surface a pneumatic tyre will generate forces distributed over the contact patch. To be able to define the resulting forces and moments unambiguously the contact centre C has been introduced (cf. Sec. 2.3). All resulting tyre forces and moments have been assumed to act on the wheel at the contact centre.

The variables, describing the position, orientation and motion of the wheel centre plane are (cf. Fig. 13):

v : the running speed, which is the component parallel to the ground plane of the velocity of the wheel centre; in view of the fact that the slip angle, the pitch angle and the steer angle are small, the value of v has been taken equal to the forward speed u .

Ω : the angular velocity of the wheel about the wheel spindle;

λ_t : the change in radial tyre spring compression (by definition zero in the nominal situation);

α : the side slip angle (the angle between the wheel centre plane and v , measured in a plane parallel to the ground plane);

γ : the camber angle (the roll angle of the wheel centre plane about the line of intersection of this plane with the ground plane);

ρ : the turn slip; $\rho = \dot{\psi}/v$ with ψ denoting the yaw angle of the line of intersection of the wheel centre plane and the ground plane;

and their derivatives. The resulting forces and moments are:

- the longitudinal force F_x , arising due to longitudinal slip;
- the lateral force F_y or side force, originating from lateral slip, camber and turn slip;
- the vertical load, denoted by $(-F_z)$ throughout this study (note that all remaining tyre forces and moments are dependent on the vertical load as will be discussed later on);
- the overturning moment M_x , generated notably when the wheel is cambered and arising as a consequence of the convention that the resulting vertical load $(-F_z)$ acts at the contact centre C; with the correct M_x introduced, the

- resultant vertical load can be shifted from the actual point of application -which is somewhere near the centre of the contact patch- to the contact centre;
- the rolling resistance moment M_y , resulting from the tyre hysteresis properties;
 - the aligning torque M_z , originating from asymmetrical side slip deformations, camber, turn slip and gyroscopic effects due to the rotating and deflecting tyre tread band, and wheel rim and tyre side wall masses.

Let us now assume the road surface to be flat and even and the friction properties of tyre and road to be constant. In that case the tyre forces and moments are fully determined by the variables mentioned above and the tyre properties, cf. Fig. 14. To suit the application as a part of a mathematical model the description of the tyre behaviour can be either in the form of a matrix of measured data or of a set of analytical expressions originating from theory or from experimental data or from a combination of both.

The symmetrical tyre behaviour, resulting in F_x , $-F_r$ (the radial force, directed along \overline{CA} , cf. Fig. 15) will be disregarded in the sequel except for $-F_r$, which is needed in the determination of the vertical load $-F_z$. The vertical load will from here on be regarded as an input variable to the description of the tyre behaviour. The radial force is composed of a part acting in the nominal situation and an increment due to the additional radial tyre spring compression λ_t :

$$-F_r = -F_{ro} + \lambda_t c_t \quad (2)$$

λ_t has been defined for the wheel being regarded as an infinitely thin disc. For a more accurate representation, the influence of camber upon F_r at fixed λ_t may be introduced, thereby accounting for the finite width of the tyre (crown radius), cf. Sec. 2.4.2.

From the force geometry, depicted in Fig. 15 we obtain an expression for the vertical load:

$$-F_z = \frac{-F_r}{\cos\gamma} - F_y \tan\gamma \quad (3)$$

Since $-F_z$ in turn will be employed to obtain F_y , recurrency arises. This may cause the iteration process which is used to obtain the steady state solution to be not well-damped. In Sec. 3.1 will be described how this problem has been avoided.

We now concentrate on the anti-symmetrical tyre behaviour (Fig. 16). The total in- and output quantities are each composed of a stationary (subscript s) and a non-stationary part (superscript ~):

INPUTS

$$\begin{aligned}\alpha &= \alpha_s + \tilde{\alpha} \\ \gamma &= \gamma_s + \tilde{\gamma} \\ \rho &= \rho_s + \tilde{\rho} \\ F_z &= F_{zs} + \tilde{F}_z\end{aligned}$$

OUTPUTS

$$\begin{aligned}F_y &= F_{ys} + \tilde{F}_y \\ M_x &= M_{xs} + \tilde{M}_x \\ M_z &= M_{zs} + \tilde{M}_z\end{aligned}$$

Note that longitudinal dynamics will not be regarded; therefore F_x has not been included in this list.

2.4.2 stationary behaviour

The sources from which the description of the stationary anti-symmetrical tyre behaviour model has been established are measurements conducted by the Vehicle Research Laboratory of the Delft University of Technology, theoretical considerations from [19] and [21] and experimental results presented by Sakai et al. [28].

Below, the origin of the equations describing the stationary anti-symmetrical tyre behaviour will be discussed. The contributions due to side slip, camber and turn slip have been indicated by the subscripts α , γ and ρ respectively. Thus we have:

$$F_{ys} = F_{yas} + F_{y\gamma s} + F_{y\rho s} \quad (4)$$

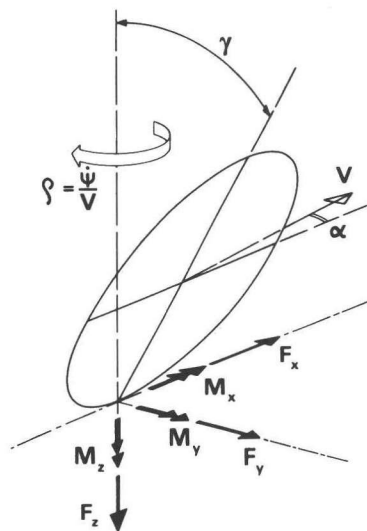
$$M_{zs} = M_{zas} + M_{z\gamma s} + M_{z\rho s} \quad (5)$$

$$M_{xs} = M_{x\gamma s} \quad (6)$$

Note that the stationary overturning moment M_{xs} has been assumed to originate from camber only.

stationary side force

The steady state relations between the slip angle, the camber angle and the resulting side force F_y of a motorcycle tyre are expected to show a course as has been depicted in Fig. 17 (cf. [8]). The curves originating from measurements on the tyres of the motorcycle in question show a less regular course, as has been depicted in Fig. 18 (below left). The oscillations in the $F_{ys}(\alpha_s)$ -



- F_x : longitudinal force
 F_y : side force
 $-F_z$: vertical load
 M_x : overturning moment
 M_y : rolling resistance moment
 M_z : aligning moment
 α : side slip angle
 γ : camber angle
 ρ : turn slip
 V : component of the velocity of the wheel centre parallel to the ground plane
 Ω : angular velocity concerning the wheel rotation about the wheel spindle, cf. Fig. 20

Fig. 13 tyre forces and moments and wheel motion variables

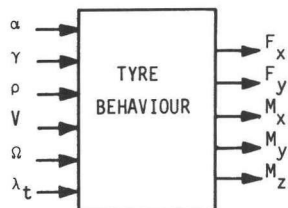


Fig. 14 inputs and outputs of the tyre behaviour model block

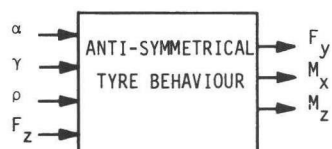


Fig. 16 inputs and outputs of the anti-symmetrical tyre behaviour block as used in this study

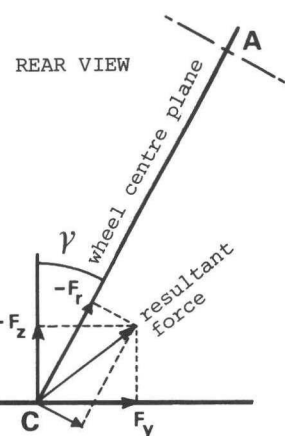


Fig. 15 forces acting on the wheel in a lateral plane

-curves at large camber angles could be due to the specific pattern of studs and ribs of the tread.

In Fig. 18 the linear approximation of the relation side force F_{ys} versus side slip angle α_s at various values of the camber angle γ_s has been indicated. In the small range of α_s , which is usually not exceeded in practice, this relation is acceptable also in quantitative respect for not too large values of γ_s . Qualitatively this approximation seems reasonable also for larger camber angles.

The side slip stiffness $C_{F\alpha} = \partial F_y / \partial \alpha$ at $\alpha = 0$ can be seen to decay at increasing camber angles, cf. Fig. 18 (top right). A linear approximation is employed. We find:

$$F_{yas} \Big|_{F_{zs} = F_{zo}} = \alpha_s (1 - p_{\alpha\gamma} |\gamma_s|) C_{F\alpha 0} \quad (7)$$

with $C_{F\alpha 0}$ being the side slip stiffness $\partial F_y / \partial \alpha$ at the nominal situation and $p_{\alpha\gamma}$ being a constant. From measurements at different vertical loads a linear load dependency has been derived:

$$F_{yas} = \alpha_s (1 - p_{\alpha\gamma} |\gamma_s|) (C_{F\alpha 0} - \eta_\alpha \Delta F_{zs}) \quad (8)$$

with:

$$\Delta F_{zs} = F_{zs} - F_{zo} \quad (9)$$

and η_α being a constant.

The side force versus camber angle relation at zero side slip, extracted from the original measured F_{ys} (α_s, γ_s)-curves appears to be well approximated by a parabola, cf. Fig. 18 (below right). The factor concerning the assumedly linear- load dependency has been derived from experimental data. Thus we obtain:

$$F_{y\gamma s} = \gamma_s (1 - p_{\gamma\gamma} |\gamma_s|) (C_{F\gamma 0} - \eta_\gamma \Delta F_{zs}) \quad (10)$$

Another contribution to the tyre side force, although small, originates from the turn slip $\rho = \dot{\psi}/v$. No data from measurements concerning this phenomenon were available. From theory, however, the following relation has been found to exist for the initial slope $C_{F\rho} = \partial F_y / \partial \rho$ if adhesion is assumed throughout the contact area (α and γ small), cf. [21]:

$$C_{F\alpha} = C_{M\alpha} \quad (11)$$

with $C_{M\alpha} = -\partial M_z / \partial \alpha$ denoting the aligning torque stiffness. Thus the following description has been chosen:

$$F_{y\alpha s} = -\rho_s C_{M\alpha} \quad (12)$$

stationary aligning moment

The aligning moment is also composed of components due to side slip, camber and turn slip respectively.

The aligning torque due to side slip arises from the pneumatic trail due to the asymmetry of the side force distribution along the contact line and has therefore been linked to the side force due to side slip:

$$M_{z\alpha s} = -F_{y\alpha s} \cdot t_p \quad (13)$$

To approximate the highly non-linear character of $M_{z\alpha s}$ (α_s) (cf. [19], [28]) a resulting parabolic relation in α_s has been employed. The pneumatic trail, t_p , is assumed to vary proportionally to the contact length, which in turn varies proportionally to $(F_{zs} / F_{zo})^{1/2}$. We obtain (note the assumed linear relation of $F_{y\alpha s}$ with α_s):

$$M_{z\alpha s} = -F_{y\alpha s} (1 - q_{\alpha\alpha} |\alpha_s|) t_p (F_{zs} / F_{zo})^{1/2} \quad (14)$$

with $q_{\alpha\alpha}$ being a constant.

The equation describing the aligning moment due to camber has partially been established with the aid of the data obtained by Sakai [28]. The load dependency factor in terms of F_{zs} / F_{zo} is made up of five parts. These respective factors are due to the dependence on (cf. [19]):

- contact length $\sim (F_{zs} / F_{zo})^{1/2}$;
- longitudinal deformation \sim contact length $\sim (F_{zs} / F_{zo})^{1/2}$;
- number of active rows of tread elements \sim contact width $\sim (F_{zs} / F_{zo})^{1/2}$;
- anti-symmetrical longitudinal slip \sim contact width $\sim (F_{zs} / F_{zo})^{1/2}$;
- moment arm \sim contact width $\sim (F_{zs} / F_{zo})^{1/2}$.

A parabolic dependence on the camber angle has been employed to suit the data from [28]:

$$M_{z\gamma s} = \gamma_s (1 + q_{\gamma\gamma} |\gamma_s|) C_{M\gamma o} \left(\frac{F_{zs}}{F_{zo}} \right)^{5/2} \quad (15)$$

with a_{YY} and $C_{M\gamma_0}$ being constants.

The mechanism giving rise to the aligning moment due to turn slip is, apart from the input, identical to that producing the aligning moment due to camber. When yawing, longitudinal deformation of tread elements at non-zero distances from the contact centre occurs. The deformation of all tread elements produces a moment, $M_{z\rho}$, counteracting the yaw motion. We obtain:

$$M_{z\rho} = - \rho_s C_{M\rho_0} \left(\frac{F_{zs}}{F_{zo}} \right)^{5/2} \quad (16)$$

The constant $C_{M\rho_0}$ may be obtained directly from dynamic tests or indirectly from static torsional stiffness and aligning moment stiffness measurements (cf. [21]). The turn slip ρ_s remains relatively small. Therefore, a linear relationship has been employed.

stationary overturning moment

The overturning moment is the moment about the line of intersection of the wheel centre plane and the road plane. At the chosen conventions and a non-zero tyre crown radius this moment arises if the camber angle differs from zero, cf. Fig. 19. From the geometry shown in this figure we obtain:

$$M_{xs} = \left(r_{tco} + \frac{F_{zs}}{C_t} \right) F_{zs} \tan \gamma_s \quad (17)$$

with r_{tco} being the tyre crown radius and C_t the radial stiffness of the tyre (note again that F_{zs} is negative!). In this case the tyre has been assumed to be laterally stiff: in expression (17) the contribution arising from the lateral deformation of the tyre due to the side force (cf. [28]) has not been accounted for. This contribution is comparatively small because of the high value of the lateral stiffness of the tyre; moreover, the effective shift of the resulting vertical force is smaller than the lateral deflection of the tyre contact patch, cf. [19].

2.4.3 non-stationary behaviour

Since detailed experimental data concerning the non-stationary anti-symmetrical behaviour of motorcycle tyres are still lacking at this moment, the expressions to be discussed in the sequel have been derived from theory. As far as possible they have been quantified with the aid of data obtained from stationary experiments.

As a basis the taut string theory, which is described in [19], has been

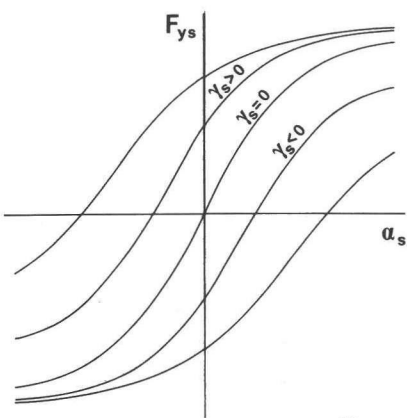


Fig. 17 expected stationary
tyre side force
characteristics
(cf. [8])

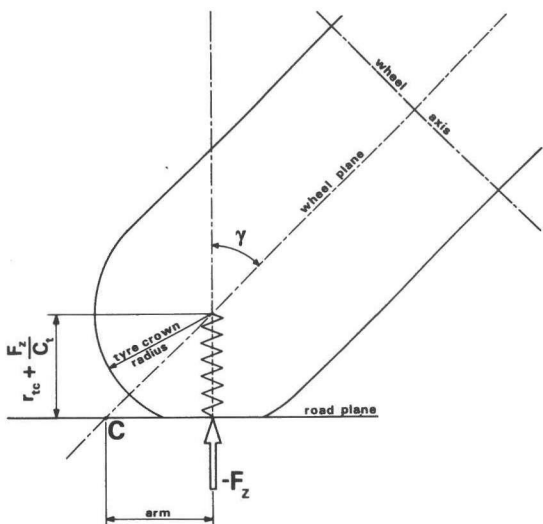


Fig. 19 derivation of the overturning
moment M_x

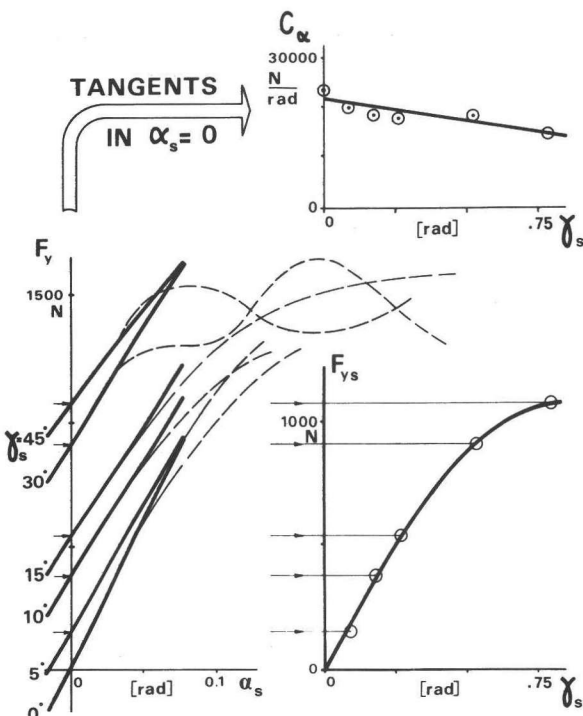


Fig. 18 measured tyre side force data and model representation of
 $C_\alpha(\gamma)$ and $F_y(\gamma) \mid_{\alpha=0}$. The data have been obtained with the
wheel rolling freely at 40 km/h on dry asphalt; $F_z \approx -1200$ N

employed. In its simplest form it describes the forces and moments generated by the deflection of a string, attached to the circumference of a rigid disk by means of an infinite number of lateral springs, cf. Fig. 20. The string touches the ground plane over a finite length. If the rolling disk is subjected to a non-zero side slip angle lateral deflections of the string occur. Figure 21 provides a top view of the situation at a stationary slip angle α_s . If we assume that no sliding of the string relative to the ground plane throughout the contact length occurs ($\mu = \infty$), in this case the contact line is straight.* Non-stationary anti-symmetrical motions of the disk cause this contact line to be curved, cf. Fig. 22. The local slip angle at the leading edge of the contact zone is assumed to govern the non-stationary properties of the tyre behaviour. This approximation is realistic for large wavelengths (with respect to the contact length) and as long as adhesion at the leading edge is retained. Thus we obtain first-order differential equations for $\tilde{F}_{y\alpha}$ and $\tilde{M}_{z\alpha}$ (cf. [19]):

$$\frac{\sigma}{u_s} \frac{d}{dt} \tilde{F}_{y\alpha} + \tilde{F}_{y\alpha} = \Delta F_{yas} \quad (18)$$

$$\frac{\sigma}{u_s} \frac{d}{dt} \tilde{M}_{z\alpha} + \tilde{M}_{z\alpha} = \Delta M_{zas} \quad (19)$$

with σ being the so-called 'relaxation length' of the tyre and the right-hand members being the instantaneous (or steady state) response to variations in input quantities. Division by the longitudinal speed u_s shows that the response is path dependent rather than time dependent.

non-stationary side force

Considering the steady-state expression for F_{yas} , Eq. (8), and the fact that apparently, F_{yas} depends on α_s , γ_s and ΔF_{zs} it is assumed that similarly the non-stationary variations of the side force to side slip will depend on small variations of the side slip angle: $\tilde{\alpha}$, the camber angle: $\tilde{\gamma}$ and the vertical load: $-\tilde{F}_z$. The right-hand member of the differential equation concerning $\tilde{F}_{y\alpha}$ is written in the form of a total differential. We obtain, together with (18):

$$\frac{\sigma}{u_s} \frac{d}{dt} \tilde{F}_{y\alpha} + \tilde{F}_{y\alpha} = \frac{\partial F_{yas}}{\partial \alpha_s} \Big|_s \tilde{\alpha} + \frac{\partial F_{yas}}{\partial \gamma_s} \Big|_s \tilde{\gamma} + \frac{\partial F_{yas}}{\partial F_{zs}} \Big|_s \tilde{F}_z \quad (20)$$

* note that the stationary model exceeds this assumption: it covers partial sliding in the contact zone, cf. Fig. 18.

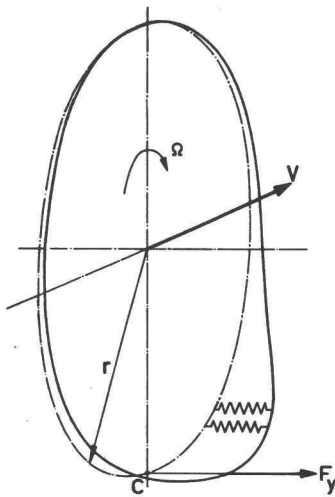


Fig. 20 physical structure of the tyre model: a taut string laterally suspended on the wheel centre plane via an infinite number of springs, only a few of which have been depicted.

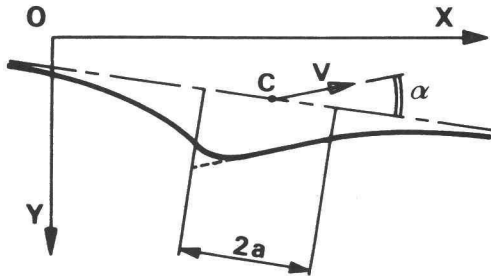


Fig. 21 top view on the deflected string with the wheel rolling at a constant slip angle and a finite friction coefficient (solid line). If no sliding is assumed throughout the contact length in this area the dashed contact line is obtained. The modelled situation includes sliding due to a finite friction coefficient, cf. Fig. 18.

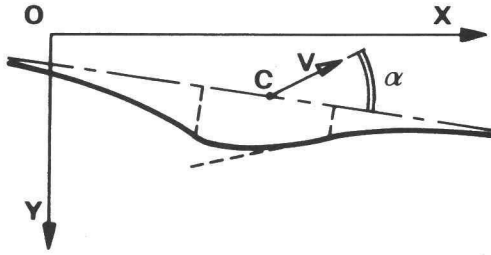


Fig. 22 the same elements as in Fig. 21, now subjected to a non-stationary slip angle. In the situation shown α_s equals zero and adhesion is assumed throughout the contact zone. At large wavelengths (relative to the contact length) the local slip angle at the leading edge of the contact zone approximates the global slip angle α and the string shape in the contact zone approximates that of the stationary case.

The partial differentials $\frac{\partial F}{\partial \gamma_s}$ / $\frac{\partial \alpha_s}{\partial \gamma_s}$ etc. can be derived from the steady state equation (8). The qualification $|_s$ denotes the substitution of the actual steady-state condition in the expression at hand (the partial differentials mentioned above are functions of the steady state variables).

The non-stationary side force due to camber is composed of a lagging and a non-lagging part, due to different camber force generating mechanisms, as assumed by Rotta [27]: a mechanism involving a lateral displacement of the equatorial line (the string in the string model) which lags the camber angle input, and the lateral component of the tyre radial force which responds instantaneously. Segel and Wilson [30] confirmed the assumption of different camber force generating mechanisms experimentally. According to their findings about 80% of \tilde{F}_{yy} lags the input, and the remaining 20% responds instantaneously. The right-hand member of the equation for the camber force is a function of small variations of the camber angle and the vertical load only. We obtain:

$$\frac{\sigma_{FyY}}{u_s} \dot{\tilde{F}}_{yy}^L + \tilde{F}_{yy}^L = \xi^L \left(\frac{\partial F_{yyS}}{\partial \gamma_s} \Big|_s \tilde{\gamma} + \frac{\partial F_{yyS}}{\partial F_{zs}} \Big|_s \tilde{F}_z \right) \quad (21)$$

$$\tilde{F}_{yy}^{NL} = \left(1 - \xi^L \right) \left(\frac{\partial F_{yyS}}{\partial \gamma_s} \Big|_s \tilde{\gamma} + \frac{\partial F_{yyS}}{\partial F_{zs}} \Big|_s \tilde{F}_z \right) \quad (22)$$

$$\tilde{F}_{yy} = \tilde{F}_{yy}^L + \tilde{F}_{yy}^{NL} \quad (23)$$

with L denoting the lagging, and NL denoting the non-lagging component. From measurements the coefficient ξ^L is expected to have a value of about 0.8. The relaxation length associated with camber, σ_{FyY} , is about twice that associated with side slip, $\sigma_{Fy\alpha}$ (data from [30]).

The minor contribution to F_y connected with turn slip is a function of small variations of the turn slip, the camber angle and the vertical load. We assume $\tilde{F}_{y\beta}$ to lag the input:

$$\frac{\sigma_{Fy\beta}}{u_s} \dot{\tilde{F}}_{y\beta} + \tilde{F}_{y\beta} = \frac{\partial F_{y\beta S}}{\partial \beta_s} \Big|_s \tilde{\beta} + \frac{\partial F_{y\beta S}}{\partial \gamma_s} \Big|_s \tilde{\gamma} + \frac{\partial F_{y\beta S}}{\partial F_{zs}} \Big|_s \tilde{F}_z \quad (24)$$

Concerning $\sigma_{Fy\beta}$ the same mechanism applies as in the case of side slip, so that:

$$\sigma_{Fy\beta} = \sigma_{Fy\alpha} \quad (25)$$

Furthermore, using the quantification of [30], for not too high frequencies it seems justified to integrate the equations (21) and (22) into one equation, with:

$$\xi^L = 1 \quad (26)$$

and, the relaxation length being assumed to vary proportionally to the contact length:

$$\sigma_{Fy\gamma} = \sigma_{Fya} = \sigma_{Fy} = \sigma_{Fyo} \left(\frac{F_{zs}}{F_{zo}} \right)^{\frac{1}{2}} \quad (27)$$

It is now obvious to integrate all four components of \dot{F}_y , described by the equations (20), (21), (22) and (24), into one differential equation:

$$\frac{\sigma_{Fy}}{u_s} \dot{F}_y + \tilde{F}_y = \frac{\partial F_{ys}}{\partial \alpha_s} \Bigg|_s \tilde{\alpha} + \frac{\partial F_{ys}}{\partial \gamma_s} \Bigg|_s \tilde{\gamma} + \frac{\partial F_{ys}}{\partial \rho_s} \Bigg|_s \tilde{\rho} + \frac{\partial F_{ys}}{\partial F_{zs}} \Bigg|_s \tilde{F}_z \quad (28)$$

non-stationary aligning torque

Likewise, the non-stationary aligning torque due to side slip depends on small variations of the side slip angle, the camber angle and the vertical load. The taut string model governs the response. Similarly to Eq. (20) we have:

$$\frac{\sigma_{Mza}}{u_s} \dot{\tilde{M}}_{za} + \tilde{M}_{za} = \frac{\partial M_{zas}}{\partial \alpha_s} \Bigg|_s \tilde{\alpha} + \frac{\partial M_{zas}}{\partial \gamma_s} \Bigg|_s \tilde{\gamma} + \frac{\partial M_{zas}}{\partial F_{zs}} \Bigg|_s \tilde{F}_z \quad (29)$$

with:

$$\sigma_{Mza} = \sigma_{Fya} \quad (30)$$

The increment of the aligning moment due to camber depends on small variations of the camber angle and the vertical load only, and is assumed to respond instantaneously to the inputs:

$$\tilde{M}_{z\gamma} = \frac{\partial M_{z\gamma s}}{\partial \gamma_s} \Bigg|_s \tilde{\gamma} + \frac{\partial M_{z\gamma s}}{\partial F_{zs}} \Bigg|_s \tilde{F}_z \quad (31)$$

The aligning moment due to turn slip, depending on turn slip and vertical load is also assumed to respond instantaneously because of its physical origin, which is related to the one of $\tilde{M}_{z\gamma}$ (not to the origin of $\tilde{F}_{y\rho}$):

$$\tilde{M}_{z\rho} = \frac{\partial M_{z\rho s}}{\partial \rho_s} \Bigg|_s \tilde{\rho} + \frac{\partial M_{z\rho s}}{\partial F_{zs}} \Bigg|_s \tilde{F}_z \quad (32)$$

A fluctuating lateral deformation of the tyre tread band mass will give rise to gyroscopic effects if the deformation is not uniformly distributed over the wheel circumference. Such deformation will be caused mainly by $\dot{\tilde{F}}_{y\alpha}$ and $\dot{\tilde{F}}_{yp}$, since the major part of the side force due to camber arises due to the horizontal component of the radial force and therefore does not evoke significant deviations of the wheel and tyre mass from the wheel centre plane. However, since $\dot{\tilde{F}}_{y\alpha}$ and $\dot{\tilde{F}}_{yp}$ are not explicitly available, $\dot{\tilde{F}}_y$ has been employed instead. This approximation seems justified since the root locus courses which are relatively sensitive to M_{zGYR} all correspond to vibrational modes in which $\dot{\tilde{F}}_y$ plays only a minor role compared with $\dot{\tilde{F}}_{y\alpha}$. We obtain:

$$\dot{\tilde{M}}_{zGYR} = - C_{GYR} u_s \dot{\tilde{F}}_y \quad (33)$$

The coefficient C_{GYR} has been estimated starting with the data from [19] and considering the differences between the mass distribution and the compliance distribution of a diagonal ply car tyre on the one hand (on which the data of [19] have been based) and a motorcycle wheel plus tyre on the other.

The dynamic part of the overturning moment depends on the camber angle variations and the normal load variations and has been assumed to respond instantaneously (cf. [30]):

$$\dot{\tilde{M}}_x = \frac{\partial M_x}{\partial \gamma_s} \left|_s \right. \dot{\tilde{Y}} + \frac{\partial M_{xs}}{\partial F_{zs}} \left|_s \right. \dot{\tilde{F}}_z \quad (34)$$

The equations for $\dot{\tilde{F}}_y$ (Eq. (28)) and $\dot{\tilde{M}}_{z\alpha}$ (Eq. (29)) have been added to the set of dynamic equations (cf. Fig. 38). The equations for $\dot{\tilde{M}}_{zy}$ (Eq. (31)), $\dot{\tilde{M}}_{zp}$ (Eq. (32)) and $\dot{\tilde{M}}_x$ (Eq. (34)) have been included in the final set as well, but with a slight modification: these algebraic equations have been converted into first-order differential equations by adding a small relaxation effect. The equations of $\dot{\tilde{M}}_{zGYR}$ (Eq. (33)) have been included implicitly in the final set of dynamic equations by means of elimination of the variable $\dot{\tilde{M}}_{zGYR}$.

The procedure, described above, has been chosen to keep the final matrices surveyable without unnecessarily raising the order of the system.

2.5 Rider behaviour

2.5.1 general

The dynamic behaviour of a motorcycle is influenced by the presence of the rider in two ways: the rider acts as a (non-linear) stabilizer and controller

and the rider body acts as a complex (non-linear) mass/spring/damper system. It is beyond the scope of this study to deal with each of these aspects thoroughly; they will be briefly discussed and a simple structure will be introduced to approximate the presence of a non-active, non-rigid rider.

active rider behaviour

The active interference by the rider takes place at several levels. The most straight-forward is the compensatory control applied to stabilize the 'capsize mode' (cf. Sec. 4.2.2). Weir [46] compared the properties of various linear feed-back structures. With respect to stochastic inputs the bandwidth of the rider controlling actions is about 1 to 1.5 Hz. It should be noted that relevant muscle activity in general can occur also at higher frequencies, for instance if the rider acts as a quasi-open loop system. This could be the case when a periodic motion of the motorcycle occurs. The bandwidth of rider activity in that case is set to bounds by neuromuscular dynamics.

2.5.2 passive rider behaviour

In most of the studies concerning motorcycle dynamics the rider body has been assumed to be rigid in itself and rigidly connected to the main frame, the connection to the handlebars being disregarded, except for a stationary moment exerted on the steer which is required to achieve a steady state when cornering. Sharp suggests investigation of the effect of alternative assumptions about the rider, notably with respect to the wobble mode [37]. The critical speed of the weave mode increases when a pillion passenger is added [4] and decreases when the main frame centre of gravity is moved up and to the rear (cf. Sec. 4.4.3). These facts suggest an important influence of the rider body passive behaviour on the weave mode also.

A blackbox approach of accounting for the rider body passive behaviour would be to develop describing functions linking output forces and moments to input motion variables (cf. Fig. 23). This method requires an extensive measuring programme.

Another approach would be to analyse the body and the function and properties of all elements (muscles, joints etc.) and to build a model based on these data. At present, this method is not feasible in practice because the complexity of the human body amply exceeds the state-of-the-art of biomechanics.

To avoid the unsatisfactory rigid rider-assumption on the one hand and to remain within the scope of this study on the other, a simple physical model

has been introduced, based on kinematic considerations. A rigid rider body has been divided into two parts, in accordance with Fig. 24, at the most flexible region of the torso with respect to the lateral bending, the region of the lumbar spine. At the motorcycle/rider system at hand the separation between the two parts is at the same height relative to the ground plane as the handlebars in the nominal situation. The lower segment of the rider body has been assumed to be rigidly attached to the main frame, the upper part to rotate about an axis, which is horizontal in the nominal condition, relative to the main frame, cf. Fig. 24 and 25. Application of even a simple rider body model like this is expected to bring the lateral behaviour of the vehicle/rider system closer to reality, especially concerning the rider body motions.

However, it is obvious that effects occur which have not been accounted for in this model. For instance lateral motions of the lower body part relative to the main frame will occur, just as a coupling between the body roll motion and the steer moment.

The inertia parameter values concerning the rider body have been taken from an anthropometric sourcebook [17]. No data were available from which the lateral bending stiffness and damping could be derived. The stiffness parameter has been estimated with the aid of experimentally obtained data [43] showing a resonance frequency of the upper part of the rider body concerning the rotation in question, of about 3 Hz. It is likely that the stiffness and damping parameter values vary in a wide range depending on the subject chosen, muscular tension, clothing etc.

2.6 Environment

At a basic level the environment of a motorcycle comprises the road surface and the air through which the vehicle moves.

The road surface is assumed to be a flat and even plane perpendicular to the direction of the local gravitational field.

The air surrounding the vehicle is assumed to be initially still relative to the ground plane. The motion of the vehicle through the air will, in general, give rise to stationary and non-stationary forces distributed over the surface of the vehicle. Decomposition of the resultant force in components parallel to the system of axes (C_2, x_2, y_2, z_2) , cf. Fig. 26, yields the drag force (in negative x-direction), the lift force (in negative z-direction) and the aerodynamic side force (in y-direction), each force having its specific line of application.

In this study only stationary drag and lift forces have been regarded,

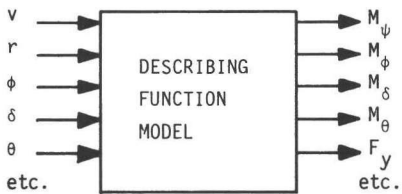


Fig. 23 ins and outs of a full passive rider body model

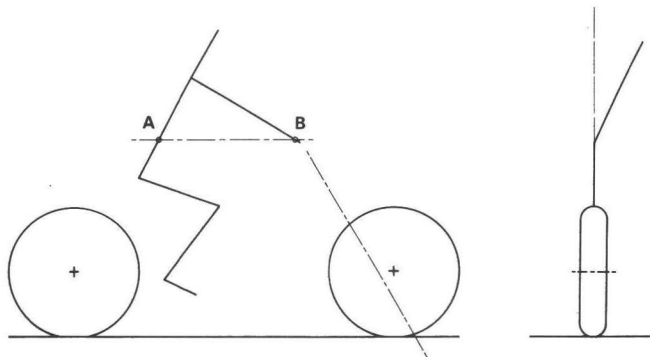


Fig. 24 rider body lean. For the specific motorcycle/rider-combination considered the resulting spinal pivot (A) is at the same height as the handlebar (B).

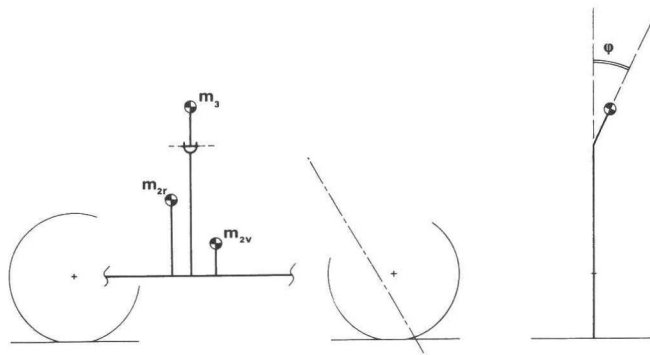


Fig. 25 rider body lean - schematically; cf. Fig. 12

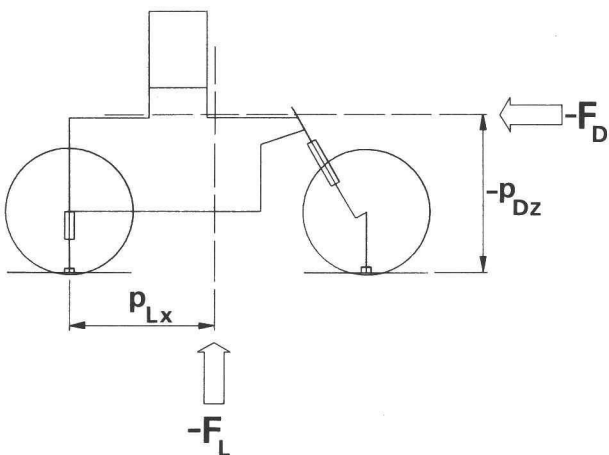


Fig. 26 direction and lines of application of the stationary aerodynamic forces F_L and F_D

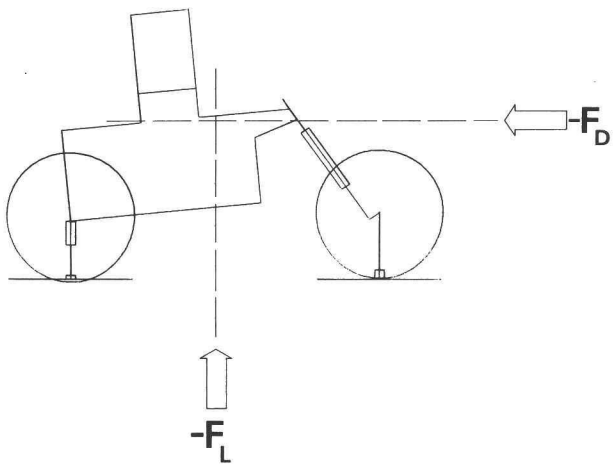


Fig. 27 general situation of the stationary aerodynamic forces. Note that the vehicle frame is tilted relative to the x_2 -axis; F_D remains horizontal. F_L remains perpendicular to F_D and both forces remain in the vehicle plane of symmetry; the lines of application of these forces retain their respective distances to the rear contact centre.

denoted by F_D and F_L respectively. The lines along which these forces act have been assumed to lie in the vehicle plane of symmetry. The position of these lines has been defined by the co-ordinates p_{Dz} and p_{Lx} respectively in the nominal situation and remains unaltered with respect to a system of axes, the x -axis of which coincides with the x_2 -axis, the positive z -axis being directed in accordance with a line through the rear wheel centre and the rear contact centre.

2.7 Derivation of the equations of motion (principles)

2.7.1 general

The outlines of the derivation of the equations of motion will be discussed in the sequel. To establish these equations, the Lagrangean approach has been chosen, employing the basic relation:

$$\frac{d}{dt} \frac{\partial T}{\partial \dot{q}_i} - \frac{\partial T}{\partial q_i} + \frac{\partial D}{\partial \dot{q}_i} + \frac{\partial U}{\partial q_i} = Q_i \quad (35)$$

in which T denotes the kinetic energy of the system, D the dissipation function, U the potential energy and Q the generalized force and moments, and q_i represents the i -th generalised co-ordinate. Specific difficulties arising due to the physical nature of the system at hand will be treated. The full derivation of the equation has been documented in [12] and [15].

modified Lagrange-equations

The main motion of the vehicle has been described by the longitudinal velocity, the lateral velocity and the yaw rate. These quantities have been defined with respect to the moving along system of axes, cf. Sec. 2.3 and Fig. 9. Employing these velocities instead of their time integrals results in a reduction of the order of the full system by two in the case at hand (the equation concerning the longitudinal motion has been disregarded since the longitudinal velocity u has been assumed to be constant).

The longitudinal velocity u and the lateral velocity v are the time derivations of so-called generalised quasi-co-ordinates (x and y). No true co-ordinates exist which by differentiation yield u and v . The yaw rate has been denoted by r . In order to obtain Lagrangean equations in u , v and r these velocities have been transformed to the fixed system of axes (indicated by 0):

$$u = \dot{x}_{C2}^0 \cos\psi + \dot{y}_{C2}^0 \sin\psi \quad (36)$$

$$v = - \dot{x}_{C2}^O \sin\psi + \dot{y}_{C2}^O \cos\psi \quad (37)$$

$$r = \dot{\psi} \quad (38)$$

in which \dot{x}_{C2}^O and \dot{y}_{C2}^O are the absolute velocity components of the origin C_2 of the moving along axis system (C_2, x_2, y_2, z_2) along the X-and the Y-axis respectively of the earth-fixed triad, cf. Fig. 9.

With the aid of the transformation (36), (37) and (38) and the basic expression (35) the Lagrangean equations for the longitudinal, the lateral and the yaw motion can be obtained, expressed in the variables u , v and r (cf. [49]):

$$\frac{d}{dt} \frac{\partial T}{\partial u} - r \frac{\partial T}{\partial v} = Q_x \quad (39)$$

$$\frac{d}{dt} \frac{\partial T}{\partial v} + r \frac{\partial T}{\partial u} = Q_y \quad (40)$$

$$\frac{d}{dt} \frac{\partial T}{\partial r} + u \frac{\partial T}{\partial v} - v \frac{\partial T}{\partial u} = Q_\psi \quad (41)$$

The equations corresponding to the remaining co-ordinates are of the form (35).

The full list of generalized co-ordinates, in addition to the variables u , v and r reads (cf. Fig. 28):

- u longitudinal velocity of the rear contact centre;
- v lateral velocity of the rear contact centre;
- $r (= \dot{\psi})$ yaw velocity of the moving along system of axes;
- ϕ roll angle of the rear wheel centre plane about the line of intersection of the wheel centre plane and the ground plane;
- δ steering angle;
- β frame torsion angle;
- ϕ_r rider body lean angle;
- θ pitch angle;
- λ_{t2} rear radial tyre spring compression;
- λ_{s2} rear suspension spring compression;
- λ_{s1} front suspension spring compression.

Note that λ_{t1} , the front radial tyre spring compression, is a dependent co-ordinate. The longitudinal velocity of the rear contact centre, u , will

later on be assumed to be constant. In consequence, equation (39) will not be relevant.

2.7.2 kinematics of the vehicle

Starting with the physical model as it has been presented in the foregoing a vector structure has been designed, shown in Fig. 29. This vector structure defines the position of each relevant point with respect to the moving along triad (C_2, x_2, y_2, z_2). The relevant points are (cf. Fig. 30):

- A_1 : front wheel centre;
- A_2 : rear wheel centre;
- B : point of the main frame which coincides with the rear wheel centre A_2 in the nominal situation;
- C_1 : front contact centre;
- C_2 : rear contact centre;
- D : point of intersection of the perpendicular from G_3 to the body roll axis and the body roll axis;
- F : point of intersection of the steering axis and the frame torsion axis (which is perpendicular to the steering axis);
- G_1 : c.g. of the front sprung part;
- G_{1a} : c.g. of the front axle assembly;
- G_{1w} : c.g. of the front wheel;
- G_{1u} : c.g. of the front unsprung part (the sum total of the front axle assembly and the front wheel);
- G_2 : c.g. of the main frame assembly;
- G_{2a} : c.g. of the rear axle assembly;
- G_{2w} : c.g. of the rear wheel;
- G_{2u} : c.g. of the rear unsprung part (the sum total of the rear axle assembly and the rear wheel);
- G_3 : c.g. of the upper part of the rider body.

In order to keep the structure surveyable, in this section a slightly simplified version of the model is employed, in which G_{1a} , G_{1w} and G_{1u} resp. G_{2a} , G_{2w} and G_{2u} coincide. The structure of the full model has been described in Appendix B.

Local systems of axes have been assigned and fixed to various parts of the structure, in accordance with Fig. 30, e.g. serving as a basis for the inertia matrix of each part:

local system of axes	fixed to	orientation in nominal situation
$(G_{2w}, x_{G2w}, y_{G2w}, z_{G2w})$		
$(G_{2a}, x_{G2r}, y_{G2r}, z_{G2r})$	G_{2a} and r_{w2}	$\left\{ \begin{array}{l} \text{conform to that of the moving-} \\ \text{-along system of axes} \\ (C_2, x_2, y_2, z_2) \end{array} \right.$
$(G_{2u}, x_{G2u}, y_{G2u}, z_{G2u})$		
$(G_2, x_{G2}, y_{G2}, z_{G2})$		
$(G_3, x_{G3}, y_{G3}, z_{G3})$		
$(G_1, x_{G1}, y_{G1}, z_{G1})$		
$(G_{1u}, x_{G1u}, y_{G1u}, z_{G1u})$	G_{1a} and r_{w1}	$\left\{ \begin{array}{l} \text{to be obtained from that of the} \\ \text{moving along triad } (C_2, x_2, y_2, z_2) \\ \text{by rotation about the } y\text{-axis over} \\ \text{the inclination angle } \varepsilon \end{array} \right.$
$(G_{1a}, x_{G1r}, y_{G1r}, z_{G1r})$		
$(G_{1w}, x_{G1w}, y_{G1w}, z_{G1w})$		$\left\{ \begin{array}{l} \text{conform to that of the moving-} \\ \text{-along system of axes} \\ (C_2, x_2, y_2, z_2) \end{array} \right.$

To account for mutually different orientations of local triads in the nominal situation and to describe the state of the system also in non-nominal situations the following transformations should be taken into account:

description	relevant angle	transformation matrix
frame torsion	β	\bar{A}^β
steer rotation	δ	\bar{A}^δ
steering axis inclination	ε	\bar{A}^ε
roll rotation of rider upper body	ϕ_r	\bar{A}^{ϕ_r}
pitch rotation of frame	θ	\bar{A}^θ
roll rotation of frame	ϕ	\bar{A}^ϕ

In Sec. 2.3 these rotations have been defined. The transformation matrices have been defined as in the following example:

$$\bar{k}^P = \bar{A}^\zeta \bar{k}^Q \quad (42)$$

The superscripts to the vector \bar{k} denote the system of axes relative to which the components of the vector have been expressed: either relative to the P-system (P, x_P, y_P, z_P) or to the Q-system (Q, x_Q, y_Q, z_Q) . The Q-system is obtained from the P-system by a rotation over the angle ζ about the relevant axis (which is defined for each transformation; cf. Sec. 2.3) of the P-system; in this example the origins Q and P at all time coincide. If more than one rotation is involved, a chain of successive transformations must be performed and a product of corresponding matrices will show up in the

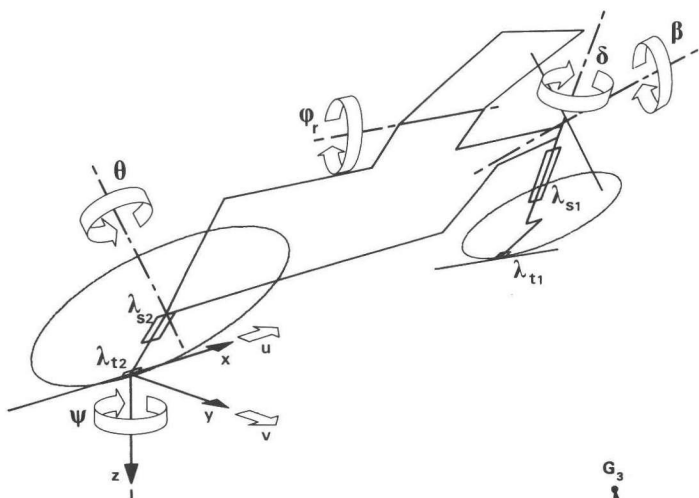


Fig. 28 generalized coordinates

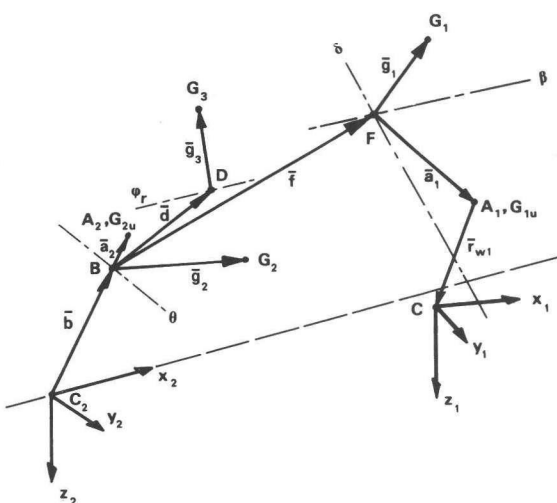


Fig. 29 vector structure of the model (depicted in an arbitrary situation). Letters G indicate mass centres. Note that $|\bar{b} + \bar{a}_2| = r_{w2}$. In this slightly simplified version the points G_{2w} , G_{2a} , G_{2u} and A_2 , resp. G_{1w} , G_{1a} and A_1 coincide (cf. Appendix B for the full model definitions).

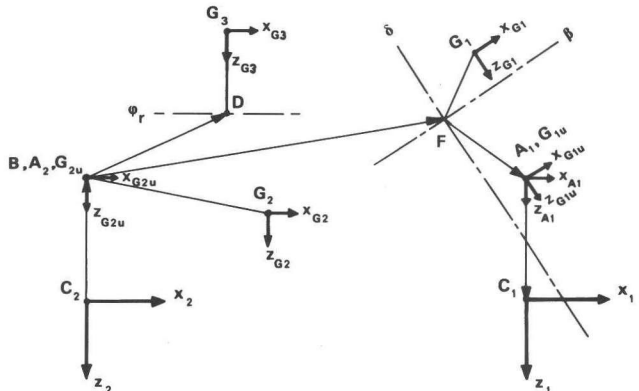


Fig. 30 local triads (depicted in the nominal situation; of the right-handed orthogonal systems of axes only the x- and z-axes have been identified). Note that z_{A1} is always directed along $\overline{A_1 C_1}$, and z_{G2u} along $\overline{A_2 C_2}$.

mathematical description.

The position of the relevant points relative to the moving along (C_2, x_2, y_2, z_2) -system can now be expressed in the variables, the vectors defining the geometry and the rotation matrices. We obtain for the position of G_{1a} relative to (C_2, x_2, y_2, z_2) (vector \bar{p}_{G1a}) in components along the axes of (C_2, x_2, y_2, z_2) :

$$\bar{p}_{G1a} = \bar{a}_2^{G2a} + \bar{a}_2^{\theta_f G2} + \bar{a}_2^{\phi_A \theta_A \epsilon_A \delta_A \beta_A G1a} \quad (43)$$

Note that:

$$|\bar{b}^{G2a}| = -|\bar{a}_2^{G2a}| + \bar{r}_{w2}^{G2a} \quad (44)$$

The lengths of the vectors \bar{b} , \bar{a}_2 and \bar{a}_1 and the length r_{w1} are dependent on changes of the spring compressions λ (zero in the nominal situation). We have:

$$b_z^{G2a} = b_{zo}^{G2a} + \lambda_{t2} + \lambda_{s2} \quad (45)$$

$$a_{2z}^{G2a} = -\lambda_{s2} \quad (46)$$

$$a_{1z}^{G1a} = a_{1zo}^{G1a} - \lambda_{s1} \quad (47)$$

$$r_{w1} = r_{w1o} - \lambda_{t1} \quad (48)$$

Note that spring compressions correspond to positive values of the respective λ 's.

2.7.3 kinematics of the wheel

In this section derivations have been developed, necessary to express the relevant quantities, concerning the kinematics of the wheel, in the system variables. The elaborated expressions can be found in Appendix C. The situation concerning the front wheel only will be discussed; the set of system variables introduced makes it possible to derive the description of the rear wheel situation from that of the front wheel situation by an appropriate adaption of the parameters concerned.

Two fundamental concepts concerning the kinematics of the wheel, which have been defined before (cf. Sec. 2.3), are the contact centre of the wheel, cf. Fig. 32, and the wheel centre plane. The contact centre of the wheel has

been defined as the point of intersection of the wheel centre plane, the ground plane and a plane, normal to the ground plane, containing the wheel spin axis. The wheel centre plane has been defined as the plane perpendicular to the wheel spin axis and through the wheel centre.

For the purpose of defining the orientation of the wheel centre plane the auxiliary unit vector \bar{j} is introduced, defined with respect to the (C_2, x_2, y_2, z_2) -triad. This vector is directed along the front wheel spin axis, and reads, with $\bar{e}_2^T = (0, 1, 0)$:

$$\bar{j} = \frac{\phi \theta \epsilon \delta \beta}{A A A A A} \bar{e}_2 \quad (49)$$

The front wheel camber angle γ_1 , which is the roll angle of the front wheel centre plane about the line of intersection of this plane and the ground plane, cf. Fig. 31, can now be obtained from $(\bar{e}_3^T = (0, 0, 1))$:

$$\sin \gamma_1 = \bar{j} \cdot \bar{e}_3 \quad (50)$$

This quantity is used in the tyre force and moment generation model.

The 'steer angle in the road plane', δ' , has been defined as the angle between the x-axis of the (C_2, x_2, y_2, z_2) -triad and the line of intersection of the front wheel centre plane and the road plane (which line coincides with the x-axis of the (C_1, x_1, y_1, z_1) -triad), cf. Fig. 33. This angle can also be obtained with the aid of the normal to the wheel centre plane, \bar{j} ($\bar{e}_1^T = (1, 0, 0)$):

$$\tan \delta' = - \frac{\bar{j} \cdot \bar{e}_1}{\bar{j} \cdot \bar{e}_2} \quad (51)$$

The front wheel radius vector \bar{r}_{w1} has been defined in the $(A_1, x_{A1}, y_{A1}, z_{A1})$ system of axes; \bar{r}_{w1} has the direction and length of $\bar{A}_1 C_1$ (cf. Fig. 31). The components of this vector (taken relative to (C_2, x_2, y_2, z_2)) can be obtained from the following conditions, all consequent from the definition of the contact centre:

- front wheel radius vector in the front wheel centre plane:

$$\bar{r}_{w1} \cdot \bar{j} = 0 \quad (52)$$

- front wheel radius vector in a plane through the front wheel spindle and perpendicular to the ground plane:

$$(\bar{j} \times \bar{r}_{w1}) \cdot \bar{e}_3 = 0 \quad (53)$$

- vertical component (relative to the ground plane) of the front

wheel radius vector equal to the height of the front wheel centre A_1 above the ground plane (i.e. the endpoint of \bar{r}_{w1} should lie in the ground plane):

$$\bar{r}_{w1} \cdot \bar{e}_3 = - p_{A1z} \quad (54)$$

After these considerations concerning the orientation of the front wheel and the location of the front wheel contact centre we will turn to the derivation of the slip quantities of the front wheel. With δ' being known, the front wheel turn slip, cf. Fig. 13, can be elaborated:

$$\rho_1 = \frac{\dot{\psi} + \dot{\delta}'}{u} \quad (55)$$

With δ' and \bar{r}_{w1} being known, the slip speed of a material point C_1^* of the front wheel, which at the moment considered coincides with the front wheel contact centre, cf. Figs. 31 and 32, can be derived:

$$\dot{\bar{s}}_1 = \begin{pmatrix} u \\ v \\ 0 \end{pmatrix} + \dot{\psi} \bar{e}_3 \times (\bar{p}_{A1} + \bar{r}_{w1}) + \dot{\bar{p}}_{A1} + \dot{\bar{r}}_{w1} - \Omega_1 \left(\frac{r_{e1}}{r_{w1}} \right) \bar{j} \times \bar{r}_{w1} \quad (56)$$

in which r_{e1} denotes the effective rolling radius and Ω_1 is the rotational velocity of the wheel about the wheel spin axis with respect to the vertical plane through this axis. The vector \bar{p}_{A1} denotes the position of the front wheel centre A_1 relative to the moving along system of axes (C_2, x_2, y_2, z_2) . The rotational velocity of the wheel Ω_1 can be written as:

$$\Omega_1 = \Omega_{1s} - \dot{\chi}_1 \quad (57)$$

with Ω_{1s} denoting the stationary value u_s/r_{e1} and $\dot{\chi}_1$ the variation with respect to Ω_{1s} . At this stage χ_1 and χ_2 are free variables, each introducing a new Lagrangean equation, cf. Sec. 2.7.7. Later on the variables χ will be eliminated by imposing requirements with respect to the tyre/ground contact situation, cf. Sec. 2.7.4. Written in components with respect to (C_1, x_1, y_1, z_1) the slip speed vector of C_1^* reads:

$$\dot{\bar{s}}_1^{C1} = (\bar{A}^{\delta'})^{-1} \dot{\bar{s}}_1 \quad (58)$$

Later on, components of this vector will be used to determine the work coefficients; furthermore, the front wheel slip angle α , cf. Fig. 13, can be obtained from $\dot{\bar{s}}_1^{C1}$:

$$\tan \alpha_1 = \frac{\dot{s}_1^{C1} \cdot e_2}{v_{C1x}^{C1}} \quad (59)$$

in which v_{C1x}^{C1} is the component along the x-axis of (C_1, x_1, y_1, z_1) of the absolute velocity of the non-material point C_1 .

Note that, concerning the kinematics of the remainder of the vehicle, the wheels have been considered to be flat discs, cf. Fig. 34. From a tyre mechanics point of view, the finite tyre crown radius has been taken into account, thus giving rise to the overturning moment, as has been described in Sec. 2.4.2.

2.7.4 derivation of the constraint equations

In this section the derivation of the equations will be discussed, which satisfy the kinematic tyre/ground contact conditions. In the previous section, the slip speed of the material point C_1^* of the wheel, cf. Figs. 31 to 33, has been derived, cf. Eq. (56). The longitudinal slip of C_1^* , which is the slip along the line of intersection of the front wheel centre plane and the ground plane, reads, expressed with respect to (C_1, x_1, y_1, z_1) :

$$\dot{s}_{1x}^{C1} = \dot{e}_1^T (\bar{A}^{\delta'})^{-1} \dot{s}_1 \quad (60)$$

With the aid of the condition of vanishing longitudinal slip:

$$\dot{s}_{ix}^{C1} = 0 \quad (61)$$

for each wheel, the time derivatives of χ_1 and χ_2 can be explicitly expressed in the other variables.

With the aid of the χ -equations (cf. Sec. 2.7.3) with χ eliminated the longitudinal forces F_{x1} and F_{x2} can be expressed in the variables in order to eliminate these forces from the right-hand members of the remaining equations.

2.7.5 kinetic energy due to the speed of the mass centres

The absolute velocity vector \bar{V}_{G1u} reads, expressed in components along the axes of the moving along triad (C_2, x_2, y_2, z_2) :

$$\bar{V}_{G1u}^{C2} = \underbrace{\begin{pmatrix} u \\ v \\ 0 \end{pmatrix}}_{\text{velocity of the origin of the moving along triad } (C_2, x_2, y_2, z_2)} + \underbrace{\dot{\psi} \bar{e}_3 \times \bar{p}_{G1u}^{C2}}_{\text{contribution due to yaw rate}} + \underbrace{\dot{\bar{p}}_{G1u}^{C2}}_{(C_2, x_2, y_2, z_2)\text{-apparent velocity (relative vel.)}} \quad (62)$$

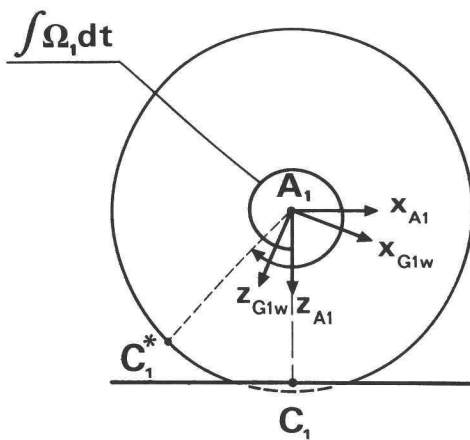


Fig. 31 the material point C_1^* is located at the circumference of a disk-like wheel. The system of axes $(A_1, x_{1w}, y_{1w}, z_{1w})$ is fixed to the front wheel, part $1w$; the z_{A1} -axis is always directed along $\overline{A_1C_1}$.

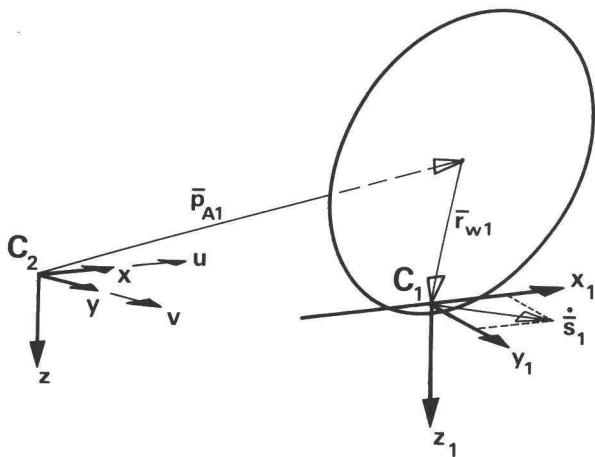


Fig. 32 the slip velocity of the material point C_1^* , considered at the time that C_1^* coincides with C_1

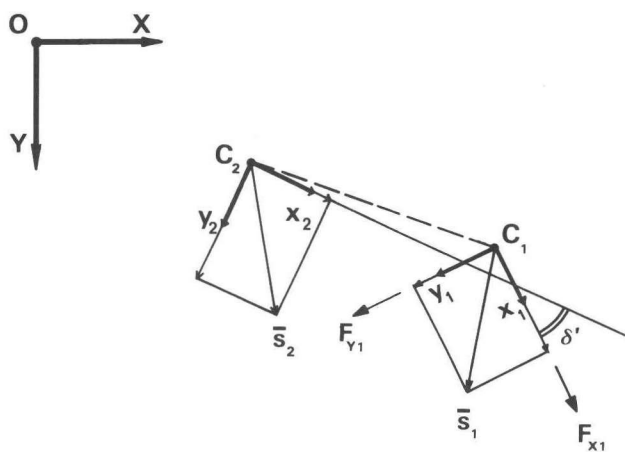


Fig. 33 top view of the road plane with the important quantities describing the vehicle/road contact

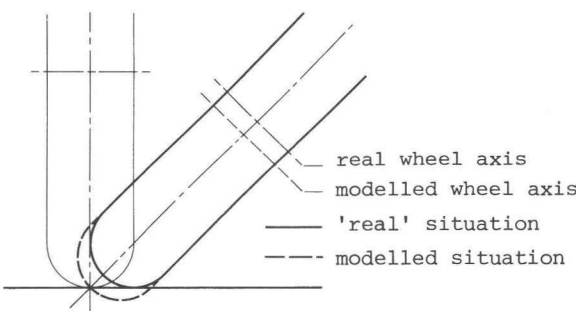


Fig. 34 'real' and modelled tyre crown effects; overturning moment realistically modelled (cf. Fig. 19); displacement of the wheel centre plane due to camber not modelled

Now the terms accounting for the kinetic energy T_{m1u} of m_{1u} , regarded as a point mass, located in G_{1u} , can be obtained:

$$T_{m1u} = \frac{1}{2} m_{1u} \bar{V}_{G1u}^{C2 T} \bar{V}_{G1u}^{C2} \quad (63)$$

with \bar{V}_{G1u} constituting the absolute value of the vector (62).

The contributions of the remaining masses can be derived from the contribution of m_{1u} . This advantage arises from the chosen chain vector structure. For instance, to obtain T_{m3} :

replace λ_{s1} in T_{m1u} by 0 ;
 \bar{a}_1 by \bar{g}_3 ;
 β by ϕ_r ;
 δ by 0 ;
 ϵ by 0 ;
 and \bar{F} by \bar{d} .

Summation of all relevant contributions yields the total kinetic energy due to the linear speeds of the masses.

2.7.6 kinetic energy due to the rotational speed of the bodies

The description of the inertia properties arising due to the continuous distribution of mass has been related to the local frame of reference of each body, cf. Fig. 30. In the nominal situation all bodies have been assumed to be symmetrical with respect to the vehicle centre plane. Since the local y -axis of each body is directed perpendicular to this plane we find for the products of inertia:

$$C_{xy} = C_{yx} = C_{yz} = C_{zy} = 0 \quad (64)$$

In consequence the inertia matrices are of the form:

$$\bar{J} = \begin{pmatrix} J_x & 0 & -C_{xz} \\ 0 & J_y & 0 \\ C_{zx} & 0 & J_2 \end{pmatrix} \quad (65)$$

In order to obtain the corresponding contributions to the kinetic energy, we need the absolute angular velocity vector of each body expressed in components along the axes of the local triad. Starting with the transformation defined by \bar{A}^{ζ} , cf. Eq. (42), first the relative angular velocity vector will be

derived, denoting the C_2 -apparent angular velocity. As an aid the position vector \bar{k} will be employed, denoting the position of the point K which is fixed in the Q-system of axes (Q, x_Q, y_Q, z_Q) , with Q fixed in (C_2, x_2, y_2, z_2) :

$$\bar{k}^{C2} = \bar{A}^{\zeta} \bar{k}^Q \quad (66)$$

$$\dot{\bar{k}}^{C2} = \dot{\bar{A}}^{\zeta} \bar{k}^Q \quad (67)$$

$$\bar{v}_{Kr}^Q = \bar{A}^{\zeta-1} \dot{\bar{k}}^{C2} = \bar{A}^{\zeta-1} \dot{\bar{A}}^{\zeta} \bar{k}^Q \quad (68)$$

$$\bar{v}_{Kr}^Q = \bar{\Omega}^Q \bar{k}^Q \quad (69)$$

so that

$$\bar{\Omega}^Q = \bar{A}^{\zeta-1} \dot{\bar{A}}^{\zeta} \quad (70)$$

Here, \bar{v}_{Kr}^Q is the vector denoting the velocity of K relative to the C_2 -system of axes expressed in components along the axes of the local Q-system of axes. On the other hand, for the same vector may be written:

$$\bar{v}_{Kr}^Q = \bar{\omega}_{Qr}^Q \times \bar{k}^Q \quad (71)$$

in which $\bar{\omega}_{Qr}^Q$ is the vector describing the angular velocity of the Q-frame relative to the C_2 -frame. The similarity between the expressions (69) and (71) indicates a relation between $\bar{\Omega}^Q$ and $\bar{\omega}_{Qr}^Q$. This relation can be obtained with the aid of Fig. 35, and reads:

$$\bar{\Omega}^Q = \begin{pmatrix} 0 & -\omega_{Qrz}^Q & \omega_{Qry}^Q \\ \omega_{Qrz}^Q & 0 & -\omega_{Qrx}^Q \\ -\omega_{Qry}^Q & \omega_{Qrx}^Q & 0 \end{pmatrix} \quad (72)$$

Thus the components of the vector $\bar{\omega}_{Qr}^Q$ of the rotational speed relative to the C_2 -system can be elaborated. The absolute angular speed may now be found by adding the vector of the yaw rate $\dot{\psi} \bar{e}_3$ but with components along the local system of axes concerned. For the front unsprung part 1u we find in this way:

$$\bar{\omega}_{G1u}^{G1u} = (\bar{A}^{\phi} \bar{A}^{\theta} \bar{A}^{\epsilon} \bar{A}^{\delta} \bar{A}^{\beta})^{-1} \bar{e}_3 \cdot \dot{\psi} + \bar{\omega}_{G1ur}^{G1u} \quad (73)$$

Now the contribution of \bar{J}_{1u} to the kinetic energy can be derived:

$$T_{J1u} = \frac{1}{2} \omega_{G1u}^T \bar{J}_{1u} \omega_{G1u} \quad (74)$$

The contribution of the remaining parts can be obtained from the elaborated version of the expression (74) by omission or replacement of variables and parameters. For example, to obtain T_{J3} : replace β by θ_r and δ and ε by 0.

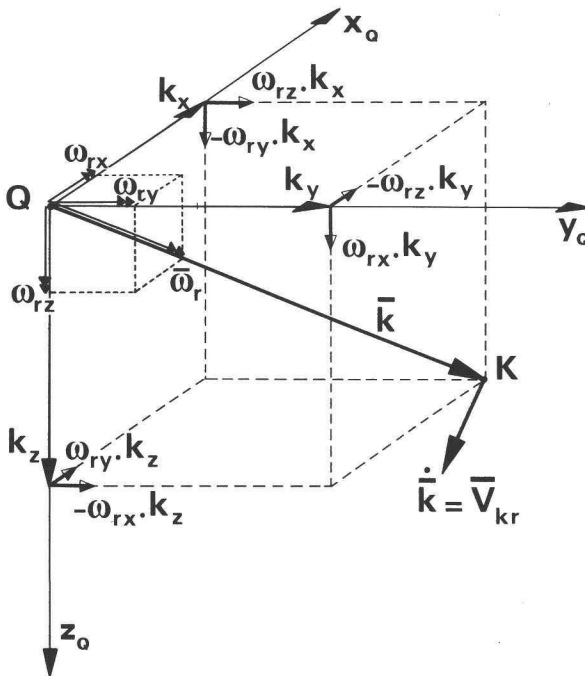


Fig. 35 derivation of the components of the relative angular velocity vector $\bar{\omega}_r$, in this figure written as $\bar{\omega}_r$

2.7.7 kinetic energy due to the speed of revolution of the wheels

The speed of revolution of the front wheel, Ω_1 (which concerns the rotation of the wheel about the wheel spin axis with respect to a vertical plane through this axis) is composed of a constant part Ω_{1s} , and a non-constant part $\dot{\chi}_1$:

$$\Omega_1 = \Omega_{1s} - \dot{\chi}_1 \quad (75)$$

with:

$$\Omega_{1s} = u_s / r_{e1} \quad (76)$$

$\dot{\chi}_1$ is a small variation, superimposed on Ω_{1s} , constrained to the forward speed of the contact centre in order to ensure pure rolling of the wheel under all circumstances. The parameter r_e denotes the effective rolling radius of the wheel, cf. [19]. For the time being the condition of constraint will be disregarded, and χ treated as a generalized co-ordinate, because of the non-holonomic nature of the constraint condition.

The contribution to the kinetic energy becomes:

$$T_{w1} = \frac{1}{2} \omega_{w1y}^2 J_{y1w} \quad (77)$$

with:

$$\omega_{w1y} = -\Omega_1 + (\dot{\psi} + \dot{\delta}') \sin \gamma_1 \quad (78)$$

which is the absolute angular velocity of the front wheel about the front wheel spin axis, still containing χ as a variable. This variable gives rise to two more equations of motion (one for each wheel) of the form:

$$\frac{d}{dt} \frac{\partial T_w}{\partial \dot{\chi}} = Q_x \quad (79)$$

since the remaining terms of Eq. (35) in this case equal zero.

Together with the equations of constraint, cf. Sec. 2.7.4, we now have a sufficient number of equations to eliminate the variables χ_1 , χ_2 , and F_{x1} , F_{x2} .

2.7.8 potential energy

The potential energy due to gravity:

$$U_g = \sum m g h \quad (80)$$

in which h denotes the height above the zero level of potential energy, g the gravitational acceleration and Σ a summation over the various parts of the vehicle, can be directly derived from the position vectors of the various centres of gravity relative to (c_2, x_2, y_2, z_2) since the road surface over which (c_2, x_2, y_2, z_2) moves is assumed to be flat and even.

The potential energy, accumulated in a spring, reads approximately,

cf. Fig. 36:

$$U_\lambda = U_0 - F_0 \lambda + \frac{1}{2} C_0 \lambda^2 \quad (81)$$

with λ positive denoting a spring compression, and with C_0 being the spring stiffness coefficient in the nominal condition. The contributions of all springs to the potential energy can now be derived except for the contribution of the front tyre spring since λ_{t1} is not an explicit variable. To elaborate this contribution the front tyre spring compression has to be expressed first (cf. Fig. 37):

$$\lambda_{t1} = \frac{p_{A1z}}{\cos \gamma_1} + r_{w10} \quad (82)$$

with γ_1 being the front wheel camber angle, cf. Sec. 2.7.3, p_{A1z} the negative of the height of the wheel centre A_1 , and r_{w10} the length of the front wheel radius vector \bar{r}_{w1} in the nominal situation.

2.7.9 dissipation function

Energy is being dissipated in:

- the suspension dampers;
- the steer damper;
- the frame structure, due to the elastic torsional deformation, described by β ;
- the rider body, due to the bending of the upper part of the body relative to the remainder of the body (cf. Sec. 2.5.2).

All damping actions have been assumed to be linear and to have an ideal viscous character. Concerning the damping in the frame structure and the rider body no data were available.

We obtain:

$$D = \frac{1}{2} \sum K_\lambda \dot{\lambda}^2 + \frac{1}{2} K_\delta \dot{\delta}^2 + \frac{1}{2} K_{\phi r} \dot{\phi}_r^2 \quad (83)$$

with Σ denoting a summation over the suspension springs. Experiments show that the damping involved in the radial tyre spring motion is very small when the tyre is rolling; these contributions have therefore been put zero.

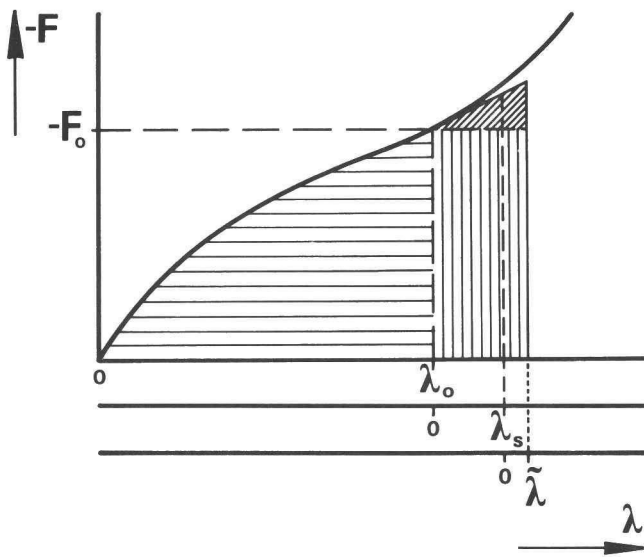


Fig. 36 spring characteristic showing the various components of the potential spring energy. The accumulated potential energy reads (exact in the case of linear springs); with $\lambda = \lambda_s + \tilde{\lambda}$:

$$U_\lambda = U_0 - F_0 \lambda + \frac{1}{2} C_0 \lambda^2$$

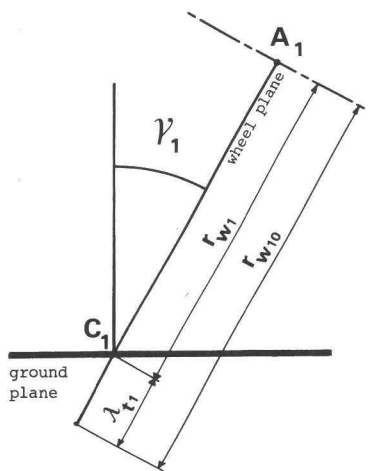


Fig. 37 definition of the front tyre spring compression

2.7.10 right-hand members

The right-hand members of the equations of Lagrange (35) have been obtained with employment of the principle of virtual work. The forces and moments* acting on the system are:

- the tyre forces and moments;
- (stationary) aerodynamic forces;
- a (stationary) steer moment, exerted on the front frame with a reaction on the main frame, the moment vector being directed parallel to the steering axis;
- a (stationary) driving moment, exerted on the rear wheel with a reaction on the main frame.

The introduction of a steer moment (and, of course, a driving moment) is in general necessary to achieve an equilibrium condition.

The relevant virtual displacements can be obtained in a straightforward manner except for the virtual displacement in the direction of the front tyre side force. This is the virtual displacement of a material point C_1^* at the wheel circumference, at the time considered located in C_1 , in the direction of F_{y1} . An expression, similar to equation (56) is obtained:

$$\delta s_{1y}^{C1} = \bar{e}_2^T (\bar{A}^{\delta'})^{-1} \left\{ \begin{pmatrix} \delta x \\ \delta y \\ 0 \end{pmatrix} + \begin{pmatrix} 0 \\ 0 \\ \delta \psi \end{pmatrix} \times (\bar{p}_{A1} + \bar{r}_{w1}) + \delta \bar{p}_{A1} + \delta \bar{r}_{w1} + \delta \chi_1 \left(\frac{r_{e1}}{r_{w1}} \right) \bar{j} \times \bar{r}_{w1} \right\} \quad (84)$$

The quantities δx , δy and $\delta \psi$ denote the virtual displacements of the (C_2, x_2, y_2, z_2) - triad in its x_2 and y_2 -directions and about its z_2 -axis respectively. The generalized forces Q can now be derived from:

$$\delta W = \sum_{i=1}^m \delta q_i Q_{qi} \quad (85)$$

in which δW denotes the total virtual work and δq_i the virtual increment of the generalized (quasi-) coordinate q_i .

2.7.11 processing the equations of motion

The full Lagrangean equations (35) which can now be elaborated in detail (described in [12] and [15]) have been processed in order to obtain the description of the stationary and the non-stationary situation (cf. Sec. 2.1) respectively.

In order to describe the nominal situation all variables are put equal to

* internal moments have been taken along as pairs of action and reaction moments, acting as external moments of parts of the system

zero (note that all geometrical parameters have been quantified in the nominal situation). The nominal wheel loads are solved from simple equilibrium conditions.

The equations describing the stationary situation can readily be obtained from the full equations of motion by omission of all terms containing first and second time derivatives of the variable quantities; note that u and v are regarded as zeroth time derivatives. These algebraic 'steady state'-equations have been kept non-linear. The stationary wheel loads can be obtained from the equations accounting for the equilibrium of stationary forces, acting on the system. The set has been completed with the equations describing the stationary behaviour of the tyres (cf. Sec. 2.4.2).

Since an eigenvalue/eigenvector-analysis will be employed to study the non-stationary situation, a set of linear dynamic equations must be obtained. This has been done by linearizing the full equations of motion about a trim condition, which in this case is the situation described by the solution of the 'steady state'-equations. The set of linear differential equations, thus obtained, has been completed with the equations describing the non-stationary behaviour of the tyres (cf. Sec. 2.4.3).

2.7.12 equations concerning the stationary situation

For the sake of simplification, the frame torsion angle β and the body lean angle ϕ_r have been disregarded and put equal to zero in the stationary situation. The forward speed of the rear contact centre, u_s' , and the vehicle roll angle ϕ_s have been regarded as given input quantities. The roll angle has been selected to be non-variable in order to minimize the number of terms in the partial derivatives, which are required in the solution process.

Thus the vector of steady state variables reads (p elements):

$$\underline{\underline{x}}_s^T = (v_s \ r_s \ M_{\delta s} \ \delta_s \ \phi_s \ \lambda_{t2s} \ \lambda_{s2s} \ \lambda_{s1s} \ F_{y1s} \ M_{z1s} \ M_{x1s} \ F_{y2s} \ M_{z2s} \ M_{x2s}) \quad (86)$$

To reduce the total number of terms the steady state variables have been divided into two groups, variables of the one group being assumed to be small relative to variables of the other group:

GROUP I (large):	GROUP II (small):
$u_s \ v_s \ r_s \ \phi_s \ F_{y1s} \ M_{z1s} \ M_{x1s} \ F_{y2s} \ M_{z2s} \ M_{x2s} \ M_{\delta s}$	$ \ \delta_s \ \theta_s \ \lambda_{t2s} \ \lambda_{s2s} \ \lambda_{s1s}$

(87)

It may be noted that the variables of group II all represent quantities which describe the change in shape of the vehicle with respect to the nominal sit-

uation.

Terms with products of variables from group II have been neglected in the final steady state equations.

The full steady state equations have been listed in Appendix B.

2.7.13 equations concerning the non-stationary situation

All variables concerning the perturbed situation -denoted by superscript \sim - have been assumed to be small. The vector of variables concerning the non-stationary motion reads:

$$\tilde{\mathbf{x}}^T = (\tilde{v} \ \tilde{r} \ \tilde{\phi} \ \tilde{\delta} \ \tilde{\beta} \ \tilde{\phi}_r \ \tilde{\theta} \ \tilde{\lambda}_{t2} \ \tilde{\lambda}_{s2} \ \tilde{\lambda}_{s1} \ \tilde{F}_{y1} \ \tilde{M}_{z1\alpha} \ \tilde{M}_{z1\gamma} \ \tilde{M}_{z1\rho} \ \tilde{M}_{x1} \ \tilde{F}_{y2} \ \tilde{M}_{z2\alpha} \ \tilde{M}_{z2\gamma} \ \tilde{M}_{z2\rho} \ \tilde{M}_{x2}) \quad (88)$$

Note that the steer moment is assumed constant so that the variable \tilde{M}_δ does not occur in $\tilde{\mathbf{x}}$. Furthermore, \tilde{M}_{zGYR} has been omitted from $\tilde{\mathbf{x}}$, since the corresponding equations have been included implicitly in the full set (cf. Sec. 2.4.3). Steady state variables from group I (cf. Sec. 2.7.12) have been taken along in coefficients of the dynamic equations. In the range of u_s and ϕ_s that will be considered in the calculations, the symmetrical change of shape of the vehicle -due to centrifugal and aerodynamic forces- is of greater importance than the anti-symmetrical change of shape. Therefore, of group II the variables describing the symmetrical change of shape of the vehicle (which are θ_s , λ_{t2s} , λ_{s2s} and λ_{s1s}) have been accounted for in the dynamic calculations; the remaining variable, δ_s , has not been accounted for. To avoid a large increase of the number of terms in the coefficients of the dynamic equations the symmetrical change of shape has been included implicitly. This has been done by an adaption of the geometry of the vehicle to include θ_s , λ_{t2s} , λ_{s2s} and λ_{s1s} . The adapted geometry has been considered to be the nominal geometry with respect to the dynamic equations, cf. Sec. 3.1.

The structure of the dynamic equations written as a homogeneous system has been depicted in matrix form in Fig. 38. The set is composed of three groups of equations:

- the equations for the anti-symmetrical motion variables
- the equations for the symmetrical motion variables
- the equations for the tyre force and moment variables

When cornering, the symmetrical and the anti-symmetrical dynamics are no longer orthogonal. Due to this phenomenon the coefficients of the equations of motions describing the dynamic situation appear to change. On the one hand this change causes existing non-zero coefficients to change value; on the other hand this change causes coefficients which are zero in the running-straight-ahead situation to assume a non-zero value giving rise to 'new' terms in the equations. Many of these terms are so-called 'coupling terms' linking up the symmetrical and the anti-symmetrical dynamic equations. The 'coupling terms' are terms with symmetrical variables when occurring in the anti-symmetrical equations and vice versa, as indicated in Fig. 38.

$$\ddot{\tilde{q}} + \begin{array}{|c|c|c|} \hline 0 & AS & C & 0 \\ \hline 0 & C & S & 0 \\ \hline 0 & 0 & 0 & 0 \\ \hline \end{array} + \begin{array}{|c|c|c|} \hline AS & C & T \\ \hline C & S & 0 \\ \hline 0 & T & T \\ \hline \end{array} + \begin{array}{|c|c|c|} \hline AS & C & T \\ \hline C & S & 0 \\ \hline T & T & T \\ \hline \end{array} = \ddot{\tilde{q}} = \bar{0}$$

Fig. 38 dynamic equations, homogeneous notation

$$\ddot{\tilde{q}}^T = (\tilde{v} \tilde{r} \tilde{\phi} \tilde{\delta} \tilde{\beta} \tilde{\phi} \tilde{\theta} \tilde{\lambda}_{t2} \tilde{\lambda}_{s2} \tilde{\lambda}_{s1} \tilde{F}_{y1} \tilde{M}_{z1\alpha} \tilde{M}_{z1\gamma} \tilde{M}_{z1\rho} \tilde{M}_{x1} \tilde{F}_{y2} \tilde{M}_{z2\alpha} \tilde{M}_{z2\gamma} \tilde{M}_{z2\rho} \tilde{M}_{x2})$$

position
number 1 2 3 4 5 6 7 8 9 10 11 12 13 14 15 16 17 18 19 20

AS: anti-symmetric motion terms/variables

S: symmetric motion terms/variables

C: coupling terms/variables

T: tyre behaviour terms/variables

Only the blocks of which all elements are principally zero have been marked with "0".

3.1 Procedure

A suitable method to achieve fundamental insight into the dynamic properties of a system is the eigenvalue/eigenvector analysis. This analysis can be applied after linearization of the homogeneous version of the set of equations describing the dynamic behaviour of the system. The equilibrium condition about which the non-linear equations at hand have been linearized may in general refer to a steady state curving motion. The problem is now divided into two parts: a set of non-linear algebraic equations, describing the equilibrium condition and a set of homogeneous linear differential equations describing the dynamic behaviour of the system.

The method of calculation which is schematically depicted in Fig. 39 will now be discussed. In order to optimize the iterative method of solving the steady state equations (cf. Sec. 2.4.1) the normal wheel loads of the stationary situations are pre-calculated from simple equilibrium considerations. Then the set of steady-state equations is solved with the aid of the method of Newton-Raphson. At this stage steady-state data become available.

The frame spring length may alter considerably (order of magnitude of .1 m) due to aerodynamic and centrifugal forces. If this effect would be taken into account in the dynamic equations in the normal way the symmetrical steady state variables would give rise to many extra terms. To avoid this the geometry of the vehicle is considered after the application of the steady state values of these variables (cf. Sec. 2.7.13). This off-zero condition is considered to be the nominal condition for the dynamic equations. To establish this state the geometrical quantities defined in Fig. 12 are recalculated to account for θ_s , λ_{t2s} , λ_{s2s} and λ_{s1s} .

At this stage the block of calculations concerning the dynamic behaviour is entered, cf. Fig. 39, and the roots of the characteristic equation are calculated.

The numerical output of the calculations is a full documentation of the dynamic state of the system. The eigenvalue courses (the root loci) plotted

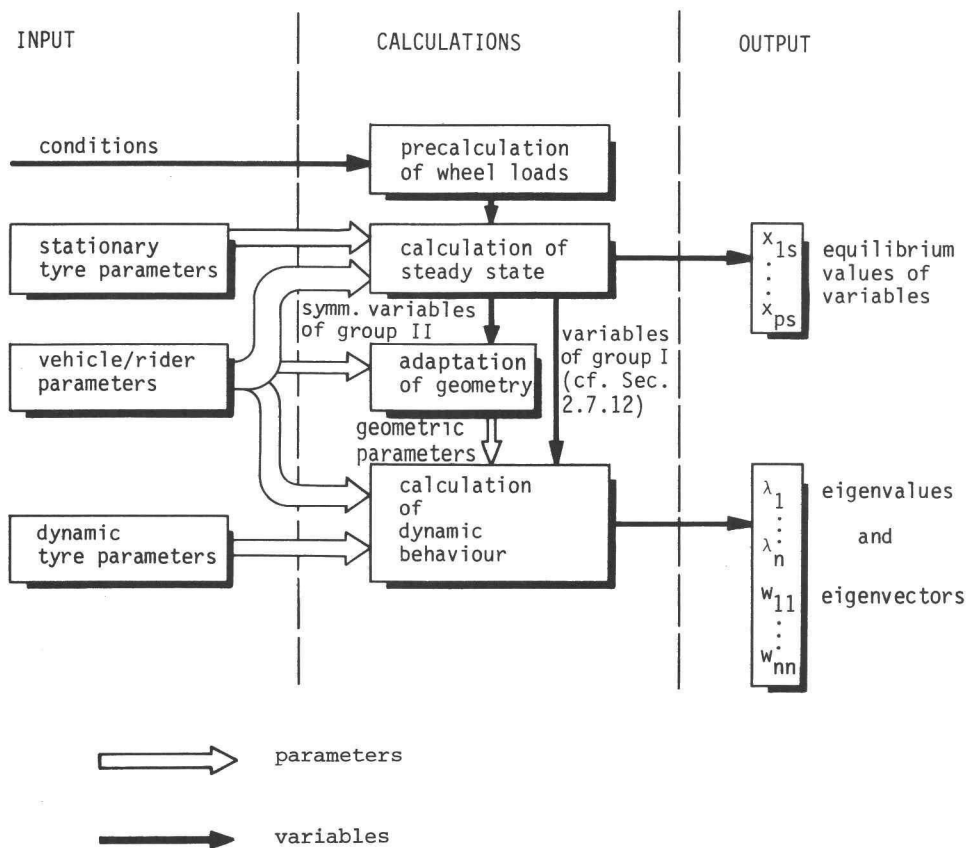


Fig. 39 calculation scheme

in the complex plane with the forward speed of the vehicle as variable parameter can be readily studied. The eigenvectors, however, which fully determine the mode shapes, can not easily be related to a complex motion of the physical system. Therefore a graphical animation technique has been employed to visualize the mode shapes.

3.2 Solution of the steady state equations

The set of p simultaneous non-linear algebraic steady state equations has been solved with the Newton-Raphson method. The steady state equations are written in the form:

$$\begin{aligned} f_{1s}(x_{1s}, x_{2s}, \dots, x_{ps}) &= 0 \\ \vdots & \\ \vdots & \\ \vdots & \\ \vdots & \\ f_{ps}(x_{1s}, x_{2s}, \dots, x_{ps}) &= 0 \end{aligned} \quad (89)$$

A starting value $x_{is,1}$ has been assigned to each variable ($i = 1 \dots p$). In the iteration process these values are adjusted by adding the increments $h_{is,n}$:

$$x_{is,n+1} = x_{is,n} + h_{is,n} \quad (90)$$

The increments $h_{is,n}$ can be obtained from:

$$\begin{aligned} h_{1s,n} \frac{\partial f_{1s}}{\partial x_{1s}}(x_{1s,n}, \dots, x_{ps,n}) + \dots + h_{ps,n} \frac{\partial f_{1s}}{\partial x_{ps}}(x_{1s,n}, \dots, x_{ps,n}) &= -f_{1s}(x_{1s,n}, \dots, x_{ps,n}) \\ \vdots & \\ \vdots & \\ h_{1s,n} \frac{\partial f_{ps}}{\partial x_{1s}}(x_{1s,n}, \dots, x_{ps,n}) + \dots + h_{ps,n} \frac{\partial f_{ps}}{\partial x_{ps}}(x_{1s,n}, \dots, x_{ps,n}) &= -f_{ps}(x_{1s,n}, \dots, x_{ps,n}) \end{aligned} \quad (91)$$

In matrix notation these equations read:

$$\bar{s} \bar{h}_{s,n} = -\bar{f}_{s,n} \quad (92)$$

with:

$$\bar{h}_{s,n}^T = (h_{1s,n}, \dots, h_{ps,n}) \quad (93)$$

$$\bar{f}_{s,n}^T = f_{1s}(x_{1s,n}, \dots, x_{ps,n}), \dots, f_{ps}(x_{1s,n}, \dots, x_{ps,n}) \quad (94)$$

and the matrix \bar{S} with elements:

$$s_{i,j} = \frac{\partial f_{is}}{\partial x_{js}} \quad (95)$$

From equation (92) $\bar{h}_{s,n}$ can be solved as follows:

$$\bar{S}^{-1} \bar{S} \bar{h}_{s,n} = -\bar{S}^{-1} \bar{f}_{s,n} \quad (96)$$

$$\bar{h}_{s,n} = -\bar{S}^{-1} \bar{f}_{s,n} \quad (97)$$

The process is now repeated until all increments have become smaller than an arbitrarily chosen small value. From the physical nature of the problem, it is expected that the process is convergent. Thus the relevant solution can be obtained, if the iteration starting values have been chosen properly.

3.3 Calculation of the eigen-solutions

The set of differential equations determining the non-stationary situation is of the form (cf. Fig. 38):

$$M \ddot{\bar{x}} + K \dot{\bar{x}} + C \bar{x} = \bar{0} \quad (98)$$

Some variables occur up to their first time derivative, the remaining up to their second time derivative. As to transform the set (98) into a set of first-order equations, new variables, related to the latter group, are introduced:

$$\begin{aligned} \tilde{z}_3 &= \dot{\tilde{\phi}} \\ \tilde{z}_4 &= \ddot{\tilde{\phi}} \\ \tilde{z}_5 &= \dot{\tilde{s}} \\ \tilde{z}_6 &= \ddot{\tilde{s}}_r \\ \tilde{z}_7 &= \dot{\tilde{\theta}} \\ \tilde{z}_8 &= \ddot{\tilde{\lambda}}_{t2} \\ \tilde{z}_9 &= \ddot{\tilde{\lambda}}_{s2} \\ \tilde{z}_{10} &= \ddot{\tilde{\lambda}}_{s1} \end{aligned} \quad (99)$$

The new vector of state variables, \bar{z} , is completed as follows:

$$\begin{aligned} \tilde{z}_1 &= \tilde{x}_1 \\ \tilde{z}_2 &= \tilde{x}_2 \end{aligned} \quad (100)$$

and for $i = 3$ to 20:

$$\tilde{z}_{i+8} = \tilde{x}_i \quad (101)$$

The state vector now reads (28 elements):

$$\begin{aligned} \tilde{z}^T = & (\dot{\tilde{v}}, \dot{\tilde{r}}, \dot{\tilde{\phi}}, \dot{\tilde{\delta}}, \dot{\tilde{\beta}}, \dot{\tilde{\phi}}, \dot{\tilde{\theta}}, \dot{\tilde{\lambda}}_{t2}, \dot{\tilde{\lambda}}_{s2}, \dot{\tilde{\lambda}}_{s1}, \dot{\tilde{\phi}}, \dot{\tilde{\delta}}, \dot{\tilde{\beta}}, \dot{\tilde{\phi}}, \dot{\tilde{\theta}}, \dot{\tilde{\lambda}}_{t2}, \dot{\tilde{\lambda}}_{s2}, \dot{\tilde{\lambda}}_{s1}, \tilde{F}_{y1}, \tilde{M}_{z1\alpha}, \tilde{M}_{z1\gamma}, \tilde{M}_{z1\rho}, \tilde{M}_{x1}, \tilde{F}_{y2}, \tilde{M}_{z2\alpha}, \tilde{M}_{z2\gamma}, \tilde{M}_{z2\rho}, \tilde{M}_{x2}) \\ & (102) \end{aligned}$$

Employing this new vector of variables the set of equations may be re-written in the form:

$$\bar{A} \dot{\tilde{z}} + \bar{B} \tilde{z} = \bar{0} \quad (103)$$

The structure of the matrices \bar{A} and \bar{B} has been shown in Fig. 40. A solution is assumed of the form:

$$\tilde{z} = \bar{Z} e^{\lambda t} \quad (104)$$

Substitution of this solution in the equations yields:

$$(\lambda \bar{A} + \bar{B}) \bar{Z} = \bar{0} \quad (105)$$

Multiplication by \bar{A}^{-1} yields:

$$(\bar{A}^{-1} \lambda \bar{A} + \bar{A}^{-1} \bar{B}) \bar{Z} = \bar{0} \quad (106)$$

The eigenvalues λ can now be solved from the characteristic equation:

$$|\lambda \bar{I} - \bar{E}| = 0 \quad (107)$$

with:

$$\bar{E} = -\bar{A}^{-1}\bar{B} \quad (108)$$

and \bar{I} being the unity matrix. From equation (106) n solutions for λ can be obtained, n being the order of the set of equations. The total solution of the homogeneous system reads:

$$\bar{z} = \sum_{i=1}^n c_i \bar{Z}_i e^{\lambda_i t} \quad (109)$$

		inertia coefficients				implicit M_{gyr}				damping coeff.				stiffness coeff.				originally right hand members										
		qualifications concerning vehicle/rider equations		vehicle/rider equations		dynamic tyre behaviour reduction equations		qualifications concerning tyre behaviour equations		qualifications concerning the relaxation effects		damping coeff.		stiffness coeff.		right hand members + load dependency terms (partially)												
1	6	1	7	2	3	10	11	18	19	28	1	6	7	10	11	18	19	28	1	6	7	10	11	18	19	28		
6	10	18	19	28	1	6	7	10	11	18	19	28	1	6	7	10	11	18	19	28	1	6	7	10	11	18	19	28
18	19	28	1	6	7	10	11	18	19	28	1	6	7	10	11	18	19	28	1	6	7	10	11	18	19	28		
19	28	1	6	7	10	11	18	19	28	1	6	7	10	11	18	19	28	1	6	7	10	11	18	19	28			

Fig. 40 structure of the matrices \bar{A} and \bar{B} in expression (103); the corresponding state vector reads:

$$\begin{aligned} \tilde{\mathbf{T}}^T = (\begin{array}{ccccccccc} \tilde{\mathbf{x}}_T & \tilde{\mathbf{v}}_T & \tilde{\mathbf{r}}_T & \tilde{\mathbf{\phi}}_T & \tilde{\mathbf{s}}_T & \tilde{\mathbf{\beta}}_T & \tilde{\mathbf{\phi}}_R & \tilde{\mathbf{r}}_R \\ \tilde{\mathbf{x}}_T & 0 & \lambda_{t2} & \lambda_{s2} & \lambda_{s1} & \phi & \delta & \beta & \phi_R \end{array} | \begin{array}{ccccccccc} \tilde{\mathbf{x}}_T & \tilde{\mathbf{v}}_T & \tilde{\mathbf{r}}_T & \tilde{\mathbf{\phi}}_T & \tilde{\mathbf{s}}_T & \tilde{\mathbf{\beta}}_T & \tilde{\mathbf{\phi}}_R & \tilde{\mathbf{r}}_R \\ 0 & \lambda_{t2} & \lambda_{s2} & \lambda_{s1} & \phi & \delta & \beta & \phi_R & \lambda_{t2} & \lambda_{s2} & \lambda_{s1} \end{array} | \begin{array}{ccccccccc} \tilde{\mathbf{x}}_T & \tilde{\mathbf{v}}_T & \tilde{\mathbf{r}}_T & \tilde{\mathbf{\phi}}_T & \tilde{\mathbf{s}}_T & \tilde{\mathbf{\beta}}_T & \tilde{\mathbf{\phi}}_R & \tilde{\mathbf{r}}_R \\ \tilde{\mathbf{F}}_{y1} & M_{z1} & M_{z1} & M_{z1} & \gamma_{z1} & \rho_{x1} & \tilde{\mathbf{F}}_{y2} & M_{z2} & M_{z2} & M_{z2} & \gamma_{z2} & \rho_{x2} \end{array}) \end{aligned}$$

The eigenvectors \bar{Z}_i can be obtained from equation (105) after substitution of the respective eigenvalues. The constants C_i follow from the initial conditions. In our case the initial conditions will be chosen to suit one eigen-mode of motion at a time. This approach leaves C_i as an arbitrary starting amplitude of the i -th mode concerned with the C 's corresponding with the remaining modes left equal to zero.

3.4 Application of computer graphics

The numerical results from the calculations described in Secs. 3.2 and 3.3 fully determine the eigenmotions. The nature of the motions in terms of frequency and damping can be studied from the root-locus plots. On the other hand, the amplitude and phase relations between the variables at a specific mode of motion can be calculated from the corresponding eigenvector. However, an impression of the whole of these amplitude and phase relations, the so-called 'mode shape' is hard to obtain from merely numerical data if the number of variables which significantly participate in the motion is not sufficiently small, as is generally the case with the system at hand.

Therefore an animation technique has been developed, employing computer graphics, in order to obtain visual impressions of the various eigenmotions by actually applying the time varying values of the variables to a visual motorcycle structure.

The inputs to the visualization programme are (cf. Fig. 41):

- the visual structure of the vehicle;
- visualization conditions (the spacial orientation of the spectator; in the nominal situation, relative to the vehicle structure);
- the relevant steady state values of the variables;
- the eigenvalues and eigenvectors.

The main optional outputs are:

- stop action images (superpositions of the situations at various points of time);
- dynamic animations with or without the introduction of exponentially decreasing or increasing amplitude according to the real part of the root.

Furthermore, various derivatives from these outputs are optional, such as the output required to produce a motion picture recording, as has been employed to obtain material for the film "Vibrational Modes of Single Track Vehicles" [1].

The visual appearance of the vehicle has been defined in Figs. 42 and 43. The wheel radii connecting the wheel centres A with the respective contact centres C have been drawn. The small rectangular blocks along these radii represent the radial tyre springs. Spring compression causes the vertical size of the block to diminish. The remaining two narrow rectangular blocks represent the suspension springs. Note that the behaviour of all springs is fully linear, which implies that negative spring lengths are not precluded and that the lower ends of the tyre springs never lose contact with the ground plane. Of the lines of intersection of the wheel planes and the ground plane parts with a length corresponding to the radius of the wheel in question have been drawn on each side of the contact centre. The wide rectangular block on top of the main frame represents the upper part of the rider body.

The mean eye position of the spectator has been defined in the nominal situation by vector \bar{s} , cf. Fig. 44. In the stationary situation the spectator moves along with the vehicle at a constant distance, cf. Fig. 45. From the visualization point of view this implies that u_s , v_s and r_s are not relevant at this stage. Concerning the non-stationary situation, the list of specified variables determining the motion of the visual structure reads:

$$\begin{aligned}
 \tilde{y} & \quad \tilde{\phi}_r \\
 \tilde{\psi} & \quad \theta_s + \tilde{\theta} \\
 \phi_s + \tilde{\phi} & \quad \lambda_{t2s} + \tilde{\lambda}_{t2} \\
 \delta_s + \tilde{\delta} & \quad \lambda_{s2s} + \tilde{\lambda}_{s2} \\
 \tilde{\beta} & \quad \lambda_{s1s} + \tilde{\lambda}_{s1}
 \end{aligned} \tag{110}$$

We will concentrate on periodic eigen-motions concerning one pair of complex conjugate eigenvalues at a time. In that case the phase shift and amplitude ratio between a variable and its time derivative is the same for all variables. Since phase and amplitude of the motion as a whole can be arbitrarily chosen with respect to the visualisation the variables:

$$\dot{\tilde{y}}, \dot{\tilde{\psi}}, \dot{\tilde{\phi}}, \dot{\tilde{\delta}}, \dot{\tilde{\beta}}, \dot{\tilde{\phi}}_r, \dot{\tilde{\lambda}}_{t2}, \dot{\tilde{\lambda}}_{s2}, \dot{\tilde{\lambda}}_{s1}$$

may be employed instead of:

$$\tilde{y}, \tilde{\psi}, \tilde{\phi}, \tilde{\delta}, \tilde{\beta}, \tilde{\phi}_r, \tilde{\lambda}_{t2}, \tilde{\lambda}_{s2}, \tilde{\lambda}_{s1}$$

and serve the same function in the visualisation programme. The lateral

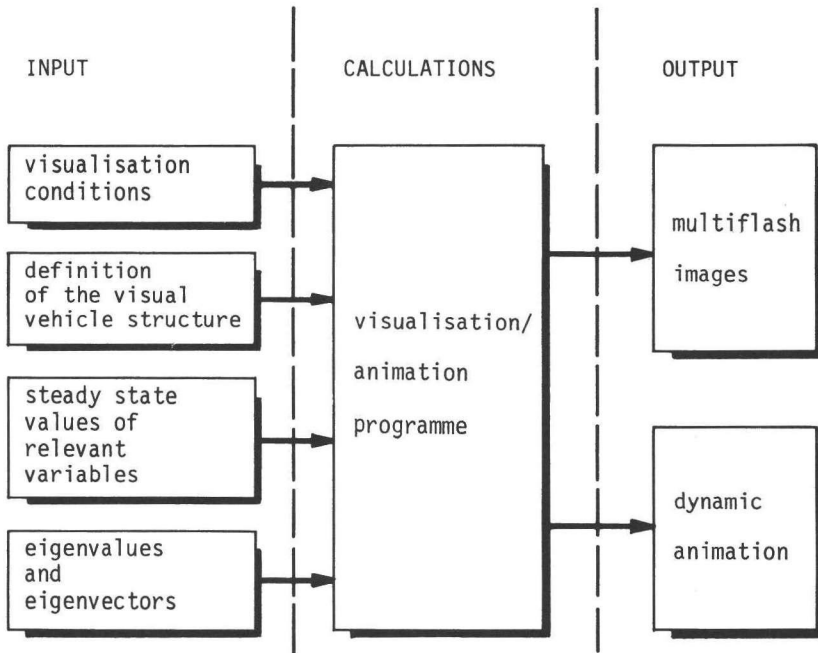


Fig. 41 generation of visual animations of the eigenmotions of the motorcycle/rider structure

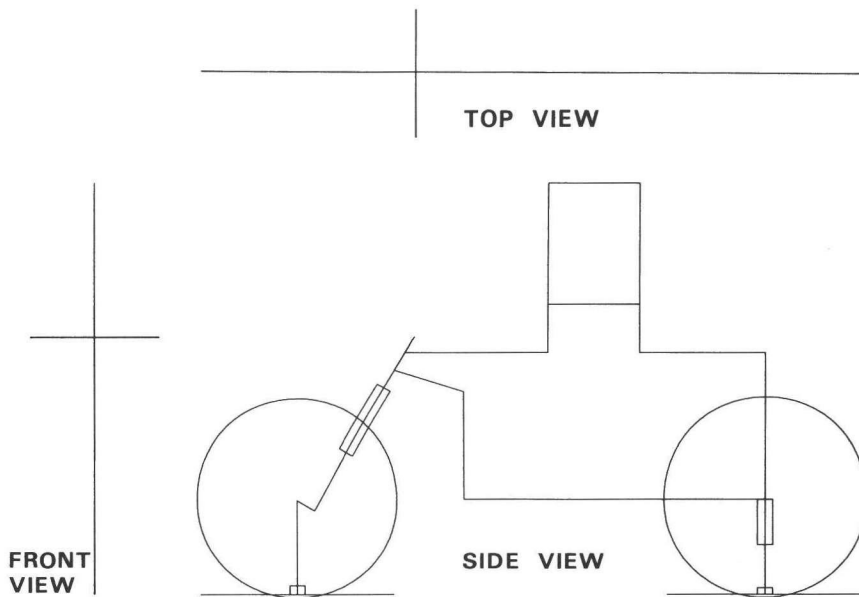


Fig. 42 visual representation of the vehicle structure

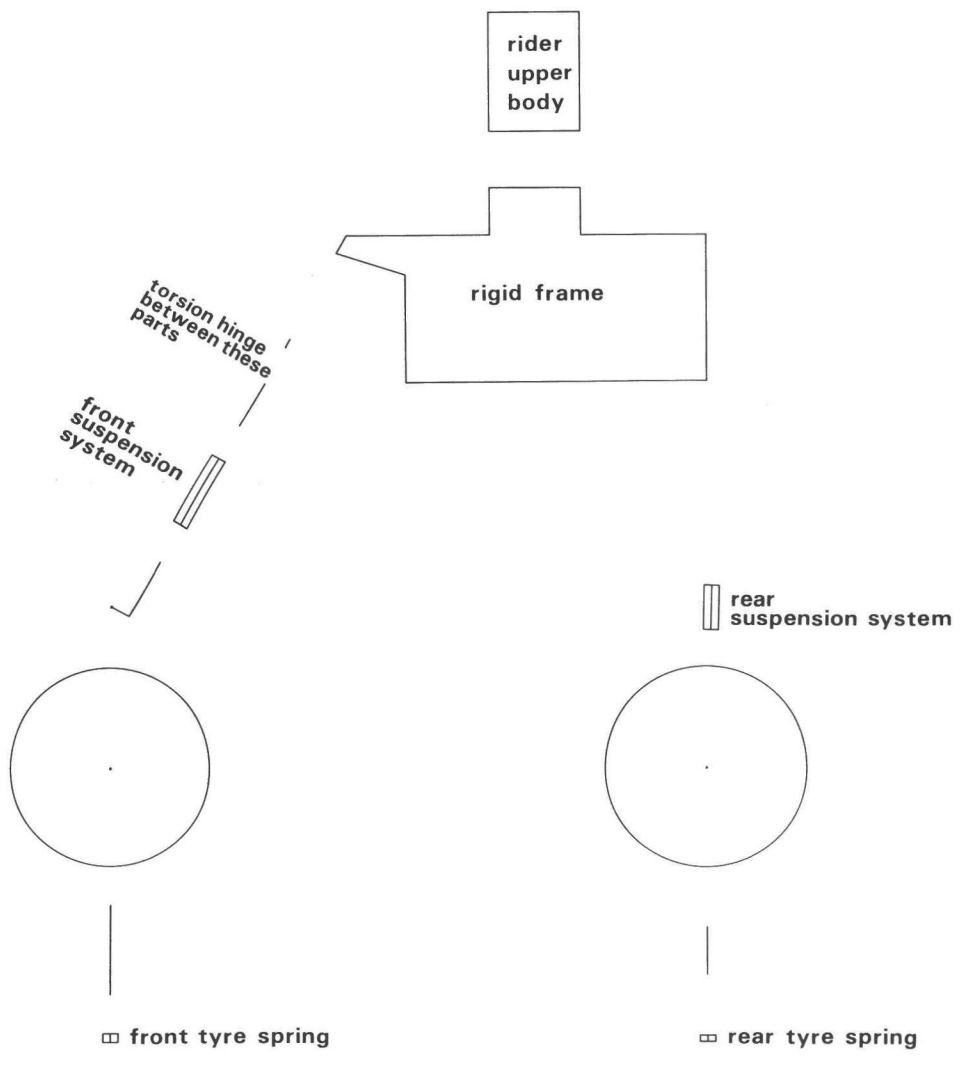


Fig. 43 specification of some parts of the visual representation
of the vehicle structure

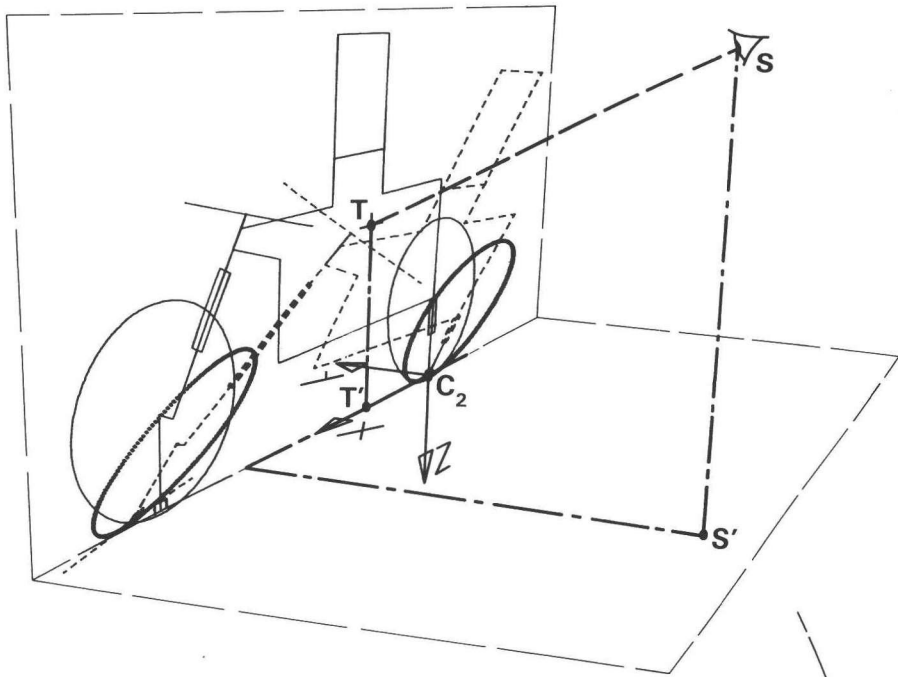


Fig. 44 definition of the mean eye position of the spectator and the target point T which have been defined in the nominal situation relative to the (C_2, x_2, y_x, z_2) -system of axes.

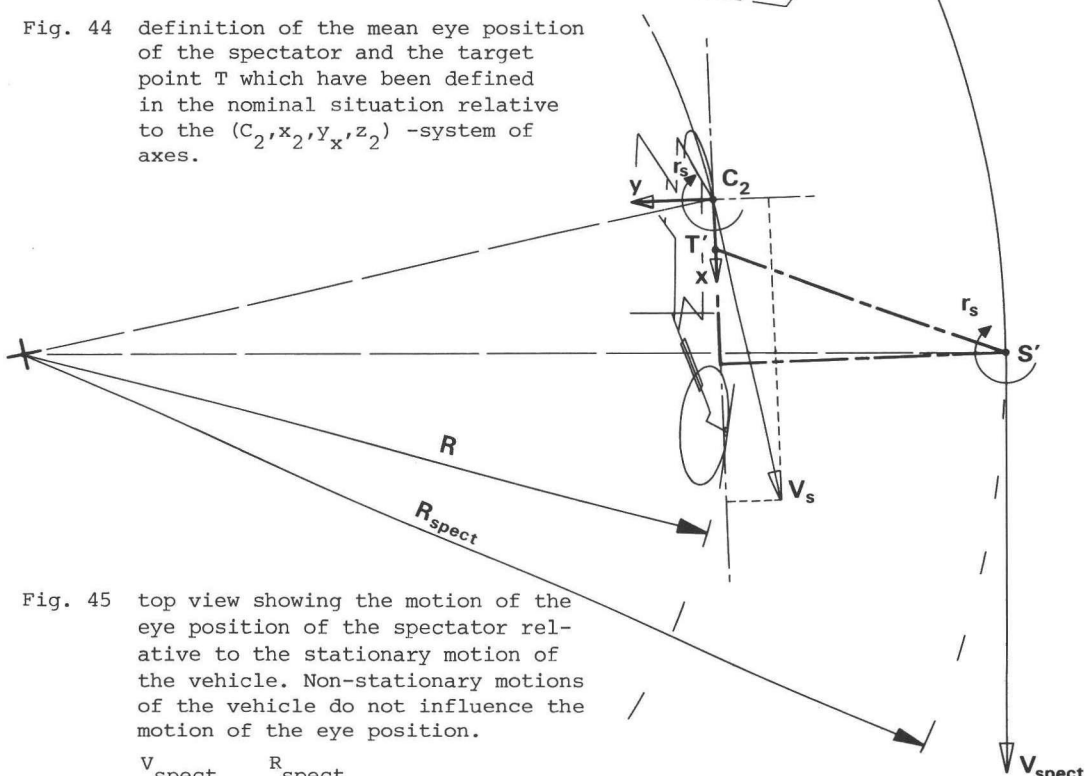


Fig. 45 top view showing the motion of the eye position of the spectator relative to the stationary motion of the vehicle. Non-stationary motions of the vehicle do not influence the motion of the eye position.

$$\frac{v_{\text{spect}}}{v_s} = \frac{R_{\text{spect}}}{R}$$

velocity \tilde{v} does not fully determine the lateral motion of the rear contact centre with respect to the observer since the forward velocity u_s may also give rise to a velocity, perpendicular to the steady-state circular course of the rear wheel contact centre:

$$\dot{\tilde{y}} = \tilde{v} + \tilde{\psi} u_s \quad (111)$$

Note that all elements of Eq. (111), except u_s , are complex. We obtain:

$$r_{RE} = \dot{\psi}_{RE} = \lambda_{RE} \psi_{RE} - \lambda_{IM} \psi_{IM} \quad (112)$$

$$r_{IM} = \dot{\psi}_{IM} = \lambda_{RE} \psi_{IM} + \lambda_{IM} \psi_{RE} \quad (113)$$

And thus:

$$\dot{y}_{RE} = v_{RE} + u_s \frac{\lambda_{RE} r_{RE} + \lambda_{IM} r_{IM}}{\lambda_{RE}^2 + \lambda_{IM}^2} \quad (114)$$

$$\dot{y}_{IM} = v_{IM} + u_s \frac{\lambda_{RE} r_{IM} - \lambda_{IM} r_{RE}}{\lambda_{RE}^2 + \lambda_{IM}^2} \quad (115)$$

4.1 Stationary behaviour

4.1.1 steady state results

The stationary situation (cf. Sec. 2.1) has been defined by the vector of steady state variables, see Eq. (86).

In Fig. 46 the values of some quantities, which are characteristic for each stationary situation, have been depicted for three values of the forward speed, as a function of the normalized lateral acceleration u_r/g , in which u is the forward speed, r the yaw rate ($= \dot{\psi}$) and g the gravitational acceleration.

The simple model according to Fig. 47 predicts:

$$\tan\phi_s = \frac{m u_s r_s}{mg} \quad (116)$$

The tangent of the roll angle of the full model can be seen to deviate from this relation; this is due to a number of factors, e.g. the gyroscopic effects and the overturning moment.

The rear slip angle can be obtained directly from the forward (u_s) and the lateral (v_s) velocities*; the front slip angle required in addition the yaw rate, the actual wheelbase and the steer angle in the road plane, cf. Appendix C. Note that the courses of the slip angles are rather insensitive to the forward speed. This is because of the fact that the camber force, which depends on the camber angle and the normal wheel load only (cf. Eq. (10)), by far dominates the equilibrium of lateral forces in a curve, and that, at the same time, the side force due to side slip is very sensitive to the side slip value. At small values of the lateral acceleration the camber force in this case is slightly too large to obtain the balance and therefore this situation needs negative slip angles. The camber stiffness, however, falls with increasing camber angles (cf. Fig. 18) and thus, above a certain value of the lateral acceleration positive slip angles are required to achieve the necessary side force. Thus the courses of the α -curves strongly depend on the camber properties of the tyres.

The steer moment M_{δ_s} is the resulting small difference of various large

$$* \alpha_{2s} = - \frac{v_s}{u_s}$$

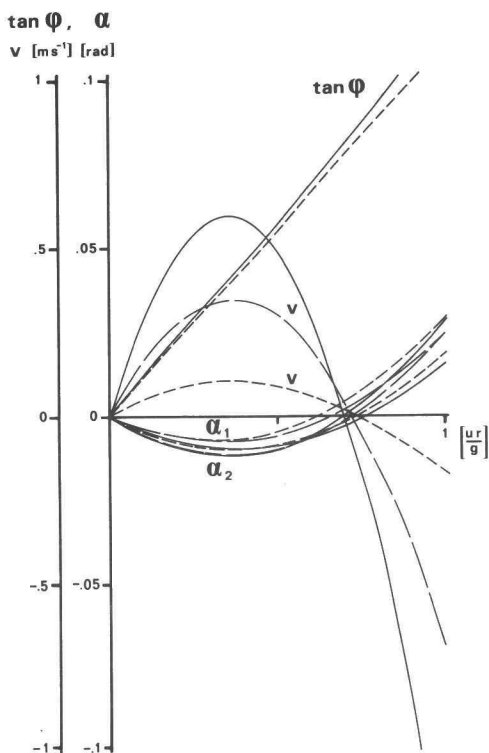
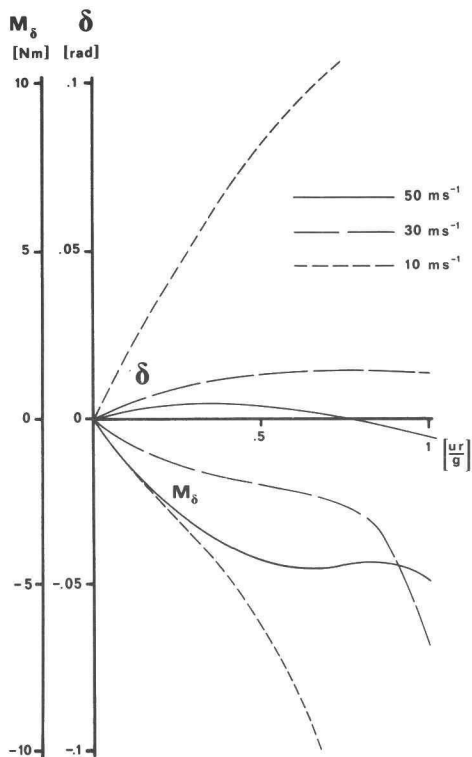


Fig. 46 the stationary behaviour of the baseline model

REAR VIEW

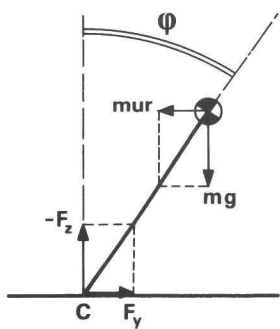


Fig. 47 simple motorcycle model showing the lateral equilibrium in a curve

components, cf. [45], as can be traced from the steady state equations, cf. Appendix E.

At this low speed, cornering requires large steer angles, as can be expected from geometrical considerations, concerning the small turn radius. At increasing speed the motion requires smaller values of δ_s , because of diminution of the geometrical contribution, which occurs due to the increase of the turn radius. Slip effects now playing the major role, the steer angle required even becomes negative beyond a certain value of ur/g .

4.1.2 front contact geometry

From a kinematic point of view the front contact geometry is the most complex aspect of the system at hand. The complexity arises from the combination of the toroidal shape of the front wheel, the inclination of the steer axis and the geometrical trail. Some effects resulting from this combination will be studied in the sequel.

First, consider the nominal situation, cf. Fig. 48a. Each tyre has been represented by a stiff torus. The suspension spring lengths have been fixed in this situation, and will remain so throughout the variations that will be applied. The front contact centre is the origin of the system of axes (C_1, x, y) . Both axes lie in the ground plane, the x -axis pointing forward along the line of intersection of the front wheel centre plane and the ground plane in the nominal situation. A coinciding system of axes (C_{10}, x_o, y_o) is now fixed to the ground plane, and will be used to describe the position of the front contact centre and some other relevant points.

Let us now assume the rear wheel centre plane to roll about its line of intersection with the ground plane, the rear tyre torus maintaining the situation of point contact with the ground plane, the distance between wheel centre and contact centre being adapted accordingly. At a specific value of ϕ the rear wheel centre plane has been fixed. Next a specific value of the steer angle δ has been applied. The pitch angle θ is now adjusted to re-establish the situation of point contact of the front tyre torus and the ground plane.

In the situation, thus achieved, the location of some relevant points has been determined:

- the front contact centre C_1 (in the wheel centre plane and in a plane through the wheel spin axis normal to the road surface), indicated by C;
- the point at which the front tyre torus touches the ground plane, indicated by P;
- the point of intersection of the steer axis and the ground plane, D, which, under the conditions mentioned above, is always located on the x -axis.

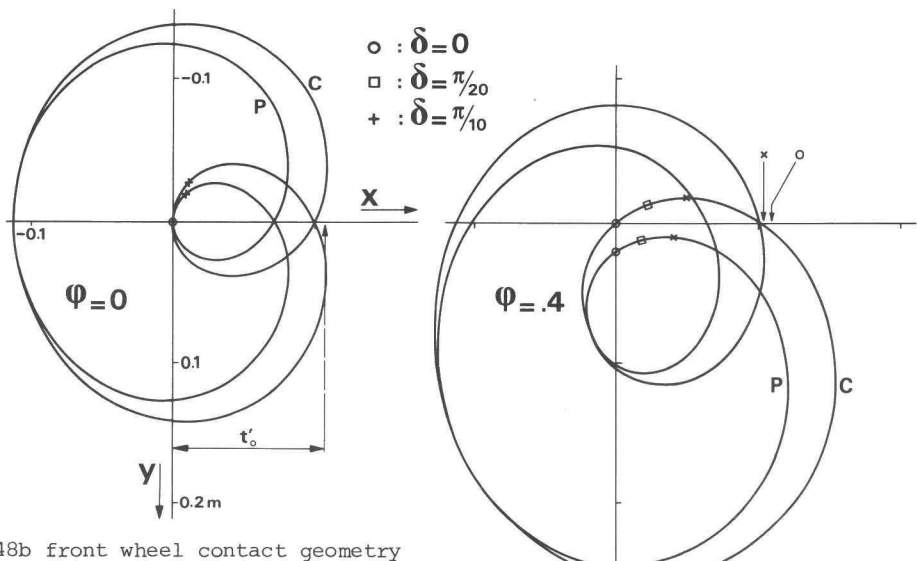


Fig. 48b front wheel contact geometry

C : front contact centre;

P : point at which the stiff torus,
representing the front tyre, touches
the ground.

For $\phi = .4, .8$ the arrows indicate the point of intersection of the steer axis and the ground plane at various values of δ . At $\phi = 0$ and $\delta = 0$ this point is located at t'_o from the origin.
The location varies slightly with δ .

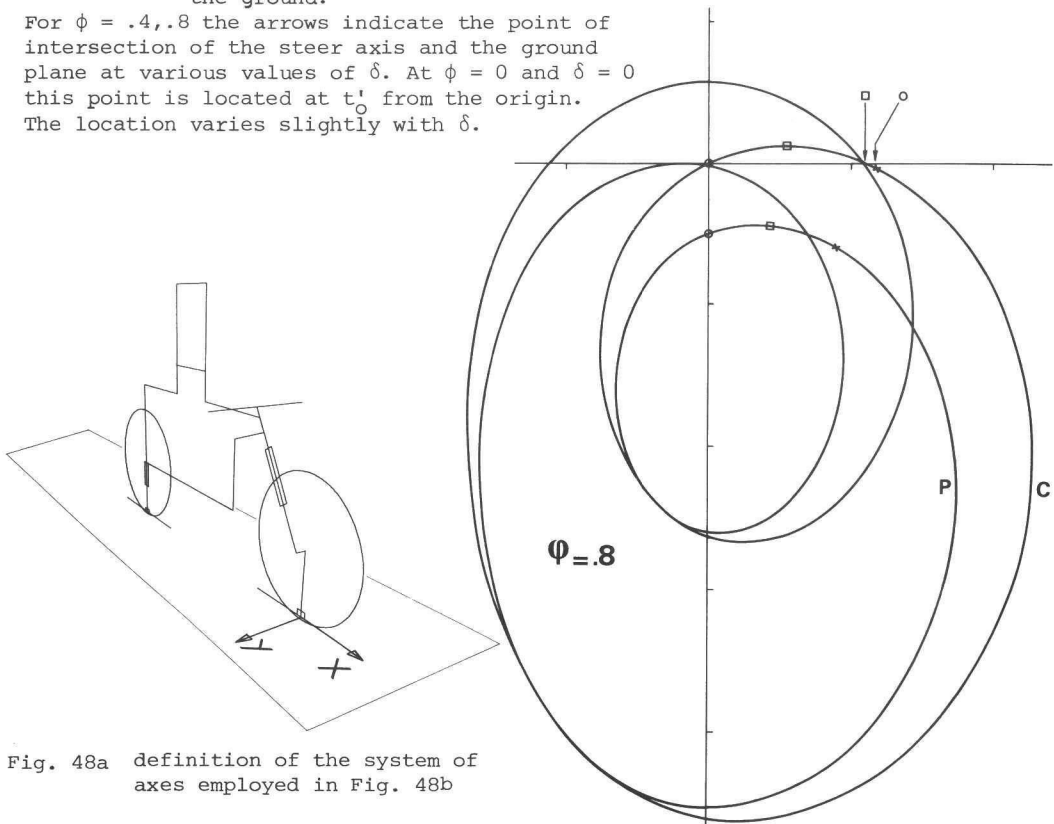


Fig. 48a definition of the system of axes employed in Fig. 48b

At a number of values of ϕ and δ these calculations have been carried out. The situations chosen cover one full revolution of the steer at three discrete values of the roll angle. Fig. 48b presents the corresponding courses of C and P; the position of D has been indicated for a few relevant cases. The most significant phenomenon to be studied in this figure is the high sensitivity of the distance $|\overline{PD}|$ to variations of the steer angle at large values of ϕ . This corresponds to a high sensitivity of the actual mechanical trail to steer angle variations. The variation of the trail has been accounted for in the steady state equations. The equations concerning the dynamic situation, however, have been based on the assumption that the steer angle (stationary plus dynamic) is very small, cf. Secs. 2.7.12 and 2.7.13 and thus the trail remains constant. To be able to investigate the consequences on the dynamic behaviour, in a special case reduction of the trail has been established, cf. Sec. 4.4.2.

4.2 Non-stationary behaviour

4.2.1 general

The dynamic behaviour of the system at hand has been studied in the form of eigenvalues and eigenvectors. Since the order of the set of dynamic equations, n, amounts to 28 (cf. Fig. 40), 28 solutions (generally complex) for λ in the characteristic equation (107) can be obtained. These solutions can be divided into:

- non-significant solutions, arising due to the fact that the algebraic equations for the tyre moments \tilde{M}_{zy} (Eq. (31)), \tilde{M}_{zp} (Eq. (32)) and \tilde{M}_x (Eq. (34)) have been converted into first-order differential equations. These 6 solutions (concerning both the front and the rear tyre) can easily be distinguished by their being heavily damped. This heavy damping is due to the very small value chosen for the dummy relaxation length σ_{DUM} (cf. Appendix G).
- significant solutions, to be divided into
 - monotonous solutions (real solutions; imaginary part zero) and
 - oscillatory solutions, described by a pair of complex conjugate values of λ .

Variation of the input variables or the parameters of the system may cause oscillatory solutions to pass into two monotonous solutions and vice versa.

4.2.2 presentation of the root-loci; baseline results

The lower half of the complex plane, in which the eigenvalues have been presented, cf. Fig. 49, has been omitted since it presents the same information as the upper half (the real axis being the horizontal axis) because the roots are either real or complex conjugate. The presentation is very suitable for complex eigenvalues. For the presentation of the real eigenvalues, however, in this case only one dimension is used, which is detrimental to the surveyability. Therefore, in a few cases the real parts of the eigenvalues have been plotted against the continuously varied parameter. Generally, the real eigenvalues have not been indicated on the real axis in the complex plane.

running-straight-ahead

Figure 50 shows the baseline root-loci of the running-straight-ahead situation ($\phi_s = 0$). The forward speed u_s varies along the curves from 5 to 70 ms^{-1} *; the arrows indicate the solutions corresponding to $u_s = 30 \text{ ms}^{-1}$ and point in the direction of increasing speed. The various modes have been named according to their nature, described by the amplitude and phase relations between the various coordinates involved in the motions. The link between the terms wobble, weave and capsiz, employed in practice to describe various phenomena and the various root locus curves has first been established by Sharp [31]. The terms pitch, bounce and front and rear hop connected with the in-plane behaviour have been transferred from automobile dynamics. The term rear wobble has first been introduced in [20]; the terms twist and shake in connection with motorcycle vibrations in [14].

The root-loci describing the in-plane behaviour vary only slightly with the forward speed. This variation is entirely due to the change of geometry due to aerodynamic forces. Two relatively high-frequency solutions correspond to the hop motion of the respective unsprung masses between the radial tyre spring and the suspension springs and have been called the *front hop mode* and the *rear hop mode* respectively; the low frequency solutions belong to the symmetrical motions of the sprung masses on the suspension springs, and have been called the *pitch mode* (front and rear spring compressions approximately in counter phase) and the *bounce mode* (front and rear spring compressions approximately in phase) respectively.

The root-loci belonging to the anti-symmetrical behaviour all vary significantly with the forward speed. The highest frequency mode, which is well damped throughout the speed range considered, arises due to the inclusion

* below $u_s = 5 \text{ ms}^{-1}$ the assumptions on which the model derivation has been based are not realistic. This matter has been discussed in the conclusions, cf. Sec. 5.1.

of the lumped frame torsional elasticity, and has therefore been called the *twist mode*. The well-known *wobble mode* is mainly a steer oscillation. This mode is lightly damped at speeds of about 15 ms^{-1} . In this speed range the wobble eigenfrequency amounts to 50 rads^{-1} approximately.

The *rear wobble mode* has been named so because, from a mode shape point of view, it can be regarded as a pendant of the wobble mode, concerning the main (rear) frame. This mode is heavily damped except at very low speeds. At a value of about $u_s = 25 \text{ ms}^{-1}$ this mode passes into two monotonous modes of motion.

The oscillatory solution arising due to inclusion of the body lean has been called the *shake mode*. Employing the baseline rider body parameters, the shake mode roots, when varying the parameter u_s , fade into roots belonging to another oscillatory mode: the *weave mode*. At slightly different rider body parameters the shake mode root-locus curve ends detach from the weave mode and constitute one continuous course. The pure shake mode root course, thus obtained, is fairly well-damped throughout the speed range. The phenomenon of the one mode fading into another will be more frequently observed when ϕ_s is being varied (running-straight-ahead \rightarrow cornering). From a root-loci point of view the merging may occur if a parameter is varied in the case of two root-locus curves close to each other in the complex plane, in the same speed range.

Thus in the baseline case the weave mode root course has split up into two parts, each fading into a part of the shake mode root course. Each branch has been named after the composing modes of motion, starting with the low speed part (cf. Fig. 50). The original *weave mode* root course shows instability at very low speed and a tendency to instability at very high speed. In the low speed range this mode shows a tendency to pass into two monotonous solutions.

The real parts of the eigenvalues against the forward speed have been depicted in Fig. 51. Employing this way of presentation monotonous solutions can also be studied. The most significant monotonous solution has been called the *capsize mode*. This commonly accepted term suggests the roll motion to play the major role, which is the case in the low speed range. At high speed, however, the dominating motion of this mode is the deviation from the straight path.

The capsizing mode (c) is slightly unstable above a critical speed of ca. 18 ms^{-1} . Below ca. 8 ms^{-1} the weave/shake mode roots are unstable. Fig. 51 clearly shows the stable speed range from 8 to 18 ms^{-1} .

The remaining monotonous solutions will not be discussed because of their relatively high damping.

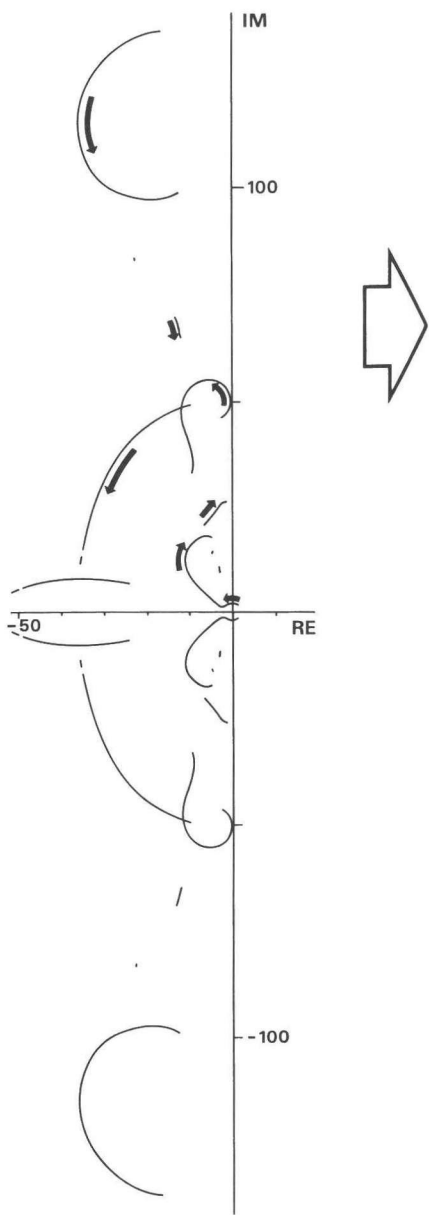


Fig. 49 baseline roots depicted in the complex plane; the arrows indicate the direction of increasing forward speed u_s ; $\phi_s = 0$

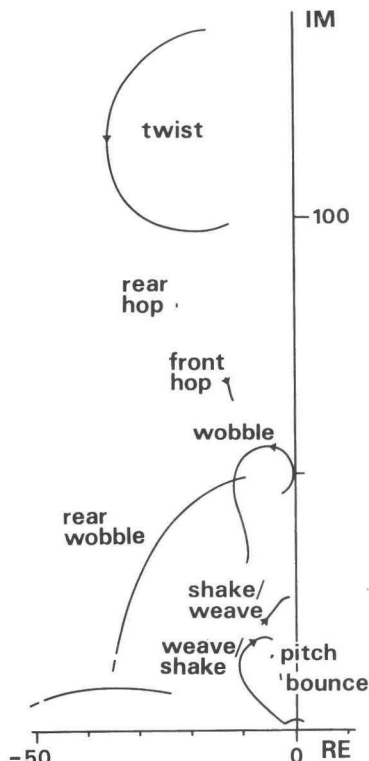


Fig. 50 baseline roots; upper half-plane only

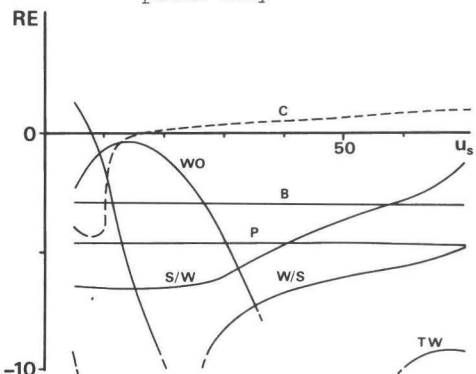


Fig. 51 baseline roots; $\phi_s = 0$; real parts plotted against the forward speed u_s . Note the course of the monotonous 'capsize' mode of motion. The abbreviations have been explained in the text (page 72).

Resuming, the most important roots of the running-straight-ahead behaviour are those of the low speed wobble mode, the low and high speed weave mode and the medium and high speed capsize mode. The phenomena, known from practice, can be identified with some of these roots. A detailed verification, however, is not possible at the moment because of lack of experimental data.

cornering

Starting with the running-straight-ahead situation ($\phi_s = 0$, cf. Fig. 52a), the mean roll angle has been increased with steps of .1 rad up to 1.0 rad (Fig. 52k), a situation beyond the cornering capabilities of the baseline machine at hand.

Regarding the situation up to .5 rad (Fig. 52a to f) a few changes that take place in the root-loci courses at increasing ϕ_s are conspicuous. The twist mode course shifts to higher frequencies, especially the low speed part. The sensitivity of the hop mode courses to the forward speed increases. The wobble mode course moves to slightly lower frequencies. A most significant change is the increase of damping of the high speed weave roots. The pitch and bounce mode root courses become more sensitive to variation of the forward speed. Between $\phi_s = .3$ rad and $\phi_s = .4$ rad a fusion of the weave and the pitch modes occurs.

From $\phi_s = .4$ rad on various more fusions and detachments of the weave/shake and pitch and bounce modes occur. These phenomena will all be traced later on. Between $\phi_s = .8$ rad and $\phi_s = .9$ rad the front hop mode and the wobble mode merge into one another. Between $\phi_s = .9$ rad and $\phi_s = 1.0$ rad they separate again.

In the region from $\phi_s = .6$ rad to $\phi_s = 1.0$ rad* two cornering effects of major importance occur. The instability of a low frequency mode increases throughout the speed range considered; between $\phi_s = .6$ rad and $\phi_s = .8$ rad this mode course entirely crosses the imaginary axis. The origin of this mode will be traced below. This mode corresponds with the phenomenon occurring in practice which is called 'cornering weave'.

The other important effect is the decrease of damping of the front hop respectively wobble/front hop mode. This mode corresponds with the cornering phenomenon known from practice by the name 'wheel patter'.

Concerning the monotonous solutions in Fig. 53 the critical speed of the capsize mode can be seen to decrease with increasing ϕ_s . At $\phi_s = .6$ rad the stable region has entirely disappeared. From $\phi_s = .8$ rad upwards the low-frequency oscillatory mode ('cornering weave') takes over maximum instability and the

* note that under these conditions the curves have been limited to $u_s = 10 \text{ ms}^{-1} \dots 70 \text{ ms}^{-1}$ because of the model validity, cf. Sec. 5.1.

capsize mode stabilizes.

Resuming, when comparing the cornering situation at large roll angles with the running-straight-ahead case the following important aspects are characteristic of the cornering situation:

- the presence of a low-frequency ($< 15 \text{ rads}^{-1}$) mode of motion which is unstable throughout the speed range considered;
- the presence of a lightly damped or (in a certain speed range and depending on the model parameters) unstable front hop respectively wobble/front hop mode of motion at frequencies between 50 and 60 rads^{-1} .

Because of the fusions and detachments of root-locus curves, most root courses of the cornering situation are not simply one-to-one related to those of the running-straight-ahead situation. In order to identify the various modes of the cornering situation, the origins (i.e. the running-straight-ahead modes from which a mode emerges) of the compound oscillatory cornering modes have been traced in detail with the aid of Fig. 54a. The following abbreviations have been employed:

<u>mode:</u>	<u>abbreviation:</u>
twist	TW
rear hop	RH
front hop	FH
wobble	WO
rear wobble	RW
weave	W
shake	S
pitch	P
bounce	B
capsize	C

These names have been defined in the running-straight-ahead case, cf. Fig. 52a. In this situation one fusion is already present: the fusion between the weave mode and the shake mode. In the case of fusions in the running-straight-ahead situation it has been determined whether parts of the fused root curves clearly represent one of the composing modes. If so, each branch has been named after the composing basic modes, starting with the low speed part. Thus the two branches of the combination weave and shake have been identified

as follows:

lower branch : W/S

upper branch : S/W

The cornering root-locus branches have been treated the same way. The following identifications have been obtained for the various root-locus curves of the situation for which $\phi_s = .8 \text{ rad}$ (cf. Fig. 52i and Fig. 54a) :

corn. TW

corn. RH

corn. FH

corn. WO

corn. S/W

P.W/S.P

B.W/S.B

W/S.B.P.W/S

The sequence of the elements of each identification is such that the first element corresponds with the low speed end of the course in question and the last element with the high speed end (just as in the running-straight-ahead case). Note that points have been used as delimiters in the case of fusions due to cornering, while the slashes of the running-straight-ahead mode fusion identification have been maintained.

The root courses corresponding to the twist and rear hop modes and the combined shake/weave mode do not fuse with other courses. In order to distinguish between these cornering modes and their running-straight-ahead counterparts in the text, their identifications have been provided with the designation "cornering" ("corn.").

The identifiactions thus obtained will be employed below to denote the various modes of motion when regarding the mode shapes.

Fig. 54b again shows the baseline root situation, now provided with the mode identification and a more detailed indication of the value of u_s .

To provide a more complete impression of the influence of cornering on the root-loci of the system the baseline results have been depicted once more, but now with the mean roll angle as the continuously varied parameter, for three discrete values of the forward speed, cf. Fig. 55. This presentation is suited to trace the real situation of entering and leaving a curve at a stationary speed of travel. The arrows point in the direction of increasing roll angle at $\phi_s = .4 \text{ rad}$ and $\phi_s = .8 \text{ rad}$.

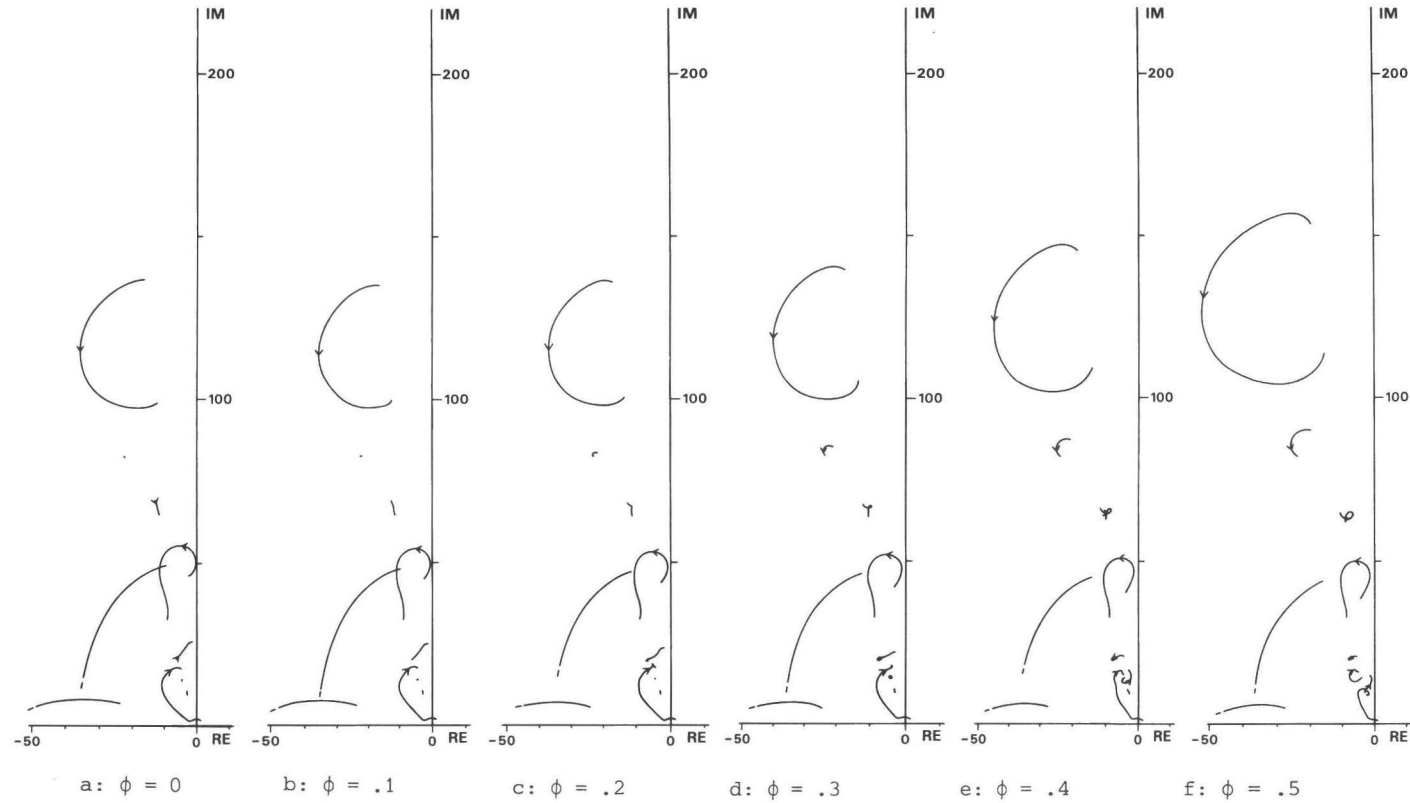
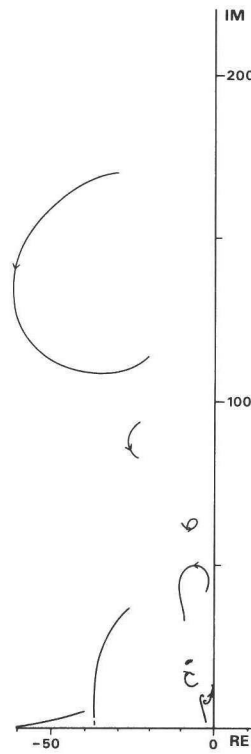
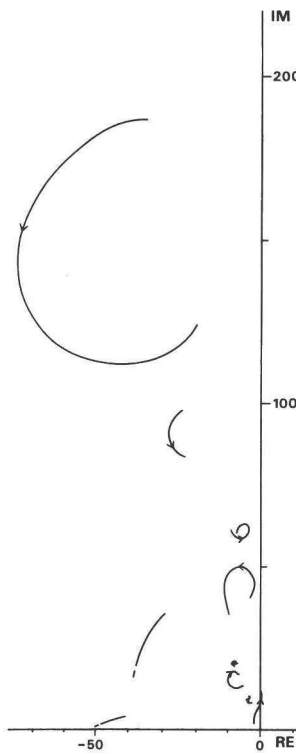


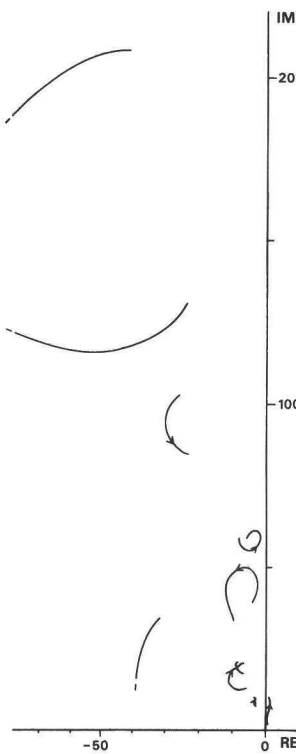
Fig. 52 baseline root-loci for various stages of cornering, starting with the running-straight-ahead situation (a); the arrows point in the direction of increasing speed at 30 ms^{-1} ; the curves start at $u_s = 5 \text{ ms}^{-1}$ ($\phi_s \leq .5$) and end at $u_s = 70 \text{ ms}^{-1}$ unless provided with a dashed line, indicating that not the entire speed range has been covered by that specific curve.



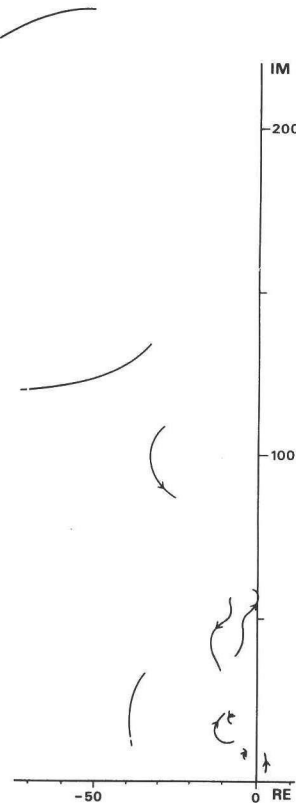
g: $\phi = .6$



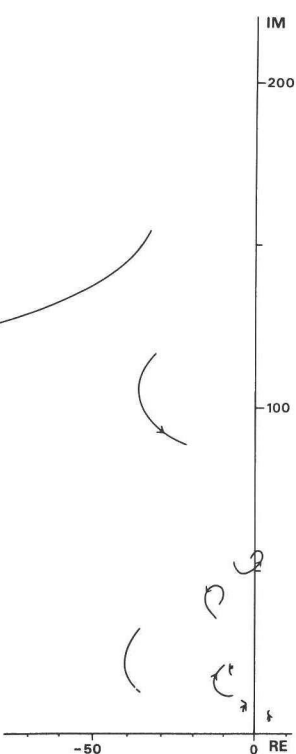
h: $\phi = .7$



i: $\phi = .8$



j: $\phi = .9$



k: $\phi = 1.0 \text{ rad}$

Fig. 52 continued; unless provided with a dashed line, the curves start at $u_s = 10 \text{ ms}^{-1}$ ($\phi_s > .5$) and end at $u_s = 70 \text{ ms}^{-1}$

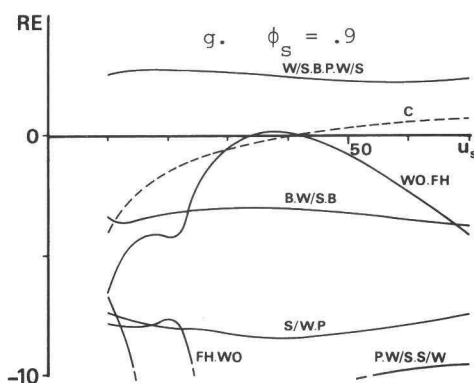
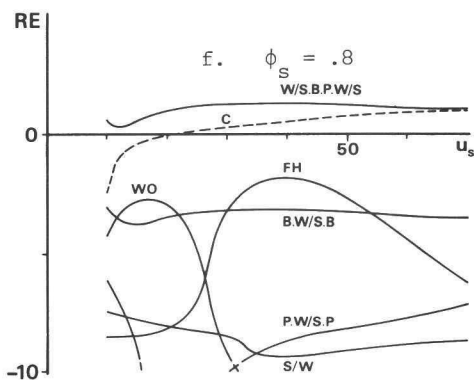
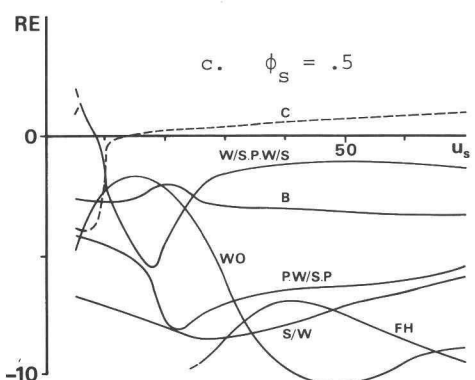
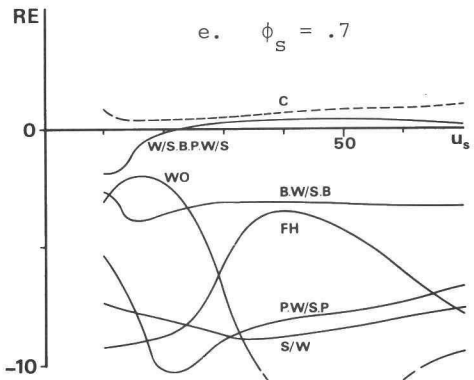
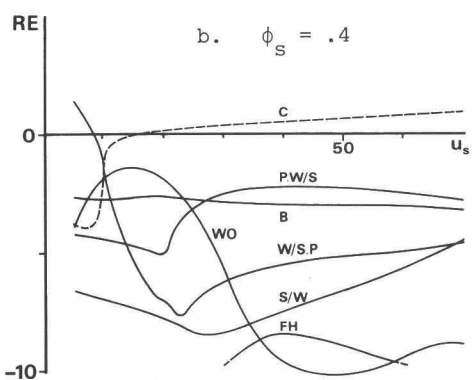
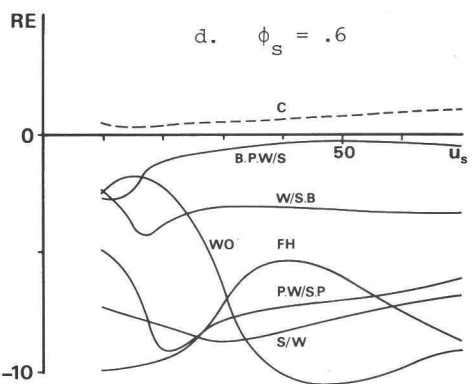
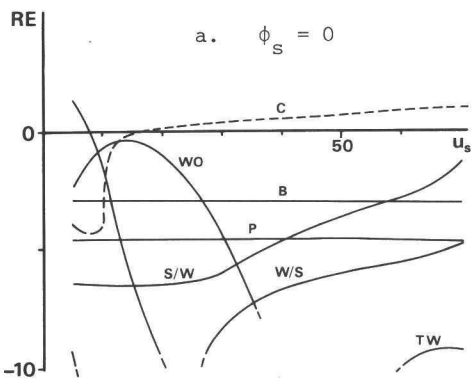


Fig. 53 real parts of the baseline eigenvalues plotted against the forward speed. Mode identification elucidated on pages 72 and 73.

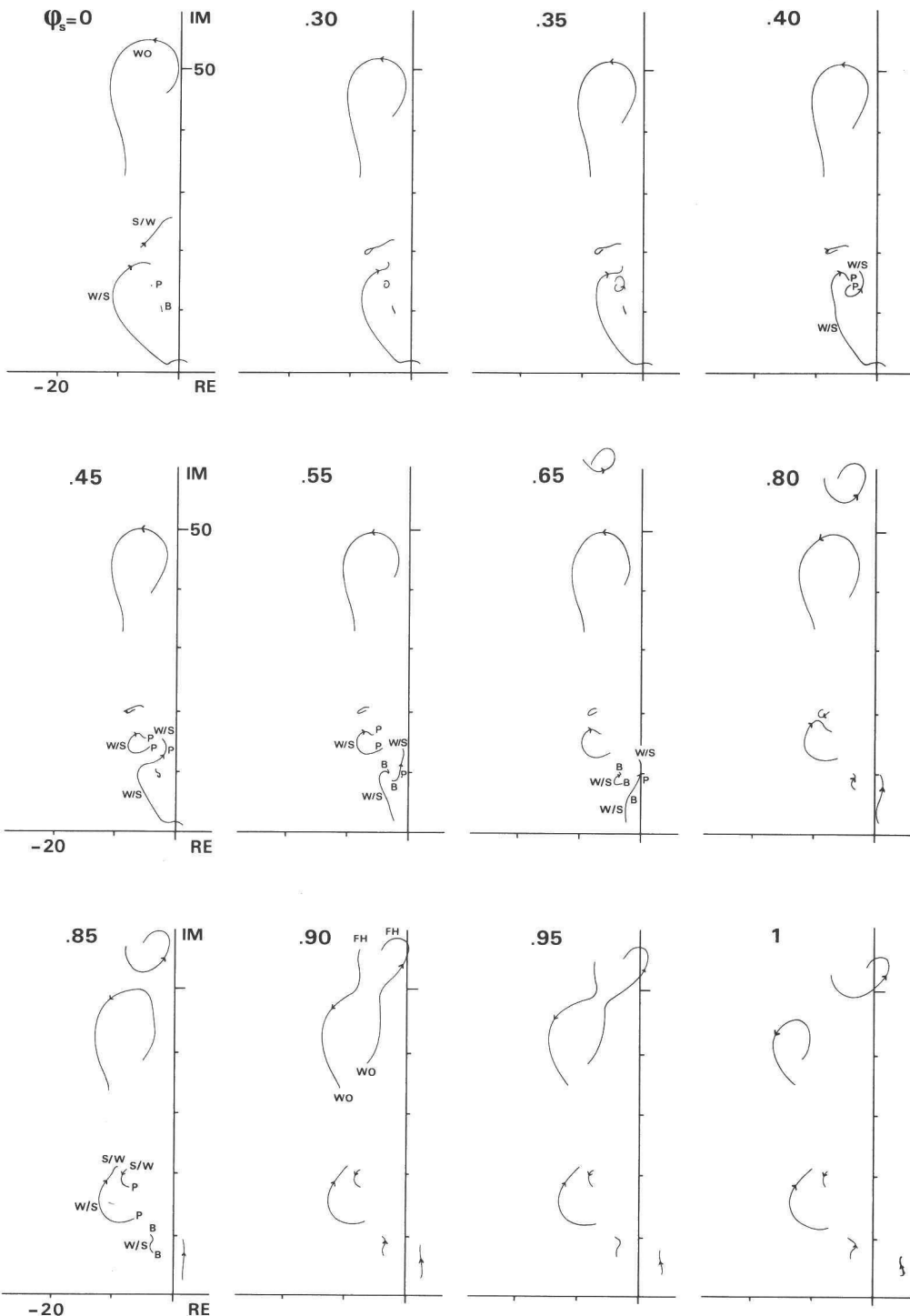


Fig. 54a fusions and detachments of root courses occurring when ϕ_s is varied; root course identification

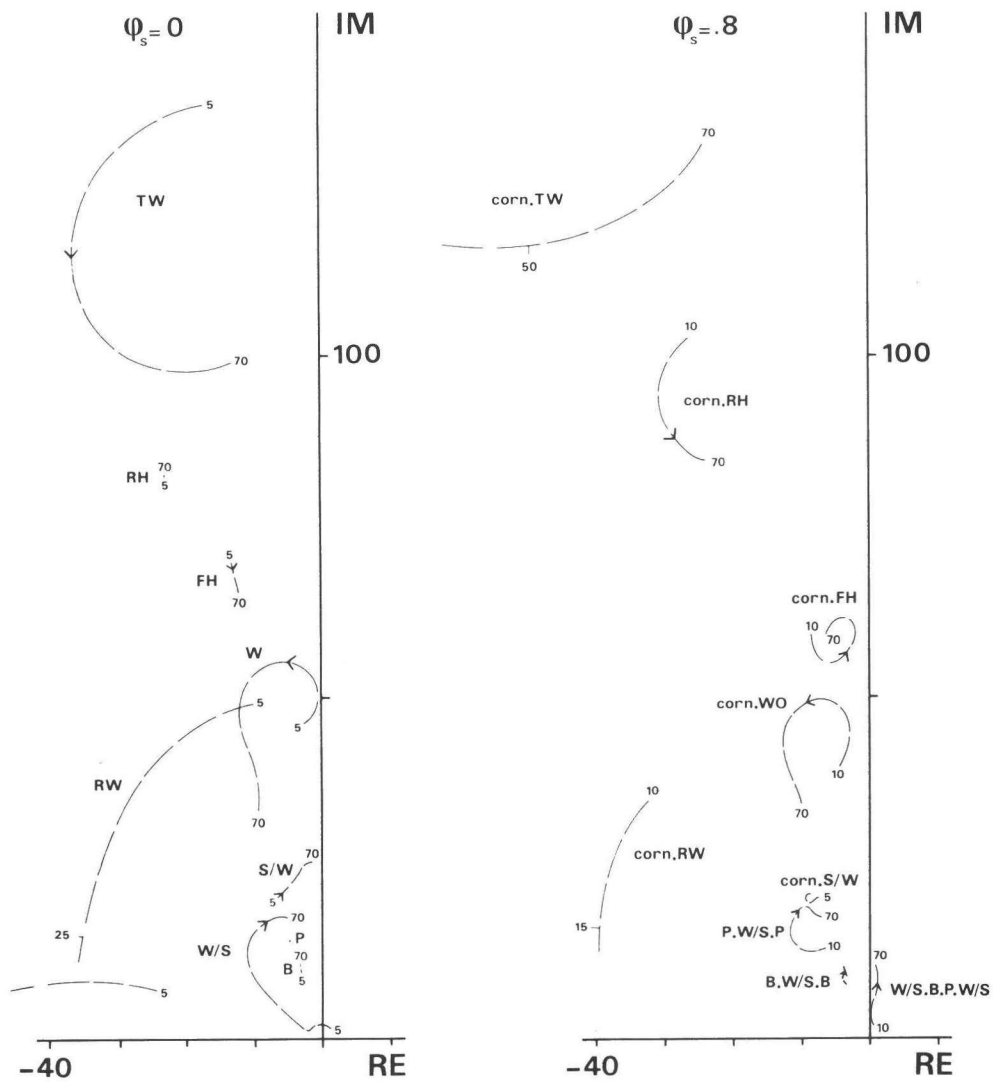
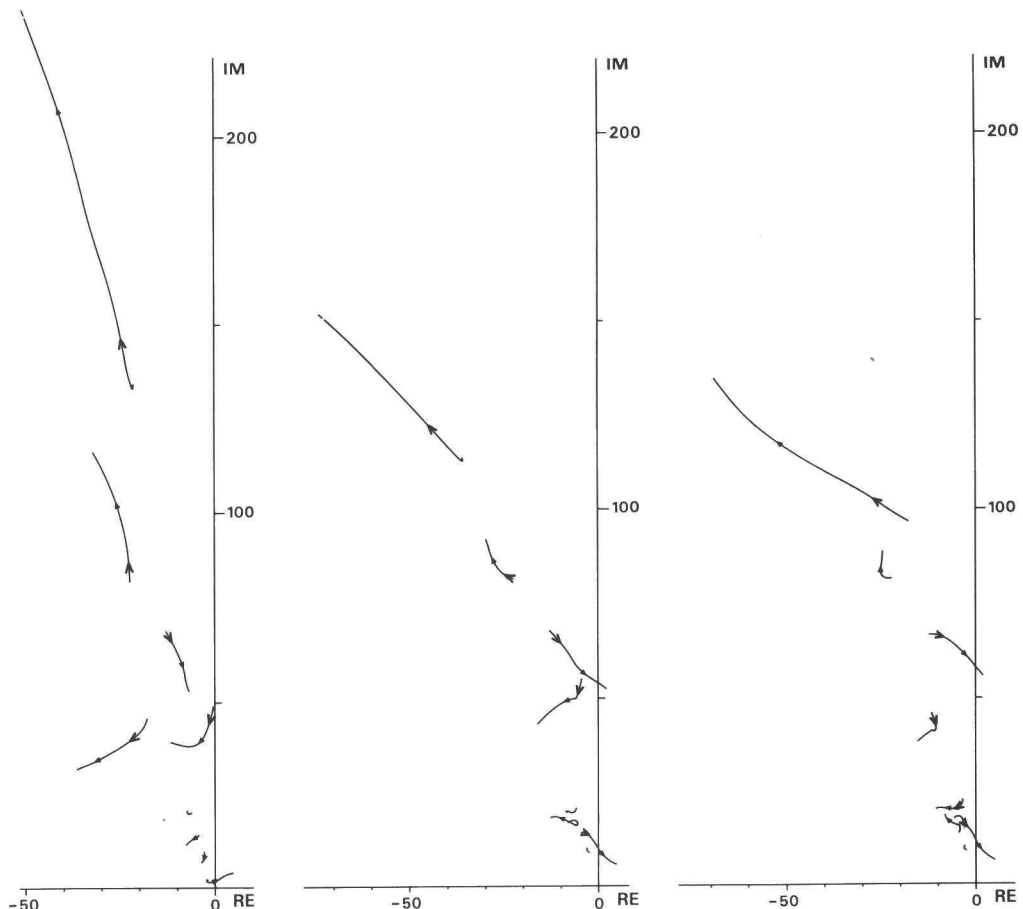


Fig. 54b baseline results; the arrows point in the direction of increasing speed at $u_s = 30 \text{ ms}^{-1}$. The numbers at the root courses denote the forward speed in ms^{-1} corresponding with either the root course end in question or the indicated root locus. The conventions concerning the root course identification are given in Sec. 4.2.2.



a.
 $u_s = 10 \text{ ms}^{-1}$

b.
 $u_s = 30 \text{ ms}^{-1}$

c.
 $u_s = 50 \text{ ms}^{-1}$

Fig. 55 baseline results with ϕ_s being continuously varied.

The curves start at $\phi_s = 0$ and end at $\phi_s = 1.0 \text{ rad}$, unless provided with a dashed line; this indicates that not the entire roll angle range has been covered by that specific curve. Arrows indicate increasing ϕ_s at the points for which $\phi_s = .4 \text{ rad}$ (\blacktriangleright) and $\phi_s = .8 \text{ rad}$ ($\blacktriangleright\!\!\!$).

4.2.3 presentation of the mode shapes; baseline results

In order to provide impressions of the mode shapes a visual animation has been developed, employing computer graphics, cf. Sec. 3.4. The technique which has been used to embody the mode shapes as has been done in this work corresponds to what in photography is called the 'multiflash'- or 'stop-action'-technique, which freezes motion by exposing the same frame at various sequential points of time. This approach will be elucidated with the aid of four examples, shown in the figures 57 to 60. The capitals between brackets employed in the text below refer to the various parts of these figures.

Starting with an arbitrarily chosen pair of complex conjugate solutions:

$$\lambda = a + ib, \quad \bar{w} = \bar{A} + i\bar{B} \quad (117)$$

$$\lambda^* = a - ib, \quad \bar{w}^* = \bar{A} - i\bar{B} \quad (118)$$

we obtain the real part of the vector of eigen-motion solutions x for the variables q :

$$\begin{aligned} \bar{x} &= C (\bar{w} e^{\lambda t} + \bar{w}^* e^{\lambda^* t}) \\ &= C' e^{at} (\bar{A} \cos bt - \bar{B} \sin bt) \end{aligned} \quad (119)$$

Obviously one solution of the pair (117), (118) already provides the information to obtain the result (119). The solution with the positive imaginary part (+ ib) has been employed in the sequel.

Starting with the numerical description (A) of the eigenvector, we obtain the graphical representation (B). The scale of this diagram can be arbitrarily chosen. To achieve time-histories of the variables the eigenvector components have been assumed to rotate with a circular frequency corresponding with the value of λ_{IM} (λ_{IM} positive: rotation from positive RE-axis to positive IM-axis). The absolute value of the components depends on the value of λ_{RE} , the time and the arbitrarily chosen scale. The real parts of the components have been plotted against time (C). These time histories correspond to equation (119).

In order to obtain clear and regular 'multiflash-images' the damping of the motion has been put zero. To show the phase relations more clearly in the time-history the time axis has been re-scaled to show the same number of periods per unit of length for each mode of motion. Of this description of the periodic course of the variables against the scaled time, one period has

been regarded, starting with the maximum of an arbitrarily chosen variable. In the cases to be studied the variable (or function of a number of variables) has been selected which visually dominates the motion. The period has been sampled (D), and each sample has been used to produce a single image of the structure described in Sec. 3.4, adapted to suit the actual values of the variables. The various images have been superimposed, thus forming the 'multi-flash-presentation' of the mode shape (E).

The first sample of the period has been drawn with dashed line to preclude the ambiguity which arises for instance in the case that the representations of the main frame for all points of time coincide, the position of the remaining parts of the vehicle relative to the main frame being different for each point of time. Compared to the graphical representation (B) and the time-history representation (C,D), the multiflash-image lacks one datum, namely the global sequence of the situation, which sequence corresponds to the direction of time in (C) and (D) or the sense of rotation in (B). This datum has been added by marking the second sample of the period with "s".

The number of samples per period has been chosen to suit the visual complexity of the resulting image.

Note that all variables employed in the visualization are first derivatives of angles and positions to the time. This has been done so since the zeroth time derivatives of the lateral position and the yaw angle have not been employed as system variables and have therefore not been represented by elements in the eigenvectors. The set of eigenvector elements corresponding to first time derivatives may be regarded as the set corresponding to the zeroth time derivatives since the amplitude and phase relations between time derivatives of different order are the same for all variables, and the amplitude and starting point ($t = 0$) may be arbitrarily chosen.

Of a selection of baseline solutions the mode shapes have been visualized. The selected roots have been indicated in Fig. 56, the corresponding visualizations in Fig. 61. The relevant root-loci in Fig. 56 have been numbered starting with the running-straight-ahead case at low frequency. These numbers identify the images of Fig. 61.

The mode shapes of the in-plane modes of motion have been presented in a side view, the remaining mode shapes in views showing lateral motion also. Note the position of the centroids of the pitch (4) and bounce (3) modes. The weave/shake mode shape shows a relatively large contribution of the roll angle in the heavily damped zone (compare (5) and (1)). From 10 ms^{-1} to 50 ms^{-1} the phase relation between the roll angle and the lateral position of the

shake/weave mode changes (cf. (7) and (8)). The rear wobble mode shape (9) shows a wobble-like phenomenon at the rear frame assembly. The wobble mode (11), in which the steer angle plays the major role, includes a fair amount of twist, as can best be seen from the original eigenvector. The front and rear hop modes (12) and (13) show only a minute involvement of coordinates other than the respective suspension and tyre spring compression. Note the mean inclination of the frame assemblies at different values of the forward speed, due to aerodynamic effects (cf. mode (3), at 10 ms^{-1} and mode (12), at 50 ms^{-1}). The twist mode (14) can be seen to include a fair amount of steer rotation.

The modes (15) to (20) concern the cornering situation at $\phi_s = .4 \text{ rad}$. In situations in which $\phi_s \neq 0$ in-plane and lateral modes of motion do not occur separately. As can be traced from the Figs. 54 and 61, the pitch phenomenon is involved in both (15) (W/S.P) and (16) (P.W/S). The visualisations clearly show a pitch-orientated location of the centroid of the in-plane motion (cf. (4)). The visualisations (18) and (17) respectively show these modes at higher speed. The W/S.P mode of motion shows a significant alteration of the phase relation between the in-plane and the lateral motion at varying speed, cf. (15) and (18). The low speed part of the P.W/S mode and the high speed part of the W/S.P mode originate from the pitch mode, cf. Fig. 54. This fact can be found again from the visualization when comparing (15) and (16) with (18) and (17) respectively: (18) and (16) show a larger pitch contribution, compared with (15) and (17) respectively. The wobble and front hop modes for $\phi_s = .4$, cf. (19) and (20) respectively can be seen to largely retain their original character. The corresponding root-locus curves are still widely separated at this value of ϕ_s , cf. Fig. 56.

The mode shapes numbered (21) to (32) concern the cornering situation at $\phi_s = .8 \text{ rad}$. The unstable mode W/S.B.P.W/S has been regarded at four different values of the forward speed, cf. (21), (22), (24) and (25). Neither pitch nor bounce motions clearly dominate at any speed. The resultant in-plane motion share increases as the pitch/bounce-frequency range is being approached (which is the case at increasing speed). The mode identified by B.W/S.B does clearly show a bounce character, cf. (23). In mode (26) both the pitch and the shake motion can be clearly recognized. Mode (27) originates directly from the shake/weave mode. Comparison of (8) ($\phi_s = 0$) and (27) ($\phi_s = .8$) provides the specific difference between running-straight-ahead and cornering for this mode: in the latter case a strong pitch-like motion is involved. The modes (29) and (30) show a variation of phase relations as a function of the forward speed. This originally in-plane phenomenon shows participation of the steering angle. Note that, at $\phi_s = .9$, the cornering front hop mode root course has

merged with that of the cornering wobble mode (cf. Fig. 52). The heavily damped rear hop mode retains its original character, cf. (31), while the cornering twist mode exhibits strong participation of the front spring compressions, cf. (32).

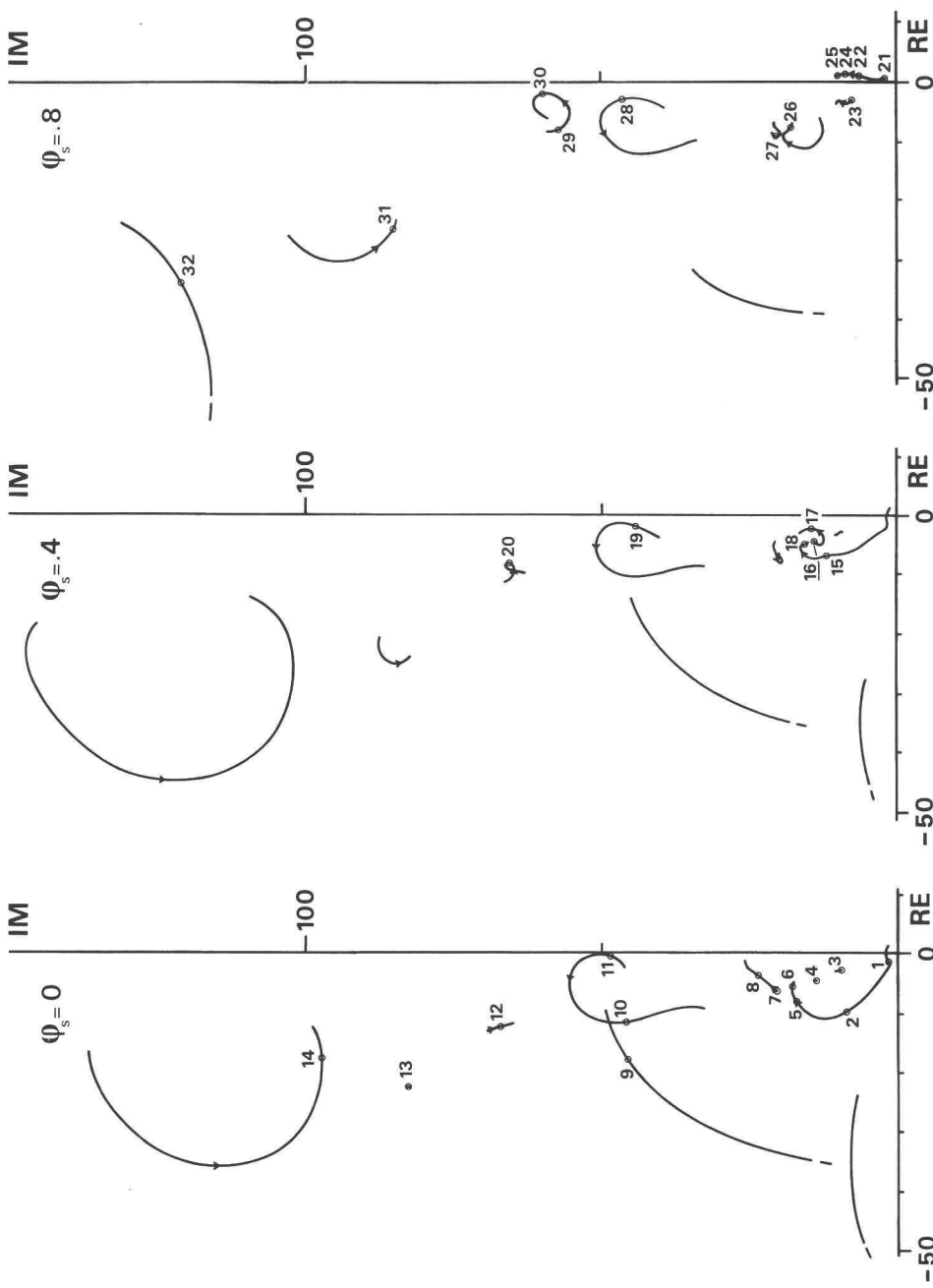
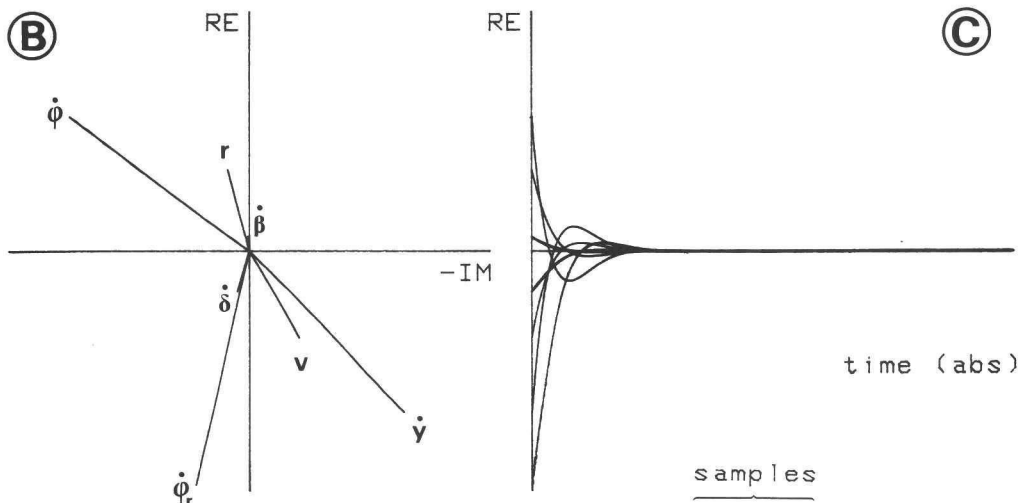


Fig. 56 selected roots of which the corresponding mode shape has been visualized. The numbers of the selected points correspond with the identification numbers of the "multiFlash" plots shown in the Figs. 57 to 61.



Us	Lre	Lim
20	-10.03	8.71
Var	Wre	Wim
y	-.119	-.115
v	-.065	-.037
r	.061	.016
phi	.100	.134
del1	-.031	.009
bet	.011	.001
phr	-.175	.040
the	0.000	0.000
lt2	0.000	0.000
ls2	0.000	0.000
ls1	0.000	0.000

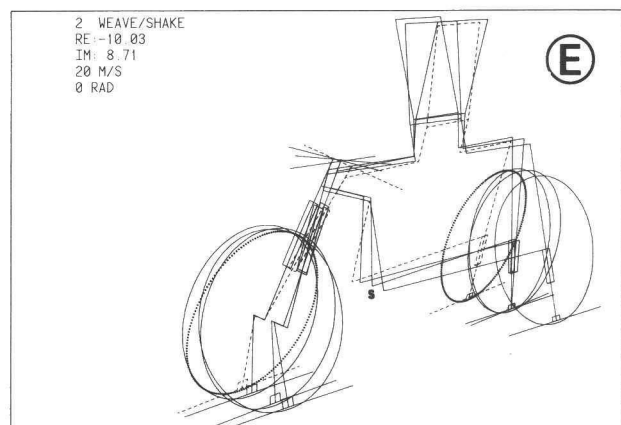
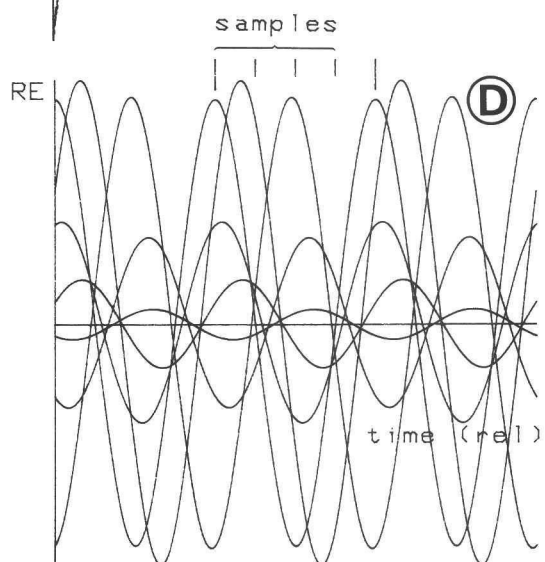


Fig. 57 visualizing the weave/shake mode ②

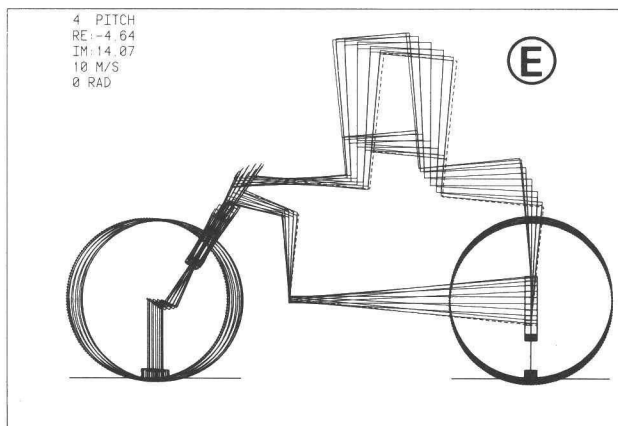
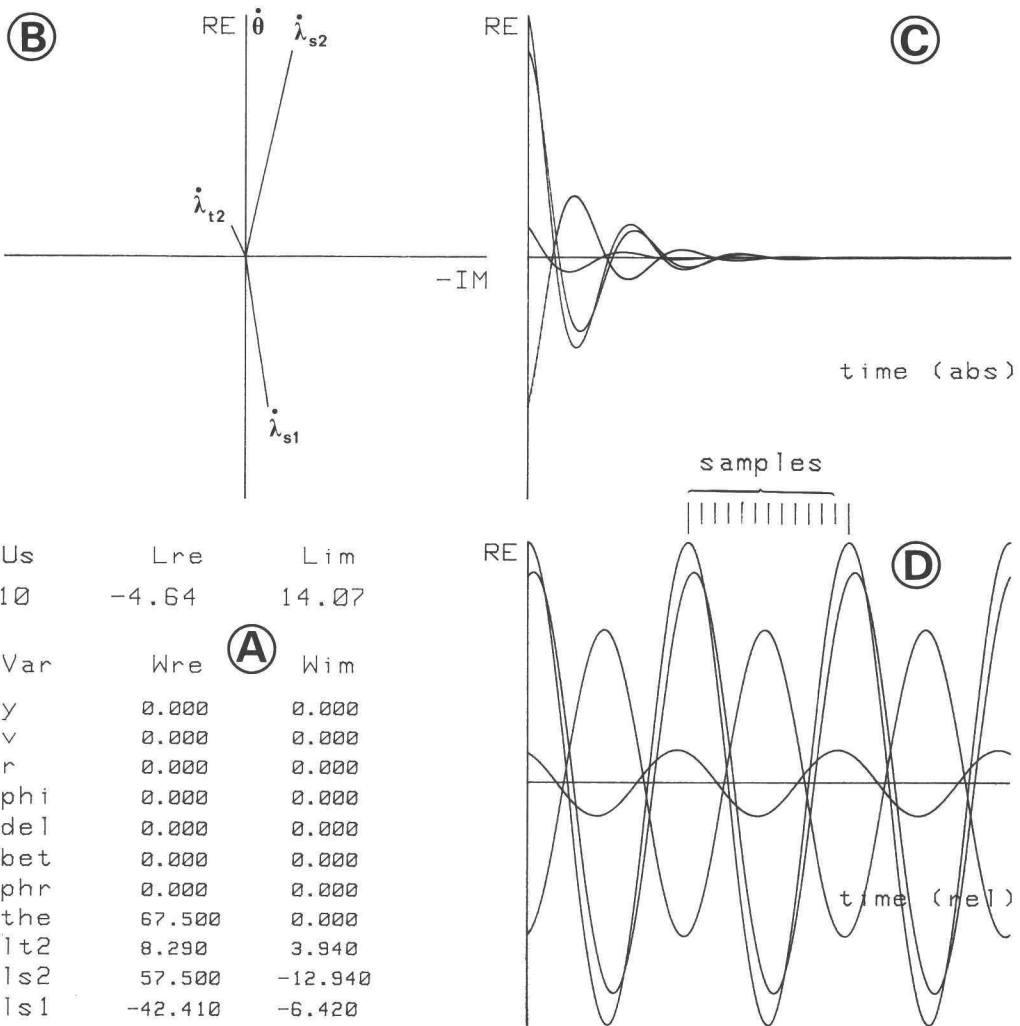
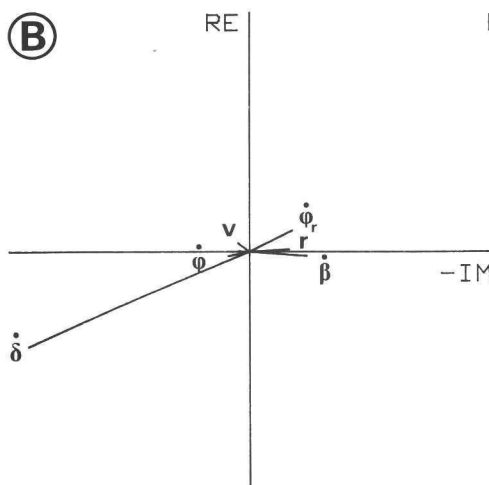


Fig. 58 visualizing the pitch mode ④

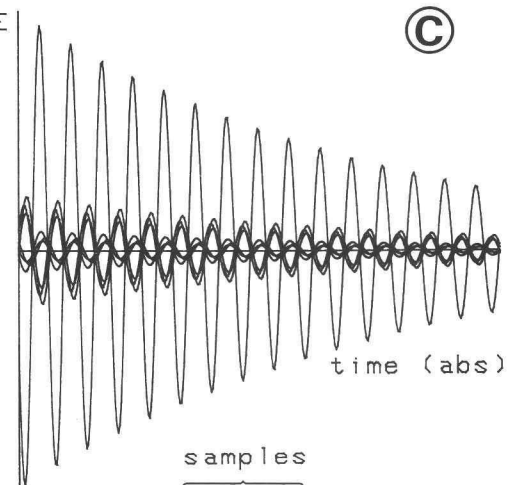
(B)



RE

-IM

(C)



samples

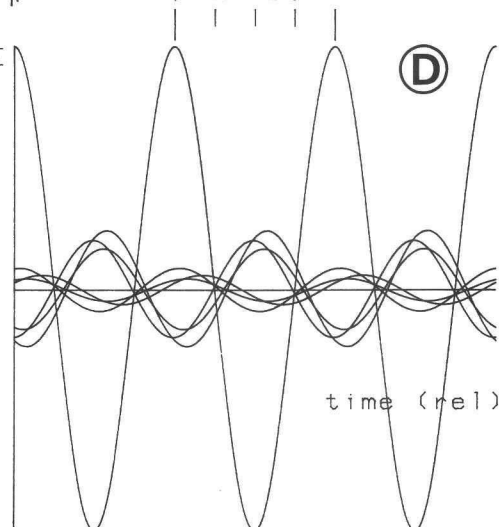
(A)

Us	Lre	Lim
10	-.68	48.50
Var	Wre	Wim
y	.001	.022
v	.018	.023
r	.005	-.080
phi	-.009	.042
del	-.188	.445
bet	-.009	-.115
phr	.044	-.086
the	0.000	0.000
1t2	0.000	0.000
ls2	0.000	0.000
ls1	0.000	0.000

RE

time (rel)

(D)



11 WOBBLE
RE: -682
IM: 48.50
10 M/S
0 RAD

(E)

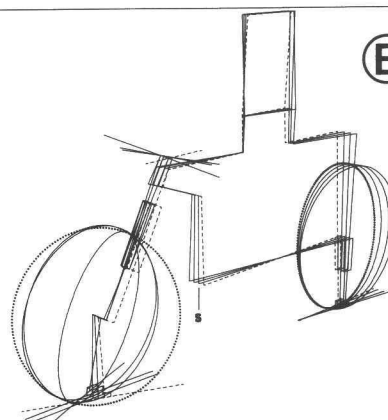


Fig. 59 visualizing the wobble mode 11

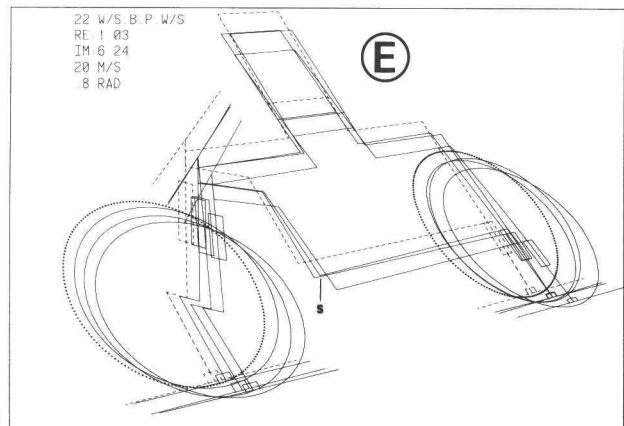
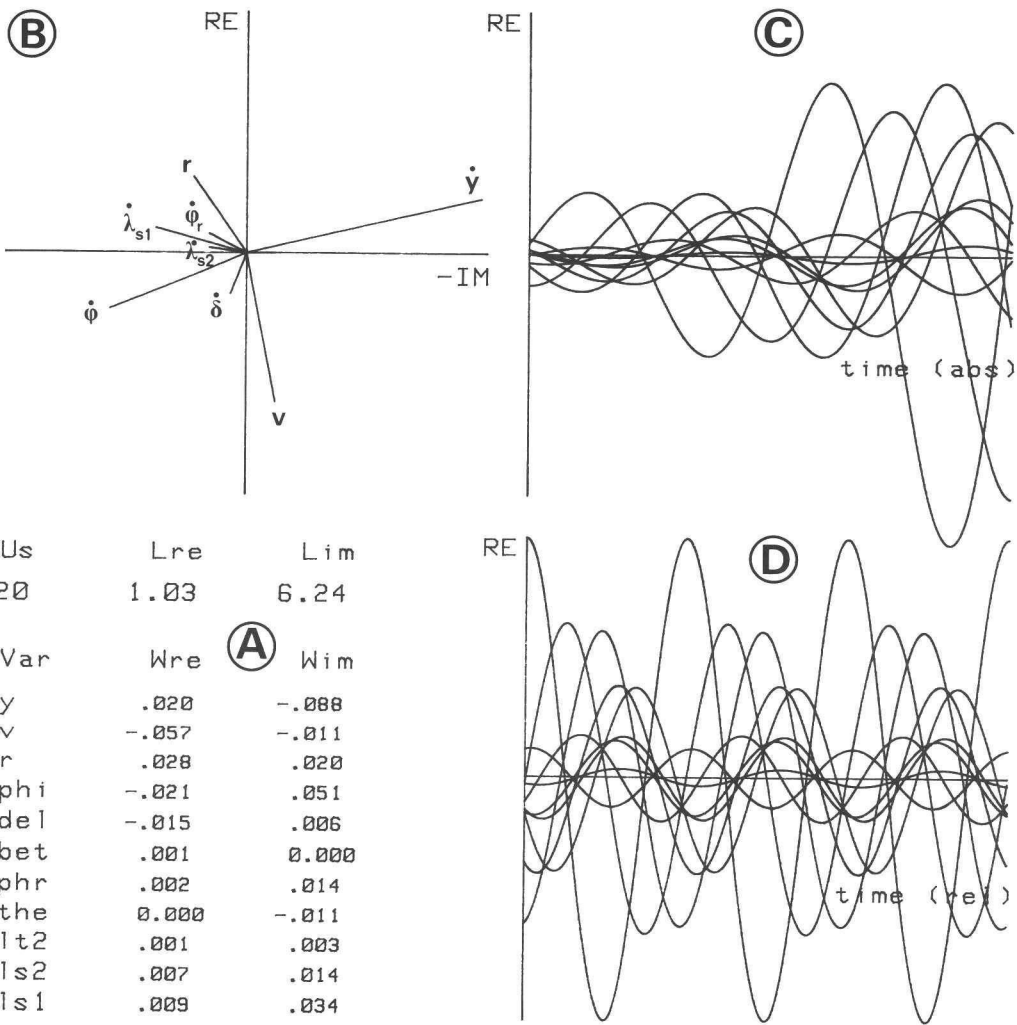


Fig. 60 visualizing the W/S.B.P.W/S mode (22)

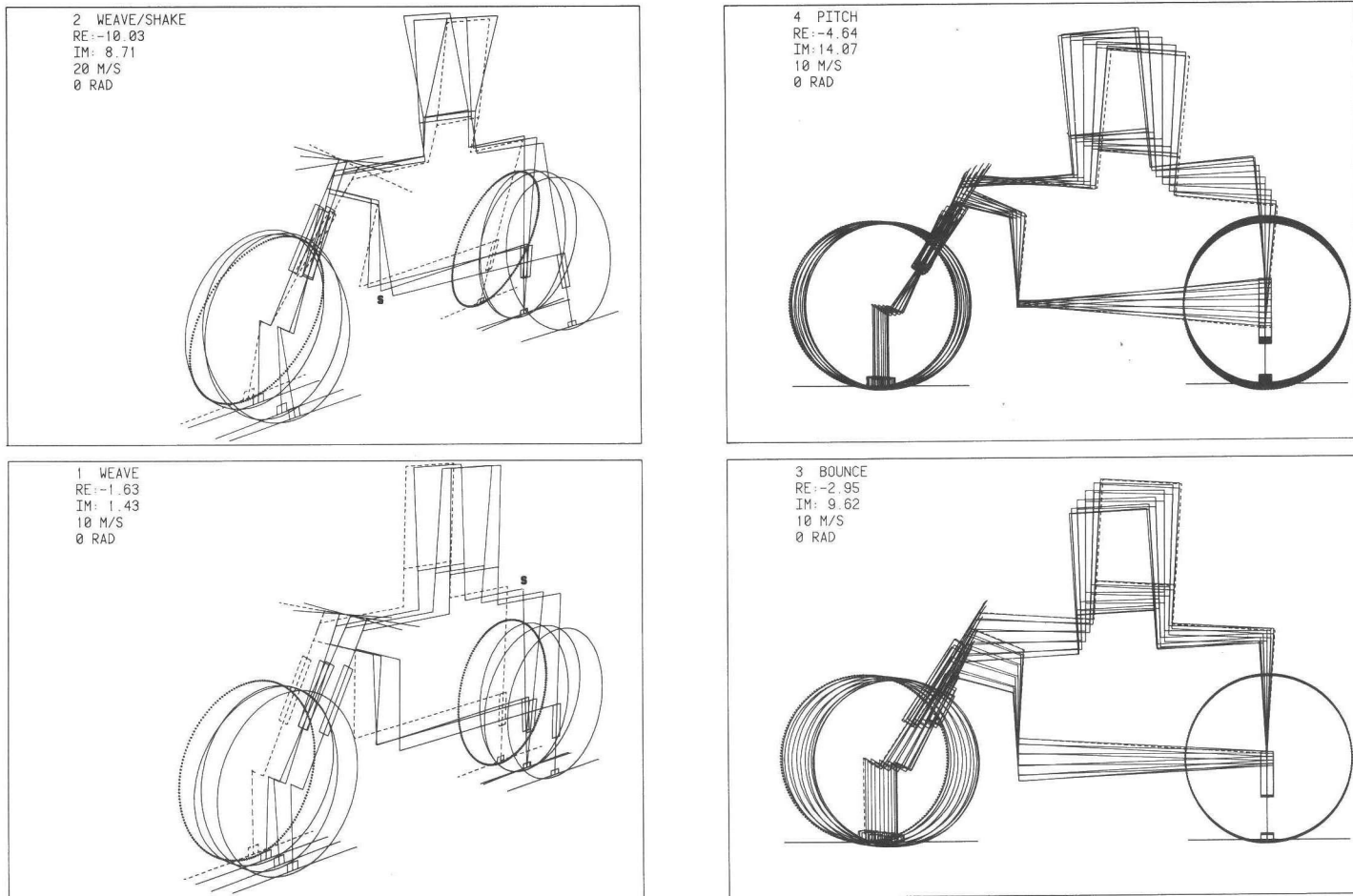
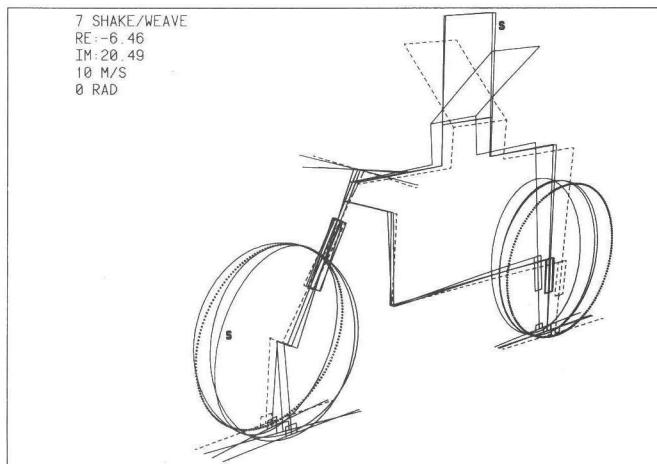
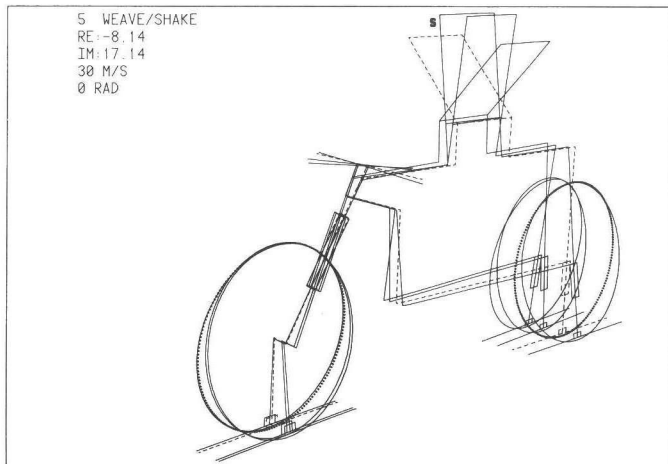
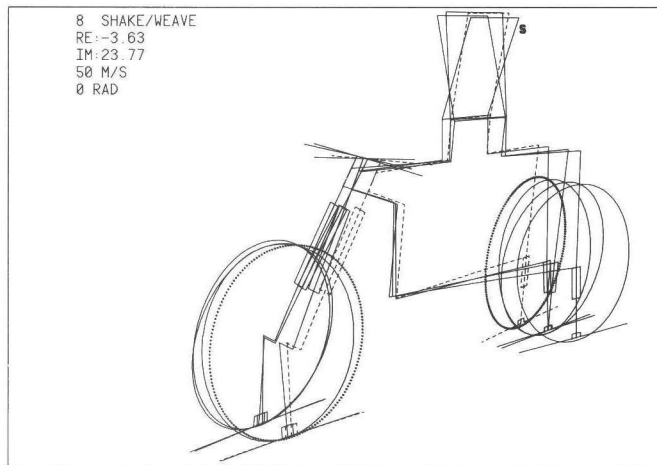
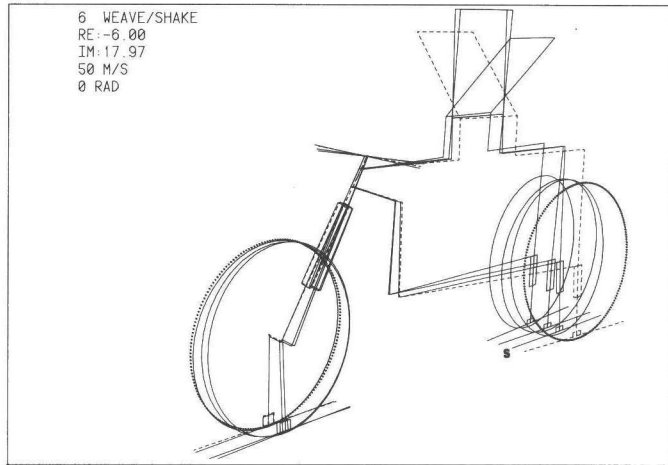


Fig. 61 visualization of some mode shapes. See Fig. 56 for the corresponding root-loci.



68 Fig. 61 (continuation)

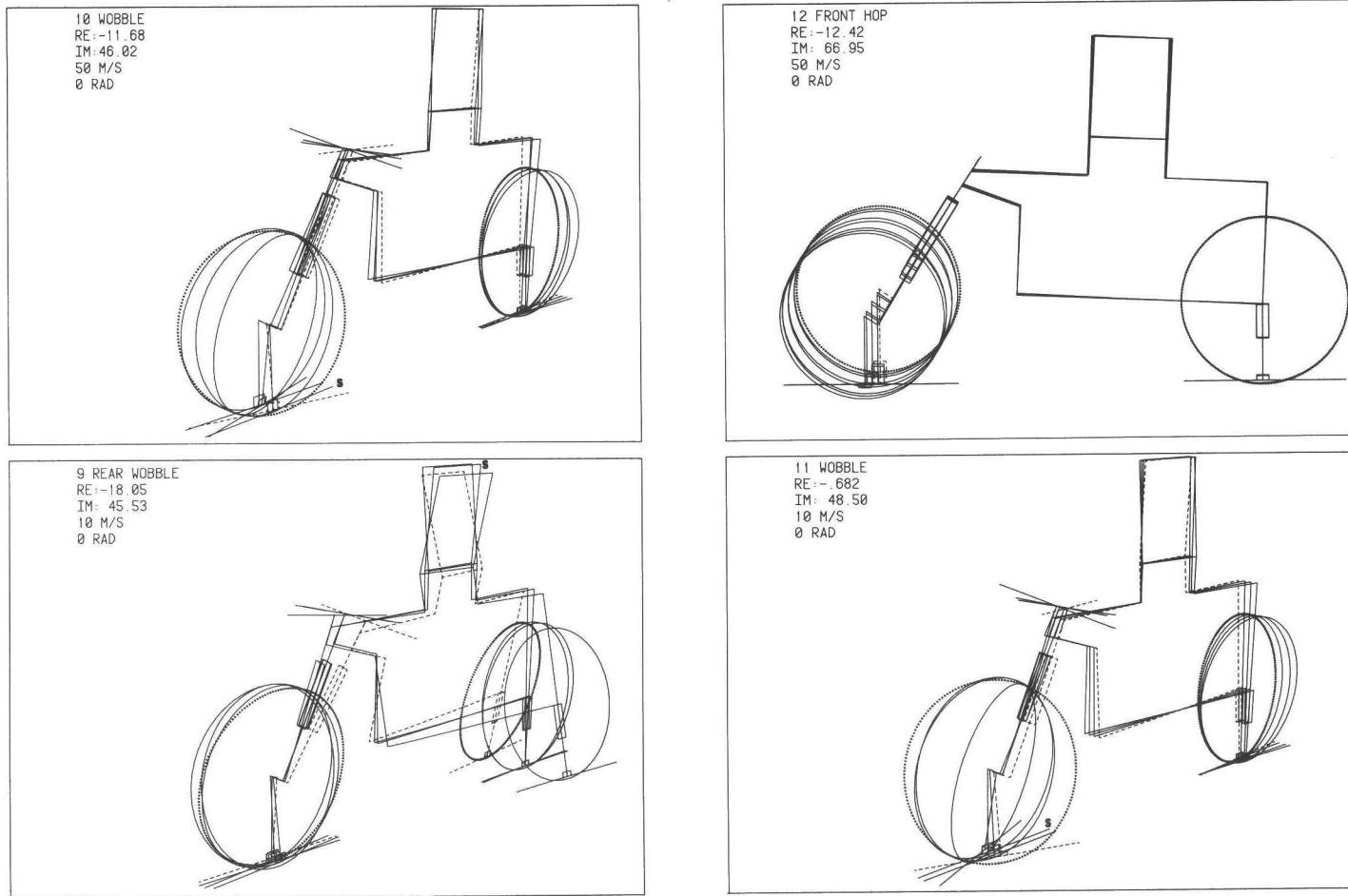
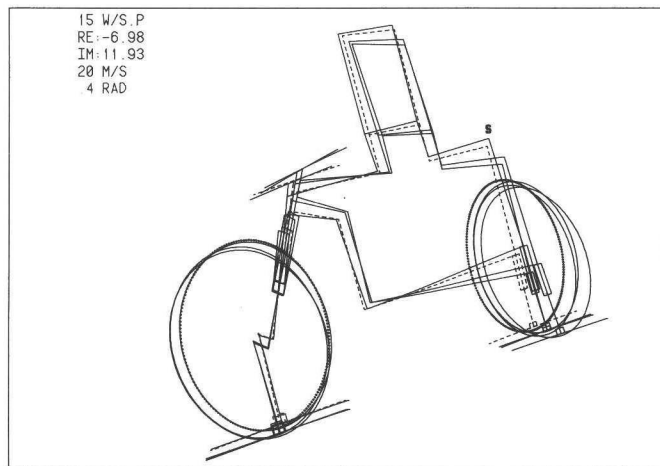
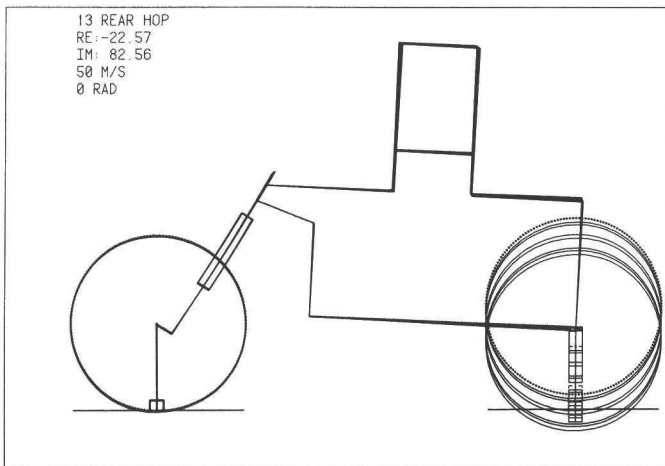
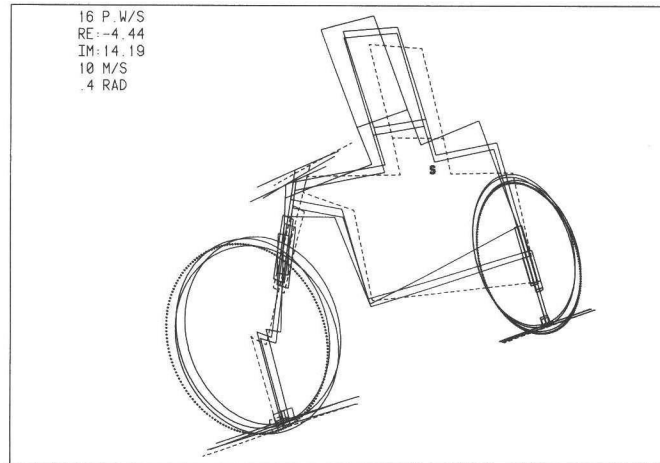
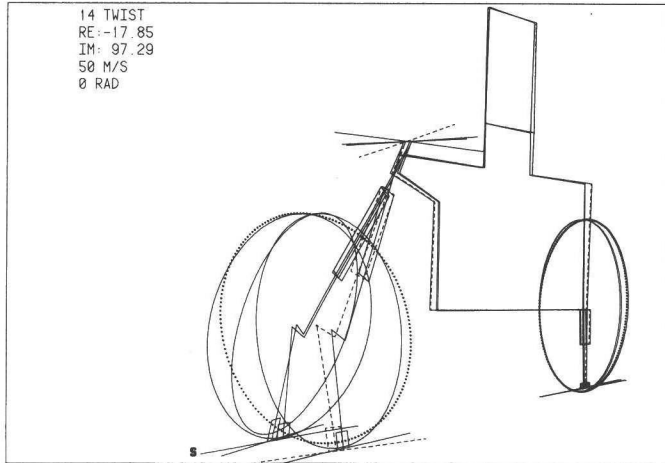


Fig. 61 (continuation)



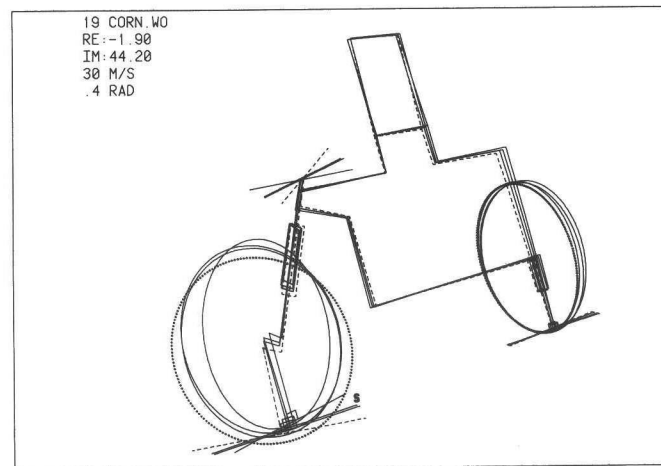
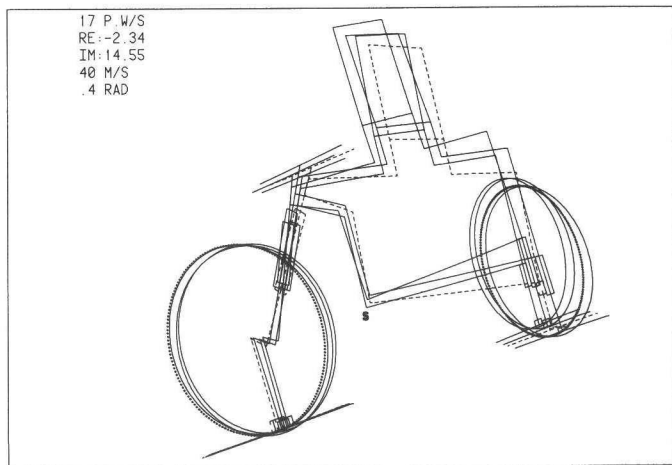
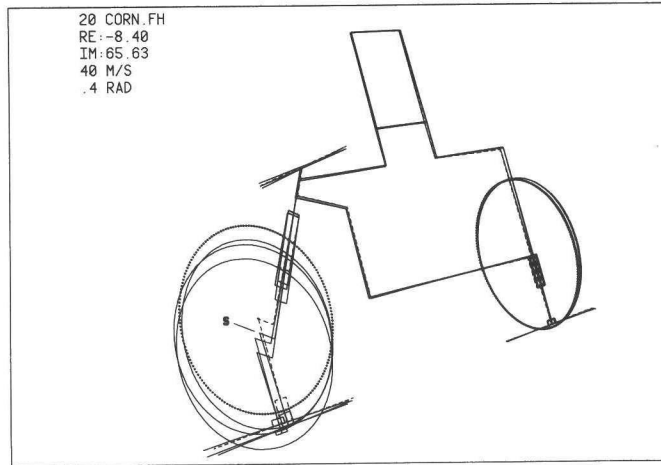
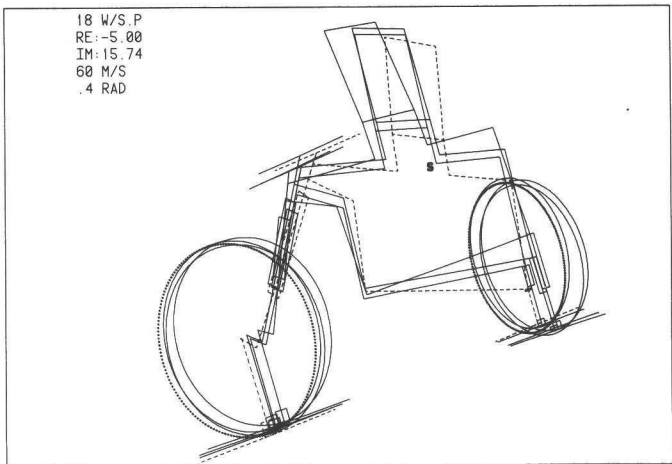


Fig. 61 (continuation)

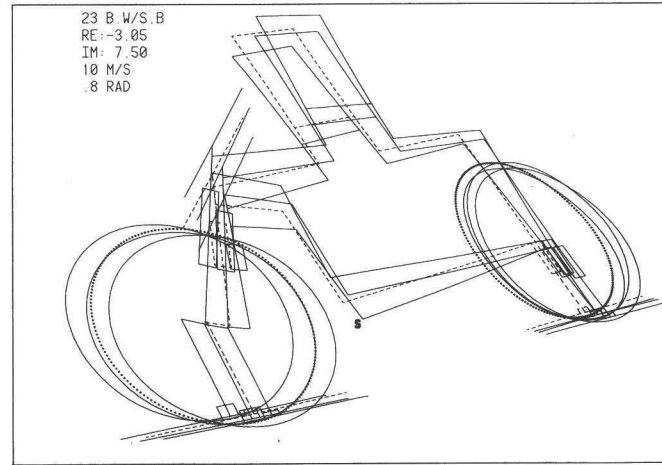
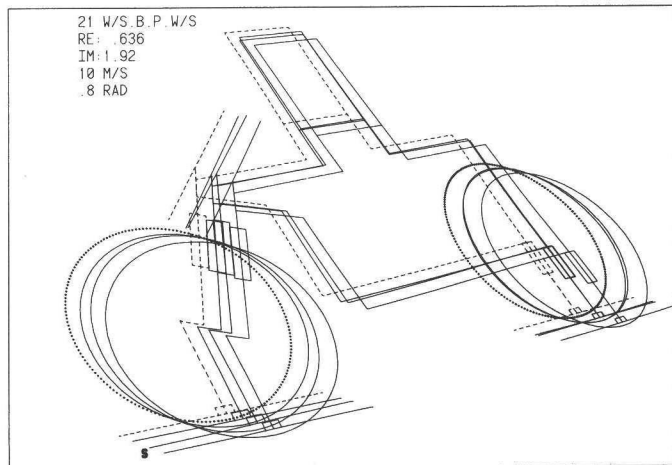
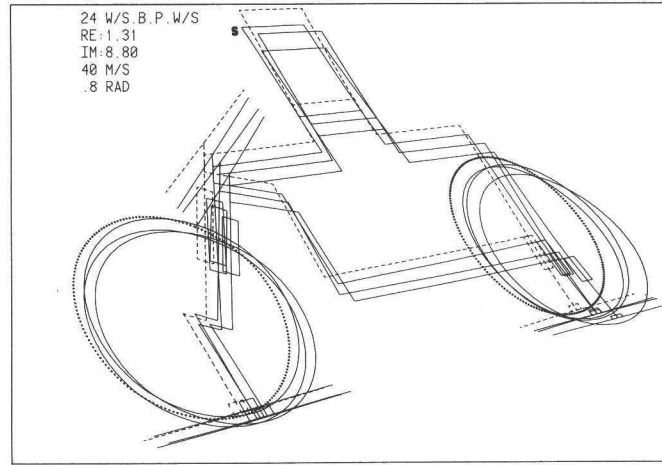
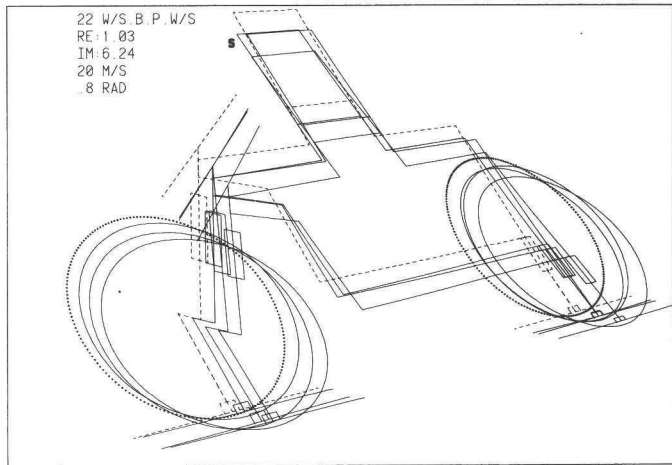


Fig. 61 (continuation)

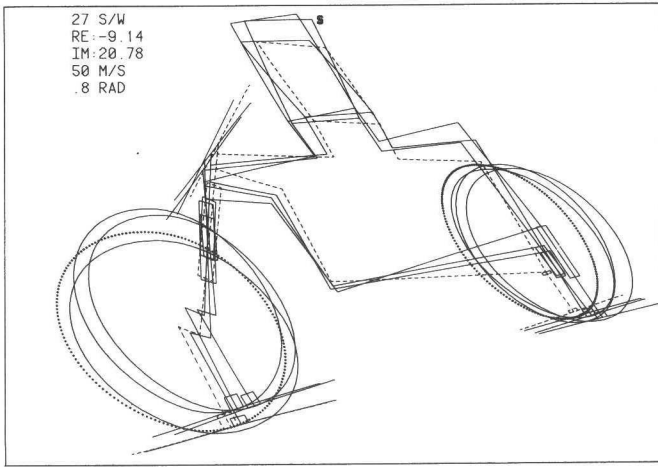
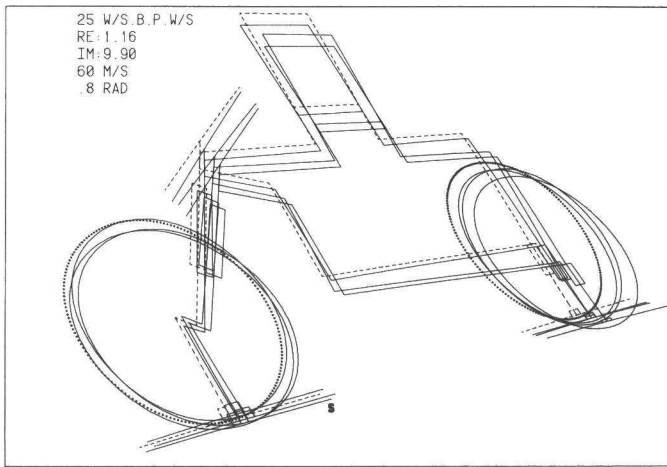
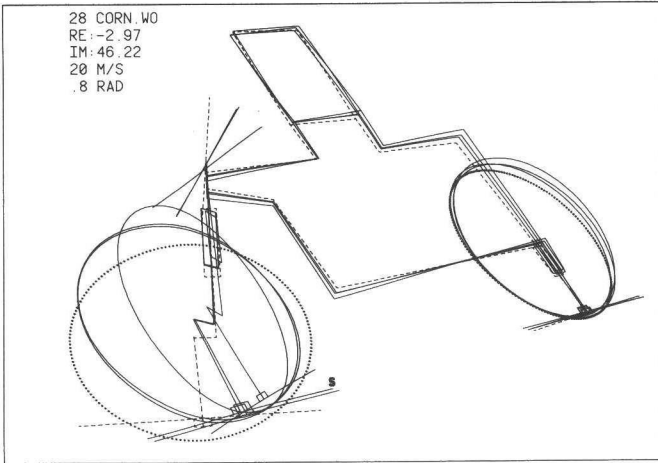
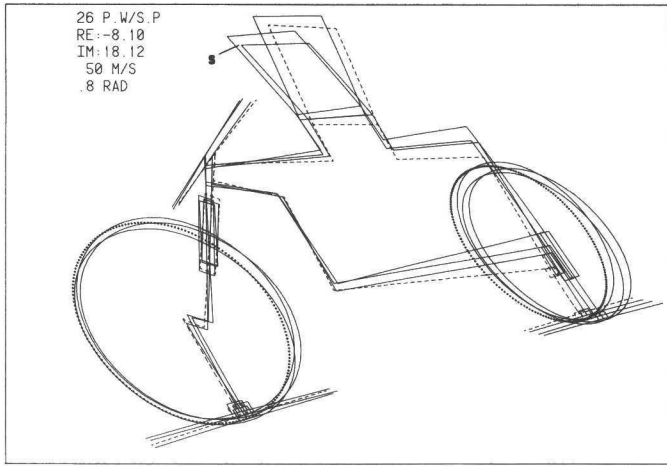


Fig. 61 (continuation)

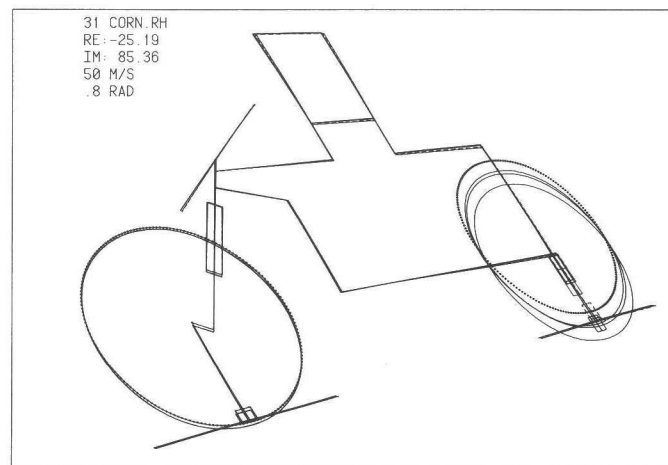
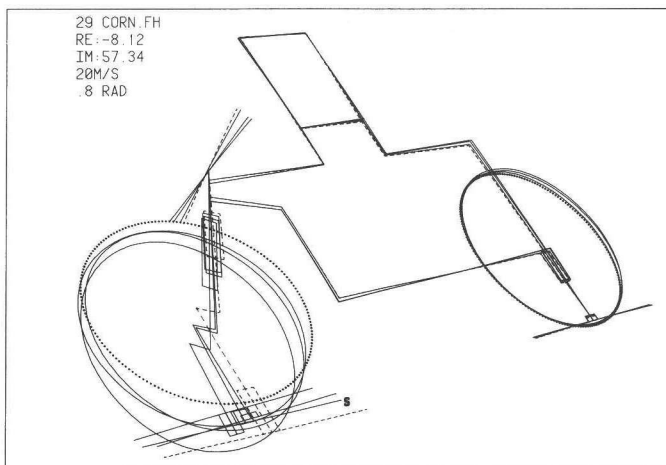
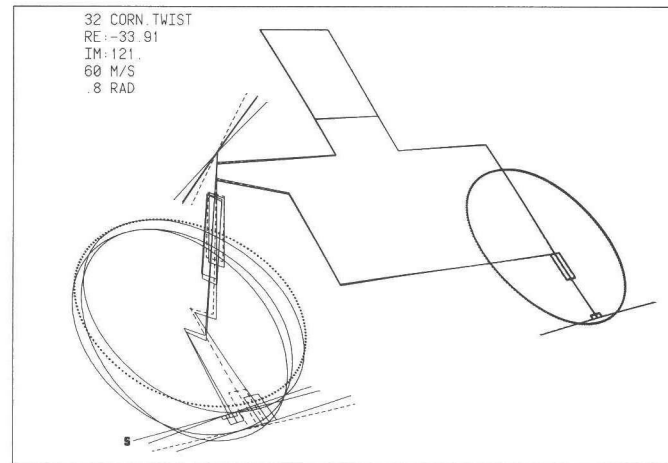
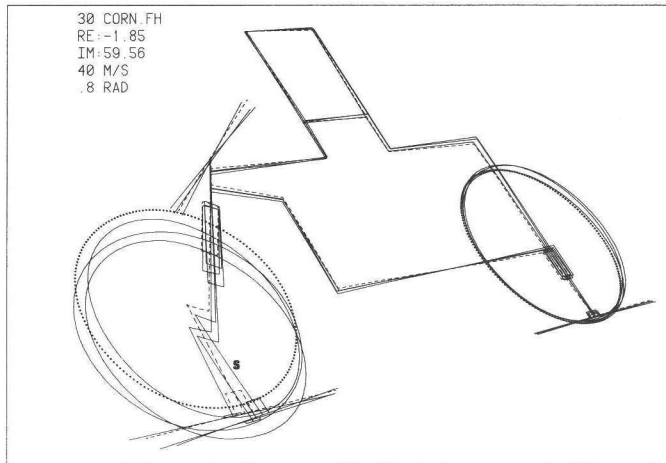


Fig. 61 (continuation)

4.3 Influence of the model structure

4.3.1 general

The mathematical model employed in this study is grafted upon the 'classical' 1971 model of Sharp [31]. Compared with this model, the model at hand comprises the following extra features:

- capability of cornering at relatively large roll angles;
- frame compliance;
- extended description of the tyre behaviour;
- simple rider body dynamics;
- stationary aerodynamic forces.

In several recent studies concerning the oscillatory behaviour of motorcycles some of these features have been included, cf. Sec. 1.1.

In the sequel the influence of the above mentioned features on the dynamic stability will be traced.

4.3.2 simplified model

In order to link up with the 'classical' theory of Sharp [31] the model at hand has been stripped down except for the cornering feature. This leaves a set of dynamic equations of the 16th order.

The root-loci of this system have been depicted in Fig. 62. The simplified equations are in agreement with those of Sharp ($\phi_s = 0$ -case). The most significant differences between the root-loci of the full (baseline) model and those of the simplified model when running straight ahead concern the wobble mode root course. Whereas the simple model shows a critical speed of about 50 ms^{-1} , above which the wobble mode is unstable, the baseline model shows a region of minimum damping in the neighbourhood of $u_s = 15 \text{ ms}^{-1}$ and shows heavy damping in the high speed region. This difference is due to the addition of air drag and frame elasticity. The weave mode exhibits one continuous course in the simplified model, because of the absence of a rider body degree of freedom.

The cornering situation exhibits a low frequency mode which is lightly unstable above a critical speed of about 20 ms^{-1} , and a "wheel patter"-mode at higher frequency, unstable at speeds above 65 ms^{-1} . This latter mode becomes well-damped when air drag is added. The front hop mode course moves to higher frequencies when cornering. The baseline model shows the contrary phenomenon due to the inclusion of frame torsional flexibility.

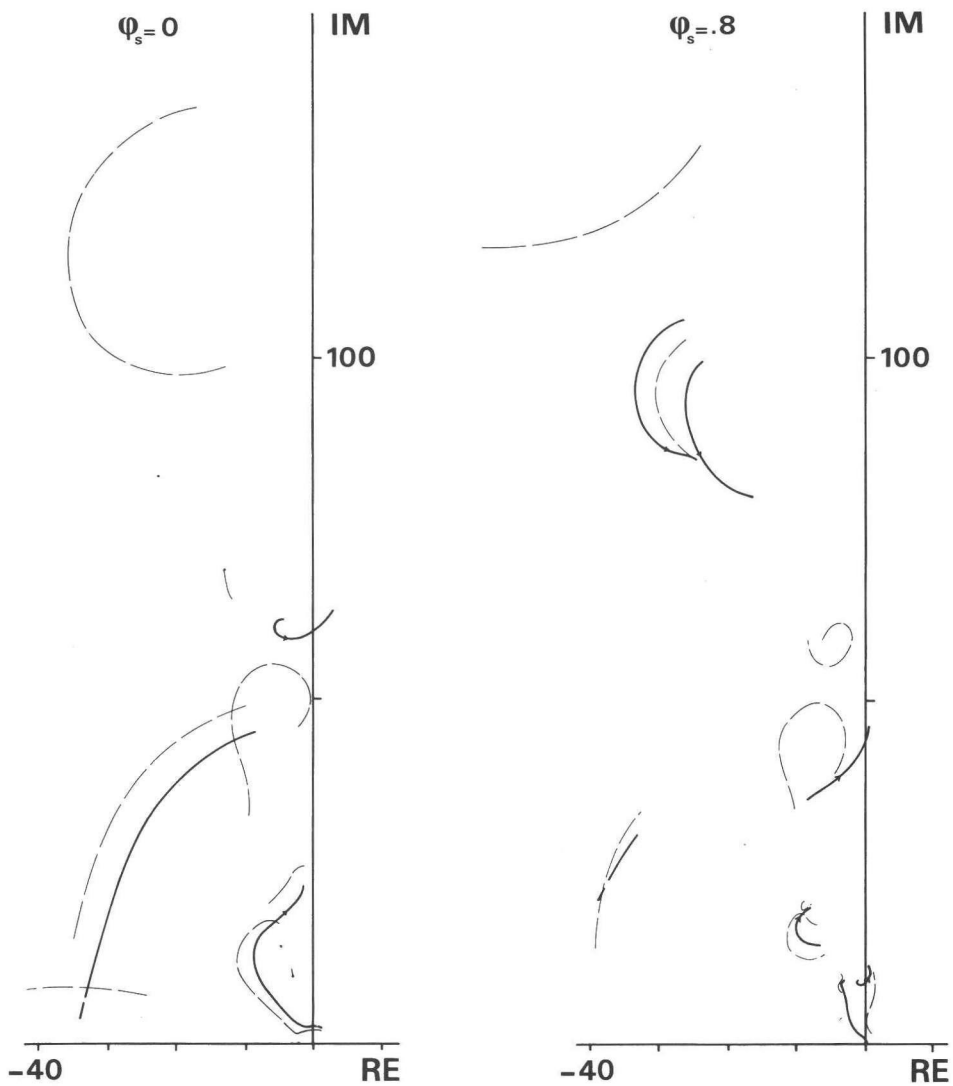


Fig. 62 simplified model

— baseline model

— simplified model: frame compliance, non-stationary tyre moments, non-stationary tyre side forces due to camber and turn slip, rider body dynamics and aerodynamic forces omitted.

4.3.3. frame elasticity

The elastic property of the motorcycle frame structure which appears to be most significant with respect to the dynamic behaviour is the torsional flexibility of the front wheel centre plane relative to the middle section of the main frame about an axis perpendicular to the steering axis (cf. [32], [38], [39], Sec. 1.1 and Appendix A). The 'twist' degree of freedom, which describes this torsional flexibility, has been included in the model; the baseline parameters have been quantified employing data from measurements (cf. Appendix A). Fig. 63 shows the location of the twist axis in the baseline case; the corresponding torsional stiffness amounts to 34100 Nmrad^{-1} .

The influence of the application of frame elasticity on the root-loci of the model can be traced from Fig. 64. Concerning running-straight-ahead, the most important influence of the frame elasticity concerns the wobble and the weave mode. Halving the torsional stiffness causes the wobble mode to slightly destabilize; rigidizing the frame causes the wobble mode to be well-damped, but at the same time destabilizes the high speed part of the wobble mode. Depending on the model parameters the frame compliance properties may be more critical with respect to the wobble mode root course, in such a way that stiffening the frame causes instability of the high speed wobble, cf. [39].

The critical speed of the high speed SH/W-mode falls as the frame stiffness decreases. In the cornering case the frame compliance strongly influences the front hop and the wobble root courses. The weak-framed version shows merging of the wobble and front hop modes at $\phi_s = .8 \text{ rad}$. This low-stiffness version strongly provokes 'wheel patter'.

The rigid-framed version stabilizes the low speed corn. WO; furthermore the original front hop mode root loci are now far less affected by cornering: there is no tendency of this mode to merge with the corn. WO-mode.

The influence of the height of the twist axis on the dynamic behaviour has been shown in Fig. 65. Two variations of the baseline case have been regarded: one with the twist axis four times as high, with respect to the wheel centre, and one with a twist axis through the point of intersection of the steering axis and ground plane in the nominal situation. In the former case the lateral translation of the front wheel centre plane due to twist strongly dominates over the rotation due to twist; in the latter case the camber motion is dominant. Thus excitation of the twist motion in the former case is mainly due to lateral forces and in the latter mainly due to gyroscopic effects and the tyre overturning moment. Furthermore it should be noted that a variation

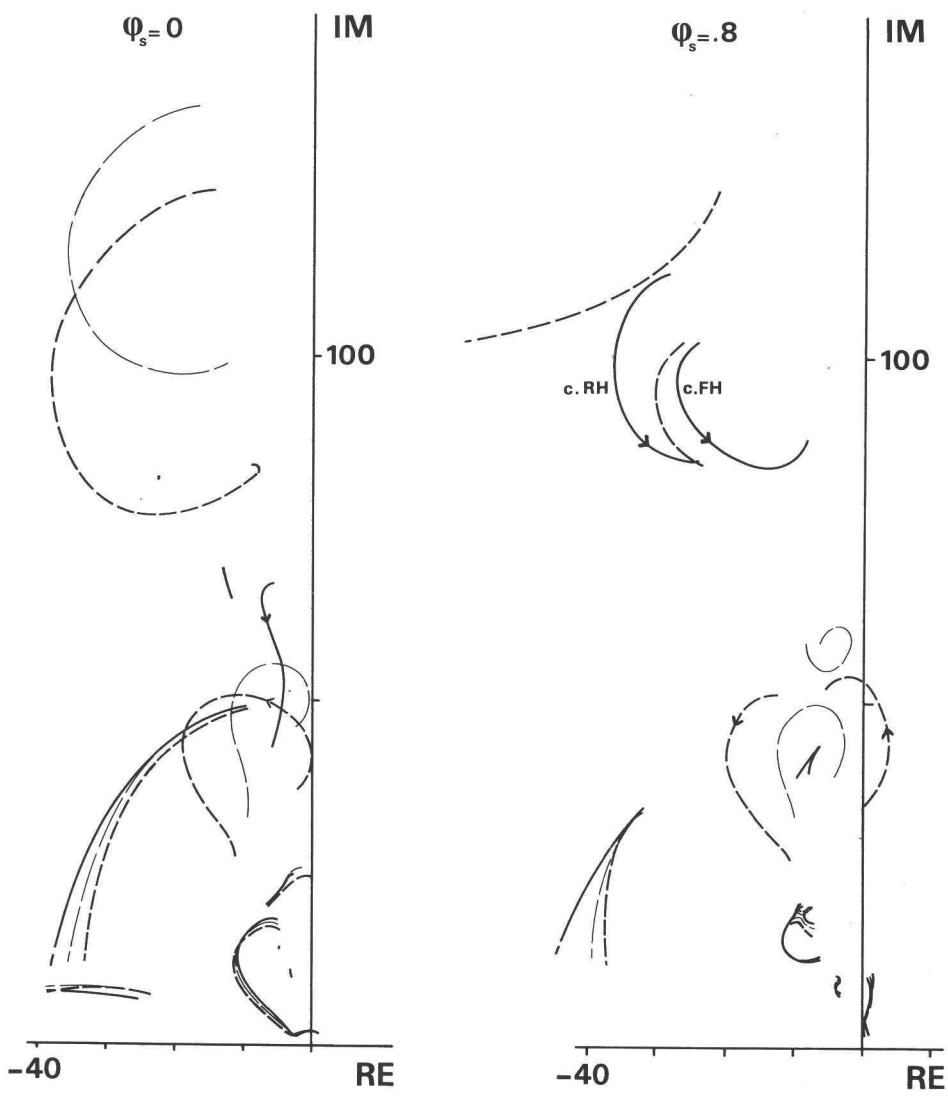


Fig. 64 variation of frame torsional compliance

— baseline model
 — $C_\beta = \infty$
 -·- $C_\beta \times .5$

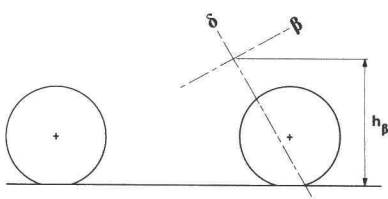


Fig. 63 baseline frame compliance properties: $h_\beta = .834$ m; $C_\beta = 3,41 \times 10^4$ Nmrad⁻¹

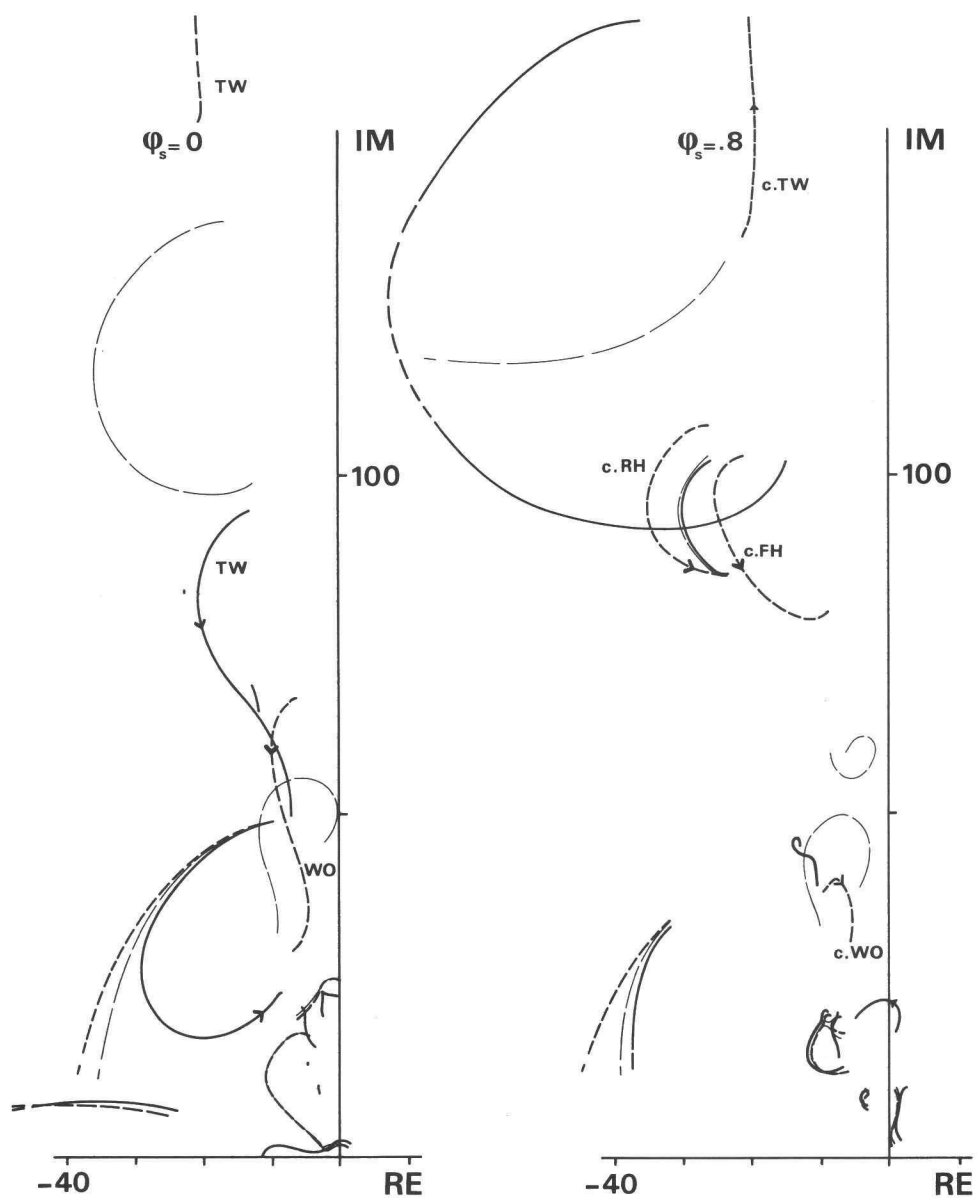
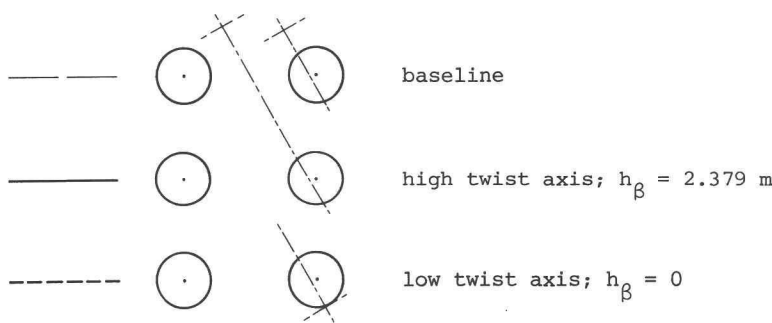


Fig. 65 high/low twist axis



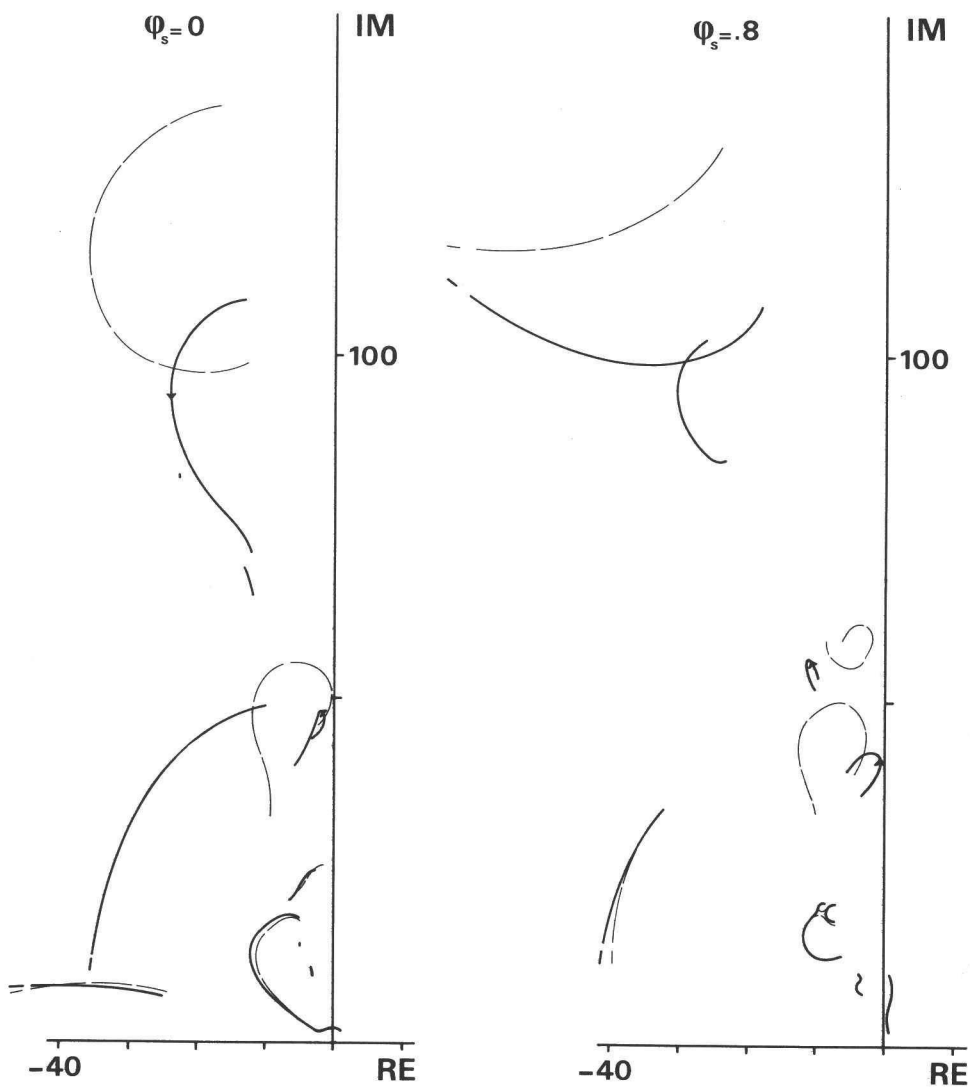
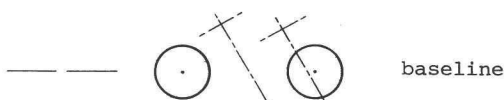


Fig. 66 'hub shift' (lateral compliance predominant over camber compliance)



hub shift; $h_\beta = 2.379 \text{ m}$;
 $C_\beta = 27.69 \times 10^4 \text{ Nmrad}^{-1}$

(providing the same lateral stiffness
at ground level as in the baseline case)

of this height alone affects the resulting lateral translational compliance of the front wheel centre plane with respect to the middle section of the main frame due to twist. Consequently a high location of the twist axis can be seen to lower the twist mode frequency range. Raising the twist axis also causes an increase of the share of the wheel lateral displacement in the twist rotation, which accounts for the marked differences between the results concerning the low compliance, cf. Fig. 64, and the results concerning the high twist axis, cf. Fig. 65. The low twist axis location provides an improvement of the damping of the critical part of the wobble mode course; the high twist axis version lowers the wobble mode frequency, and causes the rear hop and W/S-modes to merge.

When cornering, raising the twist axis can be seen to provoke high speed corn. TW and to give rise to the crossing of the imaginary axis of a second mode course in the low frequency region. In the case of the low twist axis the twist mode root frequency strongly varies with the forward speed, the damping remaining at the same level. In this case merging of corn. FH and corn. WO is suppressed.

Fig. 66 shows the results of a case in which both the twist axis location and the torsional stiffness parameter have been changed. This case provides dominating lateral translation of the front wheel centre plane due to twist ('hub shift'), but now with the same effective lateral stiffness at the front contact centre as in the baseline case. The 'hub shift' can be seen to slightly increase the damping of both the low speed wobble mode and the high speed S/W-mode. In the cornering case the 'wheel patter' damping decreases.

4.3.4 tyre behaviour

The influence of the various extensions to the description of the tyre behaviour (relative to the simplified model, cf. Sec. 4.3.2) has been studied by omission of one feature at a time, cf. Figs. 67 to 69. It should be noted that the description of the non-stationary behaviour only has been varied; the same steady state equations serve all cases studied in this chapter.

Omission of the contributions to the side force \tilde{F}_y due to camber variations ($\tilde{\gamma}$), cf. Fig. 67, causes some root-locus courses to change significantly. In the running-straight-ahead case the monotonous capsizing mode has taken over the low speed instability from the weave mode*. In the cornering case the front hop and wobble modes have merged, and the WO.FH-mode shows low damping in the middle speed range ('wheel patter'). The damping of the

* this information has been taken from the respective RE vs. u-plots, which have not been depicted here.

'cornering weave'-mode W/S.B.P.W/S has been increased; below the critical speed of 17 ms^{-1} this mode has become stable. The rear hop mode has been destabilized, but is still well-damped.

Omission of the effects due to turn slip variations ($\tilde{\rho}$) from the side forces hardly influences the results, except for a slight stabilization of the lightly-damped part of the wobble mode course and of the low-speed corn. WO-mode root course in the cornering case.

Omission of the components of the aligning torque due to side slip, cf. Fig. 68, causes a slight increase of the low-speed wobble mode damping and a significant decrease of the critical speed of the capsize mode, which speed in this case almost coincides* with the critical speed of the low speed weave mode, thus minimizing the speed range of inherent stability of the system at running-straight-ahead. The root-locus course shown in the part below left of the complex half plane disappears. Apparently the corresponding vibrational mode has been evoked by the original inclusion of \tilde{M}_{z0} with a lagging component. In the cornering case the 'cornering weave' mode W/S.B.P.W/S destabilizes except for the high speed part. The front hop and wobble modes separate.

Omission of the components of the aligning torque due to camber also evokes the last mentioned effect. However, the most striking effect of this case concerns the 'cornering weave'-like phenomena: the bounce-governed mode (baseline: B.W/S.B) and the W/S-governed mode (baseline: W/S.B.P.W/S) interchange positions, the latter now being damped throughout the speed range considered, the former showing a critical speed of about 30 ms^{-1} above which this mode is unstable.

The running-straight-ahead case is hardly affected by the omission of \tilde{M}_{zy} .

Omission of the aligning torque components due to turn slip causes a minimal decrease of the low speed wheel patter mode damping; the root-loci of this case have not been depicted. The aligning torque arising in consequence of gyroscopic effects due to the fluctuation of the wheel mass distribution relative to the wheel centre plane increases the middle and high speed wobble mode damping (and, of less importance, the twist mode damping) at running-straight-ahead, cf. Fig. 69. In the cornering case \tilde{M}_{zGYR} appears to be especially beneficial to the damping of the 'wheel patter' mode corn. FH.

Omission of the overturning moment \tilde{M}_x causes the critical speed of the capsize mode to increase from 18 ms^{-1} to 24 ms^{-1} .* Obviously in this speed range \tilde{M}_x provokes capsize-instability, which is plausible when the component of \tilde{M}_x along the steer axis is considered.

* this information has been taken from the respective RE vs. u-plots, which have not been depicted here.

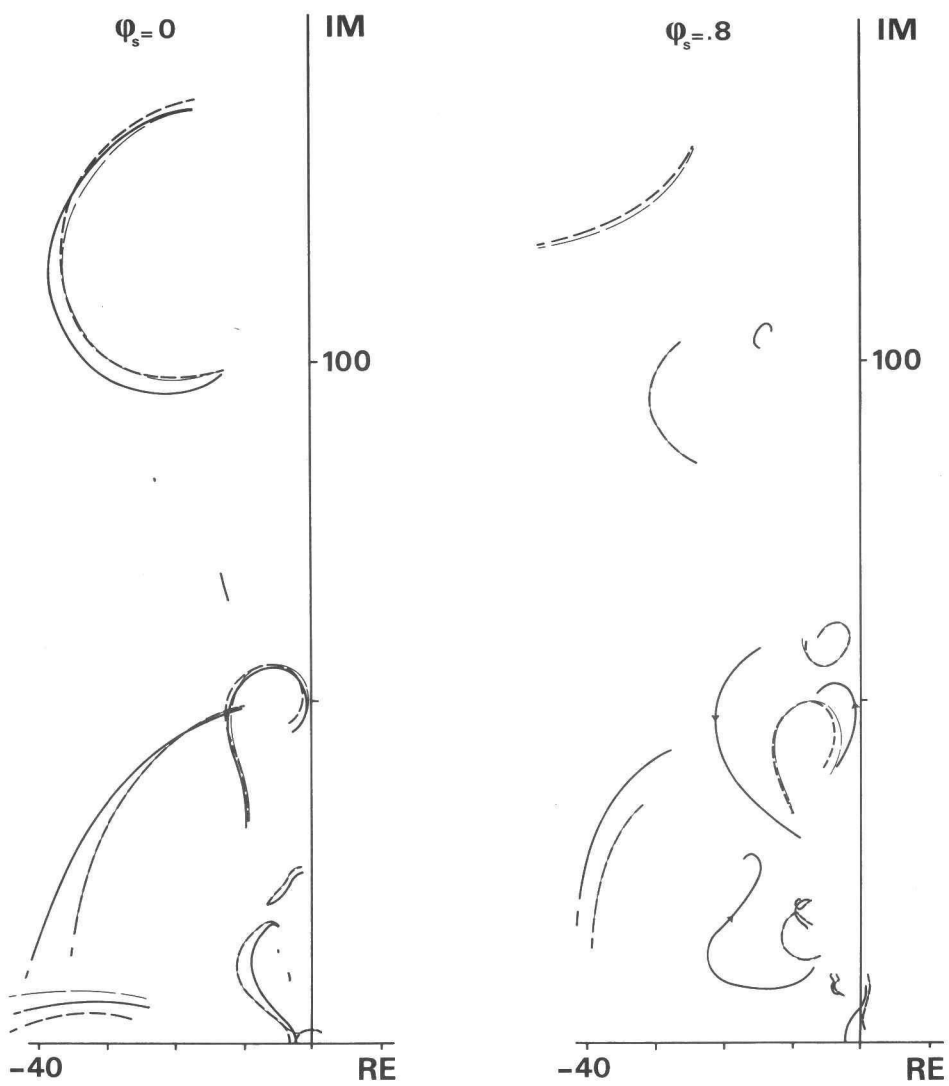


Fig. 67 influence of tyre model features

——— baseline
 ——— $\tilde{F}_{YY} = 0$
 - - - - $\tilde{F}_{YP} = 0$

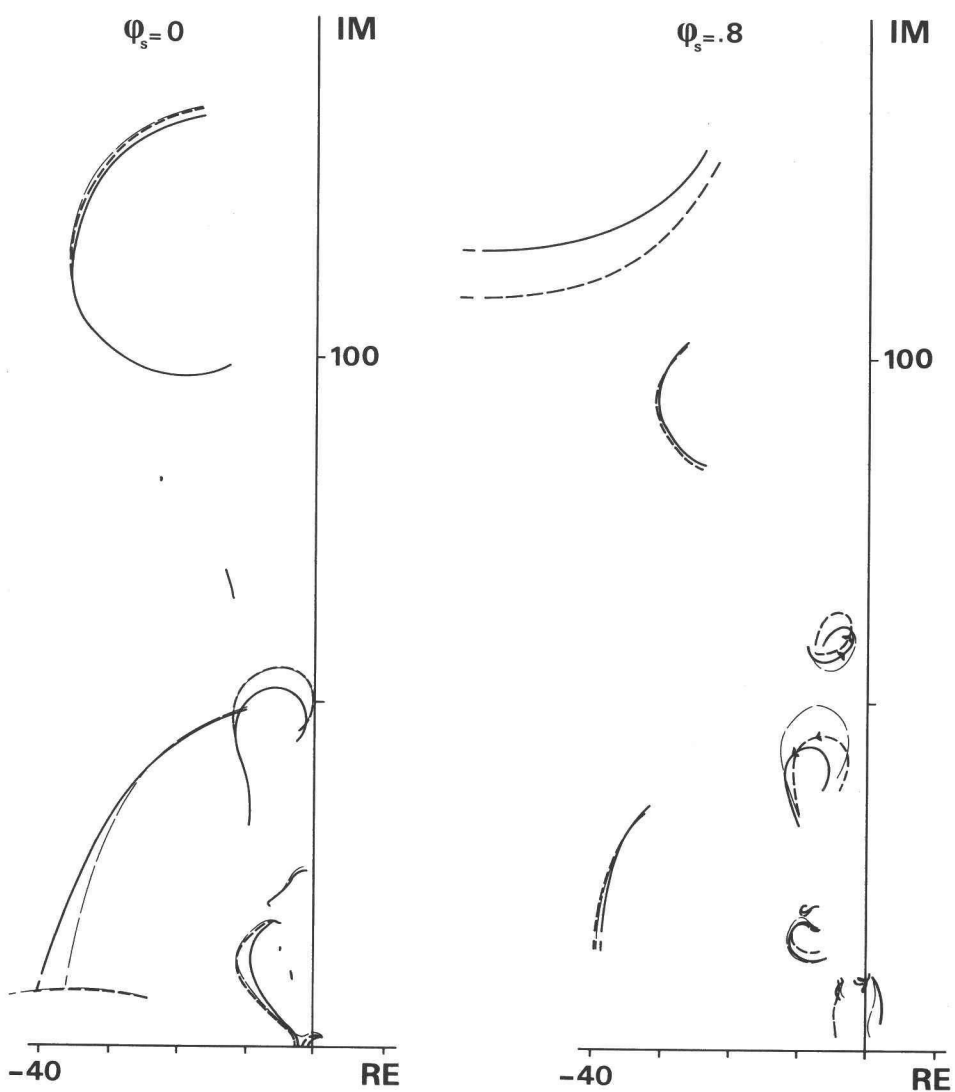


Fig. 68 influence of tyre model features

——— baseline
 ——— $\tilde{M}_{z\alpha} = 0$
 - - - - $\tilde{M}_{z\gamma} = 0$

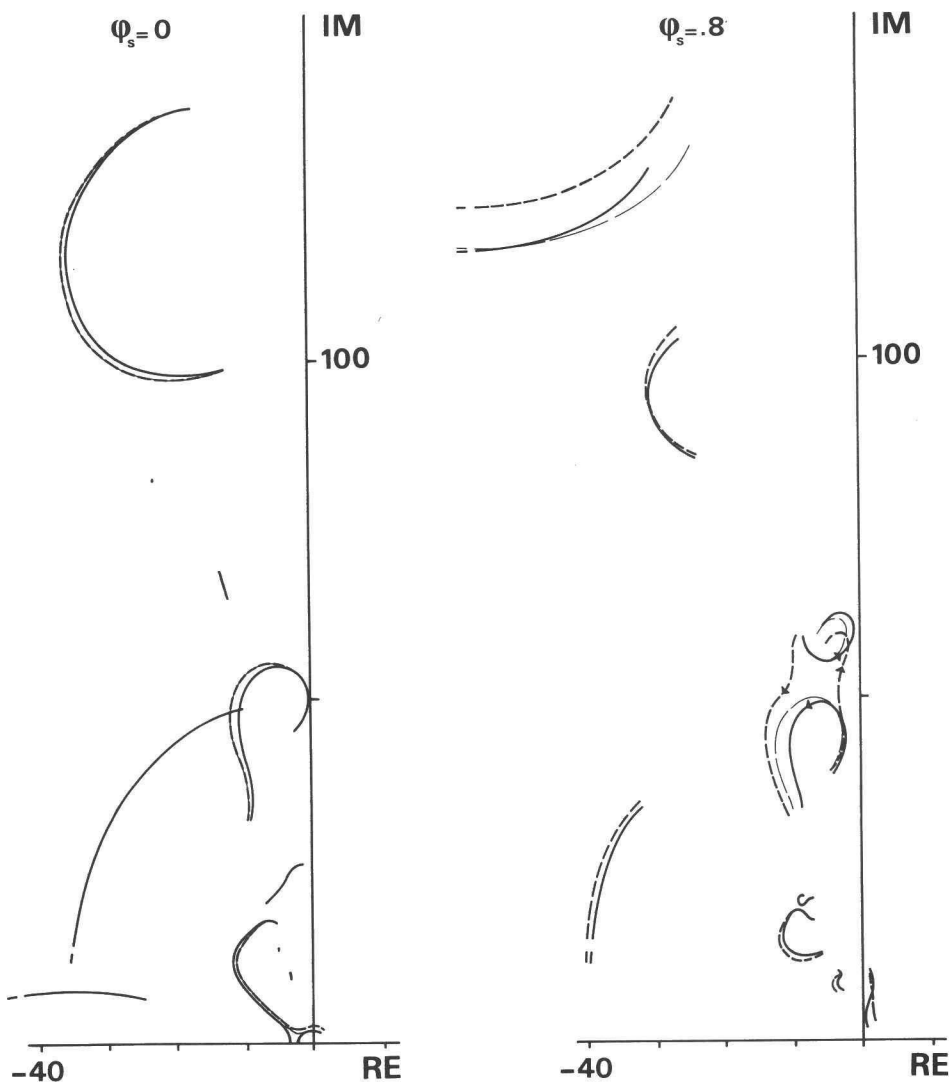


Fig. 69 influence of tyre model features

— — baseline
 — $\tilde{M}_{zGYR} = 0$
 - - - $\tilde{M}_x = 0$

In the cornering case omission of \tilde{M}_x causes the corn. FH and corn. WO modes to merge already at $\phi_s = .8$ (in the baseline case this even occurs between $\phi_s = .85$ and $\phi_s = .9$). The 'cornering weave' mode course W/S.B.P.W/S rotates slightly about an invariant point at $u_s = 25 \text{ ms}^{-1}$ which results in a decrease of damping below and a slight increase above this speed.

4.3.5 rider passive behaviour

The rider body has been modelled as two parts, rigid in themselves, the lower being rigidly attached to the main frame and the upper being hinged to the lower part as an inverted pendulum. This approach approximates one aspect of the rider body passive behaviour which is obviously present in reality (compare [4] with mode shape (5) of Fig. 61). Many more aspects are involved in reality, but have not been modelled.

At the estimated compliance and damping parameter values concerning the body lean motion ('shake') the inclusion of the body lean degree of freedom causes the weave mode root course of the rigid-rider case to mix up with the shake mode root course.

Rigidizing the rider body as a whole destabilizes the high speed weave mode when running-straight-ahead, and slightly destabilizes the low speed wobble mode, as can be seen from Fig. 70.

The cornering results are not significantly influenced by the rider passive behaviour as it has been modelled, except for the fact that rigidizing the rider body provokes the merging of the corn. FH and the corn. WO modes.

4.3.6 aerodynamic effects

The stationary aerodynamic forces, as they have been modelled, result in:

- wheel load transfer;
- a change of the vehicle geometry at high speed, due to spring length variations;
- a yaw moment arising only when cornering.

The first phenomenon causes the side forces to change in such a way that the last phenomenon is counteracted. The dynamic situation is influenced particularly by the load transfer. Fig. 71 shows the baseline results vs. the results obtained with omission of air drag. The air drag is found to decrease the running-straight-ahead wobble mode damping except for the low speed range, and to decrease the high speed S/W-mode damping. The latter phenomenon is demonstrated in reality in the film 'Weave and Wobble' [4], in which the rider

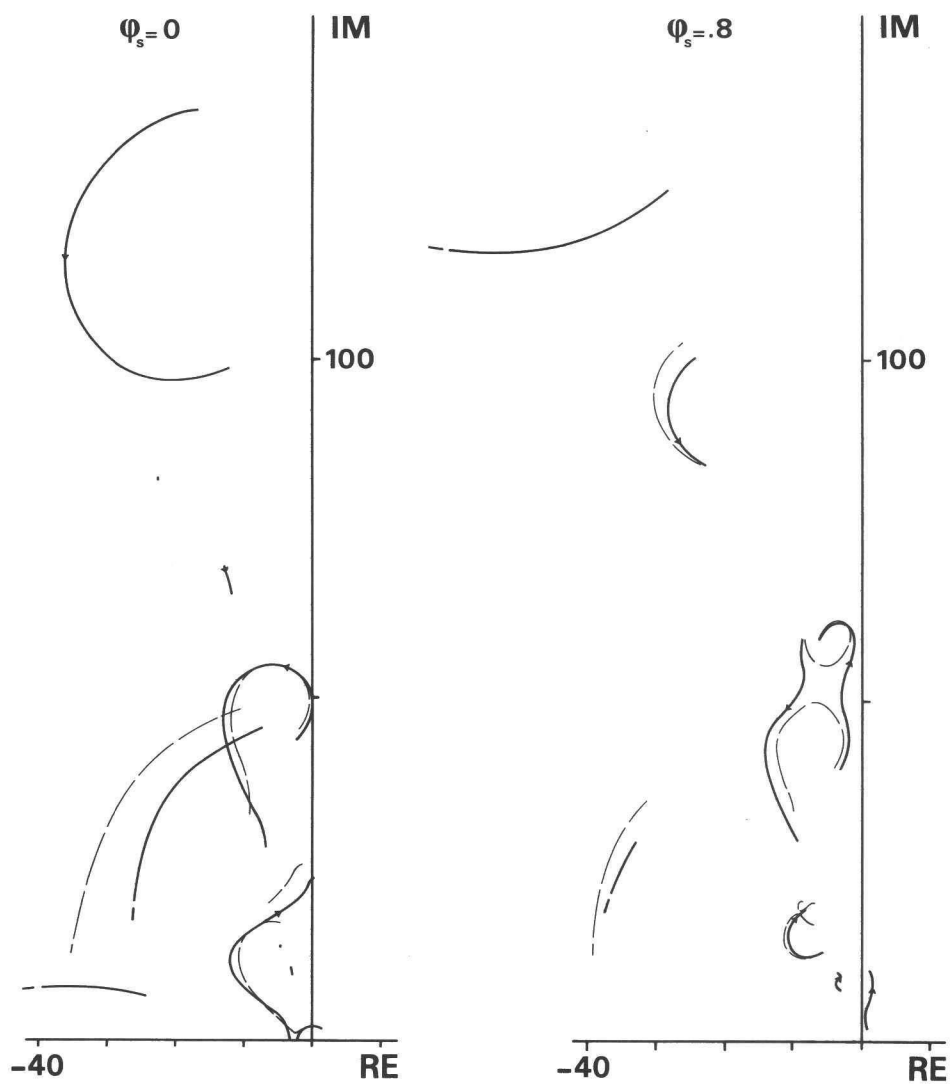


Fig. 70 influence of rider body dynamics

— — baseline

— rigid rider

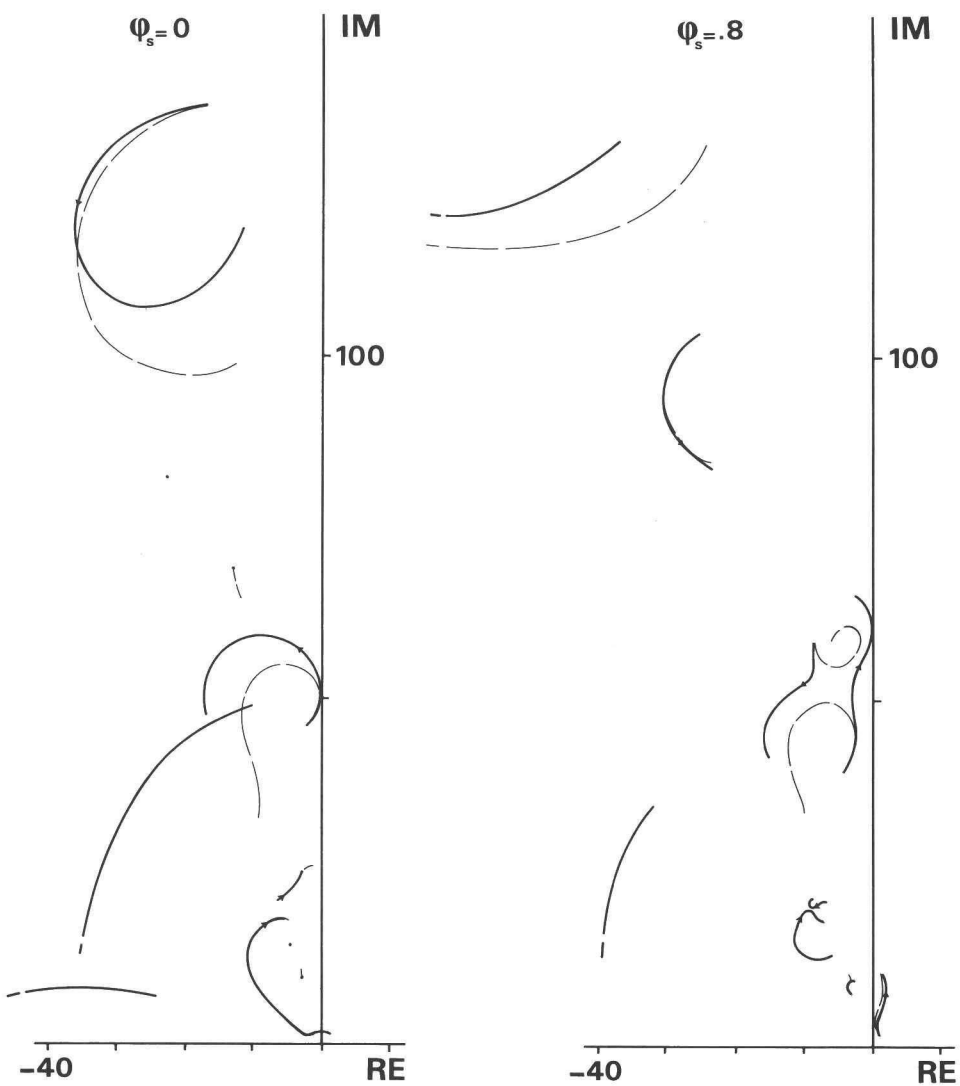


Fig. 71 influence of air drag

— — baseline

— — no air drag

stabilizes a severe weave oscillation by lying down and thus reducing the frontal area. As a secondary effect lying down results in slightly moving forward the resulting centre of gravity which is also beneficial to the high speed weave damping.

In the cornering situation the aerodynamic forces stabilize the high-speed wobble course (i.c. FH.WO) and destabilize the cornering twist and high-speed front hop course (i.c. WO.FH). The 'cornering weave'-mode W/S.B.P.W/S is slightly stabilized by the inclusion of air drag.

4.3.7 *miscellaneous*

The geometry of the vehicle which serves as an input to the dynamic calculations has been adapted to include large spring deflections arising from cornering and air drag. The effects of including this feature can be seen from Fig. 72. The influence on the running-straight-ahead root-loci is small and mainly concerns the in-plane modes of motion and the high speed part of the well-damped twist mode. In the cornering situation at $\phi_s = .8$ rad adaptation of the geometry influences the merging of the corn. FH and corn. WO modes of motion.

4.4 Influence of some parameters

4.4.1 *suspension*

In practice, much attention is paid to suspension properties. These properties seem especially relevant to cornering dynamic stability, cf. [9]. The influence of some suspension parameters on the model behaviour will be traced in the sequel. The running-straight-ahead case will not be regarded.

Fig. 73a shows the effects of changing the front and rear suspension stiffnesses. The most important effect of lowering the stiffnesses by 50% is the increase of damping of the high speed 'cornering weave' W/S.B.P.W/S. The low speed part of this mode shows increasing instability. Increasing the stiffness of the suspension springs by 100% hardly influences this mode, but does influence the remaining modes, the most important effect being an increase of damping of the corn. FH mode.

In Fig. 73b can be seen how the suspension damping influences the dynamic behaviour of the system. Omission of the damping causes a general decrease of damping of the vibrational modes. The 'cornering weave' mode W/S.B.P.W/S is least affected; the corn. FH mode course almost entirely moves into the right half-plane.

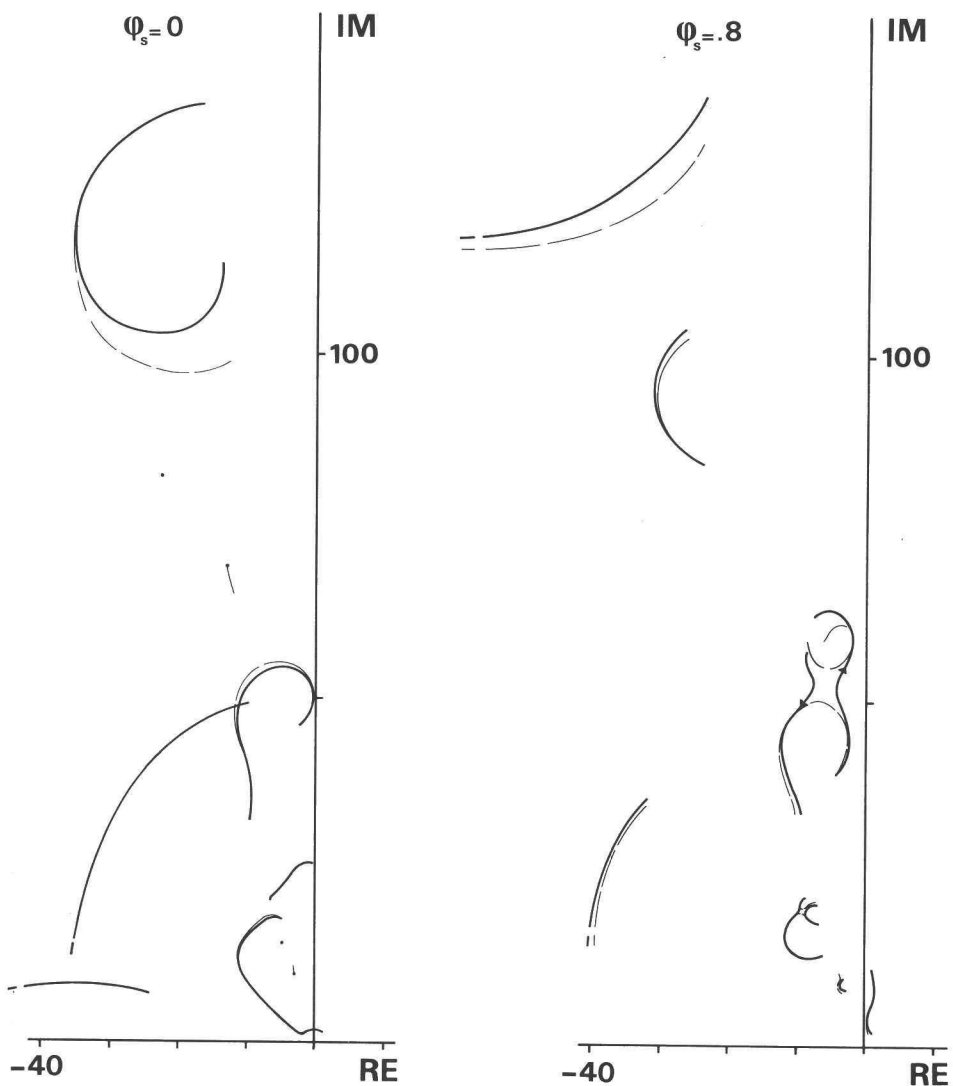


Fig. 72 influence of adaptation of the geometry (cf. Fig. 39)

— baseline

— without adaptation of the geometry

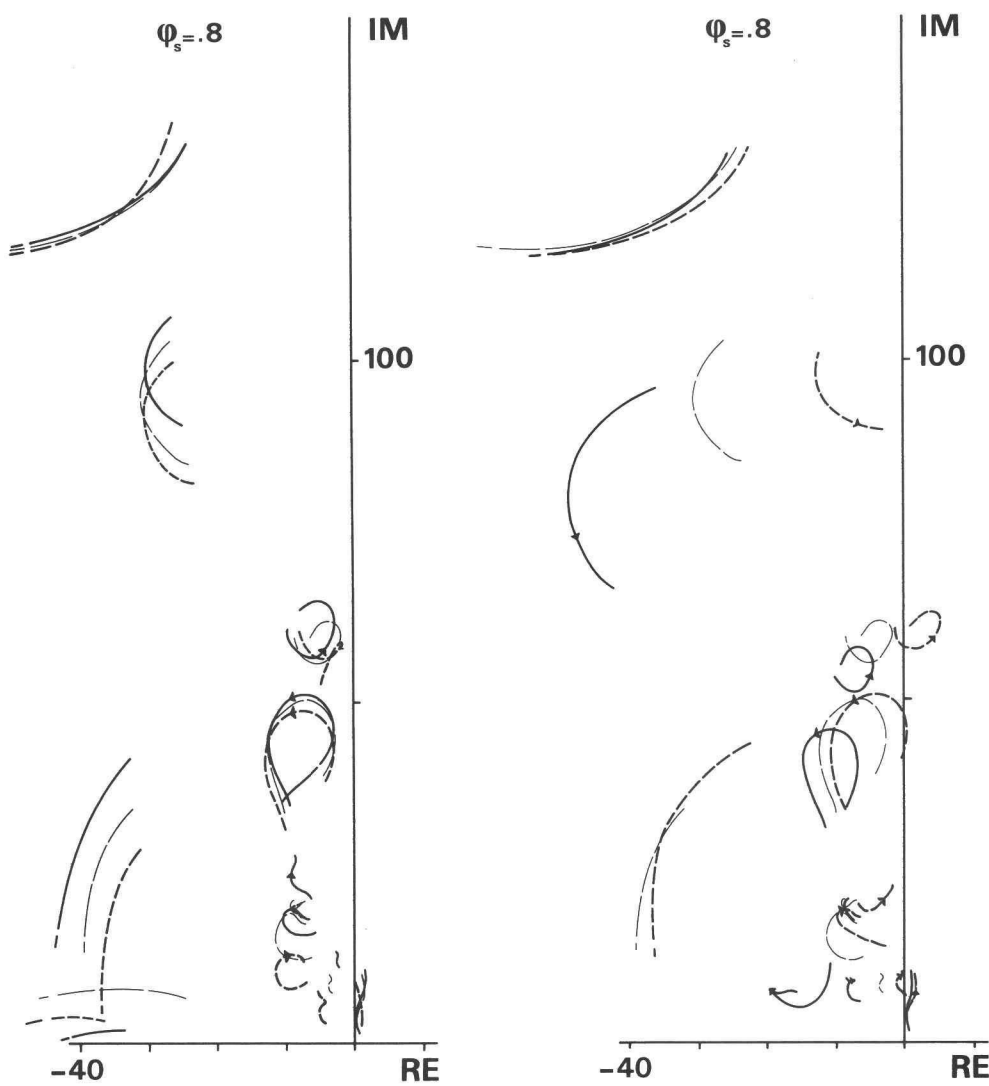


Fig. 73 influence of suspension parameters

a (left):

- — baseline
- $C_s \times 2$
- - - $C_s \times .5$

b (right):

- — baseline
- $K_s \times 2$
- - - $K_s = 0$

Increasing the damping by a factor 2 has the opposite effect; in this case the cornering weave mode remains unstable.

4.4.2 geometrical parameters

Of all geometrical parameters in the model at hand the trail has been chosen to be the subject of investigation, as has been reasoned in the sequel.

Throughout this study δ_s has been put zero in the equations describing the non-stationary motion. This approximation can be justified except for cases in which the roll angle value is high and at the same time the forward speed is very low, cf. Fig. 46. At large roll angles the trail varies strongly with the steer angle, cf. Fig. 48b. At large roll angles and low speed the stationary steer angle attains maximum values, cf. Fig. 46. In order to investigate the consequences of disregarding the trail variations the trail has been varied by altering the front frame geometry. The location of the mass centres remains unchanged. The results of these calculations have been shown in Fig. 74. Concerning the problem mentioned above the cornering case only is relevant; the trail being generally considered an important design parameter the running-straight-ahead results have also been depicted.

In the running-straight-ahead case, trail variations can be seen to affect the root-loci quantitatively. Reducing the trail causes the wobble mode frequency to decrease. Furthermore the W/SW-mode damping decreases. The critical speed of the SH/W-mode moves to lower values.

In the cornering case qualitative changes also occur, the most significant concerning the cornering weave mode. Decreasing the trail by 25% can be seen to cause the low speed part of the cornering weave to become stable, with a critical speed of about 20 ms^{-1} . Especially these low-speed results are relevant because maximal trail reduction occurs at maximal steer angle, which in turn occurs at minimal speed. For example: at $u = 10 \text{ ms}^{-1}$ and $\phi = .8 \text{ rad}$ the steering angle amounts to 0.12 rad (cf. Fig. 46) which causes the trail to fall to about 60% of its nominal value, cf. Fig. 48b; at $u = 5 \text{ ms}^{-1}$ and $\phi = .5 \text{ rad}$: $\delta = 0.34 \text{ rad}$; at this value of ϕ causing the trail to reduce to about the same proportion as in the former case.

The facts mentioned above, in combination with the results shown in Fig. 74, should be considered when interpreting the baseline results at low speed and high values of the roll angle, especially concerning the cornering weave mode root course.

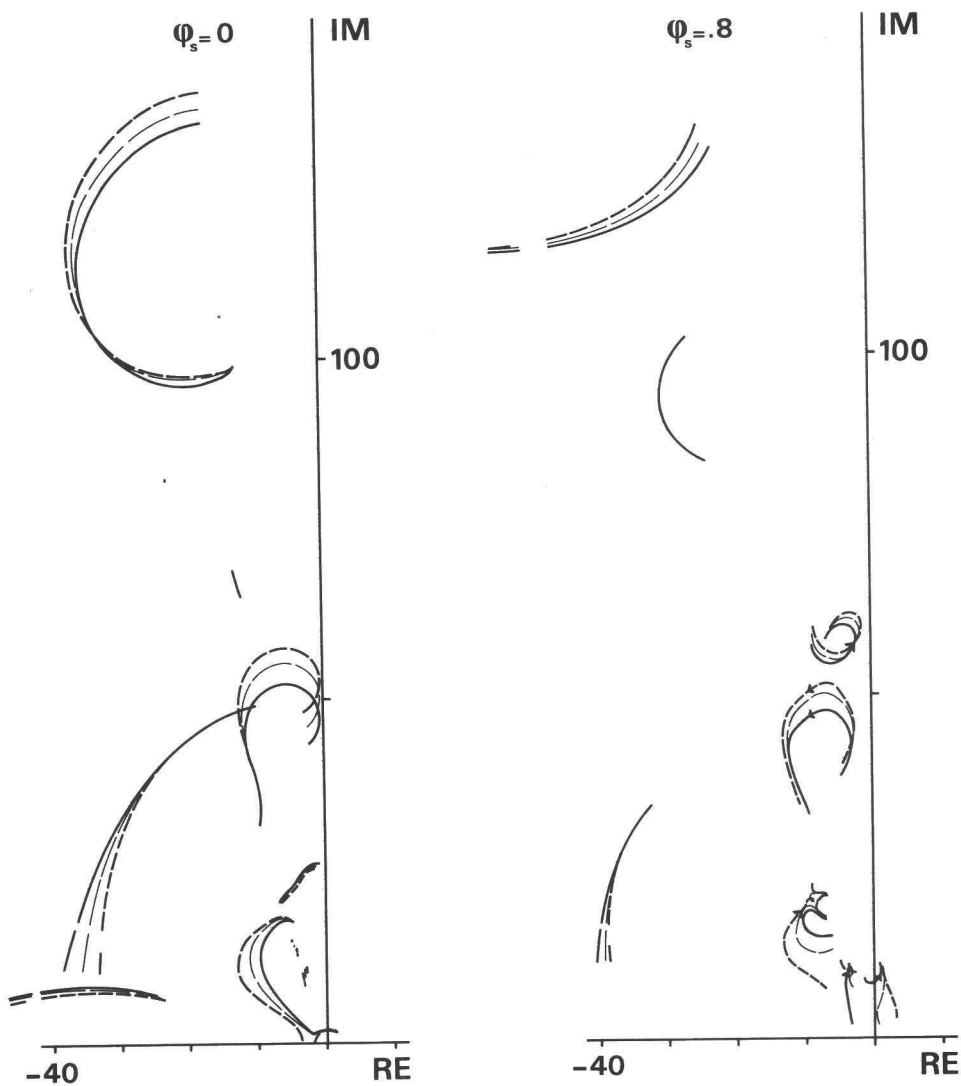


Fig. 74 variation of the mechanical trail

— baseline

— $t \times 0.75$: $a_{1x} = .090$ m ; $a_{1z} = .646$ m

-·-·- $t \times 1.25$: $a_{1x} = .043$ m ; $a_{1z} = .619$ m

Note that the inertia properties remain unchanged (\bar{a}_1 determines the location of the centre of gravity of the body \textcircled{lu} ; which is the sum total of $\textcircled{1a}$ and $\textcircled{1w}$; a_1 determines the location of the massless point A_1).

4.4.3 *inertia properties*

In this section variations of the inertia properties of the motorcycle have been regarded, bearing in mind the typical differences in this respect between racing and touring machines.

Decreasing the inertia properties of the motorcycle by 50% appears to be beneficial to the non-stationary running-straight-ahead properties: the damping of both wobble and weave increases. In the cornering case wheel patter is suppressed and the cornering weave stabilizes, although only at very high speed, cf. Fig. 75.

Moving the centre of gravity of the main frame towards the front and downwards, increases the stability of the high-speed weave (i.c. S/W) in the running-straight-ahead case, cf. Fig. 76, which is a well-known fact from practice. However, moving the main frame centre of gravity forward also causes the low-speed wobble mode to destabilize. In the cornering case, lowering the centre of gravity causes the wobble and front hop to be merged at $\phi_s = .8$ rad and causes the thus arising wheel patter mode W.O.FH to destabilize. Moving the centre of gravity forward destabilizes the corn. FH mode. Note that in the case of the lowered centre of gravity at running-straight-ahead the rear wobble fades into the high speed weave; the low speed weave (per definition an oscillatory mode of motion) only exists in two limited intervals of the forward speed.

The two hypothetical cases studied in Fig. 76 have been integrated into one practical case, the inclusion of a top box, the extra mass being 25 kg, cf. Fig. 77. The top box addition can be seen to decrease both the wobble and the weave mode damping at running straight ahead (note that the shake mode and the weave mode have not merged in this case, in contrast with the baseline case). The rear wobble and W/S-modes merge. In the cornering case adding the top box causes the wheel patter mode to destabilize. The cornering weave mode further destabilizes (this result was also experimentally obtained by Weir [47]).

Note that the change in nominal wheel load does not effect the tyre characteristics in the nominal situation; in off-nominal situations the change of wheel load with respect to the nominal wheel load does influence the tyre characteristics as it does in the baseline case.

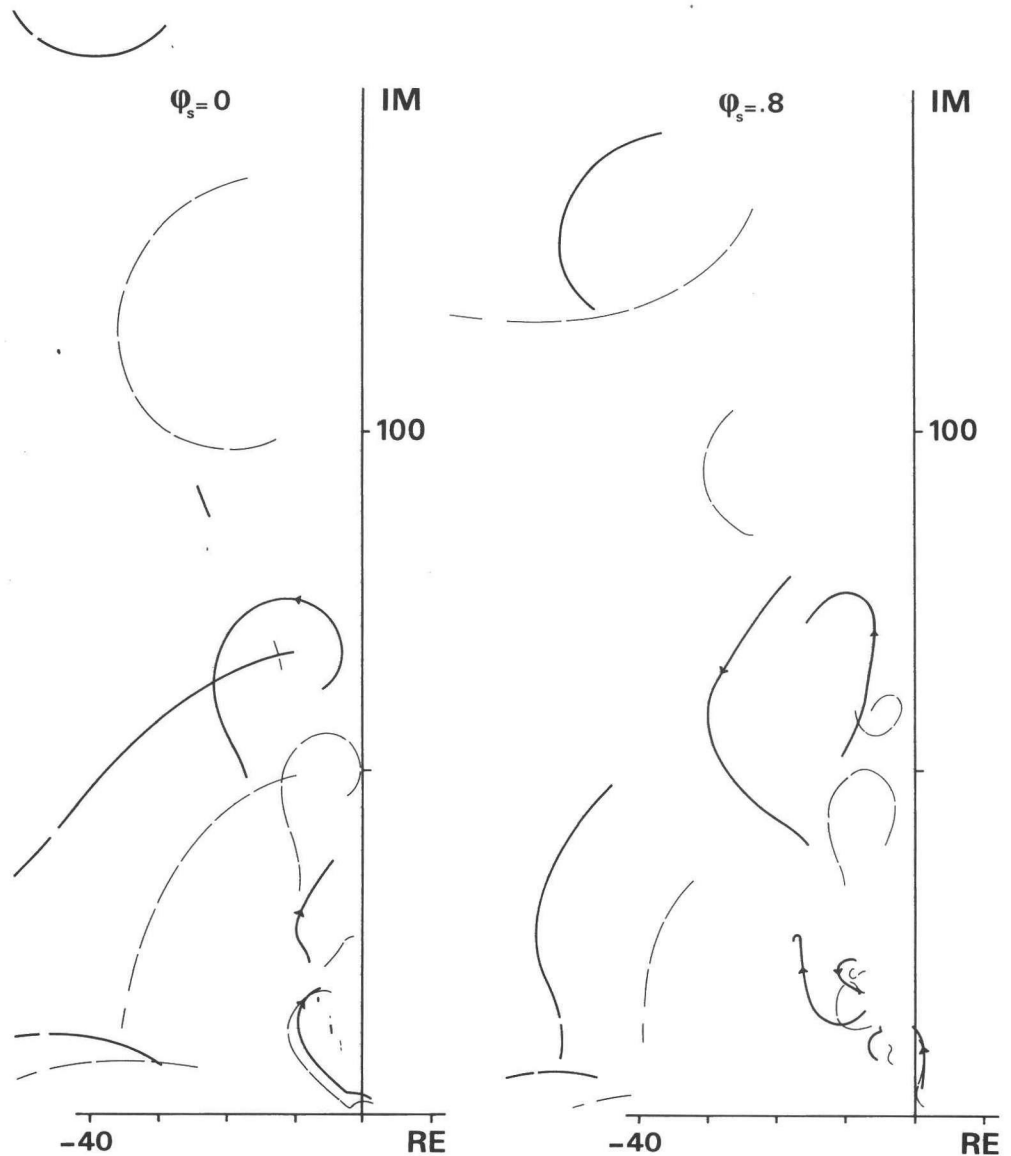


Fig. 75 influence of the inertia magnitude

— — baseline

— main frame inertia reduced: $m_1 = (13.1/2)$ kg

$$m_{1u} = (17.5/2) \text{ kg}$$

$$m_2 = (209.6 - 35.9)/2 + 35.9 \text{ kg}$$

$$m_{2u} = (25.6/2) \text{ kg}$$

All moments of inertia concerning the motorcycle have been halved.
Note that the rider inertia remains unchanged (35.9 kg is the mass of the lower part of the rider body).

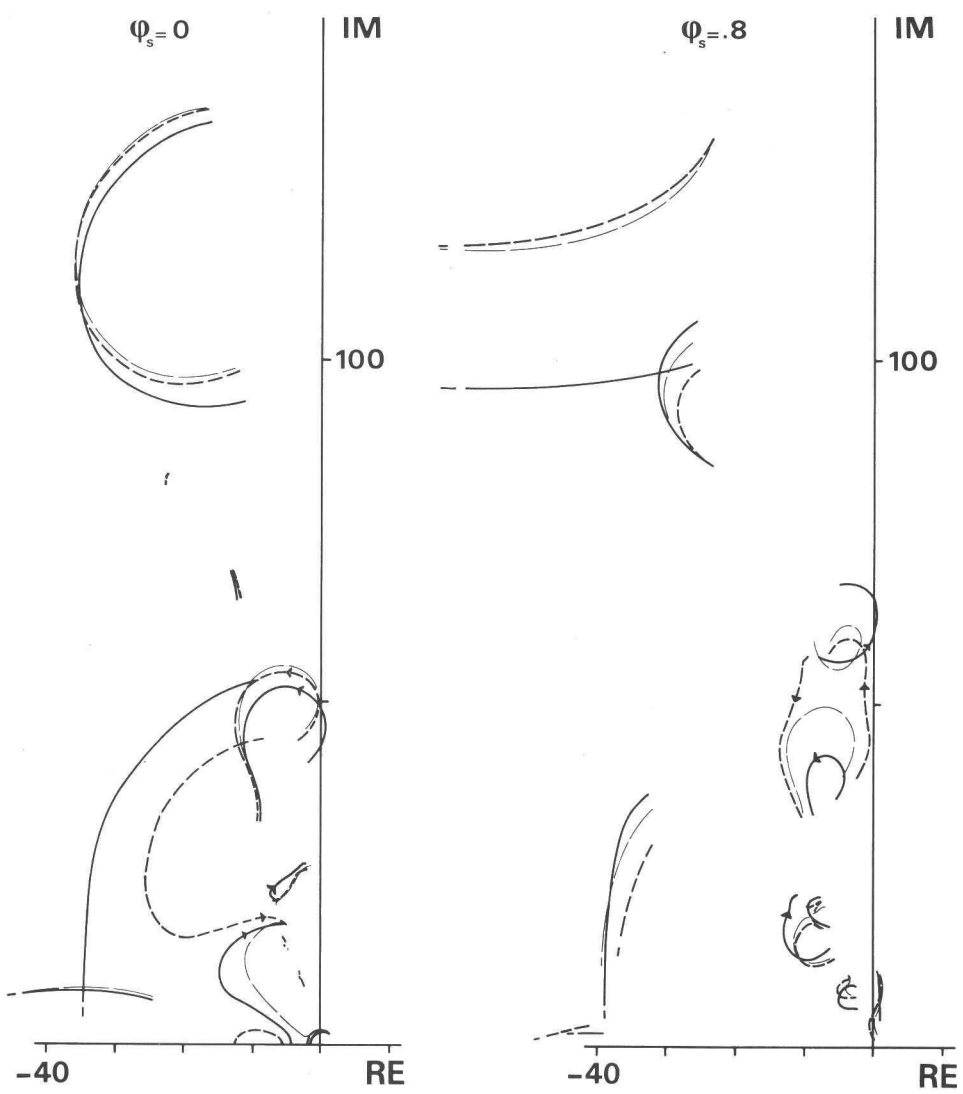


Fig. 76 influence of the location of the main frame centre of gravity

——— baseline ($g_{2x} = .680$ m; $g_{2z} = -.211$ m)
 ——— centre of gravity forward; $g_{2x} = .880$ m
 -·-·- centre of gravity downward; $g_{2z} = -.110$ m

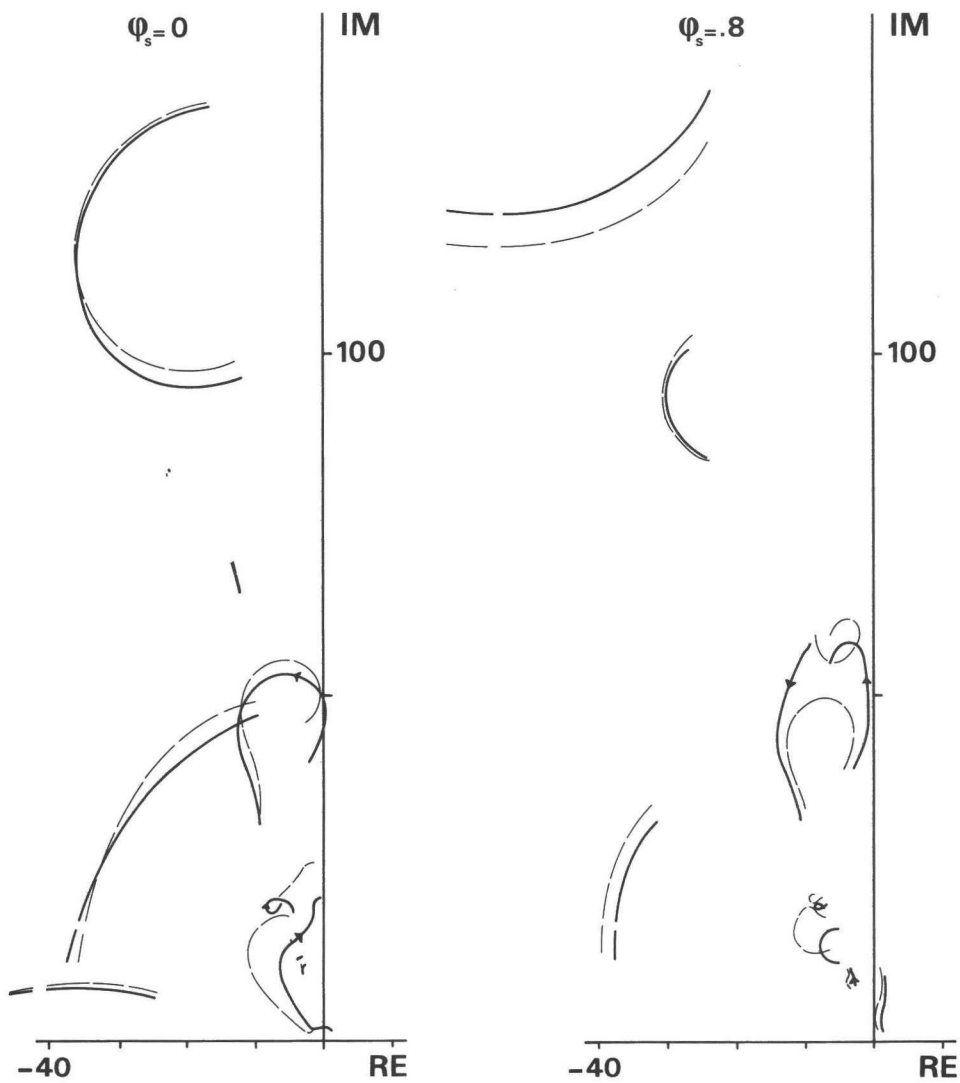


Fig. 77 influence of the addition of a top box (mass 25 kg; location of the top box centre of gravity in the nominal situation .30 m behind and .50 m above the rear wheel centre)

— baseline

$$\text{top box added: } m_2 = (209.6 + 25) \text{ kg}$$

$$\sum_m J_x = (6.9 + 1.87) \text{ kgm}^2$$

$$\sum_m J_y = (34.1 + 23.32) \text{ kgm}^2$$

$$\sum_m J_z = (21.1 + 21.45) \text{ kgm}^2$$

$$g_{2x} = .576 \text{ m}$$

$$g_{2z} = -.242 \text{ m}$$

5.1 Validity of the model

From the choice of the properties and features of the mechanical model, as described in chapter 2, various limitations arise with respect to the validity of the model.

model structure

The physical model is composed of several rigid bodies, interconnected by kinematic restraints, cf. Sec. 2.3. The distributed frame elasticity in front of the engine block has in the model been lumped at the twist axis; the lumped compliance properties have been quantified by means of static experiments. This approximation employed in the model structure seems reasonable for a large variety of motorcycles, as long as the rear wheel twist may be neglected (cf. [38]).

The rider body has been represented by two rigid parts, the lower being rigidly attached to the main frame, the upper being allowed to rotate about a horizontal axis in the vehicle plane of symmetry. The required compliance parameter has been determined from resonance experiments on a moving-base simulator. This two-body approximation of the rider restricts utilization of the full model to parametersets of middle- and heavyweight motorcycles. It is likely that true to life representation of the influence of the passive rider on the dynamic behaviour of a lightweight motorcycle requires a more complex rider body model.

non-stationary tyre model

The non-stationary tyre model has been based on the straight-tangent approximation of the taut string model, cf. Sec. 2.4.3. This approximation is valid in cases for which the wavelength of the wheel motion in question (related to the ground plane) is large with respect to the tyre contact length.

By limiting the minimum speed considered to 5 ms^{-1} this requirement has been met for the most relevant results presented in this study, which, as far as the anti-symmetrical motions are concerned, are all within the frequency

range below 60 rads^{-1} .*

The low-speed results of other than symmetrical modes with higher frequencies should be regarded with suspicion.

rider control

The bandwidth of the controlling actions of the rider amounts to 1 à 1.5 Hz. The fact that the model at hand features a non-controlling rider should be considered when regarding the practical importance of solutions in this low-frequency region.

magnitude of variables

Some variables describing the stationary situation have been assumed to be small, cf. Sec. 2.7.12. Of this group the symmetrical variables have been accounted for in the final results by an intermediate adaptation of the vehicle geometry, cf. Sec. 3.1. The remaining variable is the stationary steer angle δ_s . The assumption of this angle being small is not justified in the case of large roll angles at low speed.

The major consequence with respect to the model validity is the variation of the mechanical trail, cf. Sec. 4.1.2. The influence of trail variation on the results has been investigated, cf. Sec. 4.4.2; on the ground of these investigations, the lower bound of the speed range considered, at roll angles greater than .5 rad, has been restricted to 10 ms^{-1} . The most important influence of the trail variation occurring within the input parameter value range regarded appears to be a significant stabilization of the low speed cornering weave.

In this study quasi-linear dynamic equations have been employed; therefore the calculations are valid only for infinitesimal deviations from the stationary situation. The real-world system exhibits limit-cycle phenomena, as have been shown in the films [1] and [4].

5.2 Discussion of the results concerning the running-straight-ahead situation

The quasi-linear, homogeneous set of differential equations, which has been derived starting from the chosen physical approximation of the real motorcycle/rider system, shows various roots corresponding to lightly or negatively damped motions.

When running-straight-ahead two oscillatory modes of motion are especially

* the front wheel contact length (2a) at low speed amounts to ca. 0.13 m.

significant in the speed range considered: a low-frequency (ca. 25 rads⁻¹) oscillation at high speed involving both the front and the main assembly of the vehicle: the 'shake/weave' mode of motion, and a high-frequency (ca. 50 rads⁻¹) oscillation at moderate speed (e.g. 15 ms⁻¹) involving mainly the front assembly of the vehicle: the 'wobble' mode of motion.

The high speed shake/weave is destabilized by increasing the frame compliance, lowering the twist axis, rigidizing the rider, increasing the air drag, moving the main frame centre of gravity towards the rear or upwards or increasing the motorcycle inertia. The low speed wobble is destabilized by increasing the frame compliance, rigidizing the rider body, increasing the motorcycle inertia or moving the main frame centre of gravity forward. The running-straight-ahead root-loci corresponding with oscillatory solutions are only slightly influenced by the inclusion of $\tilde{F}_{y\gamma}$, $\tilde{F}_{x\rho}$, $\tilde{M}_{z\alpha}$, $\tilde{M}_{z\gamma}$, \tilde{M}_{zGYR} and \tilde{M}_x in the description of the tyre behaviour.

The one important monotonous eigen-motion at running-straight-ahead is the 'capsize' mode, lightly unstable from ca. 17 ms⁻¹ on. This monotonous solution remains when cornering, but the critical speed ultimately shifts to higher values.

5.3 Discussion of the results concerning the cornering situation

When cornering, all eigen-modes of motion contain both symmetrical and anti-symmetrical motions. Many root courses (arising from each mode of motion when the speed is continuously varied) exhibit fusions with and detachments from each other. Thus in-plane and lateral modes of motion can be seen to fade into one another and vice versa. The most significant oscillatory cornering mode of motion is a low-frequency phenomenon, originating from the combined weave/shake mode and the pitch and bounce modes in the running-straight-ahead case. At a mean roll angle of .8 rad, this mode, which has been called the 'cornering weave', is unstable throughout the speed range considered, regarding the base-line model. Another important mode of the cornering case originates from the front hop mode and/or the wobble mode at running-straight-ahead. In the base-line case at $\phi_s = .8$ rad this mode, which is called the 'wheel patter' mode of motion, exhibits frequencies from 40 to 60 rads⁻¹ in the speed range considered and is still damped. Minimal damping generally occurs at higher speed than the minimal damping roots of the running-straight-ahead wobble course.

The cornering weave is destabilized by increasing the frame compliance, raising the twist axis, decreasing the air drag, increasing the mechanical trail or moving the main frame centre of gravity upwards. The cornering weave root course is not affected by rigidizing the rider. The wheel patter is de-

stabilized by increasing the frame compliance, raising the twist axis, rigidizing the rider body, reducing the air drag, decreasing the suspension damping, increasing the motorcycle inertia, or lowering the main frame centre of gravity or shifting it forward. In contrast to the running-straight-ahead root-loci, the cornering root-loci generally are influenced considerably by the inclusion of $\tilde{F}_{y\gamma}$, $\tilde{F}_{y\rho}$, $\tilde{M}_{z\alpha}$, $\tilde{M}_{z\gamma}$, \tilde{M}_{zGYR} and \tilde{M}_x in the description of the tyre behaviour.

5.4 Conclusion

The model and the investigations presented in this study may improve the insight into the motorcycle as a dynamic system, especially concerning the cornering phenomena. After a detailed experimental verification of the behaviour of both the tyre subsystem and the motorcycle as a whole a practically useful design tool will have been obtained. The model will be employed to investigate the influence of road properties, such as surface geometry and friction.

Qualitatively, the main aspects of the oscillatory dynamic behaviour of the vehicle match reality (weave: cf. [4]; wobble: cf. [1]; cornering weave: cf. [47]; about 'wheel patter' information from experienced motorcyclists has been obtained).

Regarding the results quantitatively, the following remarks should be made:

At about the speed at which minimum damping of the wobble mode occurs, the wheel rate of revolution matches the wobble mode frequency. Therefore first harmonics of tyre and wheel rim non-uniformities may substantially influence the real wobble damping quantitatively. The same holds for the wheel patter phenomenon when cornering.

The high-speed shake/weave mode root location depends only slightly on the forward speed. Changing the vehicle parameters, however, may shift the high speed part of the shake/weave root course as a whole, thus strongly influencing the high speed weave critical speed.

Regarding the cornering situation it should be noted that .8 rad is an extreme value for the (touring) machine under consideration.

For more detailed conclusions be referred to the paragraphs in which the results of the calculations have been presented.

introduction

The model has been provided with a lumped frame elasticity, described by β , in accordance with Fig. 28, to describe the torsional compliance between the middle section of the main frame and the front wheel centre plane, about an axis perpendicular to the steer axis. Two parameters define this lumped compliance: the torsional stiffness C_β and the nominal height of the torsion axis above the ground plane in the nominal situation ($r_{w2o} - f_z$), cf. Figs. A1 and B2.

frame compliance measurements

Compliance measurements have been conducted, providing an overview of the distribution and the magnitude of the relevant elastic properties. Regarding the motorcycle structure as a whole and at the same time minimizing the experimental effort the (dummy) rear wheel hub has been fixed, and a load has been applied either on the front wheel hub or at the lowest point of the front wheel rim inside, cf. Fig. A2. The frame springs have been fixed to suit the nominal situation (at zero speed loaded with 1 person).

Several loading cases have been regarded (lateral force, moment parallel to the steering axis, moment perpendicular to the steering axis in the vehicle plane of symmetry) and in each case rotations and translations of a number of measuring points (cf. Fig.A3) have been recorded. The front wheel compliance has been regarded separately. Fig. A4 shows the results in the case of a lateral force applied on the lowest point of the front wheel rim inside. Of the effects on the dynamic behaviour of the motorbike due to frame elasticity, front wheel camber and lateral displacement play a major role because of gyroscopic coupling, camber force and tyre sideslip respectively. Therefore, the deflection of the front wheel plane has been regarded (in the deflected state this plane is defined as the plane through the front axle centre perpendicular to the axle at this point). The wheel rim deflection relative to the deflected wheel plane has been corrected for, in that finally the zeroth and first-order harmonics of the wheel rim deflection have been taken into account. This yields the effective deflected front wheel plane.

The deflection of the original front wheel plane of symmetry has been regarded relative to the engine plane of symmetry because we assume the compliance in front* of the great mass concentration in the structure (which is the sum total of engine block and lower part of the rider body) to play the major role in the case of a wobble oscillation, which is obviously the fault-

* directions indicated relative to the forward speed.

iest predicted mode of the rigid-framed model. The elasticity causing this deflection has been lumped into the torsional stiffness about the β -axis. The torsional compliance behind* the engine block could also be determined from the measurements and was found to be well within the range of which Sharp predicts this specific torsional compliance to have no significant influence on the dynamic behaviour [38].

The data-processing of the measurements will now be discussed on the basis of Fig. A4. The left-hand part of this figure constitutes a side view of the motorcycle, which has been rotated over the inclination angle ϵ . In a front view (right-hand part of Fig. A4) the torsional axis will now reduce to a point. This point will be determined as the point of intersection of the (deflected) engine plane of symmetry and the effective deflected front wheel plane defined above and a plane through the front wheel centre, parallel to the steering axis and perpendicular to the original vehicle plane of symmetry. The side view (Fig. A4) exhibits the measuring points (cf. Fig. A3) and the lines W-W and E-E. W-W is fixed in the 'effective wheel plane', E-E in the engine plane of symmetry. In the unloaded case both planes coincide with the vehicle plane of symmetry, and W-W with E-E. In that case these lines contain the front wheel centre and are parallel to the steering axis. When applying a lateral force F_y (in accordance with Fig. A2) the measuring points move laterally from the vehicle plane of symmetry to the positions, indicated by the circles, shown in the front view (Fig. A4). For clarity the deflections have been proportionally exaggerated. If the elastic behaviour of the structure is considered to be completely linear with respect to lateral deflection the depicted state would correspond to a load F_y (cf. Fig. A2) of 30 kN. With the aid of the measured displacement and rotation of measuring point 2 the deflected engine plane can be determined. This yields the displaced line E-E in the front view.

With the aid of the deflections of 5, 6 and 10 and the rotation of 5 an approximation of the position of two points of the deformed deflected wheel plane can be derived. In this case the elastic behaviour of the wheel rim itself plays a role. In the mathematical model, however, the wheel rim is assumed to be stiff. Therefore the effective deflected wheel plane is employed defined by the zeroth and first-order harmonics of the wheel rim deflections measured at the points 7 to 11. Through this procedure the line W-W in the effective deflected wheel plane can be found. The point of intersection of E-E and W-W constitutes the height of the torsional axis in the model structure assumed.

* directions indicated relative to the direction of travel.

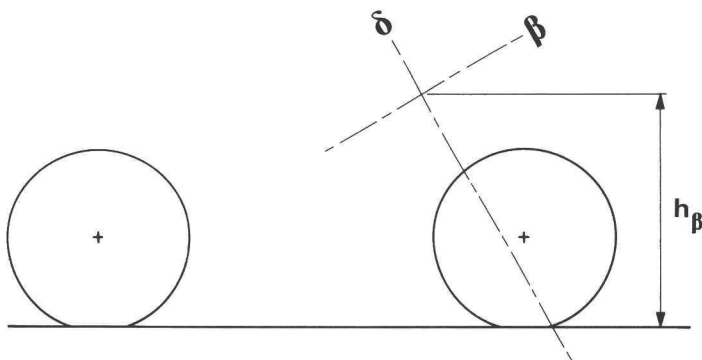


Fig. A1 location of the lumped frame elasticity; $k_\beta = .834 \text{ m}$; $c_\beta = 3.41 \times 10^4 \text{ Nmrad}^{-1}$

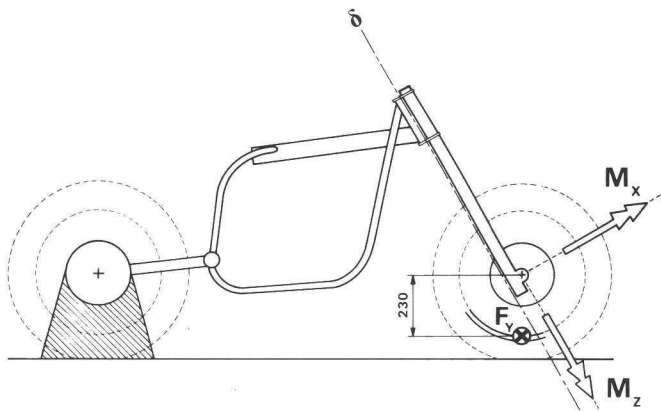


Fig. A2 test configuration and loading cases

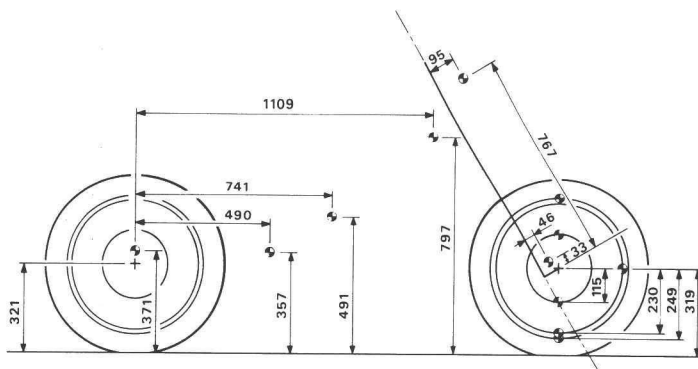


Fig. A3 location of measuring points

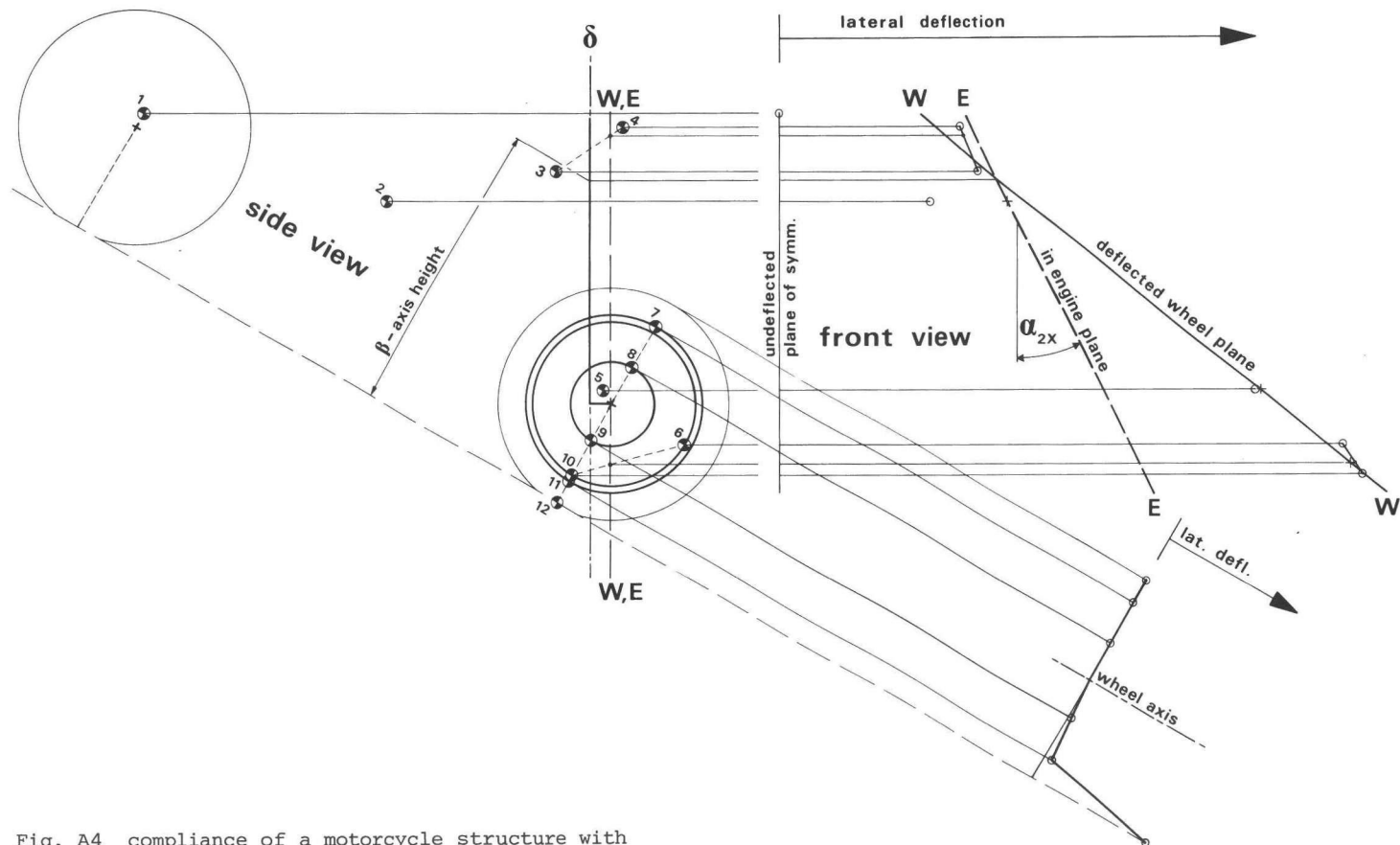


Fig. A4 compliance of a motorcycle structure with a lateral force applied in accordance with Fig. A2

Appendix B - definition of the full model

In order to keep the introduction of the mathematical model surveyable, in the foregoing chapters a simplified version has been employed. The full model, the equations of which being listed in Appendix F, provides for the following extra features:

- ascription of mass to the twisting, sprung part of the front frame (part (1s) in Fig. B1);
- no coincidence required of the mass centre of the front axle assembly G_{1a} and the mass centre of the front wheel G_{1w} , cf. Fig. B4 to Fig. 30.

The various parts, composing the full model, have been shown in Fig. B1 (to be compared with Fig. 11, applying to the simplified version). The location of the mass centre has been defined in Fig. B2 (to be compared with Fig. 12, applying to the simplified version). The vector structure and the orientation of the local triads concerning the full model have been depicted in Figs. B3 and B4 respectively (to be compared with the Figs. 29 and 30 respectively, applying to the simplified version).

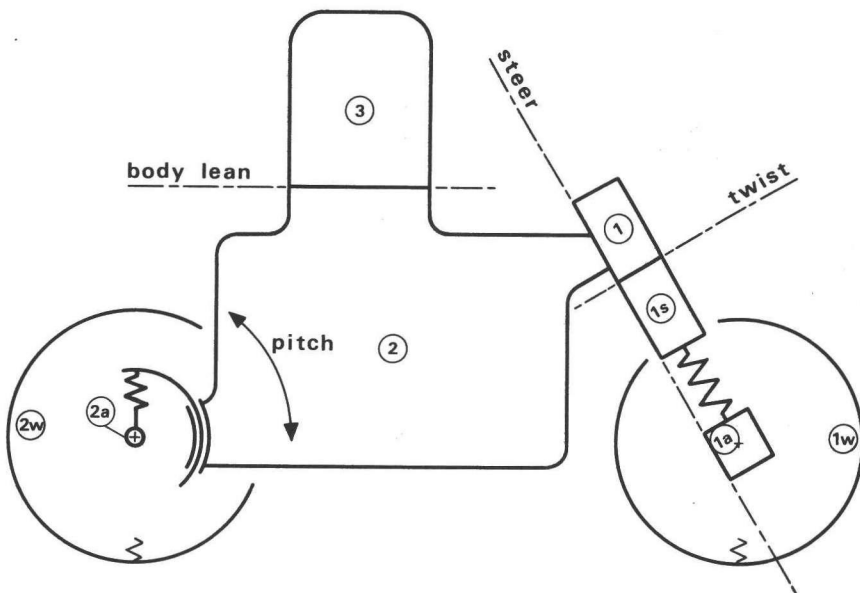


Fig. B1 the various parts composing the vehicle; full model.

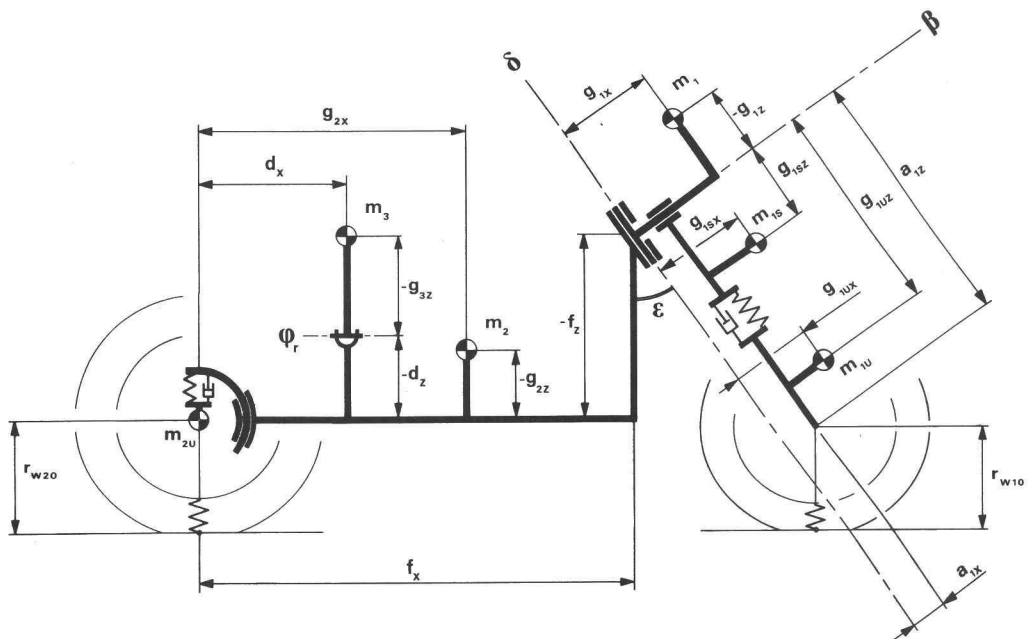


Fig. B2 geometry of the full model.

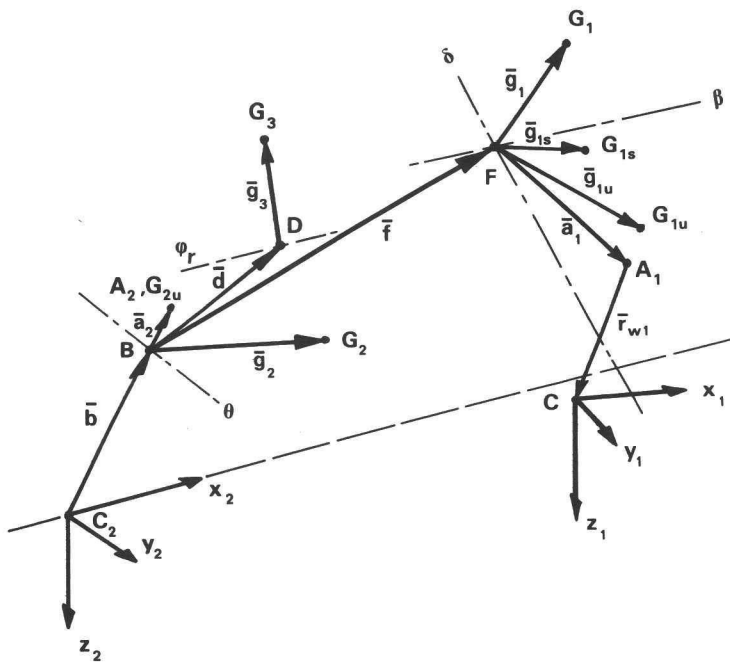


Fig. B3 vector structure of the full model (depicted in an arbitrary situation). Letters G indicate mass centres. Note that $|\bar{b} + \bar{a}_2| = r_{w2}$.

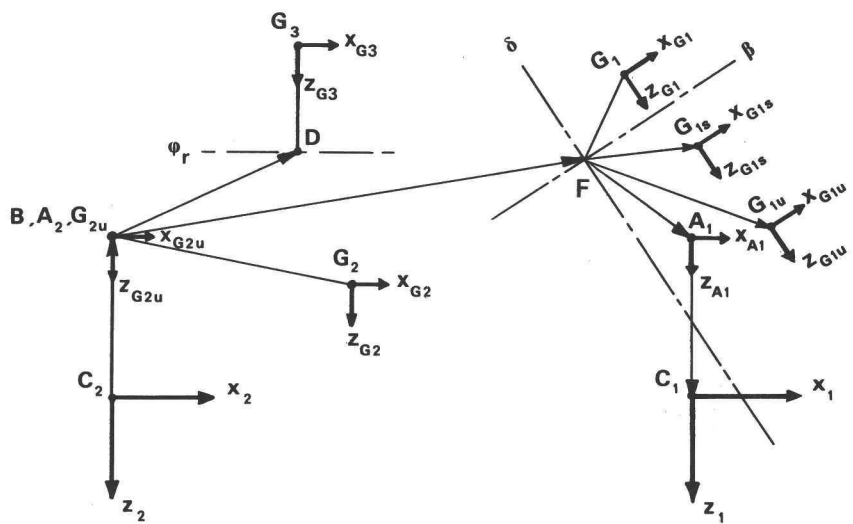


Fig. B4 local triads (depicted in the nominal situation; of the right-handed orthogonal systems of axes only the x- and z-axes have been indicated). Note that z_{A1} is always directed along $\overline{A_1 C_1}$, and z_{G2u} along $\overline{A_2 C_2}$.

Appendix C - elaborated quantities

This appendix constitutes the link between the global description of the derivation of the equations of motion as this has been given in chapter 2 on the one hand and the detailed description as it is provided by the Appendices E and F on the other. In many of the equations to be presented in this appendix terms smaller than a certain (e.g. i-th) order of magnitude have been omitted (indicated by: $+O^{i+1}$) in order to keep this appendix and the expressions themselves surveyable. Many derivations are covered by the, thus rounded, expressions given below. For the remaining cases be referred to the reports [12] and [15]. The quantities l have been defined in Appendix D.

quantities serving the derivation of the kinetic energy

The position of the front wheel centre A_1 relative to (c_2, x_2, y_2, z_2) , is described by \bar{p}_{A1} . Expressed in the generalised co-ordinates, the components of this vector read:

$$p_{A1x} = l_{A1x} + \theta (l_{A1z} - b_z) - \lambda_{s1} \sin \varepsilon + o^2 \quad (C1)$$

$$\begin{aligned} p_{A1y} = & - l_{A1z} \sin \phi - \lambda_{t2} \sin \phi - \lambda_{s2} \sin \phi + \theta l_{A1x} \sin \phi + \\ & + \delta g_{A1x} \cos \phi - \beta g_{A1z} \cos \phi + \lambda_{s1} \sin \phi \cos \varepsilon + o^2 \end{aligned} \quad (C2)$$

$$\begin{aligned} p_{A1z} = & l_{A1z} \cos \phi + \lambda_{t2} \cos \phi + \lambda_{s2} \cos \phi - \theta l_{A1z} \cos \phi + \\ & + \delta g_{A1z} \sin \phi - \beta g_{A1x} \sin \phi - \lambda_{s1} \cos \phi \cos \varepsilon + o^2 \end{aligned} \quad (C3)$$

The vector $\bar{\omega}_{G1u}^{G1u}$ describes the rotation of body 1a (cf. Figs. 11 and B1) expressed in components related to the system of axes $(G_{1u}, x_{G1u}, y_{G1u}, z_{G1u})$. Expressed in the generalized co-ordinates, the components of this vector read:

$$\omega_{G1ux}^{G1u} = r \delta \sin \phi - r \cos \phi \sin \varepsilon + \dot{\phi} \cos \varepsilon + \dot{\beta} + o^2 \quad (C4)$$

$$\omega_{G1uy}^{G1u} = r \sin \phi + r \delta \cos \phi \sin \varepsilon + r \beta \cos \phi \cos \varepsilon + \dot{\theta} + o^2 \quad (C5)$$

$$\omega_{G1uz}^{G1u} = - r \beta \sin \phi - r \theta \cos \phi \sin \varepsilon + r \cos \phi \cos \varepsilon + \dot{\phi} \sin \varepsilon - \dot{\delta} + o^2 \quad (C6)$$

With the O^2 terms taken into account, \dot{p}_{A1} and $\dot{\omega}_{G1u}^{G1u}$ serve as the basis for the derivation of the kinetic energy of the system, with the exclusion of the wheels with respect to their main rotation, cf. Eqs. (62), (63) and (74). The kinetic energy due to the speed of revolution of the wheels has been derived separately, cf. Sec. 2.7.7.

quantities concerning the tyre behaviour

The tyre/ground contact problem requires an explicit description of the front wheel radius vector \bar{r}_{w1} (having the direction and length of $\overline{A_1C_1}$, cf. Fig. 32). In order to obtain this description and that of the kinematic variables serving the tyre model input, the normal to the front wheel centre plane, \bar{j} , is required, which can be derived in accordance with Eq. (49). The components of \bar{j} relative to (C_2, x_2, y_2, z_2) read, in elaborated form:

$$j_x = -\delta \cos\epsilon + \beta \sin\epsilon + O^2 \quad (C7)$$

$$j_y = \cos\phi - \delta \sin\phi \sin\epsilon - \beta \sin\phi \cos\epsilon + O^2 \quad (C8)$$

$$j_z = \sin\phi + \delta \cos\phi \sin\epsilon + \beta \cos\phi \cos\epsilon + O^2 \quad (C9)$$

Together with the Eqs. (C1), (C2) and (C3) we now obtain, following the Eqs. (52), (53) and (54):

$$r_{w1x} = -\delta l_{A1z} \tan\phi \cos\epsilon + \beta l_{A1z} \tan\phi \sin\epsilon + O^2 \quad (C10)$$

$$\begin{aligned} r_{w1y} = & \sin\phi (l_{A1z} + \lambda_{t2} + \lambda_{s2} - \theta l_{A1x} + \delta g_{A1x} \tan\phi - \beta g_{A1z} \tan\phi + \\ & - \lambda_{s1} \cos\epsilon) + \frac{l_{A1z}}{\cos\phi} (\delta \sin\epsilon + \beta \cos\epsilon) + O^2 \end{aligned} \quad (C11)$$

$$r_{w1z} = -p_{A1z} \quad (C12)$$

The derivation of the front slip angle α_1 requires the slip velocity vector \dot{s}_1 , cf. Eq. (56), which now can readily be obtained, and the steer angle in the ground plane, δ' , which can be obtained from Eqs. (C7) and (C8), in accordance with (5), and reads:

$$\delta' = \delta \frac{\cos\epsilon}{\cos\phi} - \beta \frac{\sin\epsilon}{\cos\phi} + O^2 \quad (C13)$$

With the aid of δ' , \dot{s}_1 can be transformed into \dot{s}_1^{C1} . From this vector α_1 can be derived, in accordance with Eq. (59). We obtain for α_1 and α_2 :

$$\begin{aligned}\alpha_1 &= \frac{1}{u} \left[-v - r \{ l_{A1x} + \theta (l_{A1z} - b_z) - \lambda_{s1} \sin \epsilon . + \right. \\ &\quad \left. - \delta l_{A1z} \tan \phi \cos \epsilon \} - \dot{\delta} t \frac{1}{\cos \phi} - \dot{\beta} (l_{A1z} \frac{\cos \epsilon}{\cos \phi} - g_{A1z} \frac{1}{\cos \phi}) \right] + \\ &\quad + \delta \frac{\cos \epsilon}{\cos \phi} - \beta \frac{\sin \epsilon}{\cos \phi} + o^2 \quad (C14)\end{aligned}$$

$$\alpha_2 = -\frac{v}{u} \quad (C15)$$

The camber angle of the front wheel, γ_1 , can directly be obtained from j_z , Eq. (C9), in accordance with Eq. (50). We obtain for γ_1 and γ_2 :

$$\gamma_1 = \phi + \delta \sin \epsilon + \beta \cos \epsilon + o^2 \quad (C16)$$

$$\gamma_2 = \phi \quad (C17)$$

From Eqs. (55) and (C13) we obtain for ρ_1 and ρ_2 :

$$\rho_1 = \frac{1}{u} (r + \dot{\delta}') \quad (C18)$$

$$\rho_2 = \frac{r}{u} \quad (C19)$$

The dynamic variations of the normal wheel loads can be elaborated in accordance with Eqs. (3) and (2). We obtain for \tilde{F}_{z1} and \tilde{F}_{z2} :

$$\begin{aligned}\tilde{F}_{z1} &= \frac{\tilde{F}_{t1}}{\cos \gamma_{1s}} + \tilde{\gamma}_1 F_{t1s} \frac{\tan \gamma_{1s}}{\cos \gamma_{1s}} + F_{y1} \tan \gamma_{1s} + \tilde{\gamma}_1 F_{y1s} \frac{1}{\cos^2 \gamma_{1s}} = \\ &= -\frac{c_{t1}}{\cos \phi_s} \{ \tilde{\delta} t \tan \phi_s + \tilde{\beta} (l_{A1z} \cos \epsilon - g_{A1z}) \tan \phi_s - \tilde{\theta} l_{A1x} + \quad (C20)\end{aligned}$$

$$\begin{aligned}&\quad + \tilde{\lambda}_{t2} + \tilde{\lambda}_{s2} - \tilde{\lambda}_{s1} \cos \epsilon \} + (\tilde{\phi} + \tilde{\delta} \sin \epsilon + \tilde{\beta} \cos \epsilon) (F_{t1s} \frac{\tan \phi_s}{\cos \phi_s} + \frac{F_{y1s}}{\cos^2 \phi_s}) \\ \tilde{F}_{z2} &= -\frac{c_{t2}}{\cos \phi_s} \tilde{\lambda}_{t2} + \tilde{\phi} (F_{t2s} \frac{\tan \phi_s}{\cos \phi_s} + F_{y2s} \frac{1}{\cos^2 \phi_s}) + \tilde{F}_{y2} \tan \phi_s \quad (C21)\end{aligned}$$

Appendix D - definition of auxiliary quantities and summation conventions

auxiliary quantities

The horizontal and vertical distance of each relevant point to C_2 in the nominal situation have been identified with a single quantity "l", in order to reduce the length of the mathematical description of the model. These lengths can be obtained from Fig. B2 and read:

$$l_{A1x} = f_x + a_{1x} \cos\epsilon + a_{1z} \sin\epsilon \quad (D1)$$

$$l_{A1z} = b_z + f_z - a_{1x} \sin\epsilon + a_{1z} \cos\epsilon \quad (D2)$$

$$l_{G1ux} = f_x + g_{1ux} \cos\epsilon + g_{1uz} \sin\epsilon \quad (D3)$$

$$l_{G1uz} = b_z + f_z - g_{1ux} \sin\epsilon + g_{1uz} \cos\epsilon \quad (D4)$$

$$l_{G1sx} = f_x + g_{1sz} \cos\epsilon + g_{1sz} \sin\epsilon \quad (D5)$$

$$l_{G1sz} = b_z + f_z - g_{1sx} \sin\epsilon + g_{1sz} \cos\epsilon \quad (D6)$$

$$l_{G1x} = f_x + g_{1x} \cos\epsilon + g_{1z} \sin\epsilon \quad (D7)$$

$$l_{G1z} = b_z + f_z - g_{1z} \sin\epsilon + g_{1z} \cos\epsilon \quad (D8)$$

$$l_{G2x} = g_{2x} \quad (D9)$$

$$l_{G2z} = b_z + g_{2z} \quad (D10)$$

$$l_{G3x} = d_x \quad (D11)$$

$$l_{G3z} = b_z + d_z + g_{3z} \quad (D12)$$

$$l_{G2ux} = 0 \quad (D13)$$

$$l_{G2uz} = b_z \quad (D14)$$

summation conventions

In order to achieve a compact notation many groups of terms have been clustered into summation expressions, denoted by Σ . The following summations are now introduced:

notation:

\sum_2
 \sum_3
 \sum_5
 \sum_6

summation over (cf. Figs. 11 and B1):

(1u) and (1s)
 (1u), (1s) and (1)
 (1u), (1s), (1), (2) and (3)
 (1u), (1s), (1), (2), (3) and (2u)

Examples:

$$\sum_2(m) = m_{1u} + m_{1s}$$

$$\sum_2(mg_x) = m_{1u}g_{1ux} + m_{1s}g_{1sx}$$

$$\sum_2(mg_z) = m_{1u}g_{1uz} + m_{1s}g_{1sz}$$

$$\sum_2(mg_{z_x}) = m_{1u}g_{1uz}^l G_{1ux} + m_{1s}g_{1sz}^l G_{1sx}$$

$$\sum_3(m) = m_{1u} + m_{1s} + m_1$$

$$\sum_3(mg_x^2) = m_{1u}g_{1ux}^2 + m_{1s}g_{1sx}^2 + m_1g_{1x}^2$$

$$\sum_5(m) = m_{1u} + m_{1s} + m_1 + m_2 + m_3$$

$$\begin{aligned}\sum_5\{m_{1x}(l_z - b_z)\} &= m_{1u}l_{G1ux}(l_{G1uz} - b_z) + m_{1s}l_{G1sx}(l_{G1xz} - b_z) + \\ &+ m_1l_{G1x}(l_{G1z} - b_z) + m_2l_{G2x}(l_{G2z} - b_z) + \\ &+ m_3l_{G3x}(l_{G3z} - b_z)\end{aligned}$$

$$\sum_6(m) = m_{1u} + m_{1s} + m_1 + m_2 + m_3 + m_{2u}$$

$$\begin{aligned}\sum_6(m l_x l_z) &= m_{1u}l_{G1ux}l_{G1uz} + m_{1s}l_{G1sx}l_{G1sz} + m_1l_{G1x}l_{G1z} + \\ &+ m_2l_{G2x}l_{G2z} + m_3l_{G3x}l_{G3z} + m_{2u}l_{G2ux}l_{G2uz}\end{aligned}$$

Concerning the moments of inertia the following summation conventions have been employed:

notation:

\sum_δ

\sum_β

\sum_m

summation over:

all parts rotating about the steering axis relative to the main frame assembly;

all parts rotating about the twist axis relative to the part of the front frame above the twist axis;

all parts concerning the main frame assembly.

Note that the rear axle assembly (2a) does not participate in the pitch rotation of the main frame (cf. Fig. B1). The same holds for the rear wheel (2w). The front wheel (1w) does not participate in rotation of the neighbouring part (1a) about the local y-axis. The centrifugal moments J_{xz} of the wheels, which have been assumed to have a rotationally homogeneous mass distribution, are zero.

Because of the facts mentioned above the summation conventions in question are not independent of the subscript of the moment of inertia on which they have been applied. We define:

$$\sum_{\delta} J_x = J_{x1} + J_{x1a} + J_{x1w} + J_{x1s}$$

$$\sum_{\delta} J_y = J_{y1} + J_{y1a} + J_{y1s}$$

$$\sum_{\delta} J_z = J_{z1} + J_{z1a} + J_{z1w} + J_{z1s}$$

$$\sum_{\delta} J_{xz} = J_{xz1} + J_{xz1a} + J_{xz1s}$$

$$\sum_{\beta} J_x = J_{x1a} + J_{x1w} + J_{x1s}$$

$$\sum_{\beta} J_y = J_{y1a} + J_{y1s}$$

$$\sum_{\beta} J_z = J_{z1a} + J_{z1w} + J_{z1s}$$

$$\sum_{\beta} J_{xz} = J_{xz1a} + J_{xz1s}$$

$$\sum_m J_x = J_{x3} + J_{x2} + J_{x2a} + J_{x2w}$$

$$\sum_m J_y = J_{y3} + J_{y2}$$

$$\sum_m J_z = J_{z3} + J_{z2} + J_{z2a} + J_{z2w}$$

$$\sum_m J_{xz} = J_{xz3} + J_{xz2} + J_{xz2a}$$

Appendix E - equations of the stationary motion

The derivation of the equations of motion has been documented in [12] and [15].

The equilibrium condition in a stationary situation ('steady state') is described by 14 non-linear algebraic equations, 8 of which concerning the vehicle structure, the remaining 6 concerning the tyre behaviour, cf. Sec.

2.4.2. The steady-state variables are:

v_s	:	stationary lateral velocity
r_s	:	" yaw rate
$M_{\delta s}$:	" steer moment
δ_s	:	" steer angle
θ_s	:	" pitch angle
λ_{t2s}	:	" rear tyre spring compression
λ_{s2s}	:	" rear suspension spring compression
λ_{s1s}	:	" front suspension spring compression
F_{y1s}	:	front tyre side force
M_{z1s}	:	" " aligning moment
M_{x1s}	:	" " overturning moment
F_{y2s}	:	rear tyre side force
M_{z2s}	:	" " aligning moment
M_{x2s}	:	" " overturning moment

The input parameters are:

u_s	:	stationary forward velocity
ϕ_s	:	stationary roll angle

To reduce the total number of terms in the steady state equations the steady state variables have been divided into two groups, variables of the one group being assumed to be small in relation to variables of the other group:

GROUP I (large)

GROUP II (small)

$u_s v_s r_s \phi_s F_{y1s} M_{z1s} F_{y2s} M_{z2s} M_{x2s} M_{\delta s}$

$\delta_s \theta_s \lambda_{t2s} \lambda_{s2s} \lambda_{s1s}$

It may be noted that the variables of group II all represent quantities which describe the change in shape of the vehicle with respect to the nominal situation.

Terms with products of variables in group II have been neglected in the final steady state equations. These steady state equations read:

$$f_{y_s} = u_s r_s \sum_6 (m) + r_s^2 \sum_5 (ml_z) \sin\phi_s - r_s^2 \delta_s \sum_3 (mg_x) \cos\phi_s + \\ - r_s^2 \theta_s \sum_5 (ml_x) \sin\phi_s + r_s^2 \lambda_{t2s} \sum_6 (m) \sin\phi_s + \\ + r_s^2 \lambda_{s2s} \sum_5 (m) \sin\phi_s - r_s^2 \lambda_{s1s} m_{1u} \sin\phi_s \cos\epsilon + \\ - F_{y1s} - F_{y2s} + F_L \sin\phi_s$$

$$f_{\psi_s} = u_s r_s \sum_6 (ml_x) - v_s r_s \sum_5 (ml_z) \sin\phi_s + u_s r_s \theta_s \sum_5 \{m (l_z - b_z)\} + \\ - u_s r_s \lambda_{s1s} m_{1u} \sin\epsilon + v_s r_s \delta_s \sum_3 (mg_x) \cos\phi_s + \\ + v_s r_s \theta_s \sum_5 (ml_x) \sin\phi_s - v_s r_s \lambda_{t2s} \sum_6 (m) \sin\phi_s + \\ - v_s r_s \lambda_{s2s} \sum_5 (m) \sin\phi_s + v_s r_s \lambda_{s1s} m_{1u} \sin\phi_s \cos\epsilon + \\ - F_{y1s} \{l_{A1x} - \delta_s l_{A1z} \tan\phi_s \cos\epsilon + \theta_s (l_{A1z} - b_z) - \lambda_{s1s} \sin\epsilon\} + \\ - M_{z1s} - M_{z2s} - F_D p_{Dz} \sin\phi_s + F_L p_{Lx} \sin\phi_s$$

$$f_{\phi_s} = - u_s r_s \sum_6 (ml_z) \cos\phi_s - r_s^2 \sum_6 (ml_z^2) \sin\phi_s \cos\phi_s + \\ - u_s r_s \delta_s \sum_3 (mg_x) \sin\phi_s + u_s r_s \theta_s \sum_5 (ml_x) \cos\phi_s + \\ - u_s r_s \lambda_{t2s} \sum_6 (m) \cos\phi_s - u_s r_s \lambda_{s2s} \sum_5 (m) \cos\phi_s + \\ + u_s r_s \lambda_{s1s} m_{1u} \cos\phi_s \cos\epsilon + r_s^2 \delta_s \sum_3 (ml_z g_x) (\cos^2 \phi_s - \sin^2 \phi_s) + \\ + 2r_s^2 \theta_s \sum_5 (ml_x l_z) \sin\phi_s \cos\phi_s - 2r_s^2 \lambda_{t2s} \sum_6 (ml_z) \sin\phi_s \cos\phi_s + \\ - 2r_s^2 \lambda_{s2s} \sum_5 (ml_z) \sin\phi_s \cos\phi_s + \\ + 2r_s^2 \lambda_{s1s} m_{1u} l_{G1uz} \sin\phi_s \cos\phi_s \cos\epsilon + \\ - r_s^2 (\sum_m J_y + \sum_\delta J_y - \sum_m J_z + \sum_m J_{xz} - \sum_\delta J_x \sin^2 \epsilon - \sum_\delta J_z \cos^2 \epsilon) \sin\phi_s \cos\phi_s + \\ - r_s^2 \delta_s (\sum_\delta J_y - \sum_\delta J_x) (\cos^2 \phi_s - \sin^2 \phi_s) \sin\epsilon + \\ + 2r_s^2 \theta_s (\sum_\delta J_x - \sum_\delta J_z) \sin\phi_s \cos\phi_s \sin\epsilon \cos\epsilon + \\ + r_s (\Omega_{1s} J_{y1w} + \Omega_{2s} J_{y2w}) \cos\phi_s + \\ - r_s^2 (J_{y1w} + J_{y2w}) \sin\phi_s \cos\phi_s +$$

$$\begin{aligned}
& - r_s \Omega_{1s} \delta_s^J s_{y1w} \sin\phi_s \sin\varepsilon + r_s^2 \delta_s^J s_{y1w} (\sin^2\phi_s - \cos^2\phi_s) \sin\varepsilon + \\
& + v_s r_s \frac{1}{r_{w1}} \delta_s^J s_{y1w} \cos\varepsilon - r_s^2 \frac{1}{r_{w1}} \delta_s (t - l_{A1x} \cos\varepsilon) + \\
& + g \sum_6 (ml_z) \sin\phi_s - g \delta_s \sum_3 (mg_x) \cos\phi_s + \\
& - g \theta_s \sum_5 (ml_x) \sin\phi_s + g \lambda_{t2s} \sum_6 (m) \sin\phi_s + \\
& + g \lambda_{s2s} \sum_5 (m) \sin\phi_s - g \lambda_{s1s} m_{1u} \sin\phi_s \cos\varepsilon + \\
& - \delta_s^F z_{1o} t \frac{1}{\cos^2\phi_s} - \delta_s^F y_{1s} t \frac{\tan\phi_s}{\cos\phi_s} - M_{x1s} - M_{x2s}
\end{aligned}$$

$$\begin{aligned}
f_{\delta_s} = & u_s r_s \sum_3 (mg_x) \cos\phi_s + r_s^2 \sum_3 (ml_z g_x) \sin\phi_s \cos\phi_s + \\
& - u_s r_s \delta_s \sum_3 (mg_x) \sin\phi_s \sin\varepsilon + v_s r_s \delta_s \sum_3 (mg_x) \cos\varepsilon + \\
& + r_s^2 \delta_s \sum_3 (ml_x g_x) \cos\varepsilon - r_s^2 \delta_s \sum_3 (ml_z g_x) \sin^2\phi_s \sin\varepsilon + \\
& - r_s^2 \delta_s \sum_3 (mg_x^2) \cos^2\phi_s - r_s^2 \theta_s \sum_3 (ml_x g_x) \sin\phi_s \cos\phi_s + \\
& + r_s^2 \lambda_{t2s} \sum_3 (mg_x) \sin\phi_s \cos\phi_s + r_s^2 \lambda_{s2s} \sum_3 (mg_x) \sin\phi_s \cos\phi_s + \\
& - r_s^2 \lambda_{s1s} m_{1u} g_{1ux} \sin\phi_s \cos\phi_s \cos\varepsilon + \\
& + r_s^2 (\sum_J x \sin\varepsilon - \sum_J y \sin\varepsilon + \sum_J xz \cos\varepsilon) \sin\phi_s \cos\phi_s + \\
& + r_s^2 \delta_s \{ (\sum_J y - \sum_J x) \sin^2\phi_s + (\sum_J x - \sum_J y) \cos^2\phi_s \sin^2\varepsilon + \\
& + \sum_J x2 \cos^2\phi_s \sin\varepsilon \cos\varepsilon \} + \\
& + r_s^2 \theta_s \{ \sum_J x \cos\varepsilon - \sum_J y \cos\varepsilon - \sum_J x2 \sin\varepsilon \} \sin\phi_s \cos\phi_s + \\
& + r_s \Omega_{1s} J_{y1w} \cos\phi_s \sin\varepsilon - r_s^2 J_{y1w} \sin\phi_s \cos\phi_s \sin\varepsilon + \\
& - r_s \Omega_{1s} \delta_s^J s_{y1w} \sin\phi_s + r_s \Omega_{1s} \theta_s^J s_{y1w} \cos\phi_s \cos\varepsilon + \\
& + r_s^2 \delta_s^J s_{y1w} \sin^2\phi_s - r_s^2 \delta_s^J s_{y1w} \cos^2\phi_s \sin^2\varepsilon + \\
& + \frac{r_s^2}{r_{w1}} \delta_s^J s_{y1w} (l_{A1x} \cos\varepsilon - t) \sin\varepsilon + \frac{1}{r_{w1}} v_s r_s \delta_s^J s_{y1w} \sin\varepsilon \cos\varepsilon + \\
& - r_s^2 \theta_s^J s_{y1w} \sin\phi_s \cos\phi_s \cos\varepsilon + \\
& - g \sum_3 (mg_x) \sin\phi_s - g \delta_s \sum_3 (mg_x) \cos\phi_s \sin\phi_s + \\
& + F_{t1s} \{ -t \tan\phi_s - \delta_s t \sin\varepsilon + \delta_s l_{A1z} \tan^2\phi_s \cos^2\varepsilon + \\
& - \theta_s l_{A1z} \tan\phi_s \cos\varepsilon + (-2 \delta_s t \tan\phi_s + \theta_s l_{A1x}) + \\
& - \lambda_{t2s} - \lambda_{s2s} + \lambda_{s1s} \cos\varepsilon \} \tan\phi_s \sin\varepsilon + \\
& + C_{t1} (\delta_s t \tan\phi_s - \theta_s t l_{A1x} + \lambda_{t2s} + \lambda_{s2s} - \lambda_{s1s} \cos\varepsilon) t \tan\phi_s +
\end{aligned}$$

$$\begin{aligned}
& + F_{y1s} \left\{ -t + \delta_s l_{A1z} \tan \phi_s \cos^2 \varepsilon - \theta_s l_{A1z} \cos \varepsilon + \right. \\
& + (-2 \frac{s_t \tan \phi_s}{s} + \theta_s l_{A1x} - \lambda_{t2s} - \lambda_{s2s} + \lambda_{s1s} \cos \varepsilon) \sin \varepsilon \} \frac{1}{\cos \phi_s} + \\
& - M_{z1s} \frac{\cos \varepsilon}{\cos \phi_s} - M_{x1s} \sin \varepsilon - M_{\delta s}
\end{aligned}$$

$$\begin{aligned}
f_{\theta_s} = & u_s r_s \sum_5 (ml_x) \sin \phi_s - v_s r_s \sum_5 \{m (l_z - b_z)\} + \\
& + u_s r_s \theta_s \sum_5 \{m (l_z - b_z)\} \sin \phi_s - u_s r_s \lambda_{s1s} m_{1u} \sin \phi_s \sin \varepsilon + \\
& + v_s r_s \theta_s \sum_5 (ml_x) + v_s r_s \lambda_{s1s} m_{1u} \cos \varepsilon + \\
& - r_s^2 \sum_5 \{m l_x (l_z - b_z)\} + r_s^2 \sum_5 (m l_x l_z) \sin^2 \phi_s + \\
& - r_s^2 \delta_s \sum_3 (m l_x g_x) \sin \phi_s \cos \phi_s + \\
& + r_s^2 \theta_s \sum_5 (m l_x^2) \cos^2 \phi_s + r_s^2 \lambda_{s1s} m_{1u} l_{G1uz} \cos^2 \phi_s \cos \varepsilon + \\
& - r_s^2 \theta_s \sum_5 \{m (l_z - b_z)^2\} + r_s^2 \lambda_{s1s} m_{1u} (l_{G1uz} - b_z) \sin \varepsilon + \\
& + r_s^2 \theta_s \sum_5 \{m l_z (l_z - b_z)\} \sin^2 \phi_s + r_s^2 \lambda_{t2s} \sum_5 (ml_x) \sin^2 \phi_s + \\
& + r_s^2 \lambda_{s2s} \sum_5 (ml_x) \sin^2 \phi_s - r_s^2 \lambda_{s1s} m_{1u} l_{G1uz} \sin^2 \phi_s \sin \varepsilon + \\
& + r_s^2 (-\sum_j \frac{m}{m} xz - \sum_j \frac{\delta}{\delta} xz \cos^2 \varepsilon - \sum_j \frac{\lambda}{\lambda} x \sin \varepsilon \cos \varepsilon + \sum_j \frac{\lambda}{\lambda} z \sin \varepsilon \cos \varepsilon + \\
& + \sum_j \frac{\lambda}{\lambda} z \sin^2 \varepsilon) \cos^2 \phi_s + r_s^2 \delta_s (\sum_j \frac{\lambda}{\lambda} x \cos \varepsilon - \sum_j \frac{\lambda}{\lambda} y \cos \varepsilon - \sum_j \frac{\lambda}{\lambda} xz \sin \varepsilon) \sin \phi_s \cos \phi_s + \\
& + r_s^2 \theta_s (-\sum_j \frac{m}{m} x - \sum_j \frac{\delta}{\delta} x \cos^2 \varepsilon + \sum_j \frac{\lambda}{\lambda} x \sin^2 \varepsilon + \sum_j \frac{m}{m} z - \sum_j \frac{\delta}{\delta} z \sin^2 \varepsilon + \sum_j \frac{\lambda}{\lambda} z \cos^2 \varepsilon + \\
& + 4 \sum_j \frac{\lambda}{\lambda} xz \sin \varepsilon \cos \varepsilon) \cos^2 \phi_s + \\
& + r_s \Omega_{1s} \delta_s J_{y1w} \cos \phi_s \cos \varepsilon - r_s^2 \delta_s J_{y1w} \sin \phi_s \cos \phi_s \cos \varepsilon + \\
& + g \sum_5 (ml_x) \cos \phi_s + g \theta_s \sum_5 \{m (l_z - b_z)\} \cos \phi_s + \\
& - g \lambda_{s1s} m_{1u} \cos \phi_s \sin \varepsilon + \\
& + F_{t1s} \{l_{A1x} + \delta_s l_{A1x} \tan \phi_s \sin \varepsilon - \delta_s l_{A1z} \tan \phi_s \cos \varepsilon + \theta_s (l_{A1z} - b_z) + \\
& - \lambda_{s1s} \sin \varepsilon\} + \\
& + C_{t1} (-\delta_s t l_{A1x} \tan \phi_s + \theta_s l_{A1x}^2 - \lambda_{t2s} l_{A1x} - \lambda_{s2s} l_{A1x} + \lambda_{s1s} l_{A1x} \cos \varepsilon) + \\
& + F_{y1s} (\delta_s l_{A1x} \frac{\sin \varepsilon}{\cos \phi_s} - \delta_s b_z \frac{\cos \varepsilon}{\cos \phi_s}) + \\
& - F_D (p_{Dz} + r_{w2o}) + F_L p_{Lx} + F_D r_{w2o}
\end{aligned}$$

$$\begin{aligned}
f_{\lambda_{t2s}} = & - u_s r_s \sum_6 (m) \sin \phi_s - r_s^2 \sum_6 (ml_z) \sin^2 \phi_s + \\
& + r_s^2 \delta_s \sum_3 (mg_x) \sin \phi_s \cos \phi_s + r_s^2 \theta_s \sum_5 (ml_x) \sin^2 \phi_s + \\
& - r_s^2 \lambda_{t2s} \sum_6 (m) \sin^2 \phi_s - r_s^2 \lambda_{s2s} \sum_5 (m) \sin^2 \phi_s + r_s^2 \lambda_{s1s} m_{1u} \sin^2 \phi_s \cos \varepsilon +
\end{aligned}$$

$$\begin{aligned}
& - g \sum_6 (m) \cos \phi_s + \\
& - F_{t1s} - F_{t2o} - F_{t1s} \delta_s \tan \phi_s \sin \epsilon + \\
& + C_{t1s} (\delta_s t \tan \phi_s - \theta_s^1 A_{1x} + \lambda_{t2s} + \lambda_{s2s} - \lambda_{s1s} \cos \epsilon) + \\
& - F_{y1s} \delta_s \frac{\sin \epsilon}{\cos \phi_s} - F_L
\end{aligned}$$

$$\begin{aligned}
f_{\lambda_{s2s}} = & - u_s r_s \sum_5 (m) \sin \phi_s - r_s^2 \sum_5 (ml_z) \sin^2 \phi_s + \\
& + r_s^2 \delta_s \sum_3 (mg_x) \sin \phi_s \cos \phi_s + r_s^2 \theta_s \sum_5 (ml_x) \sin^2 \phi_s + \\
& - r_s^2 \lambda_{t2s} \sum_5 (m) \sin^2 \phi_s - r_s^2 \lambda_{s2s} \sum_5 (m) \sin^2 \phi_s + r_s^2 \lambda_{s1s} \cos \epsilon + \\
& - g \sum_5 (m) \cos \phi_s + \\
& - F_{t1s} - F_{t2o} - F_{t1s} \delta_s \tan \phi_s \sin \epsilon + \\
& + C_{t1s} (\delta_s t \tan \phi_s - \theta_s^1 A_{1x} + \lambda_{t2s} + \lambda_{s2s} - \lambda_{s1s} \cos \epsilon) + \\
& - F_{y1s} \delta_s \frac{\sin \epsilon}{\cos \phi_s} - F_L
\end{aligned}$$

$$\begin{aligned}
f_{\lambda_{s1s}} = & u_s r_s m_{1u} \sin \phi_s \cos \epsilon + v_s r_s m_{1u} \sin \epsilon + \\
& + r_s^2 m_{1u}^1 G_{1ux} \sin \epsilon + r_s^2 m_{1u}^1 G_{1uz} \sin^2 \phi_s \cos \epsilon + \\
& - u_s r_s m_{1u} \theta_s \sin \phi_s \sin \epsilon + v_s r_s \theta_s m_{1u} \cos \epsilon + \\
& - r_s^2 \delta_s m_{1u} g_{1ux} \sin \phi_s \cos \phi_s \cos \epsilon + r_s^2 \theta_s m_{1u}^1 G_{1ux} \cos^2 \phi_s \cos \epsilon + \\
& + r_s^2 \theta_s m_{1u} (l_{G1uz} - b_z) \cos^2 \phi_s \sin \epsilon + r_s^2 \lambda_{t2s} m_{1u} \sin^2 \phi_s \cos \epsilon + \\
& + r_s^2 \lambda_{s2s} m_{1u} \sin^2 \phi_s \cos \epsilon - r_s^2 \lambda_{s1s} m_{1u} \sin^2 \phi_s \cos^2 \epsilon + \\
& - r_s^2 \lambda_{s1s} m_{1u} \sin^2 \epsilon + g m_{1u} \cos \phi_s \cos \epsilon - g \theta_s m_{1u} \cos \phi_s \sin \epsilon + \\
& + F_{t1s} \cos \epsilon - F_{s1o} - F_{t1s} \theta_s \sin \epsilon + F_{t1s} \delta_s \tan \phi_s \sin \epsilon \cos \epsilon + \\
& + C_{t1s} (\delta_s t \tan \phi_s \cos \epsilon + \theta_s^1 A_{1x} \cos \epsilon - \lambda_{t2s} \cos \epsilon - \lambda_{s2s} \cos \epsilon + \lambda_{s1s} \cos^2 \epsilon + \lambda_{s1})
\end{aligned}$$

Appendix F - equations of the non-stationary motion

The 20 original first and second-order differential equations (cf. Sec. 2.7.13) have been rewritten into 28 differential equations of the first order (cf. Sec. 3.3):

$$\overline{A} \dot{\overline{z}} + \overline{B} \overline{z} = \overline{0}$$

The structure of the matrices \overline{A} and \overline{B} has been depicted in Fig. F1; their elements have been described in the sequel.

The linkage between stationary and non-stationary equations has been described in Sec. 3.1.

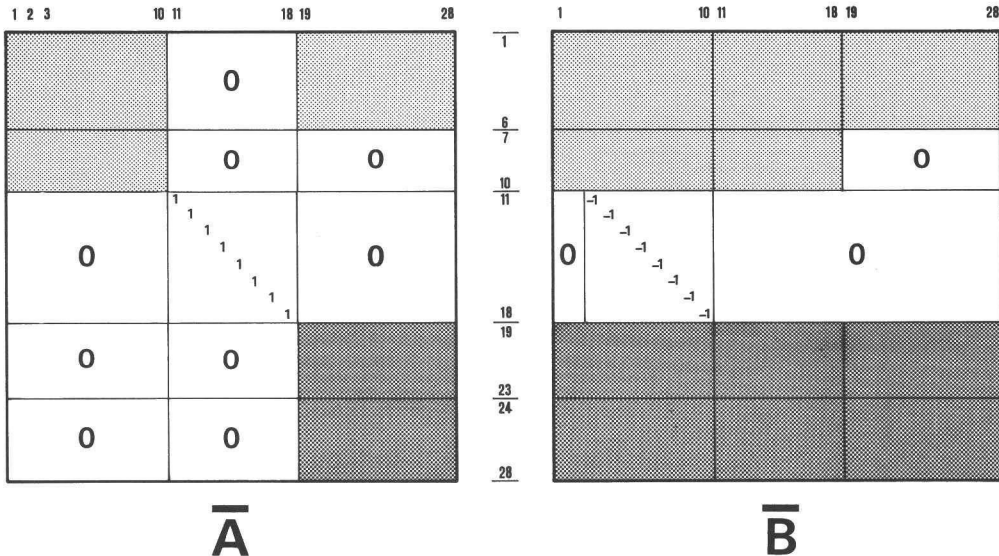


Fig. F1 structure of the matrices \overline{A} and \overline{B} . The various blocks have been specified in Fig. 40, Sec. 3.3. The corresponding vector of variables reads:

$$\overline{z} =$$

$$(\dot{v} \dot{r} \dot{\phi} \dot{\delta} \dot{\beta} \dot{\phi}_r \dot{\theta} \dot{\lambda}_{t2} \dot{\lambda}_{s2} \dot{\lambda}_{s1} \dot{\phi} \dot{\delta} \dot{\beta} \dot{\phi}_r \dot{\theta} \dot{\lambda}_{t2} \dot{\lambda}_{s2} \dot{\lambda}_{s1} \dot{F}_{y1} \dot{M}_{z1\alpha} \dot{M}_{z1\gamma} \dot{M}_{z1\beta} \dot{M}_{x1\alpha} \dot{M}_{x1\gamma} \dot{M}_{x2\alpha} \dot{M}_{x2\gamma} \dot{M}_{x2\beta})$$

$$1 \ 2 \ 3 \ . \ . \ . \ 10 \ 11 \ . \ . \ . \ 18 \ 19 \ . \ . \ . \ 28$$

MATRIX A

$$\begin{aligned}
 a_{1\ 1} &= \sum_6 (m) \\
 a_{1\ 2} &= \sum_6 (ml_x) \\
 a_{1\ 3} &= -\sum_6 (ml_z) \cos\phi_s \\
 a_{1\ 4} &= \sum_3 (mg_x) \cos\phi_s \\
 a_{1\ 5} &= -\sum_2 (mg_z) \cos\phi_s \\
 a_{1\ 6} &= -m_3 g_{3z} \cos\phi_s \\
 a_{1\ 7} &= \sum_5 (ml_x) \sin\phi_s \\
 a_{1\ 8} &= -\sum_6 (m) \sin\phi_s \\
 a_{1\ 9} &= -\sum_5 (m) \sin\phi_s \\
 a_{1\ 10} &= m_{1u} \sin\phi_s \cos\varepsilon
 \end{aligned}$$

$$\begin{aligned}
 a_{2\ 1} &= \sum_6 (ml_x) \\
 a_{2\ 2} &= \sum_6 (ml_x^2) + \sum_6 (ml_z^2) \sin^2\phi_s + \sum_J Y + \sum_m Y \sin^2\phi_s + \\
 &\quad + (\sum_J x \sin^2\varepsilon + \sum_J z \cos^2\varepsilon + 2\sum_J xz \sin\varepsilon \cos\varepsilon + \sum_J z) \cos^2\phi_s + \\
 &\quad + (J_{y1w} + J_{y2w}) \sin^2\phi_s \\
 a_{2\ 3} &= -\sum_6 (ml_x l_z) \cos\phi_s + \{(\sum_J z - \sum_J x) \sin\varepsilon \cos\varepsilon + \sum_J xz (\sin^2\varepsilon - \cos^2\varepsilon) + \\
 &\quad - \sum_m xz\} \cos\phi_s \\
 a_{2\ 4} &= \sum_3 (mg_x l_x) \cos\phi_s + \sum_J z \cos\phi_s \cos\varepsilon + \sum_J xz \cos\phi_s \sin\varepsilon \\
 a_{2\ 5} &= -\sum_2 (mg_z l_x) \cos\phi_s - \sum_J x \cos\phi_s \sin\varepsilon - \sum_J xz \cos\phi_s \sin\varepsilon \\
 a_{2\ 6} &= -m_3 g_{3z} d_x \cos\phi_s - J_{xz3} \cos\phi_s \\
 a_{2\ 7} &= [\sum_5 \{ml_z (l_z - a_{2z})\} + \sum_5 (ml_x^2)] \sin\phi_s + (\sum_J Y + \sum_m Y) \sin\phi_s + \\
 &\quad - \frac{1}{r_{w1}} (l_{A1z} - b_z) J_{y1w} \sin\phi_s \\
 a_{2\ 8} &= -\sum_6 (ml_x) \sin\phi_s \\
 a_{2\ 9} &= -\sum_5 (ml_x) \sin\phi_s \\
 a_{2\ 10} &= m_{1u} (l_{G1ux} \cos\varepsilon - l_{G1uz} \sin\varepsilon) \sin\phi_s + \frac{1}{r_{w1}} J_{y1w} \sin\phi_s \sin\varepsilon \\
 a_{2\ 19} &= u_s C_{GYR1} \\
 a_{2\ 24} &= u_s C_{GYR2}
 \end{aligned}$$

$$\begin{aligned}
a_{3 \ 1} &= -\sum_6 (ml_z) \cos\phi_s \\
a_{3 \ 2} &= -\sum_6 (ml_x l_z) \cos\phi_s + \left\{ (\sum_j z - \sum_j x) \sin\epsilon \cos\epsilon + \sum_j xz (\sin^2 \epsilon - \cos^2 \epsilon) + \right. \\
&\quad \left. - \sum_m xz \right\} \cos\phi_s \\
a_{3 \ 3} &= \sum_6 (ml_z^2) + \sum_j x \cos^2 \epsilon + \sum_j z \sin^2 \epsilon + \sum_m x \\
a_{3 \ 4} &= -\sum_3 (mg_x l_z) + \sum_j z \sin\epsilon - \sum_j xz \cos\epsilon \\
a_{3 \ 5} &= \sum_2 (mg_z l_z) + \sum_j x \cos\epsilon - \sum_j xz \sin\epsilon \\
a_{3 \ 6} &= m_3 g_{3z} l_{3z} + J_{x3}
\end{aligned}$$

$$\begin{aligned}
a_{4 \ 1} &= \sum_3 (mg_x) \cos\phi_s \\
a_{4 \ 2} &= \sum_3 (mg_x l_x) \cos\phi_s + \sum_j z \cos\phi_s \cos\epsilon + \sum_j xz \cos\phi_s \sin\epsilon \\
a_{4 \ 3} &= -\sum_3 (mg_x l_z) + \sum_j z \sin\epsilon - \sum_j xz \cos\epsilon \\
a_{4 \ 4} &= \sum_3 (mg_x^2) + \sum_j z \\
a_{4 \ 5} &= -\sum_2 (mg_x g_z) - \sum_j xz \\
a_{4 \ 19} &= u_s C_{GYR1} \frac{\cos\epsilon}{\cos\phi_s}
\end{aligned}$$

$$\begin{aligned}
a_{5 \ 1} &= -\sum_2 (mg_z) \cos\phi_s \\
a_{5 \ 2} &= -\sum_2 (mg_z l_x) \cos\phi_s - \sum_j x \cos\phi_s \sin\epsilon - \sum_j xz \cos\phi_s \cos\epsilon \\
a_{5 \ 3} &= \sum_2 (mg_z l_z) + \sum_j x \cos\epsilon - \sum_j xz \sin\epsilon \\
a_{5 \ 4} &= -\sum_2 (mg_x g_z) - \sum_j xz \\
a_{5 \ 5} &= \sum_2 (mg_z^2) + \sum_j x \\
a_{5 \ 19} &= -u_s C_{GYR2} \frac{\sin\epsilon}{\cos\phi_s}
\end{aligned}$$

$$\begin{aligned}
a_{6 \ 1} &= -m_3 g_{3z} \cos\phi_s \\
a_{6 \ 2} &= -m_3 g_{3z} d_x \cos\phi_s - J_{xz3} \cos\phi_s \\
a_{6 \ 3} &= m_3 g_{3z} l_{3z} + J_{x3} \\
a_{6 \ 6} &= m_3 g_{3z}^2 + J_{x3}
\end{aligned}$$

$$a_{7 \ 1} = \sum_5 (ml_x) \sin\phi_s$$

$$\begin{aligned}
a_{7 \ 2} &= \left[\sum_5 \{ m l_z (l_z - b_z) \} + \sum_5 (m l_x^2) \right] \sin \phi_s + \frac{(\sum J_y + \sum J_z)}{\delta} \sin \phi_s + \\
&\quad - \frac{1}{r_{w1}} (l_{A1z} - b_z) J_{y1w} \sin \phi_s \\
a_{7 \ 7} &= \sum_5 \{ m (l_z - b_z)^2 \} + \sum_5 (m l_x^2) + \frac{\sum J_y}{\delta} + \frac{\sum J_z}{m} + \frac{1}{r_{w1}^2} (l_{A1z} - b_z)^2 J_{y1w} \\
a_{7 \ 8} &= -\sum_5 (m l_x) \\
a_{7 \ 9} &= -\sum_5 (m l_x) \\
a_{7 \ 10} &= m_{1u} l_{G1ux} \cos \varepsilon - m_{1u} (l_{G1uz} - b_z) \sin \varepsilon - \frac{1}{r_{w1}^2} (l_{A1z} - b_z) J_{y1w} \sin \varepsilon
\end{aligned}$$

$$\begin{aligned}
a_{8 \ 1} &= -\sum_6 (m) \sin \phi_s \\
a_{8 \ 2} &= -\sum_6 (m l_x) \sin \phi_s \\
a_{8 \ 7} &= -\sum_5 (m l_x) \\
a_{8 \ 8} &= \sum_6 (m) \\
a_{8 \ 9} &= \sum_5 (m) \\
a_{8 \ 10} &= -m_{1u} \cos \varepsilon
\end{aligned}$$

$$\begin{aligned}
a_{9 \ 1} &= -\sum_5 (m) \sin \phi_s \\
a_{9 \ 2} &= -\sum_5 (m l_x) \sin \phi_s \\
a_{9 \ 7} &= -\sum_5 (m l_x) \\
a_{9 \ 8} &= \sum_5 (m) \\
a_{9 \ 9} &= \sum_5 (m) \\
a_{9 \ 10} &= -m_{1u} \cos \varepsilon
\end{aligned}$$

$$\begin{aligned}
a_{10 \ 1} &= m_{1u} \sin \phi_s \cos \varepsilon \\
a_{10 \ 2} &= -m_{1u} (l_{G1uz} \sin \varepsilon - l_{G1ux} \cos \varepsilon) \sin \phi_s + \frac{1}{r_{w1}} J_{y1w} \sin \phi_s \sin \varepsilon \\
a_{10 \ 7} &= -m_{1u} \{ (l_{G1uz} - b_z) \sin \varepsilon - l_{G1ux} \cos \varepsilon \} - \frac{1}{r_{w1}^2} (l_{A1z} - b_z) J_{y1w} \sin \varepsilon \\
a_{10 \ 8} &= -m_{1u} \cos \varepsilon \\
a_{10 \ 9} &= -m_{1u} \cos \varepsilon \\
a_{10 \ 10} &= m_{1u} + \frac{1}{r_{w1}^2} J_{y1w} \sin^2 \varepsilon
\end{aligned}$$

$$\begin{aligned}
a_{11} \cdot 11 &= a_{12} \cdot 12 = a_{13} \cdot 13 = a_{14} \cdot 14 = a_{15} \cdot 15 = a_{16} \cdot 16 = a_{17} \cdot 17 = a_{18} \cdot 18 = 1 \\
a_{19} \cdot 19 &= -\sigma_{Fy1} / u_s \\
a_{20} \cdot 20 &= -\sigma_{Mz1\alpha} / u_s \\
a_{21} \cdot 21 &= -\sigma_{DUM} / u_s \\
a_{22} \cdot 22 &= -\sigma_{DUM} / u_s \\
a_{23} \cdot 23 &= -\sigma_{DUM} / u_s \\
a_{24} \cdot 24 &= -\sigma_{Fy2} / u_s \\
a_{25} \cdot 25 &= -\sigma_{Mz2\alpha} / u_s \\
a_{26} \cdot 26 &= -\sigma_{DUM} / u_s \\
a_{27} \cdot 27 &= -\sigma_{DUM} / u_s \\
a_{28} \cdot 28 &= -\sigma_{DUM} / u_s
\end{aligned}$$

MATRIX B

$$\begin{aligned}
b_{1 \cdot 2} &= u_s \sum_6 (m) + 2r_s \sum_6 (ml_z) \sin\phi_s \\
b_{1 \cdot 7} &= 2r_s \sum_5 \{ m(l_z - b_z) \} \\
b_{1 \cdot 10} &= -2r_s m_{1u} \sin\epsilon \\
b_{1 \cdot 11} &= r_s^2 \sum_6 (ml_z) \cos\phi_s \\
b_{1 \cdot 12} &= -r_s^2 \sum_3 (mg_x) \cos\phi_s \\
b_{1 \cdot 13} &= r_s^2 \sum_2 (mg_z) \cos\phi_s \\
b_{1 \cdot 14} &= r_s^2 m_3 g_{3z} \cos\phi_s \\
b_{1 \cdot 15} &= -r_s^2 \sum_5 (ml_x) \sin\phi_s \\
b_{1 \cdot 16} &= r_s^2 \sum_6 (m) \sin\phi_s \\
b_{1 \cdot 17} &= r_s^2 \sum_5 (m) \sin\phi_s \\
b_{1 \cdot 18} &= -r_s^2 m_{1u} \sin\phi_s \cos\epsilon \\
b_{1 \cdot 19} &= -1 \\
b_{1 \cdot 24} &= -1
\end{aligned}$$

$$\begin{aligned}
b_{2,1} &= -r_s \sum_6 (ml_z) \sin\phi_s \\
b_{2,2} &= -v_s \sum_6 (ml_z) \sin\phi_s + u_s \sum_6 (ml_x) \\
b_{2,3} &= 2r_s \sum_6^2 (ml_z) \sin\phi_s \cos\phi_s + \\
&\quad + 2r_s (\sum_j \frac{\delta}{y} - \sum_j \frac{\delta}{z} \cos^2 \epsilon - \sum_j \frac{\delta}{x} \sin^2 \epsilon - 4 \sum_j \frac{\delta}{xz} \sin\epsilon \cos\epsilon + \\
&\quad + \sum_m \frac{\delta}{y} - \sum_m \frac{\delta}{z}) \sin\phi_s \cos\phi_s - (\Omega_{1s}^j y_{1w} + \Omega_{2s}^j y_{2w}) \cos\phi_s + \\
&\quad + 2r_s (J_{y1w} + J_{y2w}) \sin\phi_s \cos\phi_s \\
b_{2,4} &= -2r_s \sum_3 (mg_x l_z) \sin\phi_s \cos\phi_s + 2r_s (\sum_j \frac{\delta}{y} - \sum_j \frac{\delta}{x}) \sin\phi_s \cos\phi_s \sin\epsilon + \\
&\quad - 2r_s \sum_j \frac{\delta}{xz} \sin\phi_s \cos\phi_s \cos\epsilon - J_{y1w} \{\Omega_{1s} \cos\phi_s \sin\epsilon - 2r_s \sin\phi_s \cos\phi_s \sin\epsilon + \\
&\quad + \frac{v_s}{r_{w1}} \tan\phi_s \cos\epsilon - \frac{r_s}{r_{w1}} (t - l_{A1x} \cos\epsilon) \tan\phi_s\} \\
b_{2,5} &= 2r_s \sum_2 (mg_z l_z) \sin\phi_s \cos\phi_s + 2r_s (\sum_j \frac{\delta}{y} - \sum_j \frac{\delta}{z}) \sin\phi_s \cos\phi_s \cos\epsilon + \\
&\quad - 2r_s \sum_j \frac{\delta}{xz} \sin\phi_s \cos\phi_s \sin\epsilon - J_{y1w} \{\Omega_{1s} \cos\phi_s \cos\epsilon - \frac{v_s}{r_{w1}} \tan\phi_s \sin\epsilon + \\
&\quad - 2r_s \sin\phi_s \cos\phi_s \cos\epsilon + \frac{r_s}{r_{w1}} (a_{1z} - l_{A1z} - l_{A1x} \sin\epsilon) \tan\phi_s\} \\
b_{2,6} &= 2r_s m_3 g_{3z} l_{3z} \sin\phi_s \cos\phi_s + 2r_s (J_{y3} - J_{z3}) \sin\phi_s \cos\phi_s \\
b_{2,7} &= -2r_s [\sum_5 (ml_x l_z) \sin^2 \phi_s - \sum_5 \{ml_x (l_z - b_z)\}] + \\
&\quad + 2r_s \{(\sum_j \frac{\delta}{x} - \sum_j \frac{\delta}{z}) \sin\epsilon \cos\epsilon + \sum_j \frac{\delta}{xz} (\cos^2 \epsilon - \sin^2 \epsilon) + \sum_m \frac{\delta}{xz}\} \cos^2 \phi_s \\
b_{2,8} &= 2r_s \sum_6 (ml_z) \sin^2 \phi_s \\
b_{2,9} &= 2r_s \sum_5 (ml_z) \sin^2 \phi_s \\
b_{2,10} &= -2r_s m_{1u} (l_{G1uz} \sin^2 \phi_s \cos\epsilon + l_{G1ux} \sin\epsilon) \\
b_{2,11} &= -v_s r_s \sum_6 (ml_z) \cos\phi_s \\
b_{2,12} &= v_s r_s \sum_3 (mg_x) \cos\phi_s + F_{y1s} l_{A1z} \tan\phi_s \cos\epsilon \\
b_{2,13} &= -v_s r_s \sum_2 (mg_z) \cos\phi_s - F_{y1s} l_{A1z} \tan\phi_s \sin\epsilon \\
b_{2,14} &= -v_s r_s m_3 g_{3z} \cos\phi_s \\
b_{2,15} &= v_s r_s \sum_5 (ml_x) \sin\phi_s + u_s r_s \sum_5 \{m (l_z - b_z)\} - F_{y1s} (l_{A1z} - b_z) \\
b_{2,16} &= -v_s r_s \sum_6 (m) \sin\phi_s \\
b_{2,17} &= -v_s r_s \sum_5 (m) \sin\phi_s \\
b_{2,18} &= v_s r_s m_{1u} \sin\phi_s \cos\epsilon - u_s r_s m_{1u} \sin\epsilon + F_{y1s} \sin\epsilon \\
b_{2,19} &= -l_{A1x} \\
b_{2,20} &= b_{2,21} = b_{2,22} = b_{2,25} = b_{2,26} = b_{2,27} = -1
\end{aligned}$$

$$\begin{aligned}
b_{3,2} &= -u_s \sum_6 (ml_z) \cos\phi_s - 2r_s \sum_6 (ml_z^2) \sin\phi_s \cos\phi_s + \\
&\quad - 2r_s \left(\frac{\sum J}{\delta} Y - \frac{\sum J}{\delta} X \sin^2 \epsilon - \frac{\sum J}{\delta} Z \cos^2 \epsilon - 2 \frac{\sum J}{\delta} XZ \sin\epsilon \cos\epsilon + \frac{\sum J}{\delta} Y + \right. \\
&\quad \left. - \frac{\sum J}{\delta} Z \right) \sin\phi_s \cos\phi_s + (\Omega_{1s}^J Y_{1w} + \Omega_{2s}^J Y_{1w}) \cos\phi_s + \\
&\quad - 2r_s \sin\phi_s \cos\phi_s \left(\frac{J}{Y_{1w}} + \frac{J}{Y_{2w}} \right) \\
b_{3,4} &= r_s \left(\frac{\sum J}{\delta} X - \frac{\sum J}{\delta} Y + \frac{\sum J}{\delta} Z \right) \sin\phi_s \cos\epsilon + \Omega_{1s}^J Y_{1w} \cos\epsilon - r_s^J Y_{1w} \sin\phi_s \cos\epsilon \\
b_{3,5} &= r_s \left(\frac{\sum J}{\beta} Y - \frac{\sum J}{\beta} Z - \frac{\sum J}{\beta} X \right) \sin\phi_s \sin\epsilon + \\
&\quad + \frac{\sum J}{\beta} Y_{1w} (-\Omega_{1s} \sin\epsilon + r_s \frac{\tan\phi_s}{\cos\phi_s} \sin\epsilon - r_s \tan^2 \phi_s \sin\epsilon) \\
b_{3,7} &= -2r_s \sum_5 \{ ml_z (l_z - b_z) \} \cos\phi_s + \\
&\quad - r_s \left\{ \left(\frac{\sum J}{\delta} X - \frac{\sum J}{\delta} Z \right) (\cos^2 \epsilon - \sin^2 \epsilon) + \frac{\sum J}{\delta} Y - 4 \frac{\sum J}{\delta} XZ \sin\epsilon \cos\epsilon + \right. \\
&\quad \left. + \frac{\sum J}{\delta} X + \frac{\sum J}{\delta} Y - \frac{\sum J}{\delta} Z + \frac{J}{X_3} \cos\phi_s + \frac{r_s}{r_{w1}} (l_{A1z} - b_z) \frac{J}{Y_{1w}} \cos\phi_s \right. \\
b_{3,10} &= 2r_s \frac{m}{1u} \frac{l}{G1uz} \cos\phi_s \sin\epsilon - \frac{r_s}{r_{w1}} \frac{J}{Y_{1w}} \cos\phi_s \sin\epsilon \\
b_{3,11} &= u_s r_s \sum_6 (ml_z) \sin\phi_s - r_s^2 \sum_6 (ml_z^2) (\cos^2 \phi_s - \sin^2 \phi_s) + \\
&\quad + r_s^2 \left(\frac{\sum J}{\delta} Y - \frac{\sum J}{\delta} X \sin^2 \epsilon - \frac{\sum J}{\delta} Z \cos^2 \epsilon - 2 \frac{\sum J}{\delta} XZ \sin\epsilon \cos\epsilon + \right. \\
&\quad \left. + \frac{\sum J}{\delta} Y - \frac{\sum J}{\delta} Z \right) (\sin^2 \phi_s - \cos^2 \phi_s) - r_s (\Omega_{1s}^J Y_{1w} + \Omega_{2s}^J Y_{2w}) \sin\phi_s + \\
&\quad + r_s^2 (J_{Y_{1w}} + J_{Y_{2w}}) (\sin^2 \phi_s - \cos^2 \phi_s) + g \sum_6 (ml_z) \cos\phi_s \\
b_{3,12} &= -u_s r_s \sum_3 (mg_x) \sin\phi_s + r_s^2 \sum_3 (mg_x l_z) (\cos^2 \phi_s - \sin^2 \phi_s) + \\
&\quad + r_s^2 \left(\frac{\sum J}{\delta} X \sin\epsilon - \frac{\sum J}{\delta} Y \sin\epsilon + \frac{\sum J}{\delta} XZ \cos\epsilon \right) (\cos^2 \phi_s - \sin^2 \phi_s) + \\
&\quad + r_s^J \frac{1}{r_{w1}} (v_s \cos\epsilon - r_s t + r_s l_{A1x} \cos\epsilon) - \Omega_{1s} \sin\phi_s \sin\epsilon + \\
&\quad + r_s (\sin^2 \phi_s - \cos^2 \phi_s) \sin\epsilon - g \sum_3 (mg_x) \cos\phi_s - F_{t1s} t \frac{1}{\cos^2 \phi_s} \\
b_{3,13} &= r_s^2 \sum_2 (mg_z l_z) (\sin^2 \phi_s - \cos^2 \phi_s) + u_s r_s \sum_2 (mg_z) \sin\phi_s + \\
&\quad + r_s^2 \left(\frac{\sum J}{\beta} Y \cos\epsilon - \frac{\sum J}{\beta} Z \cos\epsilon - \frac{\sum J}{\beta} XZ \sin\epsilon \right) (\sin^2 \phi_s - \cos^2 \phi_s) + \\
&\quad + r_s^J \frac{r_s}{r_{w1}} (a_{1z} - l_{A1z} \cos\epsilon - l_{A1x} \sin\epsilon) + \\
&\quad - \frac{v_s}{r_{w1}} \sin\epsilon - \Omega_{1s} \sin\phi_s \cos\epsilon + r_s (\sin^2 \phi_s - \cos^2 \phi_s) \cos\epsilon + \\
&\quad + g \sum_2 (mg_z) \cos\phi_s - F_{t1s} \frac{(l_{A1z} \cos\epsilon - a_{1z})}{\cos^2 \phi_s} + \\
&\quad + F_{y1s} (a_{1z} \frac{\tan\phi_s}{\cos\phi_s} - l_{A1z} \frac{\tan\phi_s}{\cos\phi_s} \cos\epsilon) \\
b_{3,14} &= r_s^2 m_3 g_3 l_{3z} (\sin^2 \phi_s - \cos^2 \phi_s) + u_s r_s m_3 g_3 z \sin\phi_s + \\
&\quad + r_s^2 (J_{z3} - J_{y3}) (\cos^2 \phi_s - \sin^2 \phi_s) + g m_3 g_3 z \cos\phi_s
\end{aligned}$$

$$\begin{aligned}
b_{3 \ 15} &= u_s r_s \sum_5 (m l_x) \cos \phi_s + 2r_s^2 \sum_5 (m l_x l_z) \sin \phi_s \cos \phi_s + \\
&\quad + 2r_s^2 \left\{ \left(\frac{\sum J}{\delta x} - \frac{\sum J}{\delta z} \right) \sin \epsilon \cos \epsilon + \sum_m xz + J_{xz3} \right\} \sin \phi_s \cos \phi_s + \\
&\quad - g \sum_5 (m l_x) \sin \phi_s + 2r_s^2 \sum_5 \frac{J}{\delta xz} (\cos^2 \epsilon - \sin^2 \epsilon) \\
b_{3 \ 16} &= - u_s r_s \sum_6 (m) \cos \phi_s - 2r_s^2 \sum_6 (m l_z) \sin \phi_s \cos \phi_s + g \sum_6 (m) \sin \phi_s \\
b_{3 \ 17} &= - u_s r_s \sum_5 (m) \cos \phi_s - 2r_s^2 \sum_5 (m l_z) \sin \phi_s \cos \phi_s + g \sum_5 (m) \sin \phi_s \\
b_{3 \ 18} &= u_s r_s m_{1u} \cos \phi_s \cos \epsilon + 2r_s^2 m_{1u} l_{Gluz} \sin \phi_s \cos \phi_s \cos \epsilon - g m_{1u} \sin \phi_s \cos \epsilon \\
b_{3 \ 23} &= b_{3 \ 28} = -1
\end{aligned}$$

$$\begin{aligned}
b_{4 \ 2} &= u_s \sum_3 (mg_x) \cos \phi_s + 2r_s \sum_3 (mg_x l_z) \sin \phi_s \cos \phi_s + \\
&\quad + 2r_s \left(\frac{\sum J}{\delta x} \sin \epsilon - \frac{\sum J}{\delta y} \sin \epsilon + \frac{\sum J}{\delta xz} \cos \epsilon \right) \sin \phi_s \cos \phi_s \sin \epsilon + \Omega_{1s} J_{y1w} \cos \phi_s \sin \epsilon + \\
&\quad - 2r_s^2 \sum_3 \frac{J}{\delta y1w} \sin \phi_s \cos \phi_s \sin \epsilon \\
b_{4 \ 3} &= r_s \left(\frac{\sum J}{\delta y} - \frac{\sum J}{\delta x} - \frac{\sum J}{\delta z} \right) \sin \phi_s \cos \epsilon - \Omega_{1s} J_{y1w} \cos \epsilon + r_s^2 \sum_3 \frac{J}{\delta y1w} \sin \phi_s \cos \epsilon \\
b_{4 \ 4} &= K_\delta \\
b_{4 \ 5} &= r_s \left(\frac{\sum J}{\beta y} - \frac{\sum J}{\beta z} - \frac{\sum J}{\beta x} \right) \sin \phi_s + J_{y1w} (r_s \sin \phi_s - \Omega_{1s}) \\
b_{4 \ 7} &= 2r_s \sum_3 (mg_x (l_z - b_z)) \cos \phi_s + r_s \left(\frac{\sum J}{\delta x} \sin \epsilon - \frac{\sum J}{\delta y} \sin \epsilon - \frac{\sum J}{\delta z} \sin \epsilon + \right. \\
&\quad \left. + \frac{\sum J}{\delta xz} \cos \epsilon \right) \cos \phi_s + \frac{r_s}{r_{w1}} (l_{A1z} - b_z) J_{y1w} \cos \phi_s \sin \epsilon \\
b_{4 \ 10} &= - 2r_s m_{1u} g_{1uz} \cos \phi_s \sin \epsilon - \frac{r_s}{r_{w1}} J_{y1w} \cos \phi_s \sin^2 \epsilon \\
b_{4 \ 11} &= - u_s r_s \sum_3 (mg_x) \sin \phi_s + r_s^2 \sum_3 (mg_x l_z) (\cos^2 \phi_s - \sin^2 \phi_s) + \\
&\quad + r_s^2 \left(\frac{\sum J}{\delta x} \sin \epsilon - \frac{\sum J}{\delta y} \sin \epsilon + \frac{\sum J}{\delta xz} \cos \epsilon \right) (\cos^2 \phi_s - \sin^2 \phi_s) + \\
&\quad - r_s^2 \sum_3 \frac{J}{\delta y1w} \sin \phi_s \sin \epsilon + r_s^2 \sum_3 \frac{J}{\delta y1w} \sin \epsilon (\sin^2 \phi_s - \cos^2 \phi_s) \\
&\quad - g \sum_3 (mg_x) \cos \phi_s - F_{t1s} t \frac{1}{\cos^2 \phi_s} - F_{y1s} t \frac{\tan \phi_s}{\cos \phi_s} \\
b_{4 \ 12} &= - u_s r_s \sum_3 (mg_x) \sin \phi_s \sin \epsilon + r_s v \sum_3 (mg_x) \cos \epsilon + \\
&\quad - r_s^2 \sum_3 (mg_x^2) \cos^2 \phi_s - r_s^2 \sum_3 (mg_x l_z) \sin^2 \phi_s \sin \epsilon + \\
&\quad + r_s^2 \sum_3 (mg_x l_x) \cos \epsilon + r_s^2 \left(\frac{\sum J}{\delta y} - \frac{\sum J}{\delta x} \right) (\sin^2 \phi_s - \cos^2 \phi_s \sin^2 \epsilon) + \\
&\quad + r_s^2 \sum_3 \frac{J}{\delta xz} \cos^2 \phi_s \sin \epsilon \cos \epsilon + r_s^2 \sum_3 \frac{J}{\delta yw1} \left\{ \frac{1}{r_{w1}} (v_s \sin \epsilon \cos \epsilon - r_s t \sin \epsilon) + \right. \\
&\quad \left. + r_s l_{A1x} \sin \epsilon \cos \epsilon \right\} + r_s^2 (\sin^2 \phi_s - \cos^2 \phi_s \sin^2 \epsilon) \\
&\quad - g \sum_3 (mg_x) \cos \phi_s \sin \epsilon + \\
&\quad + F_{t1s} \left\{ - 2 \tan^2 \phi_s t \sin \epsilon + l_{A1z} \tan^2 \phi_s \cos^2 \epsilon - t \sin \epsilon \right\} + t^2 C_{t1} \tan^2 \phi_s + \\
&\quad - F_{y1s} \left(2t \sin \epsilon - l_{A1z} \cos^2 \epsilon \right) \frac{\tan \phi_s}{\cos \phi_s}
\end{aligned}$$

$$\begin{aligned}
b_{4 \ 13} &= r_s^2 \sum_2 (mg_x g_z) \cos^2 \phi_s + r_s^2 \sum_2 (mg_z l_z) \sin^2 \phi_s \sin \epsilon + \\
&\quad + u_s r_s \sum_2 (mg_z) \sin \phi_s \sin \epsilon - r_s^2 \sum_2 (mg_z l_x) \cos \epsilon + \\
&\quad - v_s r_s \sum_2 (mg_z) \cos \epsilon + r_s^2 (\sum_j \frac{\beta_z}{\beta_y} - \sum_j \frac{\beta_y}{\beta_z}) \cos^2 \phi_s \sin \epsilon \cos \epsilon + \\
&\quad + r_s^2 \sum_j \frac{\beta_{xz}}{\beta_{xz}} (\cos^2 \phi_s \sin^2 \epsilon - \sin^2 \phi_s) + \\
&\quad - r_s^2 \sum_j \frac{1}{rw1} (v_s \sin^2 \epsilon - r_s a_{1z} \sin \epsilon + r_s a_{1z} \sin \epsilon \cos \epsilon + r_s l_{A1x} \sin^2 \epsilon) + \\
&\quad + r_s \cos^2 \phi_s \sin \epsilon \cos \epsilon \} + g \sum_2 (mg_z) \cos \phi_s \sin \epsilon + \\
&\quad + F_{t1s} \left\{ a_{1z} \frac{\sin \epsilon}{\cos^2 \phi_s} - t \tan^2 \phi_s \cos \epsilon - l_{A1z} (1 + 2 \tan^2 \phi_s) \sin \epsilon \cos \epsilon \right\} + \\
&\quad + t (l_{A1z} \cos \epsilon - a_{1z}) c_{t1} \tan^2 \phi_s + \\
&\quad + F_{y1s} \left(a_{1z} \frac{\tan \phi_s}{\cos \phi_s} \sin \epsilon - 3 l_{A1z} \frac{\tan \phi_s}{\cos \phi_s} \sin \epsilon \cos \epsilon - a_1 \frac{\tan \phi_s}{\cos \phi_s} \cos \epsilon \right) \\
b_{4 \ 15} &= - r_s^2 \sum_3 (mg_x l_x) \sin \phi_s \cos \phi_s + r_s^2 \sum_2 \left(\frac{\sum_j \cos \epsilon}{\delta_x} - \frac{\sum_j \cos \epsilon}{\delta_y} \right) + \\
&\quad - \sum_j \frac{\sin \epsilon}{\delta_{xz}} \sin \phi_s \cos \phi_s + r_s \Omega_{1s}^J yw1 \cos \phi_s \cos \epsilon + \\
&\quad + r_s^2 \sum_j yw1 \sin \phi_s \cos \phi_s \cos \epsilon + F_{t1s} (l_{A1x} \sin \epsilon - l_{A1z} \cos \epsilon) \tan \phi_s + \\
&\quad - t l_{A1x} c_{t1} \tan \phi_s + F_{y1s} (l_{A1x} \sin \epsilon - l_{A1z} \cos \epsilon) \frac{1}{\cos \phi_s} \\
b_{4 \ 16} &= r_s^2 \sum_3 (mg_x) \sin \phi_s \cos \phi_s - F_{t1s} \tan \phi_s \sin \epsilon + t c_{t1} \tan \phi_s - F_{y1s} \frac{\sin \epsilon}{\cos \phi_s} \\
b_{4 \ 17} &= r_s^2 \sum_3 (mg_x) \sin \phi_s \cos \phi_s - F_{t1s} \tan \phi_s \sin \epsilon + t c_{t1} \tan \phi_s - F_{y1s} \frac{\sin \epsilon}{\cos \phi_s} \\
b_{4 \ 18} &= - r_s^2 m_{1u} g_{1ux} \sin \phi_s \cos \phi_s \cos \epsilon + F_{t1s} \tan \phi_s \sin \epsilon \cos \epsilon + \\
&\quad - t c_{t1} \tan \phi_s \cos \epsilon + F_{y1s} \frac{\sin \epsilon}{\cos \phi_s} \cos \epsilon \\
b_{4 \ 19} &= - t \frac{1}{\cos \phi_s} \\
b_{4 \ 20} &= b_{4 \ 21} = b_{4 \ 22} = - \frac{\cos \epsilon}{\cos \phi_s} \\
b_{4 \ 23} &= - \sin \epsilon
\end{aligned}$$

$$\begin{aligned}
b_{5 \ 2} &= - 2r_s \sum_2 (mg_z l_z) \sin \phi_s \cos \phi_s - u_s \sum_2 (mg_z) \cos \phi_s + \\
&\quad + 2r_s \left(\sum_j \frac{\beta_z \cos \epsilon}{\beta_y} - \sum_j \frac{\beta_y \cos \epsilon}{\beta_z} + \sum_j \frac{\beta_{xz} \sin \epsilon}{\beta_x} \right) \sin \phi_s \cos \phi_s + \\
&\quad - 2r_s^2 \sum_j yw1 \sin \phi_s \cos \phi_s \cos \epsilon + \Omega_{1s}^J yw1 \cos \phi_s \cos \epsilon \\
b_{5 \ 3} &= r_s \left(\sum_j \frac{\beta_x \sin \epsilon}{\beta_z} - \sum_j \frac{\beta_y \sin \epsilon}{\beta_z} - \sum_j \frac{\beta_z \sin \epsilon}{\beta_x} \right) \sin \phi_s \sin \epsilon + \Omega_{1s}^J yw1 \sin \epsilon - r_s^2 \sum_j yw1 \sin \phi_s \sin \epsilon \\
b_{5 \ 4} &= r_s \left(\sum_j \frac{\beta_x \sin \epsilon}{\beta_y} - \sum_j \frac{\beta_y \sin \epsilon}{\beta_z} + \sum_j \frac{\beta_z \sin \epsilon}{\beta_x} \right) \sin \phi_s + \Omega_{1s}^J yw1 - r_s^2 \sum_j yw1 \sin \phi_s \\
b_{5 \ 5} &= 2k_\beta \left[c_\beta \left\{ \sum_2 (m g_z^2) + \sum_j \frac{\beta_{xz}}{\beta_x} \right\} \right] \\
b_{5 \ 7} &= - 2r_s \sum_2 mg \left\{ (l_z - b_z) \right\} \cos \phi_s + r_s \left(\sum_j \frac{\beta_z \cos \epsilon}{\beta_x} - \sum_j \frac{\beta_x \cos \epsilon}{\beta_z} + \right. \\
&\quad \left. - \sum_j \frac{\beta_y \cos \epsilon}{\beta_z} + 2 \sum_j \frac{\beta_{xz} \sin \epsilon}{\beta_x} \right) \cos \phi_s + \frac{r_s}{r_{w1}} \sum_j yw1 (l_{A1z} - b_z) \cos \phi_s \cos \epsilon
\end{aligned}$$

$$\begin{aligned}
b_{5 \ 10} &= 2r_s \sum_2 (m_{1u} g_{1uz}) \cos \phi_s \sin \epsilon - \frac{r_s}{r_{w1}} J_{y1w} \cos \phi_s \sin \epsilon \cos \epsilon \\
b_{5 \ 11} &= r_s^2 \sum_2 (mg_z l_z) (\sin^2 \phi_s - \cos^2 \phi_s) + u_s r_s \sum_2 (mg_z) \sin \phi_s + \\
&\quad + r_s^2 \left(\frac{\sum_J \cos \epsilon}{\beta z} - \frac{\sum_J \cos \epsilon}{\beta y} + \frac{\sum_J \sin \epsilon}{\beta xz} \right) (\cos^2 \phi_s - \sin^2 \phi_s) + \\
&\quad - r_s \Omega_{1s} J_{y1w} \sin \phi_s \cos \epsilon + r_s^2 J_{y1w} (\sin^2 \phi_s - \cos^2 \phi_s) \cos \epsilon + g \sum_2 (mg_z) \cos \phi_s + \\
&\quad - F_{t1s} (l_{A1z} \cos \epsilon - a_{1z}) \frac{1}{\cos^2 \phi_s} - F_{y1s} (l_{A1z} \cos \epsilon - a_{1z}) \frac{\tan \phi_s}{\cos \phi_s} \\
b_{5 \ 12} &= r_s^2 \sum_2 (mg_x g_z) \cos^2 \phi_s + r_s^2 \sum_2 (mg_z l_z) \sin^2 \phi_s \sin \epsilon + \\
&\quad + u_s r_s \sum_2 (mg_z) \sin \phi_s \sin \epsilon - r_s^2 \sum_2 (mg_z l_x) \cos \epsilon - v_s r_s \sum_2 (mg_z) \cos \epsilon + \\
&\quad + r_s^2 \left(\frac{\sum_J}{\beta z} - \frac{\sum_J}{\beta y} \right) \cos^2 \phi_s \sin \epsilon \cos \epsilon + r_s^2 \sum_J (\cos^2 \phi_s \sin^2 \epsilon - \sin^2 \phi_s) + \\
&\quad - \frac{r_s^2}{r_{w1}} J_{y1w} (t - l_{A1x} \cos \epsilon) \cos \epsilon - r_s^2 J_{y1w} \cos^2 \phi_s \sin \epsilon \cos \epsilon + \\
&\quad + r_s \frac{v_s}{r_{w1}} J_{y1w} \cos^2 \epsilon + g \sum_2 (mg_z) \cos \phi_s \sin \epsilon + \\
&\quad + F_{t1s} a_{1z} \frac{\sin \epsilon}{\cos^2 \phi_s} - t \tan^2 \phi_s \cos \epsilon - l_{A1z} (1 + 2 \tan^2 \phi_s) \sin \epsilon \cos \epsilon + \\
&\quad + t (l_{A1z} \cos \epsilon - a_{1z}) c_{t1} \tan^2 \phi_s + \\
&\quad + F_{y1s} (a_{1z} \sin \epsilon - 3l_{A1z} \sin \epsilon \cos \epsilon - a_{1x} \cos \epsilon) \frac{\tan \phi_s}{\cos \phi_s} \\
b_{5 \ 13} &= C_\beta - r_s^2 \sum_2 (mg_z^2) \cos^2 \phi_s + r_s^2 \sum_2 (mg_z l_z) \sin \phi_s \cos \epsilon + \\
&\quad + u_s r_s \sum_2 (mg_z) \sin \phi_s \cos \epsilon + r_s^2 \sum_2 (mg_z l_x) \sin \epsilon + \\
&\quad + v_s r_s \sum_2 (mg_z) \sin \epsilon + \\
&\quad + r_s^2 \left(\frac{\sum_J}{\beta z} - \frac{\sum_J}{\beta y} \right) \cos^2 \phi_s \cos^2 \epsilon + r_s^2 \left(\frac{\sum_J}{\beta y} - \frac{\sum_J}{\beta z} \right) \sin^2 \phi_s + \\
&\quad + r_s^2 J_{xz} \cos^2 \phi_s \sin \epsilon \cos \epsilon + r_s J_{y1w} \{ r_s \sin^2 \phi_s - \Omega_{1s} \sin \phi_s + \\
&\quad + r_s \cos^2 \phi_s \cos^2 \epsilon - \frac{v_s}{r_{w1}} \sin \epsilon \cos \epsilon + \frac{r_s}{r_{w1}} (a_{1z} - l_{A1z} \cos \epsilon + \\
&\quad - l_{A1x} \sin \epsilon) \cos \epsilon \} + g \sum_2 (mg_z) \cos \phi_s \cos \epsilon + \\
&\quad + F_{t1s} |a_{1z} (1 + 2 \tan^2 \phi_s) \cos \epsilon + l_{A1z} \{ (\sin^2 \epsilon - \cos^2 \epsilon) \tan^2 \phi_s + \\
&\quad - \frac{\cos^2 \epsilon}{\cos^2 \phi_s} \}| + (l_{A1z} \cos \epsilon - a_{1z})^2 c_{t1} \tan^2 \phi_s + \\
&\quad + F_{y1s} (l_{A1z} \frac{\tan \phi_s}{\cos \phi_s} - 3l_{A1z} \frac{\tan \phi_s}{\cos \phi_s} \cos^2 \epsilon + 2a_{1z} \frac{\tan \phi_s}{\cos \phi_s} \cos \epsilon) \\
b_{5 \ 15} &= r_s^2 \sum_2 (mg_z l_x) \sin \phi_s \cos \phi_s - r_s^2 \left(\frac{\sum_J}{\beta z} \sin \epsilon - \frac{\sum_J}{\beta y} \sin \epsilon - \frac{\sum_J}{\beta xz} \cos \epsilon \right) \sin \phi_s \cos \phi_s + \\
&\quad - r_s \Omega_{1s} J_{y1w} \cos \phi_s \sin \epsilon + r_s^2 J_{y1w} \sin \phi_s \cos \phi_s \sin \epsilon + \\
&\quad + F_{t1s} (l_{A1x} \cos \epsilon + l_{A1z} \sin \epsilon) \tan \phi_s + \\
&\quad - l_{A1x} (l_{A1z} \cos \epsilon - a_{1z}) c_{t1} \tan \phi_s + F_{y1s} (l_{A1x} \cos \epsilon + l_{A1z} \sin \epsilon) \frac{1}{\cos \phi_s}
\end{aligned}$$

$$\begin{aligned}
b_{5 \ 16} &= -r_s^2 \sum_2 (mg_z) \sin\phi_s \cos\phi_s - F_{t1s} \tan\phi_s \cos\epsilon + (l_{A1z} \cos\epsilon - a_{1z}) C_{t1} \tan\phi_s + \\
&\quad - F_{y1s} \frac{\cos\epsilon}{\cos\phi_s} \\
b_{5 \ 17} &= -r_s^2 \sum_2 (mg_z) \sin\phi_s \cos\phi_s + \\
&\quad - F_{t1s} \tan\phi_s \cos\epsilon + \\
&\quad + (l_{A1x} \cos\epsilon - a_{1z}) C_{t1} \tan\phi_s + \\
&\quad - F_{y1s} \frac{\cos\epsilon}{\cos\phi_s} \\
b_{5 \ 18} &= r_s^2 m_{1u} (l_{G1uz} + g_{1uz} \cos\epsilon) \sin\phi_s \cos\phi_s + u_s r_s m_{1u} \cos\phi_s + \\
&\quad - gm_{1u} \sin\phi_s + \\
&\quad - F_{t1s} \tan\phi_s \sin^2 \epsilon + \\
&\quad - (l_{A1z} \cos\epsilon - a_{1z}) C_{t1} \tan\phi_s \cos\epsilon + \\
&\quad - F_{y1s} \frac{\sin^2 \epsilon}{\cos\phi_s} \\
b_{5 \ 19} &= (a_{1z} - l_{A1z} \cos\epsilon) \frac{1}{\cos\phi_s} \\
b_{5 \ 20} &= b_{5 \ 21} = b_{5 \ 22} = \frac{\sin\epsilon}{\cos\phi_s} \\
b_{5 \ 23} &= -\cos\epsilon
\end{aligned}$$

$$\begin{aligned}
b_{6 \ 2} &= -2r_s m_3 g_{3z} l_{3z} \sin\phi_s \cos\phi_s - u_s m_3 g_{3z} \cos\phi_s + \\
&\quad + 2r_s (J_{z3} - J_{y3}) \sin\phi_s \cos\phi_s \\
b_{6 \ 6} &= 2k_{\phi r} \{C_r (m_3 g_{3z}^2 + J_{x3})\} \\
b_{6 \ 7} &= -2r_s m_3 g_{3z} (l_{3z} - b_z) \cos\phi_s + \\
&\quad + r_s (J_{z3} - J_{x3} - J_{y3}) \cos\phi_s \\
b_{6 \ 11} &= r_s^2 m_3 g_{3z} l_{3z} (\sin^2 \phi_s - \cos^2 \phi_s) + u_s r_s m_3 g_{3z} \sin\phi_s + \\
&\quad + r_s^2 (J_{z3} - J_{y3}) (\cos^2 \phi_s - \sin^2 \phi_s) + \\
&\quad + gm_3 g_{3z} \cos\phi_s + \\
&\quad + C_{\phi r} \\
b_{6 \ 15} &= r_s^2 m_3 g_{3z} d_x \sin_s \cos\phi_s + r_s^2 J_{xz3} \sin\phi_s \cos\phi_s \\
b_{6 \ 16} &= -r_s^2 m_3 g_{3z} \sin\phi_s \cos\phi_s \\
b_{6 \ 17} &= -r_s^2 m_3 g_{3z} \sin\phi_s \cos\phi_s
\end{aligned}$$

$$\begin{aligned}
b_7 \cdot 1 &= -r_s \sum_{S5} \{m(l_z - b_z)\} \\
b_7 \cdot 2 &= u_s \sum_{S5} (ml_x) \sin\phi_s - v_s \sum_{S5} \{m(l_z - b_z)\} + \\
&\quad + 2r_s \sum_{S5} (ml_x l_z) \sin^2 \phi_s - \sum_{S5} \{ml_x (l_z - b_z)\} + \\
&\quad + 2r_s \left\{ \frac{(\Sigma J_z - \Sigma J_x)}{\delta z} \sin\epsilon \cos\epsilon + \frac{\Sigma J_{xz}}{\delta xz} (\sin^2 \epsilon - \cos^2 \epsilon) - \frac{\Sigma J_{xz}}{m_{xz}} \right\} \cos^2 \phi_s \\
b_7 \cdot 3 &= 2r_s \sum_{S5} \{ml_z (l_z - b_z)\} \cos\phi_s + \\
&\quad + r_s \left\{ \frac{(\Sigma J_x - \Sigma J_z)}{\delta x - \delta z} (\cos^2 \epsilon - \sin^2 \epsilon) + \right. \\
&\quad \left. + \frac{\Sigma J_y}{\delta y} - 4 \frac{\Sigma J_{xz}}{\delta xz} \sin\epsilon \cos\epsilon + \frac{\Sigma J_y}{m_y} + \frac{\Sigma J_x}{m_x} - \frac{\Sigma J_z}{m_z} \right\} \cos\phi_s + \\
&\quad - \frac{r_s}{r_{w1}} (l_{A1z} - b_z) J_{y1w} \cos\phi_s \\
b_7 \cdot 4 &= -2r_s \sum_{S3} \{mg_x (l_z - b_z)\} \cos\phi_s + \\
&\quad + r_s \left(\frac{\Sigma J_y \sin\epsilon}{\delta y} - \frac{\Sigma J_x \sin\epsilon}{\delta x} + \frac{\Sigma J_z \sin\epsilon}{\delta z} + \frac{\Sigma J_{xz} \cos\epsilon}{\delta xz} \right) \cos\phi_s + \\
&\quad - \frac{r_s}{r_{w1}} (l_{A1z} - b_z) (t - l_{A1x} \cos\epsilon) J_{y1w} \frac{1}{\cos\phi_s} + \\
&\quad + \frac{s}{r_{w1}^2} (l_{A1z} - b_z) J_{y1w} \frac{\cos\epsilon}{\cos\phi_s} + \\
&\quad - \frac{r_s}{r_{w1}} (l_{A1z} - b_z) J_{y1w} \cos\phi_s \sin\epsilon \\
b_7 \cdot 5 &= 2r_s \sum_{S2} \{mg_z (l_z - b_z)\} \cos\phi_s + \\
&\quad + r_s \left(\frac{\Sigma J_x \cos\epsilon}{\beta x} + \frac{\Sigma J_y \cos\epsilon}{\beta y} - \frac{\Sigma J_z \cos\epsilon}{\beta z} + 2 \frac{\Sigma J_{xz} \sin\epsilon}{\beta xz} \right) \cos\phi_s + \\
&\quad + \frac{1}{r_{w1}} J_{y1w} (l_{A1z} - b_z) \left[\frac{r_s}{r_{w1}} (a_{1z} - l_{A1z} \cos\epsilon - l_{A1x} \sin\epsilon) \frac{1}{\cos\phi_s} + \right. \\
&\quad \left. - \frac{v_s}{r_{w1}} \frac{\sin\epsilon}{\cos\phi_s} - r_s \cos\phi_s \cos\epsilon \right] \\
b_7 \cdot 6 &= 2r_s m_3 (l_{3z} - b_z) \cos\phi_s + r_s (J_{x3} + J_{y3} - J_{z3}) \cos\phi_s \\
b_7 \cdot 8 &= 2r_s \sum_{S5} \{m(l_z - b_z)\} \sin\phi_s \\
b_7 \cdot 9 &= 2r_s \sum_{S5} \{m(l_z - b_z)\} \sin\phi_s \\
b_7 \cdot 10 &= -2r_s m_{1u} \{(l_{G1uz} - b_z) \cos\epsilon + l_{G1ux} \sin\epsilon\} \sin\phi_s \\
b_7 \cdot 11 &= u_s r_s \sum_{S5} (ml_x) \cos\phi_s + 2r_s^2 \sum_{S5} (ml_x l_z) \sin\phi_s \cos\phi_s + \\
&\quad + 2r_s^2 \left\{ \frac{(\Sigma J_x - \Sigma J_z)}{\delta x - \delta z} \sin\epsilon \cos\epsilon + \frac{\Sigma J_{xz}}{\delta xz} (\cos^2 \epsilon - \sin^2 \epsilon) + \frac{\Sigma J_{xz}}{m_{xz}} \right\} \\
&\quad + J_{xz3} \} \sin\phi_s \cos\phi_s - g \sum_{S5} (ml_x) \sin\phi_s \\
b_7 \cdot 12 &= -r_s^2 \sum_{S3} (mg_x l_x) \sin\phi_s \cos\phi_s + \\
&\quad + r_s^2 \left(\frac{\Sigma J_x \cos\epsilon}{\delta x} - \frac{\Sigma J_y \cos\epsilon}{\delta y} - \frac{\Sigma J_z \sin\epsilon}{\delta z} \right) \sin\phi_s \cos\phi_s + \\
&\quad + r_s 1s^J J_{y1w} \cos\phi_s \cos\epsilon +
\end{aligned}$$

$$\begin{aligned}
& + F_{t1s} (l_{A1x} \sin\epsilon - l_{A1z} \cos\epsilon) \tan\phi_s + \\
& - l_{A1x} (a_{1x} + l_{A1z} \sin\epsilon) C_{t1} \tan\phi_s + \\
& - F_{y1s} \left\{ - (l_{A1z} - b_z) \cos\epsilon - (l_{A1x} \sin\epsilon - l_{A1z} \cos\epsilon) \right\} \frac{1}{\cos\phi_s} + \\
& - r_s^2 J_{y1w} \sin\phi_s \cos\phi_s \cos\epsilon \\
b_{7 13} & = r_s^2 \sum_2 (m g_z l_x) \sin\phi_s \cos\phi_s + \\
& + r_s^2 \left(\sum_j \sin\epsilon - \sum_z \sin\epsilon + \sum_x \cos\epsilon \right) \sin\phi_s \cos\phi_s + \\
& - r_s^2 l_{1s} J_{y1w} \cos\phi_s \sin\epsilon + r_s^2 J_{y1w} \sin\phi_s \cos\phi_s \sin\epsilon + \\
& + F_{t1s} (l_{A1x} \cos\epsilon + l_{A1z} \sin\epsilon) \tan\phi_s + \\
& - l_{A1x} (l_{A1z} \cos\epsilon - a_{1z}) C_{t1} \tan\phi_s + \\
& + F_{y1s} \left\{ l_{A1z} \sin\epsilon + l_{A1x} \cos\epsilon - (l_{A1z} - b_z) \sin\epsilon \right\} \frac{1}{\cos\phi_s} \\
b_{7 14} & = r_s^2 m_3 g_{3z} d_x \sin\phi_s \cos\phi_s + r_s^2 J_{xz3} \sin\phi_s \cos\phi_s \\
b_{7 15} & = u_s r_s \sum_5 \{m (l_z - b_z)\} \sin\phi_s + v_s r_s \sum_5 (ml_x) + \\
& - r_s^2 \left(- \sum_5 (ml_x^2) \cos^2 \phi_s - \sum_5 \{ml_z (l_z - b_z)\} \sin^2 \phi_s + \sum_5 \{m (l_z - b_z)^2\} \right) + \\
& + r_s^2 \left\{ (\sum_j x - \sum_j z) (\sin^2 \epsilon - \cos^2 \epsilon) + 4 \sum_j x z \sin\epsilon \cos\epsilon + \right. \\
& \left. - \sum_m x - \sum_j x z + \sum_m z \right\} \cos^2 \phi_s + g \sum_5 \{m (l_z - b_z)\} \cos\phi_s + \\
& + F_{t1s} (l_{A1z} - b_z) + \\
& + C_{t1} l_{A1x} \\
b_{7 16} & = r_s^2 \sum_5 (ml_x) \sin^2 \phi_s + \\
& - l_{A1x} C_{t1} \\
b_{7 17} & = r_s^2 \sum_5 (ml_x) \sin^2 \phi_s + \\
& - l_{A1x} C_{t1} \\
b_{7 18} & = - r_s^2 m_{1u} (u_s \sin\phi_s \sin\epsilon - v_s \cos\epsilon) + \\
& - r_s^2 m_{1u} \left\{ (l_{G1uz} \sin\epsilon + l_{G1ux} \cos\epsilon) \sin^2 \phi_s - l_{G1ux} \cos\epsilon + \right. \\
& \left. - (l_{G1uz} - b_z) \sin\epsilon \right\} - g m_{1u} \cos\phi_s \sin\epsilon + \\
& - F_{t1s} \sin\epsilon + \\
& + l_{A1x} C_{t1} \cos\epsilon
\end{aligned}$$

$$\begin{aligned}
b_{8 \ 2} &= - u_s \sum_6 (m) \sin \phi_s - 2r_s \sum_6 (ml_z) \sin^2 \phi_s \\
b_{8 \ 7} &= - 2r_s \sum_5 \{m (l_z - b_z)\} \sin \phi_s \\
b_{8 \ 10} &= 2r_s m_{1u} \sin \phi_s \sin \epsilon \\
b_{8 \ 11} &= - u_s r_s \sum_6 (m) \cos \phi_s - 2r_s^2 \sum_6 (ml_z) \sin \phi_s \cos \phi_s + \sum_6 (m) g \sin \phi_s \\
b_{8 \ 12} &= r_s^2 \sum_3 (mg_x) \sin \phi_s \cos \phi_s + \\
&\quad - F_{t1s} \tan \phi_s \sin \epsilon + \\
&\quad + t C_{t1} \tan \phi_s \\
&\quad - F_{y1s} \frac{\sin \epsilon}{\cos \phi_s} \\
b_{8 \ 13} &= - r_s^2 \sum_2 (mg_z) \sin \phi_s \cos \phi_s + \\
&\quad - F_{t1s} \tan \phi_s \cos \epsilon + \\
&\quad + (l_{A1z} \cos \epsilon - a_{1z}) C_{t1} \tan \phi_s + \\
&\quad - F_{y1s} \frac{\cos \epsilon}{\cos \phi_s} \\
b_{8 \ 14} &= - r_s^2 m_3 g_{3z} \sin \phi_s \cos \phi_s \\
b_{8 \ 15} &= r_s^2 \sum_5 (ml_x) \sin^2 \phi_s + \\
&\quad - l_{A1x} C_{t1} \\
b_{8 \ 16} &= - r_s^2 \sum_6 (m) \sin^2 \phi_s + \\
&\quad + C_{t2} + \\
&\quad + C_{t1} \\
b_{8 \ 17} &= - r_s^2 \sum_5 (m) \sin^2 \phi_s + \\
&\quad + C_{t1} \\
b_{8 \ 18} &= r_s^2 m_{1u} \sin^2 \phi_s \cos \epsilon + \\
&\quad - C_{t1} \cos \epsilon
\end{aligned}$$

$$\begin{aligned}
b_{9 \ 2} &= - u_s \sum_5 (m) \sin \phi_s - 2r_s \sum_5 (ml_z) \sin^2 \phi_s \\
b_{9 \ 7} &= - 2r_s \sum_5 \{m (l_z - b_z)\} \sin \phi_s \\
b_{9 \ 9} &= K_{s2} \\
b_{9 \ 10} &= 2r_s m_{1u} \sin \phi_s \sin \epsilon \\
b_{9 \ 11} &= - r_s u_s \sum_5 (m) \cos \phi_s - 2r_s^2 \sum_5 (ml_z) \sin \phi_s \cos \phi_s + \sum_5 (m) g \sin \phi_s
\end{aligned}$$

$$b_{9\ 12} = r_s^2 \sum_3 (mg_x) \sin\phi_s \cos\phi_s +$$

$$- F_{t1s} \tan\phi_s \sin\varepsilon +$$

$$+ t c_{t1} \tan\phi_s +$$

$$- F_{y1s} \frac{\sin\varepsilon}{\cos\phi_s}$$

$$b_{9\ 13} = - r_s^2 \sum_2 (mg_z) \sin\phi_s \cos\phi_s +$$

$$- F_{t1s} \tan\phi_s \cos\varepsilon +$$

$$+ (l_{A1z} \cos\varepsilon - a_{1z}) c_{t1} \tan\phi_s +$$

$$- F_{y1s} \frac{\cos\varepsilon}{\cos\phi_s}$$

$$b_{9\ 14} = - r_s^2 m_3 g_{3z} \sin\phi_s \cos\phi_s$$

$$b_{9\ 15} = r_s^2 \sum_5 (ml_x) \sin^2\phi_s +$$

$$- l_{A1x} c_{t1}$$

$$b_{9\ 16} = - r_s^2 \sum_5 (m) \sin^2\phi_s +$$

$$+ c_{t1}$$

$$b_{9\ 17} = - r_s^2 \sum_5 (m) \sin^2\phi_s +$$

$$+ c_{s2} +$$

$$+ c_{t1}$$

$$b_{9\ 18} = r_s^2 m_{1u} \sin^2\phi_s \cos\varepsilon +$$

$$+ c_{t1} \cos\varepsilon$$

$$b_{10\ 1} = r_s m_{1u} \sin\varepsilon$$

$$b_{10\ 2} = u_s m_{1u} \sin\phi_s \cos\varepsilon + 2r_s m_{1u} l_{G1uz} \sin^2\phi_s \cos\varepsilon +$$

$$+ 2r_s m_{1u} l_{G1uz} \sin\varepsilon + v_s m_{1u} \sin\varepsilon$$

$$b_{10\ 3} = - 2r_s m_{1u} l_{G1uz} \cos\phi_s \sin\varepsilon +$$

$$+ \frac{r_s}{r_{w1}} J_{y1w} \cos\phi_s \sin\varepsilon$$

$$b_{10\ 4} = 2r_s m_{1u} g_{1ux} \cos\phi_s \sin\varepsilon +$$

$$+ \frac{1}{r_{w1}} J_{y1w} \sin\varepsilon \left\{ \frac{r_s}{r_{w1}} (t - l_{A1x} \cos\varepsilon) \frac{1}{\cos\phi_s} - \frac{v_s}{r_{w1}} \frac{\cos\varepsilon}{\cos\phi_s} + r_s \cos\phi_s \sin\varepsilon \right.$$

$$b_{10\ 5} = - 2r_s m_{1u} g_{1uz} \cos\phi_s \sin\varepsilon +$$

$$+ \frac{1}{r_{w1}} J_{y1w} \sin\varepsilon \left\{ \frac{r_s}{r_{w1}} (l_{A1x} \sin\varepsilon + l_{A1z} \cos\varepsilon - a_{1z}) \frac{1}{\cos\varepsilon} + \right.$$

$$+ \frac{v_s}{r_{w1}} \frac{\sin\varepsilon}{\cos\phi_s} + r_s \cos\phi_s \cos\varepsilon$$

$$\begin{aligned}
b_{10 \ 7} &= 2r_s m_{1u} \{ l_{G1ux} \sin\epsilon + (l_{G1uz} - b_z) \cos\epsilon \} \sin\phi_s \\
b_{10 \ 8} &= -2r_s m_{1u} \sin\phi_s \sin\epsilon \\
b_{10 \ 9} &= -2r_s m_{1u} \sin\phi_s \sin\epsilon \\
b_{10 \ 10} &= K_{s1} \\
b_{10 \ 11} &= r_s^2 m_{1u} \cos\phi_s \cos\epsilon + 2r_s^2 m_{1u} l_{G1uz} \sin\phi_s \cos\phi_s \cos\epsilon + \\
&\quad + g m_{1u} \sin\phi_s \cos\epsilon \\
b_{10 \ 12} &= -r_s^2 m_{1u} g_{1ux} \sin\phi_s \cos\phi_s \cos\epsilon + \\
&\quad + F_{t1s} \tan\phi_s \sin\epsilon \cos\epsilon + \\
&\quad - t C_{t1} \tan\phi_s \cos\epsilon \\
b_{10 \ 13} &= r_s^2 m_{1u} (l_{G1uz} + g_{1uz} \cos\epsilon) \sin\phi_s \cos\phi_s + u_s r_s m_{1u} \cos\phi_s + \\
&\quad - g m_{1u} \sin\phi_s + \\
&\quad - F_{t1s} \tan\phi_s \sin^2 \epsilon + \\
&\quad - (l_{A1z} \cos\epsilon - a_{1z}) C_{t1} \tan\phi_s \cos\epsilon \\
b_{10 \ 15} &= -u_s r_s m_{1u} \sin\phi_s \sin\epsilon + v_s r_s m_{1u} \cos\epsilon + \\
&\quad - r_s^2 m_{1u} (l_{G1uz} \sin\epsilon + l_{G1ux} \cos\epsilon) \sin^2 \phi_s + \\
&\quad + r_s^2 m_{1u} \{ l_{G1ux} \cos\epsilon + (l_{G1uz} - b_z) \sin\epsilon \} + \\
&\quad - g m_{1u} \cos\phi_s \sin\epsilon + \\
&\quad - F_{t1s} \sin\epsilon + \\
&\quad + l_{A1x} C_{t1} \cos\epsilon \\
b_{10 \ 16} &= r_s^2 m_{1u} \sin^2 \phi_s \cos\epsilon + \\
&\quad - C_{t1} \cos\epsilon \\
b_{10 \ 17} &= r_s^2 m_{1u} \sin^2 \phi_s \cos\epsilon + \\
&\quad - C_{t1} \cos\epsilon \\
b_{10 \ 18} &= -r_s^2 m_{1u} (\sin^2 \phi_s \cos^2 \epsilon + \sin^2 \phi_s) + \\
&\quad + C_{s1} + \\
&\quad + C_{t1} \cos^2 \epsilon
\end{aligned}$$

$$b_{11 \ 3} = b_{12 \ 4} = b_{13 \ 5} = b_{14 \ 6} = b_{15 \ 7} = b_{16 \ 8} = b_{17 \ 9} = b_{18 \ 10} = -1$$

$$\begin{aligned}
b_{19 \ 1} &= -\frac{1}{u_s} \frac{\partial F_{y1s}}{\partial \alpha_{1s}} \\
b_{19 \ 2} &= -\frac{1}{u_s} l_{A1x} \frac{\partial F_{y1s}}{\partial \alpha_{1s}} + \frac{1}{u_s} \frac{\partial F_{y1s}}{\partial \rho_{1s}} \\
b_{19 \ 4} &= -\frac{1}{u_s} t \frac{\partial F_{y1s}}{\partial \alpha_{1s}} \frac{1}{\cos \phi_s} + \frac{1}{u_s} \frac{\partial F_{y1s}}{\partial \rho_{1s}} \frac{\cos \epsilon}{\cos \phi_s} \\
b_{19 \ 5} &= -\frac{1}{u_s} (l_{A1z} \cos \epsilon - a_{1z}) \frac{\partial F_{y1s}}{\partial \alpha_{1s}} \frac{1}{\cos \phi_s} - \frac{1}{u_s} \frac{\partial F_{y1s}}{\partial \rho_{1s}} \frac{\sin \epsilon}{\cos \phi_s} \\
b_{19 \ 11} &= \frac{\partial F_{y1s}}{\partial \gamma_{1s}} + (F_{t1s} \frac{\tan \phi_s}{\cos \phi_s} + F_{y1s} \frac{1}{\cos^2 \phi_s}) \frac{\partial F_{y1s}}{\partial F_{z1s}} \\
b_{19 \ 12} &= (\frac{r_s}{u_s} l_{A1z} \sin \phi_s + 1) \frac{\partial F_{y1s}}{\partial \alpha_{1s}} \frac{\cos \epsilon}{\cos \phi_s} + \frac{\partial F_{y1s}}{\partial \gamma_{1s}} \sin \epsilon + \\
&\quad + (F_{t1s} \frac{\tan \phi_s \sin \epsilon}{\cos \phi_s} - t c_{t1} \frac{\tan \phi_s}{\cos \phi_s} + F_{y1s} \frac{\sin \epsilon}{\cos \phi_s}) \frac{\partial F_{y1s}}{\partial F_{z1s}} \frac{1}{\cos \phi_s} \\
b_{19 \ 13} &= -(\frac{r_s}{u_s} l_{A1z} \sin \phi_s + 1) \frac{\partial F_{y1s}}{\partial \alpha_{1s}} \frac{\sin \epsilon}{\cos \phi_s} + \frac{\partial F_{y1s}}{\partial \gamma_{1s}} \cos \epsilon + \\
&\quad + \{F_{t1s} \frac{\tan \phi_s \cos \epsilon}{\cos \phi_s} - (l_{A1z} \cos \epsilon - a_{1z}) c_{t1} \frac{\tan \phi_s}{\cos \phi_s} + F_{y1s} \frac{\cos \epsilon}{\cos \phi_s}\} \frac{F_{y1s}}{F_{z1s}} \frac{1}{\cos s} \\
b_{19 \ 15} &= -\frac{r_s}{u_s} (l_{A1z} - b_z) \frac{\partial F_{y1s}}{\partial \alpha_{1s}} + l_{A1x} c_{t1} \frac{\partial F_{y1s}}{\partial F_{z1s}} \frac{1}{\cos \phi_s} \\
b_{19 \ 16} &= -c_{t1} \frac{\partial F_{y1s}}{\partial F_{z1s}} \frac{1}{\cos \phi_s} \\
b_{19 \ 17} &= -c_{t1} \frac{\partial F_{y1s}}{\partial F_{z1s}} \frac{1}{\cos \phi_s} \\
b_{19 \ 18} &= \frac{r_s}{u_s} \frac{\partial F_{y1s}}{\partial \alpha_{1s}} \sin \epsilon + c_{t1} \frac{\partial F_{y1s}}{\partial F_{z1s}} \frac{\cos \epsilon}{\cos \phi_s} \\
b_{19 \ 19} &= -1 + \tan \phi_s \frac{\partial F_{y1s}}{\partial F_{z1s}}
\end{aligned}$$

$$\begin{aligned}
b_{20 \ 1} &= -\frac{1}{u_s} \frac{\partial M_{z1as}}{\partial \alpha_{1s}} \\
b_{20 \ 2} &= -\frac{1}{u_s} l_{A1x} \frac{\partial M_{z1as}}{\partial \alpha_{1s}} \\
b_{20 \ 4} &= -\frac{1}{u_s} t \frac{\partial M_{z1as}}{\partial \alpha_{1s}} \frac{1}{\cos \phi_s} \\
b_{20 \ 5} &= -\frac{1}{u_s} (l_{A1z} \cos \epsilon - a_{1z}) \frac{\partial M_{z1as}}{\partial \alpha_{1s}} \frac{1}{\cos \phi_s}
\end{aligned}$$

$$\begin{aligned}
b_{20 \ 11} &= \frac{\partial M}{\partial \gamma} z_{1\alpha s} + (F_{t1s} \tan \phi_s + F_{y1s} \frac{1}{\cos \phi_s}) \frac{\partial M}{\partial F} z_{1\alpha s} \frac{1}{\cos \phi_s} \\
b_{20 \ 12} &= (\frac{r_s}{u_s} l_{A1z} \sin \phi_s + 1) \frac{\partial M}{\partial \alpha} z_{1\alpha s} \frac{\cos \epsilon}{\cos \phi_s} + \frac{\partial M}{\partial \gamma} z_{1\alpha s} \frac{1}{\cos^2 \phi_s} \sin \epsilon + \\
&\quad + (F_{t1s} \sin \phi_s \sin \epsilon - t c_{t1} \sin \phi_s + F_{y1s} \sin \epsilon) \frac{\partial M}{\partial F} z_{1\alpha s} \frac{1}{\cos^2 \phi_s} \\
b_{20 \ 13} &= - \frac{\partial M}{\partial \alpha} z_{1\alpha s} (\frac{r_s}{u_s} l_{A1z} \sin \phi_s + 1) \frac{\sin \epsilon}{\cos \phi_s} + \frac{\partial M}{\partial \gamma} z_{1\alpha s} \cos \epsilon + \\
&\quad + \{F_{t1s} \sin \phi_s \cos \epsilon - (l_{A1x} \cos \epsilon - a_{1z}) c_{t1} \sin \phi_s + F_{y1s} \cos \epsilon\} \frac{\partial M}{\partial F} z_{1\alpha s} \frac{1}{\cos^2 \phi_s} \\
b_{20 \ 15} &= - \frac{r_s}{u_s} (l_{A1z} - b_z) \frac{\partial M}{\partial \alpha} z_{1\alpha s} + l_{A1x} c_{t1} \frac{\partial M}{\partial F} z_{1\alpha s} \frac{1}{\cos \phi_s} \\
b_{20 \ 16} &= - c_{t1} \frac{\partial M}{\partial F} z_{1\alpha s} \frac{1}{\cos \phi_s} \\
b_{20 \ 17} &= - c_{t1} \frac{\partial M}{\partial F} z_{1\alpha s} \frac{1}{\cos \phi_s} \\
b_{20 \ 18} &= \frac{r_s}{u_s} \frac{\partial M}{\partial \alpha} z_{1\alpha s} \sin \epsilon + c_{t1} \frac{\partial M}{\partial F} z_{1\alpha s} \frac{\cos \epsilon}{\cos \phi_s} \\
b_{20 \ 19} &= \frac{\partial M}{\partial F} z_{1\alpha s} \tan \phi_s \\
b_{20 \ 20} &= -1
\end{aligned}$$

$$\begin{aligned}
b_{21 \ 11} &= \frac{\partial M}{\partial \gamma} z_{1\gamma s} + (F_{t1s} \sin \phi_s + F_{y1s}) \frac{\partial M}{\partial F} z_{1\gamma s} \frac{1}{\cos^2 \phi_s} \\
b_{21 \ 12} &= \frac{\partial M}{\partial \gamma} z_{1\gamma s} \sin \epsilon + (F_{t1s} \sin \phi_s \sin \epsilon - t c_{t1} \sin \phi_s + \\
&\quad + F_{y1s} \sin \epsilon) \frac{\partial M}{\partial F} z_{1\gamma s} \frac{1}{\cos^2 \phi_s} \\
b_{21 \ 13} &= \frac{\partial M}{\partial \gamma} z_{1\gamma s} \cos \epsilon + \{F_{t1s} \sin \phi_s \cos \epsilon - (l_{A1x} \cos \epsilon - a_{1z}) c_{t1} \sin \phi_s + \\
&\quad + F_{y1s} \cos \epsilon\} \frac{\partial M}{\partial F} z_{1\gamma s} \frac{1}{\cos^2 \phi_s} \\
b_{21 \ 15} &= l_{A1x} c_{t1} \frac{\partial M}{\partial F} z_{1\gamma s} \frac{1}{\cos \phi_s} \\
b_{21 \ 16} &= - c_{t1} \frac{\partial M}{\partial F} z_{1\gamma s} \frac{1}{\cos \phi_s}
\end{aligned}$$

$$b_{21\ 17} = - c_{t1} \frac{\partial M}{\partial F} \frac{z_{1s}\gamma_s}{z_{1s}} \frac{1}{\cos\phi_s}$$

$$b_{21\ 18} = c_{t1} \frac{\partial M}{\partial F} \frac{z_{1s}\gamma_s}{z_{1s}} \frac{\cos\varepsilon}{\cos\phi_s}$$

$$b_{21\ 19} = \frac{\partial M}{\partial F} \frac{z_{1s}\gamma_s}{z_{1s}} \tan\phi_s$$

$$b_{21\ 21} = - 1$$

$$b_{22\ 2} = \frac{1}{u_s} \frac{\partial M}{\partial \rho_{1s}} z_{1s}\rho_s$$

$$b_{22\ 4} = \frac{1}{u_s} \frac{\partial M}{\partial \rho_{1s}} \frac{z_{1s}\rho_s}{z_{1s}} \frac{\cos\varepsilon}{\cos\phi_s}$$

$$b_{22\ 5} = - \frac{1}{u_s} \frac{\partial M}{\partial \rho_{1s}} \frac{z_{1s}\rho_s}{z_{1s}} \frac{\sin\varepsilon}{\cos\phi_s}$$

$$b_{22\ 11} = (F_{t1s}\sin\phi_s + F_{y1s}) \frac{\partial M}{\partial F} \frac{z_{1s}\rho_s}{z_{1s}} \frac{1}{\cos^2\phi_s}$$

$$b_{22\ 12} = (F_{t1s}\sin\phi_s \sin\varepsilon - t c_{t1}\sin\phi_s + F_{y1s}\sin\varepsilon) \frac{\partial M}{\partial F} \frac{z_{1s}\rho_s}{z_{1s}} \frac{1}{\cos^2\phi_s}$$

$$b_{22\ 13} = \{F_{t1s}\sin\phi_s \cos\varepsilon - (l_{A1z}\cos\varepsilon - a_{1z}) c_{t1}\sin\phi_s - F_{y1s}\cos\varepsilon\} \frac{\partial M}{\partial F} \frac{z_{1s}\rho_s}{z_{1s}} \frac{1}{\cos^2\phi_s}$$

$$b_{22\ 15} = l_{A1x} c_{t1} \frac{\partial M}{\partial F} \frac{z_{1s}\rho_s}{z_{1s}} \frac{1}{\cos\phi_s}$$

$$b_{22\ 16} = - c_{t1} \frac{\partial M}{\partial F} \frac{z_{1s}\rho_s}{z_{1s}} \frac{1}{\cos\phi_s}$$

$$b_{22\ 17} = - c_{t1} \frac{\partial M}{\partial F} \frac{z_{1s}\rho_s}{z_{1s}} \frac{1}{\cos\phi_s}$$

$$b_{22\ 18} = c_{t1} \frac{\partial M}{\partial F} \frac{z_{1s}\rho_s}{z_{1s}} \frac{\cos\varepsilon}{\cos\phi_s}$$

$$b_{22\ 19} = \frac{\partial M}{\partial F} \frac{z_{1s}\rho_s}{z_{1s}} \tan\phi_s$$

$$b_{22\ 22} = - 1$$

$$b_{23\ 11} = \frac{\partial M}{\partial \gamma} \frac{x_{1s}}{z_{1s}} + (F_{t1s}\sin\phi_s + F_{y1s}) \frac{\partial M}{\partial F} \frac{x_{1s}}{z_{1s}} \frac{1}{\cos^2\phi_s}$$

$$b_{23\ 12} = \frac{\partial M}{\partial \gamma} \frac{x_{1s}}{z_{1s}} \sin\varepsilon + (F_{t1s}\sin\phi_s \sin\varepsilon - t c_{t1}\sin\phi_s + F_{y1s}\sin\varepsilon) \frac{\partial M}{\partial F} \frac{x_{1s}}{z_{1s}} \frac{1}{\cos^2\phi_s}$$

$$\begin{aligned}
b_{23 \ 13} &= \frac{\partial M_{x1s}}{\partial \gamma_{1s}} \cos \varepsilon + \{ F_{t1s} \sin \phi_s \cos \varepsilon - (l_{A1z} \cos \varepsilon - a_{1z}) c_{t1} \sin \phi_s + \\
&\quad + F_{y1s} \cos \varepsilon \} \frac{\partial M_{x1s}}{\partial F_{z1s}} \frac{1}{\cos^2 \phi_s} \\
b_{23 \ 15} &= l_{A1x} c_{t1} \frac{\partial M_{x1s}}{\partial F_{z1s}} \frac{1}{\cos \phi_s} \\
b_{23 \ 16} &= - c_{t1} \frac{\partial M_{x1s}}{\partial F_{z1s}} \frac{1}{\cos \phi_s} \\
b_{23 \ 17} &= - c_{t1} \frac{\partial M_{x1s}}{\partial F_{z1s}} \frac{1}{\cos \phi_s} \\
b_{23 \ 18} &= c_{t1} \frac{\partial M_{x1s}}{\partial F_{z1s}} \frac{\cos \varepsilon}{\cos \phi_s} \\
b_{23 \ 19} &= \frac{\partial M_{x1s}}{\partial F_{z1s}} \tan \phi_s \\
b_{23 \ 23} &= - 1
\end{aligned}$$

$$\begin{aligned}
b_{24 \ 1} &= - \frac{1}{u_s} \frac{\partial F_{y2s}}{\partial \alpha_{2s}} \\
b_{24 \ 2} &= \frac{1}{u_s} \frac{\partial F_{y2s}}{\partial \rho_{2s}} \\
b_{24 \ 11} &= \frac{\partial F_{y2s}}{\partial \gamma_{2s}} + (F_{t2s} \sin \phi_s + F_{y2s}) \frac{\partial F_{y2s}}{\partial F_{z2s}} \frac{1}{\cos^2 \phi_s} \\
b_{24 \ 16} &= - c_{t2} \frac{\partial F_{y2s}}{\partial F_{z2s}} \frac{1}{\cos \phi_s} \\
b_{24 \ 24} &= - 1 + \frac{\partial F_{y2s}}{\partial F_{z2s}} \tan \phi_s
\end{aligned}$$

$$\begin{aligned}
b_{25 \ 1} &= - \frac{1}{u_s} \frac{\partial M_{z2as}}{\partial \alpha_{2s}} \\
b_{25 \ 11} &= \frac{\partial M_{z2as}}{\partial \gamma_{2s}} + (F_{t2s} \sin \phi_s + F_{y2s}) \frac{\partial M_{z2as}}{\partial F_{z2s}} \frac{1}{\cos^2 \phi_s} \\
b_{25 \ 16} &= - c_{t2} \frac{\partial M_{z2as}}{\partial F_{z2s}} \frac{1}{\cos \phi_s} \\
b_{25 \ 24} &= \frac{\partial M_{z2as}}{\partial F_{z2s}} \tan \phi_s \\
b_{25 \ 25} &= - 1
\end{aligned}$$

$$b_{27\ 2} = \frac{1}{u_s} - \frac{\partial M_{z2ps}}{\partial p_{2s}}$$

$$b_{27\ 11} = (F_{t2s} \sin \phi_s + F_{y2s}) \frac{\partial M_{z2ps}}{\partial F_{z2s}} - \frac{1}{\cos^2 \phi_s}$$

$$b_{27\ 16} = - c_{t2} \frac{\partial M_{z2ps}}{\partial F_{z2s}} \cos \phi_s$$

$$b_{27\ 24} = \frac{\partial M_{z2ps}}{\partial F_{z2s}} \tan \phi_s$$

$$b_{27\ 27} = - 1$$

$$b_{28\ 11} = \frac{\partial M_{x2s}}{\partial \gamma_{2s}} + (F_{t2s} \sin \phi_s + F_{y2s}) \frac{\partial M_{x2s}}{\partial F_{z2s}} - \frac{1}{\cos^2 \phi_s}$$

$$b_{28\ 16} = - c_{t2} \frac{\partial M_{x2s}}{\partial F_{z2s}} \frac{1}{\cos \phi_s}$$

$$b_{28\ 24} = \frac{\partial M_{x2s}}{\partial F_{z2s}} \tan \phi_s$$

$$b_{28\ 28} = - 1$$

Appendix G - parameter values

The baseline results, discussed in this report, are based on the following set of parameters:

inertia parameters (cf. App. D for the J-summation conventions)

$m_1 = 13.1$ [kg]	$m_3 = 44.5$ [kg]
$m_{1u} = 17.5$ [kg]	$m_2 = 209.6$ [kg]
$m_{1s} = 0$	$m_{2u} = 25.6$ [kg]
$\sum_J \beta_x = .3$ [kgm^2]	$\sum_J \delta_x = .8$ [kgm^2]
$\sum_J \beta_y = 0$	$\sum_J \delta_y = 1.2$ "
$\sum_J \beta_z = .3$ "	$\sum_J \delta_z = .5$ "
$\sum_J \beta_{xz} = 0$	$\sum_J \delta_{xz} = 0$
$J_{y1w} = .58$ [kgm^2]	$J_{y2w} = .74$ [kgm^2]
$J_{x3} = 1.3$ [kgm^2]	$J_{y3} = 2.1$ "
$J_{z3} = 1.4$ "	$J_{xz3} = .3$ "

geometrical parameters (cf. Figs. B2 and B3)

$a_{1x} = .066$ [m]	$g_{1x} = .015$ [m]	$r_{tc1o} = .049$ [m]
$a_{1z} = .632$ "	$g_{1z} = .032$ "	$r_{tc2o} = .070$ "
$b_z = -.321$ "	$g_{1ux} = .066$ "	$r_{w1o} = .319$ "
$d_x = .600$ "	$g_{1uz} = .632$ "	$r_{w2o} = .321$ "
$d_z = -.679$ "	$g_{2x} = .680$ "	$\epsilon = .52$ [rad]
$f_x = 1.168$ "	$g_{2z} = -.211$ "	$p_{Lx} = .770$ m
$f_z = -.513$ "	$g_{3z} = -.190$ "	$p_{Dz} = -.900$ "

suspension parameters

$C_{s1} = 9000$ [Nm^{-1}]	$C_{t1} = 115000$ [Nm^{-1}]	$K_{s1} = 550$ [Nsm^{-1}]
$C_{s2} = 25700$ [Nm^{-1}]	$C_{t2} = 170000$ [Nm^{-1}]	$K_{s2} = 1100$ [Nsm^{-1}]

miscellaneous

$k_\beta = .1$ [-]	$C_\beta = 3.41 \times 10^4$ [Nmrad^{-1}]	$C_D A = .488$ [m^2]
$k_{\phi r} = .25$ [-]	$C_r = 1.0 \times 10^4$ [Nmrad^{-1}]	$C_L A = .114$ [m^2]
$K_\delta = 7.4$ [Nmsrad^{-1}]		

tyre parameters

C_{GYR1}	$= 0.5 \times 10^{-5}$	$[s^2]$
C_{GYR2}	$= 1.0 \times 10^{-5}$	"
$C_{M\gamma 1o}$	$= 4.8$	$[Nmrad^{-1}]$
$C_{M\gamma 2o}$	$= 7.9$	"
C_{Mp1o}	$= 18.7$	$[Nm s rad^{-1}]$
C_{Mp2o}	$= 19.5$	"
$C_{F\alpha 1o}$	$= 1.85 \times 10^4$	$[N rad^{-1}]$
$C_{F\alpha 2o}$	$= 2.58 \times 10^4$	"
$C_{F\gamma 1o}$	$= 1.71 \times 10^3$	"
$C_{F\gamma 2o}$	$= 2.8 \times 10^3$	"
$p_{\alpha\gamma 1}$	$= .46$	$[rad^{-1}]$
$p_{\alpha\gamma 2}$	$= .40$	"
$p_{\gamma\gamma 1}$	$= .36$	"
$p_{\gamma\gamma 2}$	$= .50$	"

$q_{\alpha\alpha 1}$	$= 10.1$	$[rad^{-1}]$
$q_{\alpha\alpha 2}$	$= 10.1$	"
$q_{\gamma\gamma 1}$	$= 5.1$	"
$q_{\gamma\gamma 2}$	$= 5.1$	"
t_{p1o}	$= .03$	"
t_{p2o}	$= .03$	"
$\eta_{\alpha 1}$	$= 14.0$	"
$\eta_{\alpha 2}$	$= 1.9$	"
$\eta_{\gamma 1}$	$= 1.30$	"
$\eta_{\gamma 2}$	$= 1.69$	"
σ_{DUM}	$= .001$	$[m]$
$\sigma_{F\gamma 1o}$	$= .25$	"
$\sigma_{F\gamma 2o}$	$= .25$	"
$\sigma_{Mz1\alpha o}$	$= .25$	"
$\sigma_{Mz2\alpha o}$	$= .25$	"

REFERENCES

1. Audio-Visual Centre, D.U.T., Vibrational Modes of Single-Track Vehicles. Motion Picture, 16mm, optical sound, 16 min. Film VT9, Vehicle Research Lab., Delft Univ. of Techn. (1980).
2. Chenchanna, P. et al., Beitrag zum Fahrverhalten eines Zweiradfahrzeuges. Automobil-Industrie no. 4 (1976) pp. 49-54.
3. Chikada, T. and Yoshida, K., Physical Characteristics of Accessory-Equipped Motorcycles. Proc. of the Int. Motorcycle Safety Conf., Washington D.C., Motorcycle Safety Foundation (1980) Vol. IV, pp. 1539-1558.
4. Dunlop, Fragments clipped from the film "weave and wobble". Film VT11 16mm opt. soundtrack. edited (1981).
5. Eaton, D.J., Man-Machine Dynamics in the Stabilization of Single-Track Vehicles. Ph.D.thesis, University of Michigan (1973).
6. Ellis, J.R. and Hayhoe, G.F., The Steady-State and Transient Handling Characteristics of a Motorcycle. Proc. of the 2nd Int. Congress on Automotive Safety, San Fransisco (1973).
7. McGaw, G.T., On the Steering of the Bicycle. The Engineer, Dec. 9th (1898) p. 557.
8. Hayhoe, G.F., An Introduction to the Dynamics of Single Track Vehicles. Ph.D.thesis (1973) Cranfield Institute of Technology.
9. Jennings, G., A Study of Motorcycle Suspension Damping Characteristics. SAE-paper 740628, Soc. of Aut. Engineers Inc. (1974).
10. Koch, J., Experimentelle und analytische Untersuchungen des Motorrad-Fahrer-Systems. Dissertation, Fortschr.-Ber. VDI-Z. Reihe 12 Nr. 40, VDI-Verlag GmbH Dusseldorf (1980).
11. Koenen, C. et al., Beweging van motorrijwielen verstoord door wegdekongrelmatigheden, een oriënterende studie. Report 104, Veh. Res. Lab., Delft Univ. of Techn. (1976).
12. Koenen, C., The Equations of Motion of a Single-Track Vehicle moving along a Circular Path. VT-report 0134, Vehicle Research Lab., Delft Univ. of Techn. (1979).
13. Koenen, C. and Pacejka, H.B., Vibrational Modes of Motorcycles in Curves. Proc. of the Int. Motorcycle Safety Conf., Washington D.C. Motorcycle Safety Foundation (1980) Vol. II, pp. 501-543.
14. Koenen, C. and Pacejka; H.B., The Influence of Frame Elasticity, Simple Rider Body Dynamics and Tyre Moments on Free Vibrations of Motorcycles in Curves. Proc. 7th VSD Symposium, Cambridge, Swets & Zeitlinger, Lisse (1981).
15. Koenen, C., Expansion of the Single-Track Vehicle Model described in report 0134. VT-report 0147, Vehicle Research Lab., Delft Univ. of Techn. (1981).
16. Koenen, C., Calculation of the Steady State and Dynamic Behaviour of a Motorcycle-Computer Programme Listing. Report 0182, Veh. Research Lab., Delft Univ. of Techn. (1981).
17. NASA, Anthropometric Sourcebook Vol.1, Anthropometry for designers. NASA Reference Publication 1024 (1978) chapter III and IV.

18. Otto, W.M., Effect of Motorcycle Accessories on Stability. Proc. of the Int. Motorcycle Safety Conference (1980) Vol. IV, pp. 1559-1581.
19. Pacejka, H.B., The Tire as a Vehicle Component. Chap. 7.4. of Mechanics of Pneumatic Tires, Ed. S.K. Clark, Washington D.C., N.B.S. Monograph 122 (1971).
20. Pacejka, H.B. and Koenen, C., Vibrational Modes of Single-Track Vehicles in Curves. Proc. 6th VSD Symposium, Berlin, Swets & Zeitlinger, Lisse (1979).
21. Pacejka, H.B., In-Plane and Out-of-Plane Dynamics of Pneumatic Tyres. State-of-the-art articles of the 7th IAVSD Symposium, Cambridge, Swets & Zeitlinger, Lisse (1981).
22. Riedl, K., Lugner, P., Nähere Untersuchungen zur stationären Kurvenfahrt. Vehicle System Dynamics No. 3 , Swets & Zeitlinger, Lisse (1982), pp. 175-193.
23. Roe, G.E., Thorpe, T.E., A Solution of the Low-Speed Wheel Flutter Instability in Motorcycles. Journ. Mech. Engng. Sci. Vol.18 no.2 (1976) pp. 57-65.
24. Roe, G.E. et al., The Oscillations of a Flexible Castor, and the Effect of Front Fork Flexibility on the Stability of Motorcycles. SAE-paper 780307, Soc. of Aut. Engineers Inc. (1978).
25. Roland, R.D., Computer Simulation of Bicycle Dynamics. ASME meeting Mechanics and Sports (1973).
26. Roland, R.D., Simulation Study of Motorcycle Stability at High Speed. Proc. of the 2nd Int. Congress on Automotive Safety, San Francisco (1973).
27. Rotta, J., Zur Statik des Luftreifens. Ingenieur-Archiv 17, pp. 129-141 (1949).
28. Sakai, H. et al., Effect of Main Factors on Dynamic Properties of Motorcycle Tires. SAE-paper 79025 (1979).
29. Schwartz, R., Accident Avoidance Characteristics of Unconventional Motorcycle Configurations. SAE-paper 790258, Soc. of Aut. Engineers Inc. (1979).
30. Segel, L. and Wilson, R., Requirements for Describing the Mechanics of Tires used on Single-Track Vehicles. Proc. IUTAM Symposium, Delft, Swets & Zeitlinger, Amsterdam (1976).
31. Sharp, R.S., The Stability and Control of Motorcycles. J. mech. Engng. Sci. 13 (No. 5), IMech.E (1971) pp. 316-329.
32. Sharp, R.S., Research Note: the Influence of Frame Flexibility on the Lateral Stability of Motorcycles. J.mech.Engng.Sci. 16 (No.2), IMech.E (1974) pp. 117-120.
33. Sharp, R.S., The Stability of Motorcycles in Acceleration and Deceleration. Proc. of the Conference on Braking of Road Vehicles, 23-25 March (1976) Loughborough University of Technology, I Mech. E, London pp. 45-49.
34. Sharp, R.S., The Dynamics of Single Track Vehicles. Vehicle System Dynamics no. 5, Swets & Zeitlinger, Lisse (1976) pp. 67-77.
35. Sharp, R.S., The Influence of the Suspension System on Motorcycle Weave-Mode Oscillations. Vehicle System Dynamics no. 5, Swets & Zeitlinger, Lisse (1976) pp. 147-154.
36. Sharp, R.S. and Jones, C.J., The Straight-Running Stability of Single Track Vehicles. Proc. 5th VSD/2nd IUTAM Symp., Vienna, Swets & Zeitlinger, Lisse (1977).
37. Sharp, R.S., A Review of Motorcycle Steering Behavior and Straight Line Stability Characteristics. SAE-paper 780303, Soc. of Aut. Engineers Inc. (1978).
38. Sharp, R.S., and Alstead, C.J., The Influence of Structural Flexibilities on the Straight-Running Stability of Motorcycles. Vehicle System Dynamics no. 9, Swets & Zeitlinger, Lisse (1980) pp. 327-357.

39. Spierings, P.T.J., The Effects of Lateral Front Fork Flexibility on the Vibrational Modes of Straight-Running Single Track Vehicles. Vehicle System Dynamics no. 10, Swets & Zeitlinger, Lisse (1980) pp. 21-35.
40. Taylor, D.L. and Adiele, C., Dynamic Stability of a Motorcycle during Cornering. Proc. of the Int. Motorcylce Safety Conf., Washinton D.C., Motorcycle Safety Foundation (1980) Vol. II, pp. 615-632.
41. Taylor, D.L. and Black, S.H., Analysis and Evaluation of Suspension Dynamic Response. Proc. of the Int. Motorcycle Safety Conf., Washington D.C., Motorcycle Safety Foundation (1980)Vol. II, pp. 633-658.
42. Thijss, C.F.P., Dynamic Computer Animations of Motorcycle Motions. Computer Programme Listing. Report VT A 016 83, Veh. Res. Lab., Delft Univ. of Techn. (1982).
43. Vehicle Research Laboratory, D.U.T., Vibrational Modes of a Motorcycle Rider (experiment). Motion Picture, 16mm, 3 min. Film VT107, Vehicle Research Lab., Delft Univ. of Techn. (1981).
44. Verma, M.K., Theoretical and Experimental Investigations of Motorcycle Dynamics. Ph.D.thesis, The Univ. of Michigan (1978).
45. Watanabe, Y. and Segel, L., Comparison of Linear Analysis with Experiment for a Single-Track Vehicle in a Steady Turn. Proc. of the Int. Motorcycle Safety Conf., Washington D.C., Motorcycle Safety Foundation (1980) Vol. II, pp. 659-690.
46. Weir, D.H., Motorcycle Handling Dynamics and Rider Control and the Effects of Design Configuration on Response and Performance. Ph.D.thesis, Univ. of California at Los Angeles (1972).
47. Weir, D.H. and Zellner, J.W., Experimental Investigation of the Transient Behavior of Motorcycles. SAE-paper 790266, Soc. of Aut. Engineers Inc. (1978).
48. Whipple, F.J.W., The Stability of the Motion of a Bicycle. Quart. Journ. Pure and Applied Mathematics no. 30 (1899) pp. 312-348.
49. Whittaker, E.T., Analytical Dynamics of Particles and Rigid Bodies. Cambridge University Press (1965).
50. Zellner, J.W. and Weir, D.H., Development of Handling Test Procedures for Motorcycles. SAE-paper 780313, Soc. of Aut. Engineers Inc. (1978).

STELLINGEN
behorende bij het proefschrift
THE DYNAMIC BEHAVIOUR OF A MOTORCYCLE

1

Wanneer zij alleen gebaseerd zijn op het gedrag bij rechtuitrijden leiden beschouwingen over de koppeling tussen het symmetrische en het anti-symmetrische niet-stationaire gedrag van motorfietsen bij een grote gemiddelde rolhoek in het algemeen niet tot realistische resultaten.

Weir, D.H. and Zellner, J.W., *Experimental Investigation of the Transient Behavior of Motorcycles*. SAE-paper 790266, Soc. of Aut. Engineers Inc. (1978).

2

Vanwege de belangrijke rol van symmetrische bewegingen in de eigentrillingsvormen is voor het bepalen van het niet-stationaire gedrag van motorfietsen in de bocht een model waarin de veersystemen van de wielophanging buiten beschouwing zijn gelaten, zoals voor dit doel toegepast door Taylor en Adiele, niet geschikt.

Taylor, D.L. and Adiele, C., *Dynamic Stability of a Motorcycle during Cornering*. Proc. of the Int. Motorcycle Safety Conf., Washington D.C., Motorcycle Safety Foundation (1980) Vo. II, pp. 615-632.

3

De aanbeveling van Roe en Thorpe [1] om de wobble-eigenschappen te verbeteren, namelijk minimalisatie van die aandelen in de totale laterale kompliantie van het voorframe ter hoogte van het wegvlak ten opzichte van het balhoofd, waarbij een verschil tussen de indrukking van het ene ten opzichte van het andere voorveerelement een grote rol speelt ('differential bending' en 'differential shear' in [1]) is in het algemeen niet de meest juiste; de camber-elastici-teit van het voorwiel, die vooral bij deze twee aandelen een grote rol speelt, kan stabiliserend werken [2].

[1] Roe, G.E. and Thorpe, T.E., *Improvements to the Stability, Handling and Braking of High-Performance Motorcycles*. Proc. of the Int. Motorcycle Safety Conference (1980) Vol. II, pp. 565-597.

[2] Spierings, P.T.J., *The Effects of Lateral Front Fork Flexibility on the Vibrational Modes of Straight-Running Single Track Vehicles*. Vehicle System Dynamics no. 10, Swets & Zeitlinger, Lisse (1980) pp. 21-35.

4

Bij de bestudering van de eigenbewegingen van komplexe meer-lichaam-systemen is een grafische animatie een zeer geschikt hulpmiddel.

Audio-Visual Centre, D.U.T., *Vibrational Modes of Single-Track Vehicles*. Motion Picture, 16 mm, optical sound, 16 min. Film VT9, Vehicle Research Lab., Delft Univ. of Techn. (1980).

5

De cultuurhistorische waarde van het rein-pneumatische regeerwerk dient tijdig te worden ingezien om te voorkomen dat in de toekomst de voor een bepaalde periode in de orgelbouw zo karakteristieke instrumenten ontbreken.

De bestrijding door Norman van de juistheid van het uitgangspunt dat inlatende wind meer nuttig vermogen levert dan drukwind is niet terecht als dit uitgangspunt betrokken wordt op een compleet traktuursysteem.

Norman, H. and Norman, H.J., The Organ Today, Barrie and Rockliff, London (1966).

De belangrijkste functie van de toepassing van de combinatie van in- en uit-slaande vuwen, respektievelijk onder en boven, bij magazijnbalgen is niet, zoals Oosterhof vermeldt, het verkrijgen van een zo regelmatig mogelijke volumevermindering bij het samenvouwen, maar een compensatie van het gewicht van het tussenraam, waardoor het schaarmechanisme minder hoog belast wordt.

Oosterhof, A.P. en Bouman, mr. A., Orgelbouwkunde (1971), Spruyt, van Mantgem & de Does, Leiden.

De doeltreffendheid van de inspanning die men zich getroost om situaties ergonomisch te optimaliseren door dit in de ontwerp fase te doen kan vergroot worden door een deel van deze inspanning aan te wenden om de mensen, geplaatst in de genoemde situaties, ertoe te bewegen zich te gedragen zoals in het ontwerp bedoeld is.

Het gebruik van een hoofdtelefoon voor het beluisteren van muziek tijdens deelname aan het verkeer bemoeilijkt de overdracht van informatie die van belang is voor de veiligheid van de drager en die van anderen en verschafft hem informatie die in het algemeen geen correlatie vertoont met de verkeerssituatie, en is daarom af te raden.

Zij die zich vanwege gemeenschappelijke belangen in verenigingsverband organiseren dienen zich te realiseren dat zij hierdoor de aanspreekbaarheid door anderen met betrekking tot het bedoelde belang vergroten en langs deze weg hun doelstellingen mogelijk ondermijnen.

Het verdient aanbeveling om bij het ontwerp van de configuratie voor die computertoepassingen waarbij een groot deel van de reakties van de gebruiker naar het systeem direct via het beeldscherm plaatsvindt, te streven naar een horizontale ligging van het beeldvlak.

Verdedigbaarheid, de enige eis waaraan stellingen behorend bij een proefschrift moeten voldoen, is een niet voldoende voorwaarde voor het controleerbaar juist zijn van de strekking van bedoelde stellingen.

